

This file is part of the following work:

Wau, Jayson Samuel (2023) *Sustainable production of commodity chemicals from renewable materials*. PhD Thesis, James Cook University.

Access to this file is available from:

<https://doi.org/10.25903/me1x%2Ddn25>

Copyright © 2023 Jayson Samuel Wau

The author has certified to JCU that they have made a reasonable effort to gain permission and acknowledge the owners of any third party copyright material included in this document. If you believe that this is not the case, please email

researchonline@jcu.edu.au

Sustainable Production of Commodity Chemicals from Renewable Materials

PhD Thesis

Jayson Samuel Wau

June 2023

College of Science and Engineering

James Cook University



Supervisor:

Professor Michael Oelgemöller

Dedication

“If people are for convenience, living will always be uncertain, vice versa”

LoJ

This dissertation is dedicated to my family, mentors, and friends mentioned below.

My late mother (Janet Wau), the bedrock of my achievements, and my father (Jack Wau) who continues to encourage me. These are two individuals I will always appreciate. Also, I wish to extend this sentiment to my siblings, Jacqueline, Jennifer, Jordan, Jedediah, and Jeremiah.

My principal Ph.D. supervisor, Prof. Michael Oelgemöller. His continual trust and guidance through my candidature.

My dear elder, late Mr. Henry Mapi, Ps. Caleb Lama and colleagues, Dr. Anthony Harakuwe and Dr. David Timi had a great impact on my initial pursuit of tertiary and higher degree education.

My parental guide while I was in Townsville, Mr. Wordman Agita and Mrs. Moera Agita, and friends, Mr. Daniel David, Mr. Wesley Kenai, the Schwartz family, and the Nockosengim family. These individuals and families contributed significantly to my pleasant stay in Townsville.

My friends of JCU Christian Students, JCU Piggies RUC, Northward RUC, and Western Suburbs RUC. These groups helped me to interact and acquaint myself well with Australian social norms.

Abstract

Due to the growing interest in green chemistry, many environmentally conscious methodologies for the synthesis of commodity chemicals have been developed. Commodity, fine or platform chemicals can be extracted directly from biomass or can alternatively be derived through chemical conversions of first-generation biomass substrates. This project followed both strategies and investigated methodologies for the synthesis of fine chemicals from renewable materials and subsequent approaches for their upscaling. The first reaction studied was based on dye-sensitised photooxygenations of bagasse-derived furfural to the platform chemical hydroxyfuranone, which was successfully further converted to important alkoxyfuranones. The second transformation involved the acid-catalyzed cyclization-hydration cascade of citronellal from the essential oil of Lemon scented gum (*Corymbia citriodora*) to para-menthane-3, 8-diol (PMD). Semitechnical-scale productions were performed, and relevant process parameters were optimized that enable a simple and cost-effective production of this powerful natural repellent. The chemical compositions of selected Xanthostemon essential oils were furthermore determined and several natural β -triketones were successfully identified and isolated. Additional synthetic analogues were likewise prepared and subjected to biological screening. Several essential oils and synthetic derivatives showed strong biological activities against mosquito larvae (*Aedes aegypti*) and *S. epidermidis*. The results from this project offer the sugarcane and essential oil industries of Australia new opportunities for waste utilization, product diversification and value adding.

Declaration

Declaration

I declare that this thesis was originally written by me and further editorial and guidance were provided by my supervisors. The contents of this thesis have not been published or submitted for a degree application unless stated otherwise by acknowledgment.

Signed: _____

ID No.: 13431303

Date: 30th September, 2024

Acknowledgements

The content of this thesis and its impact on the organic chemistry community is a success owing to the assistance and contributions of certain individuals and institutions.

Firstly, I wish to express my indebted thanks to my principal supervisor, Professor Michael Oelgemöller. His trust and relentless push on me to complete designated tasks had increased my capability to simultaneously work on different projects, both independently and in a group. A prized aspect of this is that the Oelgemöller lab is hands-on-oriented and composed of a good diversity of members. Also, Prof. Oelgemöller's invaluable editorial support in the preparations of my candidature milestone submissions, grant applications, publication manuscripts, and oral presentation slides is greatly appreciated.

I also wish to thank my secondary supervisors, Dr. Mark Robertson and Dr. Mark Barnes. Dr. Robertson's spirited efforts in training and providing guidance to handle LC-MS, HPLC, NMR, and occasional interpretation of results thereof. It was a great bonus to acquire this know-how, and I very much appreciate it. Dr. Barnes was helpful in comprehending and providing a general perspective on pressing concerns I faced during the course of the program.

My colleagues, interns, undergraduate students, and volunteers also contributed immensely to the success of my Ph.D. work. I wish to thank Dr. Madyan Yaseen for his help in getting me familiarized in the group. I also would like to thank Lida Baba, Denice Gamper, Anthony Traineau, Connor Clark, Marie LeGal, Alex Myhill, Flore Monnot, and Tyler Goodine for their initial work and assistance in the PMD study. Likewise, I thank Aiden Kemp for his assistance with the furfural conversion study.

Special acknowledgment is extended to Brandan Espe and Gary Sankowsky for their priceless help in identifying and approving the collection of various Myrtaceae species. In addition, I wish to thank Assoc. Prof. Nicolas Lebouvier and Dr. Nicolas Pocquet for their assistance with the biological screening.

I also would like to thank Rare Earth Oils and the Distillerie of Boulouparis for partial funding of the PMD study and PIURN and the French Embassy of Australia (Fonds Pacifique) for funding the Myrtaceae-Xanthostemon study.

Many thanks to the GRS for facilitating my candidature program and JCU International student support for paying my tuitions. I also thank CSE for research grants since 2018 and the PNG

Acknowledgment

University of Technology for providing my living allowance during the course of my candidature.

My gratitude to my parents, Jack Wau and the late Janet Wau, for encouraging and supporting me in this endeavour. Finally, I thank GOD for HIS blessings.

List of Abbreviations

^{13}C -NMR	carbon nuclear magnetic resonance
^1H -NMR	proton nuclear magnetic resonance
Acetone- d_6	deuterated acetone
Ar	aryl
BET	back electron transfer
Bn	benzyl group
CDCl_3	deuterated chloroform
CO_2	carbon dioxide
DCM	dichloromethane
d	doublet
dd	doublet of doublet
ddd	doublet of doublet of doublet
DMF	dimethylformamide
DMSO- d_6	deuterated dimethyl sulphoxide
eq.	equivalents
EnT	energy transfer
ET	electron transfer
Et	ethyl group
<i>et al.</i>	et alii (and others)
g	gram
H_2O	water (distilled)
H_2SO_4	sulphuric acid
$\text{H}_{\text{arom.}}$	aromatic proton
HCl	hydrochloric acid
$\text{H}_{\text{olef.}}$	olefinic proton
h or hr(s)	hour(s)
h ν	light photon
<i>i</i> -Bu or <i>i</i> -butyl	iso butyl group
<i>i</i> -Pr or <i>i</i> -propyl	iso propyl group
IUPAC	Internal Union of Pure and Applied Chemistry
<i>J</i>	coupling constant
K_2CO_3	potassium carbonate
m	multiplet

List of Abbreviations

Me	methyl group
MgSO ₄	magnesium sulphate
ml	millilitre(s)
mmol	millimole(s)
NaCl	sodium chloride
nm	nanometres
NMR	nuclear magnetic resonance
°C	degree Celsius
PET	photoinduced electron transfer
Ph	phenyl group
ppm	parts per million
Pr	propyl group
R	(organic) rest group
s	singlet
<i>s</i> -Bu or <i>s</i> -butyl	secondary butyl group
t	triplet
<i>t</i> -Bu or <i>t</i> -butyl	tertiary butyl group
TFA	trifluoroacetic acid
TLC	thin layer chromatography
UV	ultraviolet
VBD	vector borne diseases
π	pi
σ	sigma
δ	chemical shift

Publication and Presentations

Publication:

1. M. Oelgemöller, M. Robertson and **J. S. Wau** “Solar Photooxygenations for the Manufacturing of Fine Chemicals—Technologies and Applications”, *Molecules*, **2021**, *26*, #1685 (27 pages).

Oral Presentations:

1. **J. S. Wau**, M. Oelgemöller and M. Robertson “Prevention of Insect Borne Diseases in PNG through Local Repellent Production from Essential Oils (based on our successful realization in New Caledonia and Queensland)”, *2nd PNG IMPACT Conference*, Port Moresby (Papua New Guinea), 2nd-3rd December 2019.
2. **J. S. Wau**, M. Oelgemöller and M. Robertson “Prevention of Insect Borne Diseases in the Tropics through local repellents”, *James Cook University HDR Forum*, Townsville (Australia), 5th August 2020.
3. **J. S. Wau**, M. Oelgemöller and M. Robertson “Assessment of xanthostemon (Myrteaceae) species essential oils as renewable sources for agrochemical and healthcare application”, *9th TESS Annual Retreat*, Cairns (Australia), 3rd-4th November 2021.
4. **J. S. Wau**, M. Oelgemöller and M. Robertson “Partnering with Developers in the sustainable production of agrochemical and healthcare products”, *AgTAC Annual Awaydays*, Townsville (Australia), 1st-2nd June 2022.
5. **J. S. Wau**, N. Lebouvier, O. Terceve, L. Guentas, V. Medevielle, D. Y. Timi, N. Pocquet, M. Oelgemöller “Biological screening of Xanthostemon and Myrtaceae essential oils from Oceania and of synthetic triketone analogues”, *1st Australian Conference on Green and Sustainable Chemistry & Engineering*, Cairns (Australia), 2nd-5th July 2023.

Poster Presentation:

1. **J. S. Wau**, N. Lebouvier, O. Terceve, L. Guentas, V. Medevielle, D. Y. Timi, N. Pocquet, M. Oelgemöller “Biological screening of Xanthostemon and Myrtaceae essential oils from Oceania and of synthetic triketone analogues”, *1st Australian Conference on Green and Sustainable Chemistry & Engineering*, Cairns (Australia), 2nd-5th July 2023.

Curriculum Vitae

Personal data:

Name: Jayson Samuel Wau
Date of birth: 10. 10. 1982
Place of birth: Bulolo, Morobe Province, Papua New Guinea



Academic qualifications:

- 2018–2024 Ph.D. (Organic Chemistry), James Cook University, College of Science and Engineering, Discipline of Chemistry, Townsville, Australia, with Associate Professor Michael Oelgemöller.
Title: Sustainable Production of Commodity Chemicals from Renewable Materials.
- 2009–2013 M. Phil. (Applied Chemistry), Papua New Guinea University of Technology, Applied Sciences Department, Applied Chemistry, Lae, Papua New Guinea.
Title: Phytochemical and antimicrobial assessment of *Ficus botryocarpa* Miq, MORACEAE.
- 2002–2005 B.Sc. (Applied Chemistry), Papua New Guinea University of Technology, Applied Sciences Department, Applied Chemistry, Lae, Papua New Guinea.

Professional activities:

- 2018–2023 Laboratory demonstrator and tutor, James Cook University, College of Science and Engineering, Discipline of Chemistry, Townsville, Australia.
- 2011–current Lecturer, Papua New Guinea University of Technology, Applied Sciences Department, Applied Chemistry, Lae, Papua New Guinea.

Table of contents

Dedication	I
Abstract	II
Declaration	III
Acknowledgements	IV
List of Abbreviations	VI
Publication and Presentations	VIII
Curriculum Vitae	IX
Table of contents	I
List of Tables	V
List of Figures	VII
List of Schemes	XI
List of Equations	XII
1. Introduction	2
1.1. 5-Hydroxy-2(5H)-furanone study	2
1.1.1. Photochemistry	2
1.1.2. 5-Hydroxy-2(5H)-furanone synthesis	4
1.1.3. Sustainable 5-Hydroxy-2(5H)-furanone syntheses	5
1.1.4. Alkoxyfuranones	9
1.2. <i>Para</i>-Menthane-3, 8-diol study	10
1.2.1. Regional vector borne diseases	10
1.2.2. <i>Para</i> -Menthane-3, 8-diol mosquito repellency	11
1.2.3. Synthetic pathways to <i>para</i> -Menthane-3, 8-diol	12
1.3. β-Triketone study	14
1.3.1. Structural features	14
1.3.2. Phytochemistry	14
1.3.3. Herbicidal use	15
1.3.4. Insecticidal properties	16
1.3.5. Bioactivities	16
1.3.6. Syntheses	17
2. Aims	19
3. Results	21
3.1. Synthesis of 5-Hydroxy-2(5H)-furanone and its alkoxy-derivatives	21
3.1.1. Purification of Furan-2-carbaldehyde	21

Table of Contents

3.1.2.	Irradiation experiments in a Rayonet chamber reactor	22
3.1.3.	Outdoor solar experiments	35
3.1.4.	Workup and isolation of 5-Hydroxyfuran-2(5H)-one	38
3.1.5.	Pseudo-esterification of crude residual 5-Hydroxyfuran-2(5H)-one to 5-Ethoxyfuran-2(5H)-one	39
3.1.6.	Isolation of 5-Ethoxyfuran-2(5H)-one by microdistillation	40
3.1.7.	Pseudo-transesterification of 5-Ethoxyfuran-2(5H)-one	42
3.1.8.	Additional assessment of parameters	46
3.2.	Sustainable synthesis of <i>para</i>-menthane-3, 8-diol	49
3.2.1.	Sampling and preparation of <i>C. citriodora</i> leaves	49
3.2.2.	Sorting of leaves	50
3.2.3.	Extraction of LSG oil	50
3.2.4.	GC-analysis parameters	55
3.2.5.	PMD synthesis	59
3.2.6.	Separation of PMD stereoisomers	82
3.3.	β-Triketone syntheses and isolation	92
3.3.1.	Syntheses of 2, 4, 6-trihydroxyphenyl ketones (acetyl phloroglucinols)	92
3.3.2.	Characterization of the 2, 4, 6-trihydroxyphenyl ketones	95
3.3.3.	Syntheses of β -triketones (acetyl- β -triketones)	101
3.3.4.	Characterization of the β -triketones	104
3.3.5.	Photolysis of β -triketones	110
3.3.6.	Photooxidation of 5-Hydroxy-4-isobutyryl-2, 2, 6, 6-tetramethylcyclohex-4-ene-1, 3-dione (54)	110
3.3.7.	Exploring Myrtaceae species for β -triketones	111
3.3.8.	Extraction of essential oils	111
3.3.9.	Separation and characterization of major β -triketone constituents	114
3.3.10.	Isolation and identification of cyclocolorenone from <i>X. umbrosus</i> oil	115
3.3.11.	Identification of 1, 3-dimethoxy-5-isopropylbenzene from <i>X. verticillatus</i> oil	118
3.3.12.	GC-MS characterization of other constituents in the essential oils	118
3.3.13.	Biological activity testing	119
4.	Discussion	133
4.1.	Synthesis of 5-Hydroxy-2(5H)-furanone and its alkoxy-derivatives	133
4.1.1.	Purification of furan-2-carbaldehyde	133
4.1.2.	Photooxygenations with artificial light	133
4.1.3.	Photooxygenation studies in an Immersion Well Reactor	137
4.1.4.	Photooxygenations with natural sunlight	138
4.1.5.	Evaporation-induced composition changes	146

Table of Contents

4.1.6.	Crystallization efficiencies	147
4.1.7.	Pseudo-esterifications using recovered materials	148
4.1.8.	Pseudo-transesterification of ethoxyfuranone	150
4.1.9.	Additional assessments	151
4.1.10.	Rose Bengal decomposition with artificial light	152
4.1.11.	Assessment of pseudo-esterification in different alcohols	153
4.2.	Sustainable synthesis of <i>para</i>-menthane-3, 8-diol	154
4.2.1.	Assessment of LSG distillation methods	154
4.2.2.	GC-FID method development	157
4.2.3.	Citronellal content of commercial LSG oils	158
4.2.4.	Laboratory-scale conversions	159
4.2.5.	Demonstration-scale conversions	160
4.2.6.	Technical-scale conversions	162
4.2.7.	Separation of PMD-stereoisomers by recrystallization	164
4.2.8.	Separation of PMD stereoisomers by fractional distillation	165
4.2.9.	Synthesis of PMD-acetals	166
4.3.	β-Triketone syntheses and isolation	167
4.3.1.	Synthesis of 2, 4, 6-trihydroxyphenyl ketones	167
4.3.2.	Synthesis of acetyl- β -triketones	168
4.3.3.	Photolytic stability testing	169
4.3.4.	Photooxidative stability testing	170
4.3.5.	Exploring Myrtaceae species as potential β -triketone resources	170
4.3.6.	Isolation and structural characterization of tasmanone	172
4.3.7.	Extraction of flavesone, leptospermone and isoleptospermone from Manuka oil	172
4.3.8.	Isolation and identification of cyclocolorenone from <i>X. umbrosus</i> oil	173
4.3.9.	Isolation and identification of 1, 3-dimethoxy-5-isopropylbenzene from <i>X. verticillatus</i> oil	174
4.3.10.	Identification of other constituents in the essential oils by GC-analyses	174
4.3.11.	Antimicrobial activity evaluations	181
4.3.12.	Larvicidal activity evaluations	181
4.3.13.	Adulticidal activity evaluations	183
5.	Summary and Outlook	187
5.1.	Synthesis of hydroxyfuranone and its alkoxy-derivatives	187
5.1.1.	Photooxygenations	187
5.2.	Sustainable synthesis of <i>para</i>-menthane-3, 8-diol	189
5.2.1.	GC-FID method development	189
5.2.2.	LSG-distillations and chemical profiling	190

Table of Contents

5.2.3.	Syntheses of PMD	190
5.2.4.	Isolation and conversion of PMD	191
5.3.	β-Triketone syntheses and isolation	192
5.3.1.	Syntheses of 2, 4, 6-trihydroxyphenyl ketones and stability testing	192
5.3.2.	Distillation of Myrtaceae species and chemical profiling	192
5.3.3.	Isolation and characterization of selected constituents	193
5.3.4.	Bioactivity screening	194
6.	Experimental Part	197
6.1.	General methods	197
6.1.1.	Analytical methods	197
6.1.2.	Purification methods	198
6.2.	Synthesis of hydroxyfuranone and its alkoxy-derivatives	199
6.2.1.	Reagents and solvents	199
6.2.2.	Photochemical and solar reactors	200
6.2.3.	Flatbed reactor and illumination procedure	200
6.3.	Sustainable synthesis of <i>para</i>- menthane-3, 8-diol	201
6.3.1.	Reagents and solvents	201
6.4.	β-Triketone syntheses and isolation	202
6.4.1.	Reagents and solvents	202
	References	205
	Appendices	223

List of Tables

Table 1.1: Comparison of key-process parameters for the photooxygenation of furfural.....	6
Table 1.2: β -Triketones and β -diketones found in certain plant extracts.	15
Table 3.1: Batches of furfural obtained by fractional distillation.....	22
Table 3.2: Experimental parameters for irradiations in a Rayonet reactor.....	24
Table 3.3: Experimental results for irradiations in a Rayonet reactor.....	24
Table 3.4: Conversion profile of Experiment 5.....	25
Table 3.5: Experimental parameters of alkoxyfuranone syntheses.	26
Table 3.6: Experimental results of alkoxyfuranone syntheses.	26
Table 3.7: Experimental parameters for irradiations in an immersion well reactor.	31
Table 3.8: Experimental results for irradiations in an immersion well reactor.	31
Table 3.9: Conversion profile of Experiment 17.....	31
Table 3.10: Experimental parameters of alkoxyfuranone syntheses.	32
Table 3.11: Experimental results of alkoxyfuranone syntheses.	32
Table 3.12: Composition-over-time profiles obtained by $^1\text{H-NMR}$ analysis.	36
Table 3.13: Composition-over-time profile obtained by GC-analysis.	37
Table 3.14: Comparison of experimental outcomes of solar reactions.	38
Table 3.15: Composition of dried crude materials and isolated yields of hydroxyfuranone.....	39
Table 3.16: Pseudo-esterification parameters using crude filtrates.	40
Table 3.17: Composition of refined filtrates.	40
Table 3.18: Composition of fractions obtained by micro-distillation.	41
Table 3.19: Compositions of fractions from bulb-to-bulb distillation.....	41
Table 3.20: Transesterification conversion parameters.....	43
Table 3.21: Composition of fractions obtained by vacuum distillation.	44
Table 3.22: Composition of fractions obtained by flash chromatography separation.....	45
Table 3.23: Constituents in fractions of preparative HPLC.	45
Table 3.24: Concentration and related peak areas of the internal standard.....	47
Table 3.25: Assessment of the rate of decomposition of RB over 4 hours of irradiation.	48
Table 3.26: Comparison between different alcohols and the product compositions.....	49
Table 3.27: Details of sampling of LSG in JCU at different times.	50
Table 3.28: Comparison of distillation performance.....	54
Table 3.29: Reference standards used to assign the main compounds of LSG oils.	58
Table 3.30: Comparison of the main constituents in LSG oil from several commercial products.....	58
Table 3.31: Reaction parameters of waste utilization assessment.....	60
Table 3.32: Composition of refined LSG oils.	61
Table 3.33: Conversion parameters for the 5 L scale production of PMD.....	62
Table 3.34: Monitoring of major constituents for the initial demonstration-scale trial.....	63

Table of Contents

Table 3.35: Monitoring of major constituents for the repeat demonstration-scale experiment.....	65
Table 3.36: Monitoring of the demonstration-scale experiment using hydrosol.....	66
Table 3.37: Monitoring of major constituents for the demonstration-scale experiment using recovered acidic solution.	68
Table 3.38: Monitoring of major constituents for the demonstration-scale experiment using distilled boiler water.....	69
Table 3.39: Reaction order data calculations.	73
Table 3.40: Comparison of k' - and R^2 -values.....	75
Table 3.41: Assignments of main constituents in commercial LSG oil.	76
Table 3.42: Reaction parameters of the technical-scale conversions.	77
Table 3.43: Monitoring of major constituents for technical-scale Experiment 55.....	78
Table 3.44: Monitoring of major constituents for technical-scale Experiment 56.....	79
Table 3.45: Monitoring of major constituents for technical-scale Experiment 57.....	80
Table 3.46: Comparison of k' and R^2 -values for Experiments 55-57.....	82
Table 3.47: Reaction parameters for PMD synthesis from synthetic citronellal.....	83
Table 3.48: Conversion profile for the neat PMD synthesis from synthetic citronellal.....	83
Table 3.49: Comparison of recorded chemical shifts for <i>cis</i> -PMD (33c) with literature values.....	85
Table 3.50: Comparison of recorded chemical shifts for <i>trans</i> -PMD (33b) with literature values.....	85
Table 3.51: Composition of main constituents in fractions obtained by vacuum distillation.	87
Table 3.52: Changes in the composition of fraction F4 during successive recrystallizations.....	88
Table 3.53: Reaction conditions for acetalization.	90
Table 3.54: Constituents and composition of the PMD-acetals.	90
Table 3.55: Reaction parameters for the synthesis of β -triketone precursors.	94
Table 3.56: Reaction parameters for the exhaustive methylation of acylphloroglucinols.	103
Table 3.57: Reaction parameters for the photolysis of selected β -triketones.....	110
Table 3.58: Reaction parameters for the photooxidation of flavesone.....	111
Table 3.59: Details of leaves collected for distillation.....	112
Table 3.60: Distillation and extraction parameters and results.	113
Table 3.61: Characterization of major peaks from the Myrtaceae essential oils.....	113
Table 3.62: $^1\text{H-NMR}$ assignments of the two major tautomeric forms of tasmanone.....	114
Table 3.63: β -Triketones of Manuka oil fractions.....	115
Table 3.64: HMBC and HSQC $^1\text{H-}^{13}\text{C}$ -correlations of cyclocolorenone.	117
Table 3.65: HMBC and HSQC $^1\text{H-}^{13}\text{C}$ -correlations of 1, 3-dimethoxy-5-isopropylbenzene.	119
Table 3.66: Identified constituents of the isolated essential oils based on MS (m/z) and KI (RI) values.	120
Table 3.67: Mean values of antimicrobial growth inhibitions expressed by selected 2, 4, 6-trihydroxyphenyl ketones, acetyl- β -triketones and Myrtaceae essential oils.....	126

Table of Contents

Table 3.68: Anti-larval activity of selected 2, 4, 6-trihydroxyphenyl ketones, acetyl- β -triketones and Myrtaceae essential oils.....	127
Table 3.69: Total number of adult mosquitoes knocked down by MOR.....	129
Table 3.70: Percentages (%) of adult mosquitoes knocked down by MOR.....	130
Table 3.71: Percentage mortality (x) of adult female mosquitoes after 24 hrs.....	131
Table 3.72: Percentage mortality (x) of adult female mosquitoes after 24 hrs.....	131
Table 4.1: Comparison of distillation yields	155
Table 4.2: Main NMR assignments of <i>cis</i> - and <i>trans</i> -PMD.....	165
Table 4.3: Comparison of experimental and calculated chemical shifts of cyclocolorenone.....	173
Table 4.4: Comparison of experimental and calculated chemical shifts of 1, 3-dimethoxy-5-isopropylbenzene.....	174
Table 4.5: Constituents identified from <i>X. chrysanthus</i> oil from the Townsville region.....	175
Table 4.6: Constituents identified from <i>X. chrysanthus</i> oil from the Tolga region.....	175
Table 4.7: Constituents identified from <i>X. umbrosus</i> oil from the Tolga region.....	176
Table 4.8: Constituents identified from <i>X. chrysanthus</i> and <i>X. verticillatus</i> hybrid oil from the Tolga region.....	176
Table 4.9: Constituents identified from <i>X. verticillatus</i> oil from the Tolga region.....	177
Table 4.10: Constituents identified from <i>E. cloeziana</i> oil from the Townsville region.....	178
Table 4.11: Constituents identified from the organic fraction of Manuka oil.....	178
Table 4.12: Constituents identified from the organic fraction of Manuka oil.....	180
Table 4.13: Constituents identified from the aqueous fraction of Manuka oil.....	180
Table 6.1: List of reagents and solvents.....	199
Table 6.2: Parameters of calibration standards.....	201
Table 6.3: List of reagents and solvents.....	201
Table 6.4: List of reagents and solvents.....	202

List of Figures

Figure 1.1: Jablonski diagram illustrating excitation of a molecule to its singlet-excited state, its subsequent electronic transitions and finally its return to the ground state.....	3
Figure 1.2: Spin positions of HOMO electrons at specific energy state.....	3
Figure 1.3: 1, 3, 5-Trione herbicides.....	16
Figure 1.4: Herbicidal 1, 3-diones.....	16
Figure 3.1: Fractional distillation setup.....	21
Figure 3.2: Distilled (left) and crude (right) furfural.....	21
Figure 3.3: Rayonet chamber reactor setup.....	23
Figure 3.4: (a) Crude hydroxyfuranone. (b) Filtration and washing of crystals. (c) Pure product.....	24
Figure 3.5: Graphical conversion profile of Experiment 5.....	25

Table of Contents

Figure 3.6: Immersion well reactor (a) prior to and (b) during early stages of irradiation.....	30
Figure 3.7: Conversion of FAL and production of HF in an IWR.	31
Figure 3.8: Dean-Stark setup used for batch synthesis of alkoxyfuranones.....	32
Figure 3.9: ¹ H-NMR spectrum of the crude reaction mixture from Experiment 19 with assignments of the diethoxy derivative 15.	34
Figure 3.10: Solar flatbed reactor without aeration and circulation.	35
Figure 3.11: Hydroxyfuranone freeze-crystallization process.	39
Figure 3.12: Micro vacuum distillation setup.....	40
Figure 3.13: Structures of compounds identified in respective crude products.	42
Figure 3.14: ¹ H-NMR spectra of compound 29 with assigned characteristic chemical shifts.	46
Figure 3.15: Chromatogram depicting subsequent constituents at 900 th minute.....	48
Figure 3.16: Structures of products obtained.	49
Figure 3.17: Sampling of <i>C. citriodora</i> leaves (at Site 2) and locations of sampling sites.	49
Figure 3.18: (1) Images of leaves with dead patches (a) and infectious patches (b); (2) moderately affected leaves and (3) fine leaves with physical integrity intact.....	50
Figure 3.19: Hydrodistillation setup.....	51
Figure 3.20: Glass-based steam distillation setup.	52
Figure 3.21: Copper-based steam distillation setup.	53
Figure 3.22: Liquid-liquid extraction using boiler (left) and distilled boiler water (right).	54
Figure 3.23: Existing GC temperature profiles used for method development.....	55
Figure 3.24: Temperature profiles of the developed in-house GC methods.	56
Figure 3.25: Chromatogram LSG oil analysed using M1.	56
Figure 3.26: Chromatogram LSG oil analysed using M2.	57
Figure 3.27: Chromatogram LSG oil analysed using M3.	57
Figure 3.28: Illustration of the top (LSG-TL) and bottom (LSG-BL) LSG oil layers and, top (TLH) and bottom (BLH) layers of distillate hydrosol.	59
Figure 3.29: 5 L demonstration-scale setup.	62
Figure 3.30: Chemical profile of PMDs vs. citronellal over time.....	63
Figure 3.31: Chemical profiles of isopulegols, citronellol and PMD-acetals over time.	64
Figure 3.32: Chemical profile of PMDs vs. citronellal over time with hourly monitoring.....	65
Figure 3.33: Chemical profiles of isopulegols, citronellol and PMD acetals over time.....	66
Figure 3.34: Compositions of PMDs vs. citronellal over time using hydrosol.....	67
Figure 3.35: Compositions of isopulegols, citronellol and PMD-acetals over time hydrosol.....	67
Figure 3.36: Chemical profile of PMDs vs. citronellal over time using recovered acidic solution.	68
Figure 3.37: Chemical profiles of isopulegols, citronellol and PMD acetals over time using recovered acidic solution.	69
Figure 3.38: Chemical profile of PMDs vs. citronellal over time using distilled boiler water.....	70

Table of Contents

Figure 3.39: Chemical profiles of isopulegols, citronellol and PMD acetals over time using distilled boiler water.....	70
Figure 3.40: First order plot of Experiment 51.....	73
Figure 3.41: Second order plot of Experiment 51.....	74
Figure 3.42: First-order plot of Experiment 52.....	74
Figure 3.43: First-order plot of Experiment 53.....	74
Figure 3.44: First-order plot of Experiment 54.....	75
Figure 3.45: GC-chromatogram of the first batch of commercial LSG oil used for bulk synthesis.....	75
Figure 3.46: Initial LSG oil-water layers and generation of a stable emulsion.....	77
Figure 3.47: Chemical profile of PMDs and citronellal in Experiment 55.....	78
Figure 3.48: Profile of the isopulegols, citronellol and PMD acetals during Experiment 55.....	78
Figure 3.49: First order plot of Experiment 55.....	79
Figure 3.50: Chemical profile of PMDs and citronellal in Experiment 56.....	80
Figure 3.51: Profile of the isopulegols, citronellol and PMD-acetals during Experiment 56.....	80
Figure 3.52: First order plot for Experiment 56.....	80
Figure 3.53: Chemical profile of PMDs and citronellal in Experiment 57.....	81
Figure 3.54: Profile of the isopulegols, citronellol and PMD acetals during Experiment 57.....	81
Figure 3.55: First order plot of Experiment 57.....	81
Figure 3.56: Structures of main isomers of PMD, (1S, 2S, 5R)-(+/-)- <i>cis</i> -PMD (33c) and (1R, 2S, 5R)-(+/-)- <i>trans</i> -PMD (33b).....	82
Figure 3.57: ¹ H-NMR spectrum of <i>cis</i> -PMD (33c) in CDCl ₃	83
Figure 3.58: ¹³ C-NMR spectrum of <i>cis</i> -PMD (33c) in CDCl ₃	84
Figure 3.59: ¹ H-NMR spectrum of <i>trans</i> -PMD (33b) in CDCl ₃	84
Figure 3.60: ¹³ C-NMR spectrum of <i>trans</i> -PMD (33b) in CDCl ₃	84
Figure 3.61: Fractional vacuum distillation setup.....	86
Figure 3.62: ¹ H-NMR spectrum of fraction F4 obtained by vacuum distillation.....	87
Figure 3.63: Characteristic ¹ H-NMR signals of the main constituents in fraction F4.....	87
Figure 3.64: ¹ H-NMR spectrum of fraction RC1 after initial recrystallization.....	88
Figure 3.65: ¹ H-NMR spectrum of fraction RC2 after successive recrystallization.....	89
Figure 3.66: GC-chromatogram of Experiment 60.....	90
Figure 3.67: Expanded ¹ H-NMR-spectrum of the crude product of Experiment 60.....	91
Figure 3.68: Characteristic ¹ H-NMR signals of <i>cis</i> -PMD acetal (39a), <i>neo</i> -isopulegol (37b) and <i>iso</i> -isopulegol (37a).....	91
Figure 3.69: GC chromatogram of crude PMD-acetals obtained after column chromatography.....	92
Figure 3.70: Reaction setup for the Friedel-Crafts' acetylation of phloroglucinols.....	93
Figure 3.71: Reaction setup for the exhaustive methylation of acylphloroglucinols.....	102
Figure 3.72: Sampling of <i>X. chrysanthus</i> in Tolga (QLD).....	111
Figure 3.73: Hydrodistillation setup.....	112

Table of Contents

Figure 3.74: ¹ H-NMR spectrum of tasmanone in CDCl ₃	114
Figure 3.75: GC-chromatogram of Fraction 2 from bulb-to-bulb purification.....	115
Figure 3.76: Structure of cyclocolorenone (69).....	116
Figure 3.77: Flash chromatogram for the isolation of cyclocolorenone (69).....	116
Figure 3.78: ¹ H-NMR spectrum of cyclocolorenone (69).....	116
Figure 3.79: Structure of 1, 3-dimethoxy-5-isopropylbenzene (70).....	118
Figure 3.80: ¹ H-NMR spectrum of 1, 3-dimethoxy-5-isopropylbenzene (70).....	118
Figure 3.81: Larvicidal test setup using 24-well plates containing seeded larvae.....	127
Figure 3.82: WHO tubes infused with adult <i>A. aegypti</i>	128
Figure 4.1: Comparison of conversions, isolated yields and purities.....	133
Figure 4.2: Reaction profile of Experiment 5.....	134
Figure 4.3: Conversion rates, selectivity and yields of alkoxyfuranones.....	135
Figure 4.4: Three possible structures of the polyethoxy-derivative.....	138
Figure 4.5: Conversions and product compositions of solar photooxygenations.....	140
Figure 4.6: Temperature-and exposure time-dependances on furfural conversion.....	142
Figure 4.7: Corrected conversion over time profile during solar exposures.....	142
Figure 4.8: Composition of the ethoxy-derivatives during solar experiments.....	145
Figure 4.9: Changes in the composition after evaporation.....	146
Figure 4.10: Percentage of hydroxyfuranone in the crude product (SY), isolated yields (YAW) and losses (LW).....	148
Figure 4.11: Composition changes during pseudo-esterification in Experiment 27.....	149
Figure 4.12: Generic general structures of pseudo-transesterification products.....	150
Figure 4.13: Product compositions of transesterification reactions.....	151
Figure 4.14: Calibration curve of the IS " <i>n</i> -butanol" used to verify the response factor (R _f).....	151
Figure 4.15: The gradual change in [RB] under visible light for 4 hours.....	153
Figure 4.16: Pseudo-esterification with different alcohols.....	154
Figure 4.17: Normalized mass distribution for all oil fractions.....	156
Figure 4.18: GC-chromatogram with (a) crowd and overlapping peaks and (b) resolved peaks.....	157
Figure 4.19: (a) Initial and (b) improved resolution of PMD peaks.....	158
Figure 4.20: (a) Absent and (b) observed PMD-acetal.....	158
Figure 4.21: Citronellal content of various commercial LSG oil.....	159
Figure 4.22: Citronellal conversions and PMD contents of laboratory-scale experiments.....	159
Figure 4.23: Citronellal conversions and PMD contents of demonstration-scale experiments.....	160
Figure 4.24: Isopulegol, citronellol and PMD-acetal contents of demonstration-scale experiments.....	161
Figure 4.25: Rate constants for citronellal conversions.....	162
Figure 4.26: Citronellal conversions and PMD contents of technical-scale experiments.....	163
Figure 4.27: Isopulegol, citronellol and PMD-acetal contents of technical-scale experiments.....	164
Figure 4.28: First-order comparison of citronellal conversion.....	164

Table of Contents

Figure 4.29: Composition of crude product from neat citronellal.....	165
Figure 4.30: Composition of crude product from RE-LSG oil.	166
Figure 4.31: Partial ¹ H-NMR spectra of (a) crude and (b) recrystallized Fraction 4 material.	166
Figure 4.32: Composition of crude acetalization products.....	166
Figure 4.33: Yields and purities of acyl phloroglucinols.	167
Figure 4.34: Yields and purities of acetyl- β -triketones.....	168
Figure 4.35: Structure of penitential rotamers of 4-(<i>sec</i> -butyl)-5-hydroxy-2, 2, 6, 6-tetramethylcyclohex-4-ene-1, 3-dione (55).....	169
Figure 4.36: Possible Norrish-type cleavages of acetyl- β -triketones.	169
Figure 4.37: Possible photo-keto-enol tautomerization of acetyl- β -triketones.	169
Figure 4.38: Reported slow photooxidation of flavesone.	170
Figure 4.39: Difference between the percent yield and actual mass of oil.....	171
Figure 4.40: Major constituents of the essential oils.	172
Figure 4.41: Composition of refined Manuka oil prior and after bulb-to-bulb purification.....	173
Figure 4.42: Chemical structures of selected constituents (>20%) of the essential oils.....	175
Figure 4.43: Inhibition of <i>S. epidermidis</i> , <i>E. coli</i> and <i>C. albicans</i> after inoculating with selected Myrtaceae extracts, trihydroxyphenyl ketones and acetyl- β -triketones.	182
Figure 4.44: Susceptibility of <i>A. aegypti</i> larvae after inoculating with selected Myrtaceae extracts, trihydroxyphenyl ketones and acetyl- β -triketones.	183
Figure 4.45: Knock down (KD) rates of adult <i>A. aegypti</i> towards untreated Manuka oil (MOr).	183
Figure 4.46: LD ₅₀ -determination for adult <i>A. aegypti</i> after 1 h exposure towards untreated Manuka oil (MOr).	184
Figure 4.47: Mortality of adult <i>A. aegypti</i> towards the untreated Manuka oil (MOr).....	184
Figure 4.48: LD ₅₀ -determination for adult <i>A. aegypti</i> after 24 hrs exposure towards the untreated Manuka oil (MOr).	185

List of Schemes

Scheme 1.1: (a) Direct photoexcitation and (b) indirect photo-excitation of a substrate.....	2
Scheme 1.2: Main types of photooxygenation reactions.....	4
Scheme 1.3: Acid catalyzed hydrolysis of pentosan and subsequent dehydration to furfural.....	7
Scheme 1.4: Synthesis of furfural from (a) D-xylose and (b) D-xylopyranose.....	7
Scheme 1.5: Photosensitized oxygenation of 2-furoic acid or furfural to hydroxyfuranone.....	8
Scheme 1.6: Formation of PMD by Prins reaction.....	12
Scheme 1.7: Alternating keto-enol tautomeric forms.....	14
Scheme 3.1: Photooxygenation of furfural to hydroxyfuranone.	23
Scheme 3.2: Pseudo-Fischer esterification of hydroxyfuranone to subsequent ester derivatives.	26
Scheme 3.3: Pseudo-transesterification of ethoxyfuranone with various alcohols.	42

Table of Contents

Scheme 3.4: Acid catalysed cyclization of citronellal to PMD.....	61
Scheme 3.5: Plausible mechanism and subsequent intermediates involved in the reaction.....	71
Scheme 3.6: The two plausible rate-determining steps of the reaction.....	71
Scheme 3.7: Synthesis of PMD acetals.....	89
Scheme 3.8: Acetylation of phloroglucinol.....	93
Scheme 3.9: Exhaustive methylation of acylphloroglucinols.....	101
Scheme 3.10: Equilibrium of the tasmanone tautomers.....	114
Scheme 4.1: (a) Reaction scheme. (b) Crucial kinetic parameters.....	143
Scheme 4.2: Reaction mechanism for the conversion of furfural.....	144
Scheme 4.3: (a) Ring-chain tautomerization of hydroxyfuranone and (b) possible <i>cis-trans</i> isomerizations to open <i>trans</i> -isomer.....	144
Scheme 4.4: Acid-catalyzed formation of (a) ethoxyfuranone and (b) isomerization to ethoxybutenal.....	146
Scheme 4.5: Reaction mechanism of PMD, isopulegol and PMD-acetal formation.....	162

List of Equations

Equation 3.1: Statistical equations used to calculate; (a) Response factor, (b) Peak area mean, (c) Response factor mean, (d) Response factor standard deviation and (e) Response factor's coefficient of variance.....	47
Equation 3.2: Equation used to calculate concentration of constituents.....	48
Equation 3.3: Non-isothermal Kovats equation.....	58
Equation 3.4: Steady state expression of the production and loss of 12.....	71
Equation 3.5: Rearranging to make [SI] subject.....	71
Equation 3.6: General expression of rate of synthesis of PMD.....	71
Equation 3.7: Expression of the rate of formation of PMD 2.....	72
Equation 3.8: Differential rate expression for the conversion of Cal.....	72
Equation 3.9: Differential rate expression with pseudo rate constant.....	72
Equation 3.10: Integrated first order (a) and second order (b) reactions.....	72

CHAPTER 1: INTRODUCTION

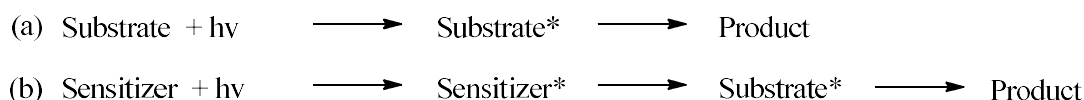
1. Introduction

1.1. 5-Hydroxy-2(5H)-furanone study

5-Hydroxy-2(5H)-furanone (HF) is a versatile chiral butenolide with stereochemical stability towards addition reactions¹⁻⁴. HF is commonly used as a substrate in the synthesis of various commodity chemicals^{5,6}. Its chlorinated derivative is also commonly used as a mutagenic pesticide^{7,8}. It furthermore functions as a bioactive moiety in sesquiterpenoids as shown in a series of structure-activity relationship studies^{7,9-11}. Due to its usefulness as a fine chemical, it is employed as a building block for four-carbon-heterocycles, particularly in the synthesis of pharmaceuticals¹²⁻¹⁴. It also has applications in the synthesis of antimicrobial agents, insecticides, and fragrant products. It is synthesized through various oxygenation processes and the photooxygenation route has been adopted and explored in this work.

1.1.1. Photochemistry

Photochemistry concerns the influence of ultraviolet, visible and infrared radiations on substrates through direct excitation or indirectly via photosensitisers or photocatalysts (Scheme 1.1)¹⁵. The following are some of the most common photochemical reactions: Photodissociation, photoinduced rearrangement or isomerization, photoaddition, photosubstitution and photo-redox reactions, respectively¹⁶. Photoactive organic molecules, among these especially alkenes and carbonyl compounds, constitute chromophores which absorb specific light photons within 200-700 nm (598-171 kJ mol⁻¹)^{4, 17-19}.



Scheme 1.1: (a) Direct photoexcitation and (b) indirect photo-excitation of a substrate.

1.1.1.1. Photoinduced excitation and transition

At ground state, molecules have electrons with an antiparallel spin configuration termed ‘singlet ground state (S_0)’. When a photon is absorbed by a molecule, the electron(s) at the highest occupied molecular orbital (HOMO) are excited and transit to the upper lowest unoccupied molecular orbital (LUMO)²⁰. Transition occurs from the S_0 to a higher energy $S_{n>0}$ state and this movement commonly involves electrons from pie bonding (π) or nonbonding (n) orbitals to the pie antibonding (π^*) orbitals²⁰. Consequently, the alternate parallel electronic spin configuration is established when the excited electron relaxes due to molecular collision to a

lower S_n state. When the electron is energetically able to cross over to the parallel spin state, it is said to have reached a ‘triplet state (T_n)’²⁰⁻²². These and other photophysical processes are illustrated in a Jablonski diagram (**Figure 1.1**).

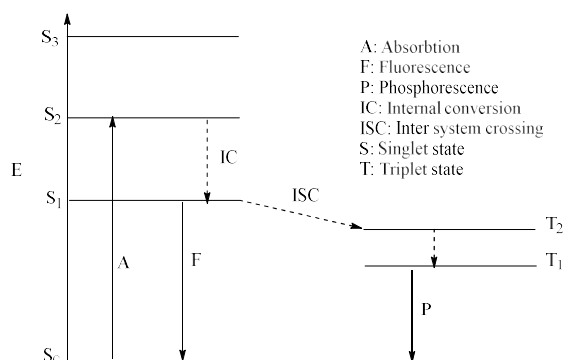


Figure 1.1: Jablonski diagram illustrating excitation of a molecule to its singlet-excited state, its subsequent electronic transitions and finally its return to the ground state.

The S_2 -state is highly energetic, unstable and therefore short lived ($\sim 10^{-12}$ s). It transits to the singlet S_1 (10^{-3} – 10^{-6} s) state or alternatively to the corresponding longer-lived T_1 state²³. In photochemical excitation, the Stark-Einstein law demands that the quantum of light absorbed is equivalent to the moles of absorbing substance and this relation is evident in the Beer-Lamberts law²⁴.

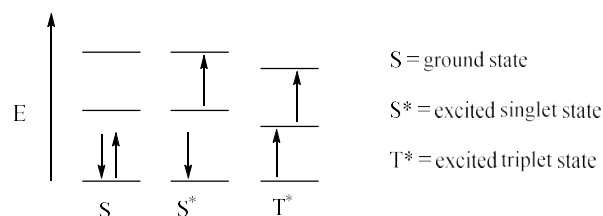


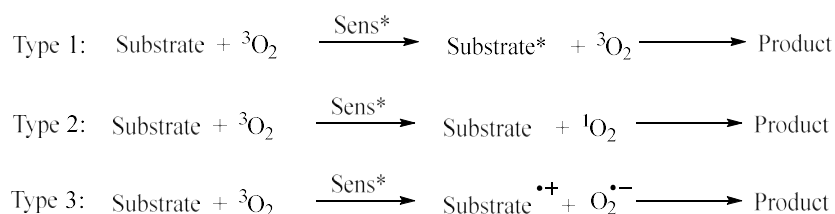
Figure 1.2: Spin positions of HOMO electrons at specific energy state.

1.1.1.2. Photooxygenations

Photooxygenation describes the light-induced incorporation of molecular oxygen (O_2) into a substrate. Typically, these transformations are mediated by organic dyes as photosensitizers. These photo-excited sensitizers interact with either the substrate or molecular oxygen, initiating different energy transfer processes and subsequently a reaction. There are three types of photooxygenation pathways that differ in the mechanism by which oxygen is reacting with the substrate (**Scheme 1.2**).

In the first type, the excited sensitizer interacts with the substrate and converts it to a (typically) biradical excited species via homolysis. This excited substrate reacts with triplet oxygen (3O_2)

to form a substrate-peroxide (bi) radical. This species is then stabilized by hydrogen quenching. The second type involves transfer of energy directly from the sensitizer to $^3\text{O}_2$ converting it to singlet oxygen ($^1\text{O}_2$). This highly reactive oxygen species then reacts with the substrate to form oxygenated products. In the third type, the excited sensitizer draws an electron from the substrate resulting in its radical cation. Molecular oxygen then gains an electron from the radical anionic sensitizer to give the superoxide radical anion ($\text{O}_2^{\bullet-}$). The radical ionic pair of oxygen and substrates reacts to form the product. In all three cases, the sensitizer returns to its neutral ground state. The [4+2]-photooxygenation reaction in this study involves the transformation of furan-2-carbaldehyde (furfural, FAL) to HF and is known to follow the Type 2 pathway.



Scheme 1.2: Main types of photooxygenation reactions.

1.1.2. 5-Hydroxy-2(5H)-furanone synthesis

Extensive research on the oxygenation of furan, FAL or furoic acid has been described in the literature^{7, 25-29}. Most of the reported processes employed inorganic oxidizing agents and solid support catalysts. These approaches are often expensive to upscale due to hazardous chemicals and specialized setups.

In 2005, Annangudi *et al* studied the homogenous Pinnick oxidation of furan and isolated HF in a yield of 35%³⁰. An improvement was achieved by Chavan *et al.* in 2021, but they discovered that further optimization of the reaction was thermodynamically challenging³¹. Interestingly, they developed a scalable protocol utilizing oxone as the oxidant to give a 75% yield, however, the highly exothermic nature of the reaction was again a disadvantage³¹.

Hydrogen peroxide is regarded as the simplest peroxide that is readily available as an oxidant⁷. In 1998, Poskonin *et al.* used vanadium sulfate in a homogenous oxidation of furan with HP. The reaction was carried out in a water-ethanol solution and produced a series of cyclic and acyclic derivatives, but with low amounts of HF³².

In 2000, Kumar *et al.* utilized titanium silicate sieves that effectively generated singlet oxygen ($^1\text{O}_2$) from hydrogen peroxide that consequently produced HF from FAL⁷.

In 2020, sulfated zirconia, another acid catalyst was used by Murzin *et al.* to facilitate hydrogen peroxide oxidation of FAL. In this work, succinic acid and maleic acid were produced with excessive amounts of formic acid and minimal amounts of HF as additional products³³.

An interesting development by Wu *et al.* in 2019 involved the oxidation of FAL in water to generate HF. In this protocol, CuS nanosheets were used as a heterogeneous catalysis to generate $^1\text{O}_2$ from water³⁴. This method gave HF with a selectivity of 84% and 70% FAL conversion. By sustainability means, water is preferred over hydrogen peroxide as an oxidant. However, the practical limitations were caused by CuS due to its instability and therefore, ability to leach from the nanosheets.

Photochemical syntheses of HF have been conducted extensively and **Table 1.1** gives a summary of recent photosynthetic approaches.

1.1.3. Sustainable 5-Hydroxy-2(5H)-furanone syntheses

To identify the most suitable sustainable synthesis method, an evaluation of existing process parameters aims to exclude the following: high stoichiometry of corrosive reagents, high reaction temperatures, steric blockages and high operational costs²¹. The photooxygenation of FAL is considered an efficient and environmentally benign access to HF. The photooxygenation of FAL, potentially obtained from sugarcane bagasse, was thus selected for this study.

1.1.3.1. Furan-2-carbaldehyde from biomass

FAL is a viscous colourless liquid with an almond scent, is marginally water soluble and readily oxidises to a brown-black appearance in air^{42,43}. It is a furan produced from the reduction of pyromucic acid⁴³. It has been predominantly synthesized from pentose biomass via xylose enolization and isomerization by acid-catalyzed dehydration⁴⁴⁻⁴⁶.

Australia has an abundance of sugar cane bagasse that can be used as biomass feedstock for the conversion to furfural. The Australian cane industry is ranked third globally, and Queensland's eastern coastline accounts for 95% of its production with 9.5 million tonnes of bagasse produced each year^{47,48}.

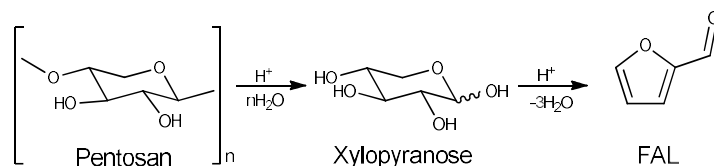
Bagasse comprises of 35.2% cellulose, 25% hemicellulose (pentosan), 22.2% lignin and 21% ash, respectively. Rezende *et al.* reported conversions of pentosan and lignin of 96% and 85%, respectively, when these materials were treated with acid (**Scheme 1.3**)^{49,50}.

Chapter 1 – Introduction

Table 1.1: Comparison of key-process parameters for the photooxygenation of furfural.

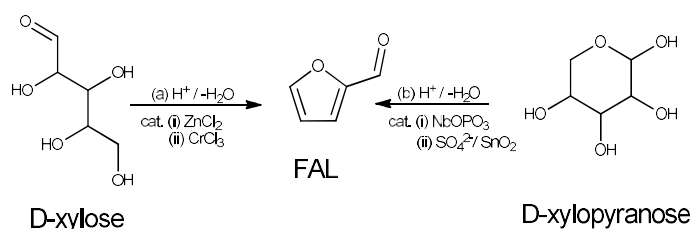
[RB]	[FAL]	Solvent	Lamp	T (°C)	t (hrs)	Detection	Yield	Ref
0.65 g	42.5 g, 0.44 mol	EtOH, 425 ml	Norelco DYH, 600 W	25-32	8	UV, 276 nm	42%	³⁵
1.3 g	90.5 g	EtOH (absolute), 850 ml	NS*	25-32	6	UV, 276 nm	43%	³⁶
2 g	236 g, 2.46 mol	95% EtOH, 2300 ml	Tungsten-Iodine lamp, 1000 W	25-31	35	TLC	70%	³⁷
1.82 g, 1.8 mmol, 0.2% mol-eq	85.84 g, 0.893 mol	MeOH (dry), 450 ml	Tungsten halogen lamp	33	18-22	TLC	81-85%	³⁸
400 mg, 0.39 mol	110 ml, 1.2 mol	MeOH, 900 ml	Medium-pressure Hg lamp, 450 W, quartz filter	25-31	8	NS	94%	³⁹
3 g	148 g	MeOH, 550 ml	Medium-pressure Hg lamp, quartz	<35	20-30	NS	91%	⁴⁰
530 mg, 52.0 mmol	100 g, 1.04 mol	EtOH/H ₂ O (475ml/25ml)	NS*	25-31	40-56	¹ H-NMR	38-60%	²⁷
4 mg polymer/ml of 1.2×10 ⁻⁵ M RB	3×10 ⁻² M	CHCl ₃ ml	Medium-pressure Hg lamp, 125 W, 450 nm cut-off	25-31	6	UV-Vis	100%	⁵
1.2×10 ⁻⁵ M	3×10 ⁻² M	CHCl ₃ ml	Medium-pressure Hg lamp, 125 W, 450 nm cut-off	25-31	6	UV-Vis	100%	⁵
150 mg, 1% on wool	200 mg, 2.04 mmol	CH ₃ CN, 30 ml	Medium-pressure mercury lamp, UV cut-off	25	10	NS*	71-82%	⁴¹

NS*: Not stated in cited literature.



Scheme 1.3: Acid catalyzed hydrolysis of pentosan and subsequent dehydration to furfural.

In 2017, Fang *et al.* reported a 55 mol-% yield of FAL from homogenous metal chloride catalyzed cyclization of D-xylose (**4**, **Scheme 1.4a**)⁴⁵. Another approach involved subjecting D-xylopyranose (**5**) to a heterogeneous acid-catalyzed two-step transformation. The pentosan hydration and acidification with bifunctional niobium phosphate was followed by pentose dehydration with tin oxide attapulgite to give FAL (**Scheme 1.4b**).



Scheme 1.4: Synthesis of furfural from (a) D-xylose and (b) D-xylopyranose.

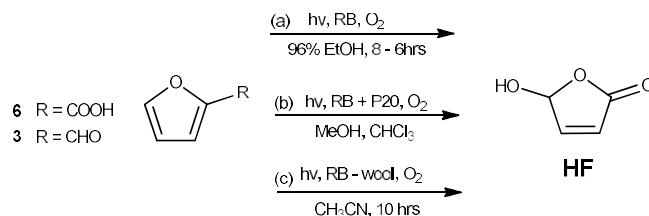
FAL has been used as a solvent for cellulose nitrates, cellulose acetates and petroleum refining⁵¹. It is a leading hemicellulose platform chemical with wide applications⁵². Cyclopentanol, furan and tetrahydrofuran are widely used as solvents and building block materials in fine chemical synthesis⁵³⁻⁵⁵. FAL alcohol represents a dispersing agent commonly used in the polymer industry^{53, 56}. Furoins, particularly C10–C12, were emphasized as alternative fuels, while γ -valerolactone is used in C5–C6 fuel production^{57, 58}. Recent studies showed that 2-methylfuran is an ideal octane booster if compared to a regular fuel⁵⁹. The acyclic levulinic ester and related alkyl levulinates have wide uses in the flavouring, fragrance, dispersant and plasticizer industries^{60, 61}.

1.1.3.2. Photooxygenation of furan-2-carbaldehyde

A review by Esser *et al.* described the transition from lamp- to solar-driven photooxygenations at up to 35 L scales. Interestingly, the latter delivered higher selectivity and yield due to the absence of harsh UV-radiation⁶². In fact, solar chemical synthesis advanced after 1944 when Schenck exposed 200×10 L glass bottles containing α -terpinene in ethanol and mixed with chlorophyll as sensitizer to sunlight. The photooxygenation ascaridole was maintained by keeping oxygen dissolved in the reaction mixture by regular shaking of the bottles⁴. With the

recent drive towards sustainable and green chemical processes for photochemical synthesis, lamp reactors may be increasingly substituted with modern solar reactors¹⁶.

Photooxygenation occurs as $^3\text{O}_2$ molecules transits to $^1\text{O}_2$ species facilitated by dye sensitizers¹⁶. The photooxygenation of FAL represents an example of a Diels-Alder reaction or [4+2] cycloaddition^{16, 23, 63}. This diene-dienophiles transformation involves the conversion of $\pi \rightarrow \sigma$ bonds and results in the formation of an endoperoxide adduct^{63, 64}. Subsequently, the initially formed endoperoxide is rearranged to the stable HF² (**Scheme 1.5**).



Scheme 1.5: Photosensitized oxygenation of 2-furoic acid or furfural to hydroxyfuranone.

In 1973, Doerr *et al.* performed a two-step synthesis that utilized the dye-sensitized photooxygenation of a FAL-ethanol mixture in an oxygen stream followed by acid hydrolysis of the initial ethylester to give HF (43%)⁶⁵. Later in 1994, a single step process utilizing methylene blue and rose bengal (RB) as the sensitizers was reported by Esser *et al.* In 2010, Burguete *et al.* attempted a heterogenous photosensitized synthesis of HF from 2-furoic acid using RB coated on divinylbenzene-crosslinked polymer as solid support⁵. The conversion in chloroform upon irradiation at 460 nm for 6 hours was higher than in methanol (**Scheme 1.5b**)⁵. In 2012, a similar study by Yan *et al.* used wool as a solid support for RB⁶⁶. In this work, a 71% yield was obtained, although this was only achieved after repeated use of the infused wool support in acetonitrile (**Scheme 1.5c**)⁶⁶.

In 2005, Morita *et al.* purged air through an absolute ethanol solution of RB and FAL under solar irradiation to produce a reasonable amount of HF (**Scheme 1.5a**)²⁷. An improved yield was achieved when the synthesis was conducted in 96%-ethanol at room temperature^{67, 68}. Marincovid *et al.* conducted a more controlled reaction and removed the solvent under vacuum and below 35°C, which resulted in an enhanced yield of 91%⁶⁹.

1.1.3.3. Application and derivatization of 5-Hydroxy-2(5H)-furanone

HF itself is a potent pesticide and a platform chemical for several thermal transformations such as the Michael reaction, Diels-Alder reaction, cyclopropanation, dipolar cycloaddition etc.^{40, 70, 71}. Thus, valuable fine chemicals such as dibenzylbutyrolactone and aryltetralin

lignans, podophyllotoxin isomers, β -lactams, grandisol, terebic acid and isostegane derivatives can be synthesized from the HF platform³⁸.

Manoalide, a compound with antibiotic, analgesic and anti-inflammatory properties, was derived from photosensitized oxygenations of 3-alkylfurans to 3-alkyl-4-hydroxy-furanones^{41, 72}. Biologically active spirocyclopropane bisbutyrolactone enantiomers with four stereogenic centres were derived from HF through asymmetric synthesis^{67, 73}. A derivative of 5HF, *i.e.* (-)-Kainic acid, displays potent anthelmintic and stimulation properties in neuropharmacology²⁷. Exceptional alkyl sulfate and sulfonate surfactants were likewise obtained from HF through fatty acid acetalization, followed by the addition of the sulfonate function⁷⁴. 3-Bromofuran-2-one and (5*S*)-(d-menthyloxy)-2(5H)-furanone were readily available from HF³⁶. The isomeric (5*R*)-5-l-menthyloxyfuran-2[5H]-one and (5*S*)-5-l-menthyloxyfuran-2[5H]-one were synthesized from HF through acetalization with L-menthol⁴⁰.

1.1.4. Alkoxyfuranones

One of the most apparent follow-up reactions involving HF is the conversion to its corresponding alkoxy derivatives. These compounds are alternatively available via transesterification of one of these alkoxyfuranones (AFN). These alkoxy derivatives have also proven useful as (photo)chemical building blocks, especially in processes involving cycloaddition reactions⁷⁵.

1.1.4.1. Synthesis and applications

Mise *et al.* reported the carbonylation of diphenylacetylene under rhodium catalysis to give various alkoxyfuranones (AFN)⁷⁶. A few years later, Zimmer *et al.* described a convenient way to synthesize 4-alkoxy-2(5H)-furanone from 4-hydroxy-2(5H)-furanone by simple pseudo-esterification⁷⁷.

Numerous studies have utilized AFN as precursors. Weigele *et al.* synthesized methoxyfuranone and used it as a precursor to produce fluorescamine⁷⁸. This product plays an important role as a fluorescent tag in the detection and quantification of primary amines. Hoffmann *et al.* developed a synthesis protocol that used 4-alkoxy-5-bromo-2-(5H)-furanones as precursors in the synthesis of aflatoxins⁷⁹. Li *et al.* reported on the synthesis of cytotoxic dithiocarbamates with alkoxy-furanone-piperazine analogues⁸⁰.

In 1988, Feringa and Lange developed a stereoselective procedure for the synthesis of 3, 4-epoxy-butanol via asymmetric additions to AFN⁸¹. A year later, Feringa *et al.* reported on the synthesis of homochiral synthons of β -amino- γ -butyrolactones via asymmetric addition of amines to menthyloxyfuranone⁸². The same authors also described the enantioselective production of the versatile (5S)-5-(d-menthyloxy)-4-(phenylsulfonyl)-2(SH)-furanone from menthyloxyfuranone via a non-epimerization route⁸³.

1.2. *Para*-Menthane-3, 8-diol study

Structurally, para-menthane-3, 8-diol (PMD) is a six-membered cyclic monoterpene diol⁸⁴. It was initially isolated from *Litsea cubeba* and *Corymbia citriodora* (lemon scented gum, LSG) distilled oil^{85, 86}. The use of “quwenling”, the hydrosol of the LSG-oil distillation process, as the traditional mosquito repellent in China resulted in the rediscovery of PMD⁸⁶⁻⁸⁸. Although PMD has been known and synthesized much earlier, it remained under-exploited until Western interest in “quwenling” as an effective repellent evolved⁸⁹. A comparative repellent assessment of the major constituents in LSG oil further confirmed that PMD was the most active molecule if compared to citronellal, citronellol and pinene⁹⁰. In 1988, the U.S. EPA approved PMD as a biochemical active ingredient for insect repellent products⁹¹. By the early 1990s, PMD was used as an active ingredient in insect repellent products such as Aerogard[®] Body Naturals (AUS), THEYE[®] Natural Mosquito Repellent (UK) and OFF[®] Botanical (USA)⁹¹. Today, PMD is a key bioactive ingredient to prevent vector borne diseases (VBD) transmitted by mosquitoes. However, access to PMD repellents is a challenge for most developing countries prone to VBD. In addition, the low global distribution of *C. citriodora* limits access or production of viable PMD enriched repellents in these countries.

Several process protocols have been developed in an attempt to optimize the production of PMD. The synthesis of PMD from citronellal using homogeneous and heterogeneous inorganic acid and metal complex catalysts represents the most dominant pathway⁹². However, these procedures commonly involve excess amounts of hazardous inorganic acids or metals. Likewise, the reported synthesis protocols lack simplicity, flexibility and cost effectiveness. A more sustainable approach uses citric acid as a versatile and green catalyst,⁹³ which subsequently formed the basis of the current study.

1.2.1. Regional vector borne diseases

Viruses transmitted by arthropods represent a significant burden for public health worldwide. The major diseases transmitted by mosquitos include dengue fever, yellow fever, Zika and

many other fatal infections. There are currently no reliable vaccines to act as preventative measures for many of these diseases. Developing countries also lack treatment facilities to cope with these infections. Thus, preventing the transmission between mosquitoes and humans is the most effective method for avoiding infections. Some of the personal measures used for this purpose include wearing long sleeves and protective clothing, using mosquito nets and applying mosquito repellents. Information campaigns have been widely conducted by national and international health organizations, but this strategy alone cannot overcome public susceptibility. Likewise, eradication of blood-sucking insects through the widespread use of insecticides has been trialled.

Mosquitos and other vector-borne diseases are extremely common in Africa and tropical regions such as North Queensland and the Pacific islands. The World Health Organisation (WHO) states that vector-borne infections are responsible for more than 700,000 deaths annually, with approximately 400,000 of those due to malaria. Locally in Queensland and on tropical Pacific islands, dengue fever is prevalent with outbreaks occurring annually. *Aedes aegypti* is the primary carrier of the dengue virus in Australia. The virus typically enters Australia from overseas via an infected human or host. Infections appear in areas with a major airport and with local *A. aegypti* populations. This is a concern for Townsville and Cairns as both places have airports with frequent international flights to Papua New Guinea and other tropical regions.

1.2.2. *Para-Menthane-3, 8-diol* mosquito repellency

The use of insecticides, particularly mosquitocides, has been a widespread strategy in disease control since the inception of DDT. However, extensive eradication programs with DDT in the 1940's and 1950's were found to have potentially carcinogenic effects on birds and other animals⁹⁴. These findings led to the desired replacement of insecticides with alternative control measures⁹⁵. One of the recommended prevention methods today is the use of effective mosquito repellents.

N, N-Diethyl-*meta*-toluamide (DEET) is the most common mosquito repellent ingredient with a 6-hours efficacy for 20-34% formulations. However, it causes skin irritation and damages textile surfaces^{98, 99}. Hydroxyethyl isobutyl piperidine carboxylate (Picaridine) is an odorless active ingredient with a broader efficacy window of 3-10 hours for a 20% formulation^{98, 99}. Ethyl *N*-acetyl-*N*-butyl- β -alaninate (IR3535) is another odourless ingredient with >8 hours efficacy for 20% formulations^{98, 99}. Citronella obtained from lemongrass (*Cymbopogon species*) oil is a popular natural repellent and is widely used due to its easy availability^{98, 99}. However, it

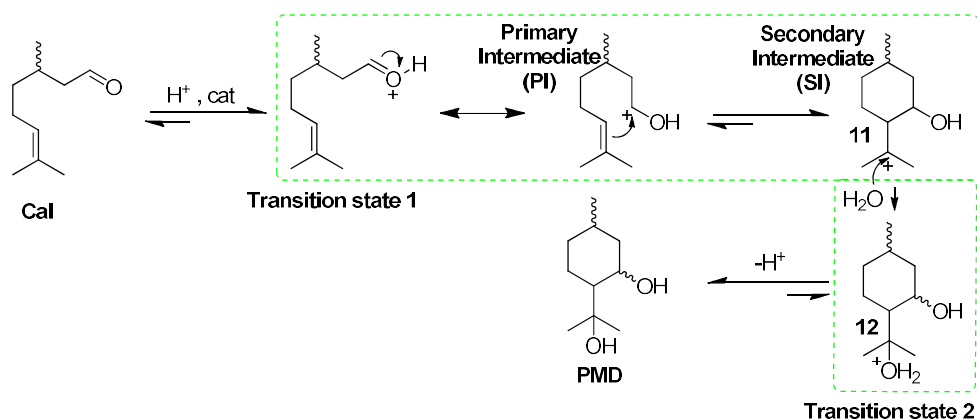
has a poor efficacy due to its volatility, which demands constant reapplication after every 30-60 minutes^{98, 99}.

Barasa *et al.* reported that all four PMD isomers were equally active against *Anopheles gambiaes*⁹⁶. Likewise, Drapeau *et al.* discovered that *p*-menthane-3, 8-diol is active against the yellow fever mosquito *A. aegypti* with repellency lasting for over 5 hours in comparison to DEET⁹⁷. PMD has been also proven active against *A. aegypti* and *A. gambiae*⁹⁸⁻¹⁰¹. It has a long efficacy of up to 12 hours at 20-50% formulations. It has a pleasant and cooling menthol-like odour and poses no risk to users^{98, 99}.

1.2.3. Synthetic pathways to *para*-Menthane-3, 8-diol

1.2.3.1. Prins reaction

Most current PMD production processes utilize the Prins reaction, which is initiated by the acid mediated protonation of aldehyde or ketone functionalities. The resulting carbocationic intermediates are susceptible to nucleophilic addition and as a result produce alcohols or diols¹⁰²⁻¹⁰⁴. The formation of PMD from 3, 7-dimethyloct-6-enal (citronellal, Cal) is depicted in **Scheme 1.6**.



Scheme 1.6: Formation of PMD by Prins reaction.

A patent by Kenmochi *et al.* described the synthesis of PMD from neat (+)-citronellal (96.0%) and 16.2 mM sulfuric acid. The reaction achieved near complete conversion of 99% with 61.9% *cis*-PMD, 36.0% *trans*-PMD and 1.1% PMD-acetal as the main constituents^{105, 106}.

Recently Sheng *et al.* synthesized PMD via H₂CO₃-mediated cyclization of citronellal. The protocol involved hydrolysis of CO₂ gas in H₂O in the presence of ZSM-5 zeolite and at pH 3.2 to produce H₂CO₃. A conversion of 97.0% was achieved when a mixture of 1 mmol (*S*)-(-)-citronellal and 10 ml water was reacted at 100°C at 7.5 MPa CO₂ for 2 hours¹⁰⁷.

Mineral acids such as sulfuric acid and solid-state metal sheets have been most commonly used as catalysts^{107, 108}. The citronellal starting material employed was either obtained from natural citronella oil or was from a synthetic source. The recent demand for more sustainable production methods calls for environmentally safe protocols and a minimum need of chemical materials. Excessive use of reagents during synthesis and of solvents during separation and purification of PMD should thus be avoided. The operation costs and safety needs for the required equipment should also be considered during the optimization process.

1.2.3.2. Synthesis of PMD-rich botanical oil

A benign approach was undertaken by Drapeau *et al.* using Cal (74%), contained in *Corymbia citriodora* leaf oil, and anhydrous citric acid⁹⁷. The reaction was carried out at 50°C for 15 hours and reached a conversion of 85% conversion with a selectivity for PMD of 80% in the crude reaction product⁹⁷. The refined oil is known as PMD-rich botanical oil (PMDRBO).

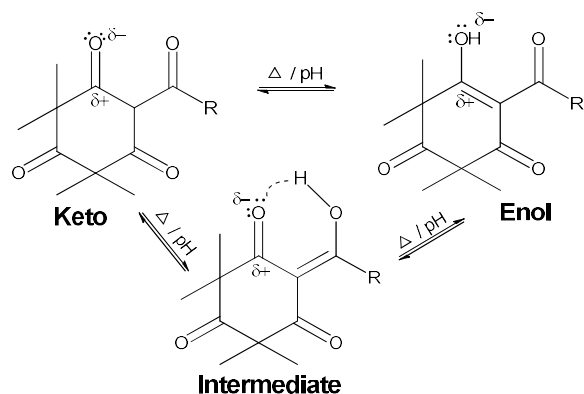
Citric acid is predominantly found in edible plants and has been recognised as a non-toxic additive by FAO and WHO, respectively¹¹⁵. Due to its trivalent configuration, it can deprotonate to facilitate reactions in its -1 to -3 ionic forms at pH 2-6. It is non-hazardous, cost effective to use and has proven itself as an efficient green catalyst in several organic transformations^{116, 117}.

C. citriodora is endemic to Australia and hence provides a stable renewable resource for chemical exploitation¹⁰⁹⁻¹¹³. Compared to its imported counterparts in China or Brazil, the native Australian tree species is also resistant to diseases and pests¹¹⁴. Several small distilleries in Australia produce *C. citriodora* oil, which is locally known as lemon scented gum (LSG) oil. Thus far, the oil is predominantly used in aromatherapy with limited commercial value. The production of PMD as an effective and valuable repellent thus provides new value adding and product diversification opportunities for local distilleries in Australia. A simple, sustainable and cost effective PMD manufacturing process may also enable tropical neighbouring countries to combat insect borne diseases. In this study, the Drapeau method was chosen to further improve citronellal conversion and PMD selectivity, and to transfer the optimized procedure to small production scales.

1.3. β -Triketone study

1.3.1. Structural features

Triketone or trione refers to three ketone groups within the same molecule. They can be on adjacent carbons, alternate carbons or distant carbons. The elementary forms include tripropanone and its cyclic form. However, these are unstable and therefore, unpopular compared to longer chain triones in the keto-enol form (**Scheme 1.7**)¹¹⁸.



Scheme 1.7: Alternating keto-enol tautomeric forms.

The ketone carbonyl experiences electron withdrawal in the direction of the electronegative oxygen atom that is involved in the oxygen-carbon double bonds. The carbonyl polarity also promotes hydrogen bonding with water, enabling them to be water soluble. Water solubility decreases with the R-group's carbon chain length. Their high polarity causes strong intermolecular attraction resulting in high boiling points than their subsequent aldehydes and esters.

Ketones are also UV active, with the electron lone pairs absorbing at 240-350 nm¹¹⁹. The electron withdrawing effect also enables deprotonation of the α -proton, hence, causing it to be acidic. This is often responsible for its enolization and keto-enol tautomerization¹²⁰. On the other hand, the ketone moiety has stable bonds and cannot undergo oxidation under mild conditions.

1.3.2. Phytochemistry

The significance of triketones arose from the traditional knowledge of plants as treatment for certain diseases. For example, the use of Manuka and kanuka leaves in New Zealand to control parasitic infections on parakeet birds led to the discovery of leptospermone, isoleptospermone and flavesone, respectively¹²¹. Another case was the observation of the herbicidal effect of

bottlebrush (*Callistemon citrinus*) on neighbouring weeds leading to the discovery of leptospermone as an herbicide¹²².

There are numerous reports of active diketones and triketones against undesired weeds and pests sourced from distilled oils of plant species from the Alliaceae, Apiaceae, Asteraceae, Cannabinaceae, Lamiaceae, Pteridaceae, Myrtaceae, Myoporaceae, Proteaceae, Rutaceae and Zingiberaceae families¹²³. Table 1.2 shows a list of phytochemical triketones and their reported uses and sources.

Table 1.2: β -Triketones and β -diketones found in certain plant extracts.

Compound	Species	Family	References
Tasmanone	<i>Eucalyptus tasmanica</i> , <i>E. risdoni</i> , <i>E. camfieldii</i> , <i>E. cloeziana</i> , <i>Baeckea frutescens</i> , <i>Campomanesia vitoris</i>	Myrtaceae	124-129
Angustione	<i>Backhousza angustifolia</i> , <i>Eruca sativa</i>	Myrtaceae, Brassicaceae	130-132
Dehydroangustione	<i>E. risdoni</i> , <i>B. angustifolia</i>	Myrtaceae	125, 131, 133
Flavesone	<i>Leptospermum scoparium</i> , <i>C. vitoris</i> , <i>L. flavescense</i> , <i>E. nitens</i>	Myrtaceae	129, 134-136
Leptospermone	<i>L. scoparium</i> , <i>L. flavescense</i> , <i>E. nitens</i> , <i>Callistemon viminalis</i> ,	Myrtaceae	130, 134-138
Isoleptospermone	<i>L. scoparium</i> , <i>E. grandis</i> , <i>L. flavescense</i> , <i>Toddalia asiatica</i> , <i>E. camaldulensis</i> , <i>E. nitens</i> , <i>Callistemon viminalis</i>	Myrtaceae, Rutaceae	134, 136, 138-140
Jensenone	<i>E. jensenii</i>	Myrtaceae	138
Agglomerone	<i>B. frutescens</i> , <i>C. vitoris</i> , <i>E. agglomerata</i>	Myrtaceae	128, 129, 141
Xanthostemone	<i>Xanthostemon oppositifolius</i> , <i>X. crenulatus</i> , <i>X. umbrosus</i>	Myrtaceae	142, 143
Papuanone	<i>E. papuana</i> , <i>Corymbia dallachiana</i>	Myrtaceae	144, 145
Grandiflorone	<i>L. scoparium</i> , <i>L. flavescense</i> , <i>Uvaria grandiflora</i>	Myrtaceae, Annonaceae	135, 146, 147
Lateriticone	<i>E. indurata</i> , <i>E. gonianthaand</i> , <i>E. perangusta</i>	Myrtaceae	148
Calythrone	<i>E. risdoni</i> , <i>Calythrix tetragona</i>	Myrtaceae	125, 149

1.3.3. Herbicidal use

The industrial importance of triketones as herbicides started when Reed *et al.* discovered the herbicidal potency of leptospermone¹²². The syncarpic acid moiety represents the important fingerprint of the leptospermone structure for bioactivity. The acetyl moiety is interchangeable and consequently, its substitution gives other active analogues. Herbicidal studies have shown that the benzoyl analogues exhibited ED₉₀ at very low doses, particular the 2-chlorobenzoyl and the 2-nitro-4-trifluoromethyl benzoyl acyl analogues (**Figure 1.3**)¹²².

Earlier work also demonstrated that the cyclohexane-1, 3-dione moiety was active and therefore, several analogues were investigated¹⁵⁰. Analogues with benzoyl moiety constituting electronegative substituents at positions C2 (R) and C4 expressed good herbicidal activity¹⁵¹⁻¹⁵³.

Methanesulfonylbenzoyl cyclohexane-1, 3-dione in particular, depicts strong affinity to 4-hydroxyphenylpyruvate dioxygenase (HPPD) enzyme¹⁵³. This finding led to the synthesis of the well-known herbicides sulcotrione in 1993 and mesotrione in 2001 (Figure 1.4)^{154, 155}.

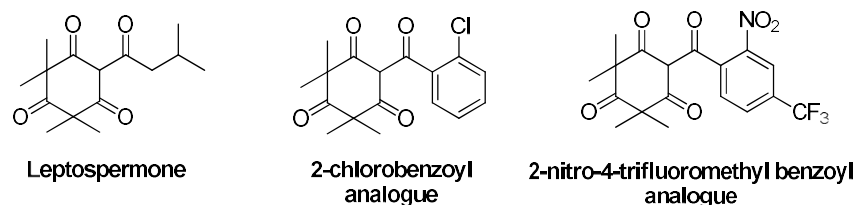


Figure 1.3: 1, 3, 5-Trione herbicides.

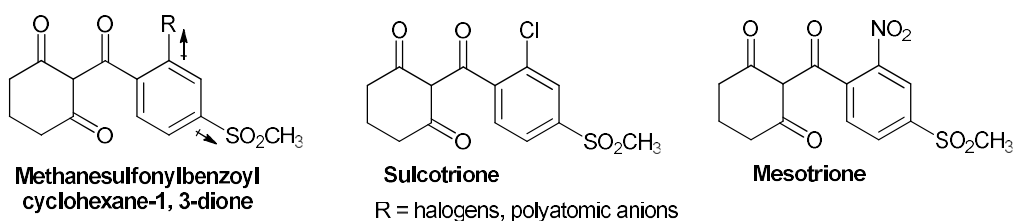


Figure 1.4: Herbicidal 1, 3-diones.

1.3.4. Insecticidal properties

Many reports of plant extracts rich in β -triketone show strong insecticidal properties. Particular cases are the essential oils of *L. scoparium* and *E. nitens* leaves exhibiting larvicidal activity against *A. aegypti* and *A. albopictus*. Interestingly these Myrtaceae plant species contain similar ratios of flavesone, leptosperme and *iso*-leptosperme. These β -triketones were suspected to be responsible for the larvicidal effect in both case^{136, 156}. In 2015 Bio-Gene, an Australian AgTech company, patented flavesone and tasmanone as active agents against a range of insects¹⁵⁷.

1.3.5. Bioactivities

A variety of synthetic and natural bioactive β -triketone analogues have antiviral, antibacterial, and antifungal activity¹⁵⁸. These properties make them important lead compounds due to the increasing spread of drug resistant microorganisms. Recent assessment of the enol β -triketone tautomer showed activity against methicillin-resistant *Staphylococcus aureus* (MRSA), vancomycin-resistant *Enterococcus faecalis* (VRE) and multi-drug resistant *Mycobacterium tuberculosis* (MDR-TB)¹⁵⁹.

A more recent assessment of tasmanone rich *E. cloeziana* oil against *Fusarium oxysporium* that causes banana wilt in North Queensland revealed significant activity¹⁶⁰. *Candida albicans* and *Aspergillus niger* were also reported to be susceptible to methoxy β -triketone^{160, 161}.

1.3.6. Syntheses

In 1973 Baigent and Bick reported the synthesis of the diketone agglomerone via a two-step reaction at 0°C. Phlorisobutyrophenone was used as the starting material and the product 2, 6-dihydroxy-4-methoxyisobutyrophenone was the subsequent precursor for diketones¹⁶².

A suitable triketone preparation protocol was described by Perry *et al.* in 1999. The protocol begins with acetylation of phloroglucinol followed by exhaustive methylation of the acetylphloroglucinol¹⁶³. This protocol was adapted in the synthesis of various β -triketone analogues in this study.

CHAPTER 2:

AIMS

2. Aims

The aim of this research project was to use renewable chemical feedstocks for the synthesis of commodity chemicals. Laboratory synthesis, optimization studies, and scale-up of production were performed. Photo-sensitized oxygenations, acid-catalyzed cyclizations, and assessments of Xanthostemon (Myrtaceae) and synthetic triketones were investigated. The main objectives of this study were as follows:

- to use photochemically activated singlet oxygen as a mild alternative to thermal oxidation agents,
- to investigate the use of biomass as a renewable source of valuable fine or commodity chemicals,
- to convert selected renewable materials into versatile and useful fine chemicals,
- to transfer reaction parameters developed in the laboratory with artificial light to outdoor conditions,
- to realize technical-scale processes and cost-effective production of the target compounds, and
- to isolate, synthesize and identify bioactive triketones.

CHAPTER 3: RESULTS

3. Results

3.1. Synthesis of 5-Hydroxy-2(5H)-furanone and its alkoxy-derivatives

3.1.1. Purification of Furan-2-carbaldehyde

Furan-2-carbaldehyde (furfural, FAL, **1**) was sourced from a 20 L drum of bulk technical grade material available in the laboratory. Batches of this oily dark red liquid were collected in a beaker and transferred to a round bottom flask. The mass was purified via fractional distillation under laboratory conditions. The flask was placed on a heating mantle and connected to a single fractional distillation unit. As depicted below in **Figure 3.1**, the setup composes of a 30 cm Vigreux column (1 cm, IØ) and a 30 cm long Liebig condenser.

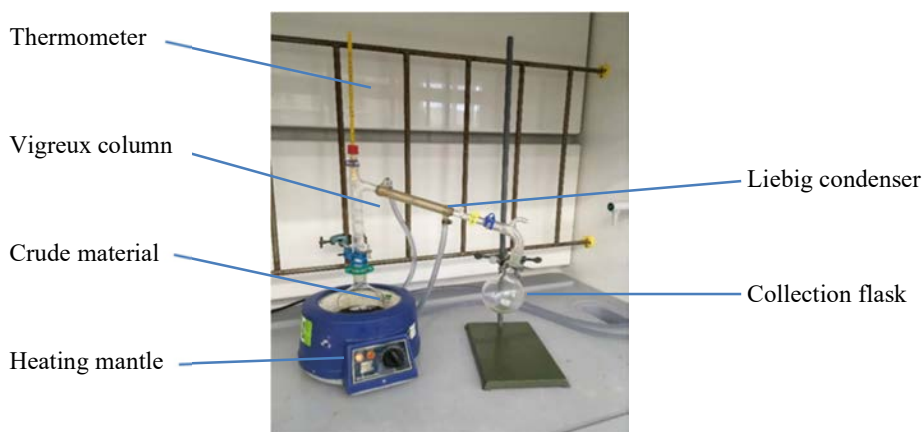


Figure 3.1: Fractional distillation setup.

Five distillations on various scales were conducted (**Table 3.1**). The distillation vapor temperature was always observed at 161°C and distillates of purified FAL were collected. High recoveries of >92% were achieved for all distillations. The distilled FAL has obtained as a pale-yellow oily liquid (**Figure 3.2**). The purity of each batch was determined by GC-analysis and their structural identification was established by NMR, IR, and MS.



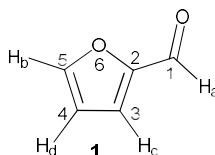
Figure 3.2: Distilled (left) and crude (right) furfural.

Table 3.1: Batches of furfural obtained by fractional distillation.

FAD	Mass (g)		Recovery (%)	Purity (%)
	Raw	Crude		
1 ^{LR}	82.513	80.615	97.7	100
2 ^{SR}	294.24	273.56	92.8	100
3 ^{SR}	261.84	247.44	94.5	100
4 ^{SR}	268.90	260.30	96.8	100
5 ^{SR}	283.77	271.85	95.8	100

LR: used for lamp irradiation; SR: used for solar illuminations.

3.1.1.1. Characterization of Furan-2-carbaldehyde



Furan-2-carbaldehyde (**1**): B.p: 160-161°C. UV abs, λ_{max} : 268.11 nm. ESI-MS: $[\text{M}+\text{H}]^+$, $\text{C}_5\text{H}_4\text{O}_2$, $m/z = 96$ (93%) and $[\text{M}+2\text{H}]^{2+}$, $\text{C}_5\text{H}_6\text{O}_2$, $m/z = 100$ (100%). $^1\text{H-NMR}$ (400 MHz, CDCl_3): δ (ppm) = 9.45 (d, $J = 0.7$ Hz, 1 H_{ac} , CHO), δ (ppm) = 7.53 (dt, $J = 1.6, 0.7$ Hz, 1 $\text{H}_{\text{bd/bc}}$, CH), 7.10 (dd, $J = 3.6, 0.7$ Hz, 1 $\text{H}_{\text{cd/cb}}$, CH), 6.42 (dd, $J = 3.6, 1.7$ Hz, 1 $\text{H}_{\text{dc/db}}$, CH). $^{13}\text{C-NMR}$: δ (ppm) = 112.6 (CH, C-3), 121.2 (HC, C-5), 147.9 (CH, C-4), 152.6 (CO, C-1), 177.5 (CHO, C-2). IR (ATR, cm^{-1}): $\tilde{\nu} = 1666.98$ (str, C-H, C=C), 1462.75 (med, C-H bending), 1391.93 (med, C-H bending, CHO), 1276.26 (str, C-O stretching), 1156.03 (str, C-O stretching), 475.46 (str, C-H bending, C=C).

3.1.2. Irradiation experiments in a Rayonet chamber reactor

A series of conversions using artificial light were done in a Rayonet photochemical reactor (RPR-200). The reactor has 32 inbuilt tombstone-like lamp holders that hold sixteen 8 W visible light fluorescent tubes (Phillips T5) and produce an intensity of 37.4 photons in a second per cm^3 at 575 nm. The reactor also has two built-in support rods holding the reaction vessels and a cooling fan mounted at the base to minimize thermal stress within the 40.6 cm deep chamber (**Figure 3.3**). Various Pyrex Schlenk flasks of 100-300 ml capacities were used as reaction vessels. Oxygen or compressed air was fed through a narrow glass side arm attached and passed through a sintered glass frit on the bottom of the flask. Alternatively, a FEP or PTFE tube with an attached porous metal inlet filter was run through a side-arm at the top of the flask. Venting of the gas-stream was provided via a second side arm at the top of the cylindrical flask. A cold finger with circulating chilled water was inserted into the vessel to cool the reacting solution during irradiation.

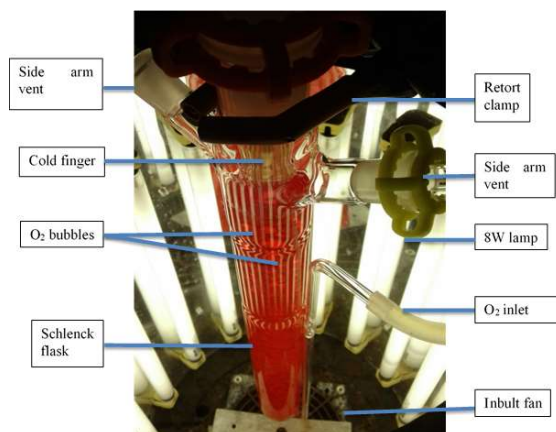
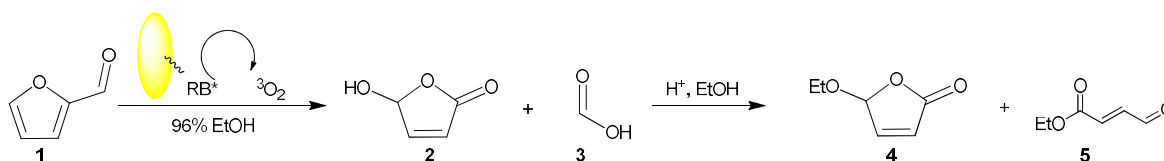


Figure 3.3: Rayonet chamber reactor setup.

3.1.2.1. Batch synthesis of 5-Hydroxy-2(5H)-furanone

The reaction protocol for the Rayonet chamber reactor was based on procedures from three previous studies to determine optimum parameters. The protocols described by Esser *et al.* (1994), Schenck *et al.* (1980), and Huan *et al.* (1999) were consequently evaluated in a series of batch conversions. FAL was obtained from FD1, while RB and ethanol (EtOH) were standard reagents available in the laboratory. Subsequent irradiation experiments revealed that the chosen 100 ml batch setup showed adequate conversions with reasonable yields of isolated HF. The selectivity and composition of the crude products obtained were determined by ¹H-NMR via comparison of characteristic integrated peak areas.



Scheme 3.1: Photooxygenation of furfural to hydroxyfuranone.

Table 3.2 shows the results of selected conversions and **Table 3.3** the obtained compositions of HF, ethoxyfuranone (EFN, **4**), ethoxybutenal (EBL, **5**) and unconverted FAL (**3**) after workup. A common issue is the persistence of residual RB in the crystal lattice of the isolated product, resulting in an orange colour. Significant losses in HF material were caused by the efforts to decolorize the crystals by repeated recrystallization. This prevalent phenomenon is seen in **Figure 3.4**, which shows decolorization beginning from the initial viscous red-orange crude material, the colourless product crystals isolated, and the orange RB washings collected in the Büchner funnel.

Table 3.2: Experimental parameters for irradiations in a Rayonet reactor.

Exp	^a EtOH (ml)	FAL			RB			HF _T Mass (g)	T _{RXN} (°C)	t _{irradiance} (min)
		Mass (g)	mmol	mM	Mass (g)	mmol	^b mol%			
^c 1	100	5.8	58.9	589.3	0.0548	0.06	0.003	5.90	21	540
^c 2	100	9.7	98.6	985.9	0.1471	0.15	0.009	9.87	21	1200
^d 3	100	5.5	55.6	555.9	0.0784	0.08	0.006	5.56	21	1200
^d 4	100	3.2	32.9	328.9	0.0832	0.09	0.008	3.29	21	1200
^d 5	100	3.2	32.6	326.5	0.0858	0.09	0.011	3.27	21	60
^d 6	100	3.2	32.9	329.4	0.0864	0.09	0.015	3.30	21	420
^d 7	100	9.7	98.6	985.7	0.1412	0.15	0.045	9.86	21	120

^a: 96% EtOH used; ^b: 4 ml H₂O was part of calculation; HF_T: theoretical mass of HF; ^c: Schlenk flask with sintered disc; ^d: Schlenk flask FEP gas-feeding tube.

Table 3.3: Experimental results for irradiations in a Rayonet reactor.

Exp	Conv (%)	Composition (%)				Isolated HF		
		HF	EFN	EBL	FAL	Mass (g)	Yield (%)	Purity (%)
1	99	94	4	1	1	2.25	36	100
2	96	87	8	1	4	5.38	47	100
3	100	73	22	5	0	2.27	30	100
4	100	98	1	1	0	1.11	33	100
5	100	100	0	0	0	1.07	33	100
6	99	99	1	0	0	1.55	46	100
7	100	100	0	0	0	5.12	52	100

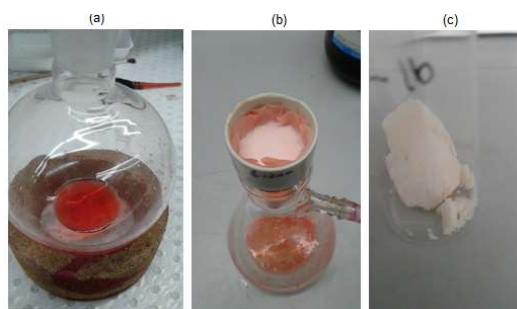
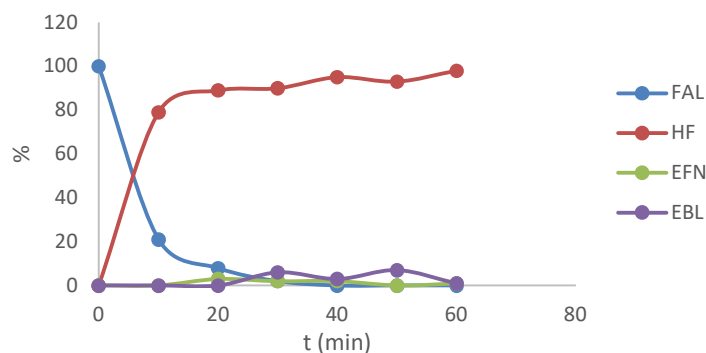


Figure 3.4: (a) Crude hydroxyfuranone. (b) Filtration and washing of crystals. (c) Pure product.

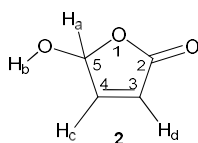
The conversion of FAL, subsequent generation of HF, and undesired formation of the ethoxy derivative were assessed by monitoring the reaction over a certain time period. Initial observations from Experiment 4 and Experiment 6 over periods of 20 hours and 6 hours confirmed that the conversion reached completion within an hour. To validate this observation, the reaction conversion was monitored at 10-minute intervals over a period of one hour in Experiment 5. To achieve this, 1 ml aliquots of reaction samples were drawn from the reaction mixture through a narrow FEP tube connected to a syringe (**Figure 3.3** and **Figure 3.5**).

Table 3.4: Conversion profile of Experiment 5.

Time (min)	Composition (%)			
	FAL	HF	EFN	EBL
0	100	0	0	0
10	21	79	0	0
20	8	89	3	0
30	2	90	2	6
40	0	95	2	3
50	0	93	0	7
60	0	98	1	1

**Figure 3.5:** Graphical conversion profile of Experiment 5.

3.1.2.2. Structural characterization of 5-Hydroxyfuran-2(5H)-one

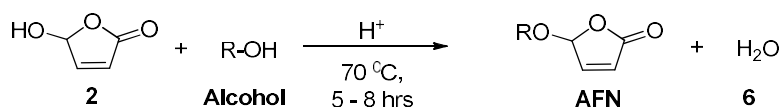


5-Hydroxyfuran-2(5H)-one (**2**): M.pt: 54-56°C. UV abs, λ_{\max} : 240.27 nm. ESI-MS: $[M-H]^-$, $C_4H_3O_3$, $m/z = 99$ (96%) and $[M+H]^+$, $C_4H_4O_3$, $m/z = 100$ (4%). $[2M-H]^-$, $C_8H_7O_6$, $m/z = 199$ (92%). $[2M]^+$, $C_8H_8O_6$, $m/z = 200$ (8%). 1H -NMR (400 MHz, $CDCl_3$): δ (ppm) = 7.29 (dd, $J = 5.6, 1.2$ Hz, 1H_c), 6.23 (dd, $J = 5.6, 1.1$ Hz, 1H_d), 6.21 (s, 1H_a), 4.21 (s, 1H_b). ^{13}C -NMR (101 MHz, $CDCl_3$): δ (ppm) = 171.6 (C, C-2), 152.2 (CH, C-5), 124.8 (CH- C-3), 99.0 (CH, C-4). IR (ATR): $\tilde{\nu}$ (cm^{-1}) = 3249.77 (brd, O-H, stretching), 1718.79 (str, C=O stretching), 1911.44 (str, C=C stretching), 1274.57 (str, C-O stretching), 1127.26 (str, C-O stretching), 704.27 (str, C=C bending).

3.1.2.3. Initial synthesis of alkoxyfuranones

Hydroxyfuranone is sensitive to esterification in the presence of acids at temperatures above 30°C. A conventional reflux system was thus used to synthesize several alkoxy derivatives. A 10 ml reaction scale setup was used with a 50 ml reaction vessel. A 23.5 cm long Dimroth

condenser with chilled water circulation was attached to this vessel. The condenser had a drying tube with a bulb fitted to the top to minimize contamination. The flask was three-quarters submerged in a silicon oil bath. Similarly, a thermometer was clamped and kept halfway in the oil to monitor the reaction temperature. The reaction was carried out on a digital hotplate with magnetic stirring capabilities. Using this setup, a mixture of **2** in the respective alcohol was subsequently heated to 70°C for 5-8 hours (**Scheme 3.2**).



Scheme 3.2: Pseudo-Fischer esterification of hydroxyfuranone to subsequent ester derivatives.

Table 3.5: Experimental parameters of alkoxyfuranone syntheses.

Exp	^a HF			Alcohol		^c FA (ml)	T (°C)	t _{rxn} (min)	AFN _T Mass (g)
	Mass (g)	mmol	mM	Name	Vol (ml)				
8	0.03	0.3	34.1	MeOH	9.0	1.0	70	240	0.04
9	0.19	1.9	194.6	<i>i</i> -PrOH	9.0	1.0	70	360	0.28
10	0.21	2.1	211.8	BuOH	9.0	1.0	70	480	0.33
11	0.21	2.1	209.8	<i>i</i> -PeOH	9.0	1.0	70	360	0.36
12	0.21	2.1	207.7	HeOH	9.0	1.0	70	360	0.38
13	0.34	3.4	337.2	PeOH	9.0	1.0	70	240	0.57
14	0.33	3.3	325.8	^b cPeOH	9.0	1.0	70	300	0.60

^a: HF sourced from LR1-7; ^b: cyclopentanol; ^c: 10% (v/v) FA in respective alcohols; AFN_T: theoretical yield of alkoxyfuranones.

Formic acid (FA) was used as the electrophilic catalyst due to its impact on the spontaneous esterification of HF to its EFN and EBL derivatives in Experiments 1-6. Pure crystals of HF for conversion were obtained from the previous Experiments 1-7 whilst the alcohols and formic acid were standard reagents obtained from laboratory stocks. After heating, the reaction mixture was neutralized in NaHCO₃, washed in brine, and dried with Na₂SO₄ before removal of the alcohol by evaporation. As shown below in **Table 3.6**, a total of seven different alkoxy-derivatives were obtained following the general reaction protocol.

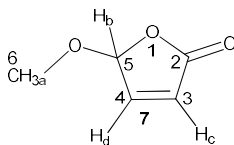
Table 3.6: Experimental results of alkoxyfuranone syntheses.

Exp	Conv (%)	Crude product					^a Isolated _{AFN}		
		Mass (g)	AFN (%)	HF (%)	ABL (%)	Alcohol (%)	Mass (g)	Yield (%)	Purity (%)
8	100	0.005	100	0	0	0	0.005	12	100
9	60	0.207	60	0	0	40	0.124	45	60
10	100	0.065	100	0	0	0	0.065	19	100
11	82	0.034	82	0	18	0	0.028	7.81	82

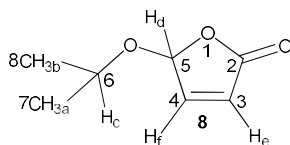
12	77	0.218	72	0	5	23	0.157	41	72
13	86	0.609	80	0	6	14	0.487	85	80
14	100	0.326	13	0	0	87	0.042	7	13

^a: isolated by azeotrope distillation; AFN: alkoxyfuranones; ABL: alkoxybutenal.

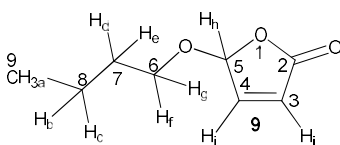
3.1.2.4. Structural characterization of alkoxyfuranones



5-Methoxyfuran-2(5H)-one (**7**): Red-orange liquid. UV abs, λ_{\max} : 198.5 nm. ESI-MS: $[M+H]^+$, $C_5H_7O_3$, $m/z = 115$ (100%). 1H -NMR (400 MHz, $CDCl_3$): δ (ppm) = 7.21 (dd, $J = 5.7, 1.2$ Hz, 1H_d), 6.25 (dd, $J = 5.7, 1.2$ Hz, 1H_c), 5.86 (t, $J = 1.2$ Hz, 1H_b), 3.58 (s, 3H_a). ^{13}C -NMR (101 MHz, $CDCl_3$): δ (ppm) = 170.5, (C=O, C-2), 150.1 (CH, C-5), 125.4 (CH, C-3), 104.2 (CH, C-4), 57.2 (CH₃, C-6). IR (ATR): $\tilde{\nu}$ (cm^{-1}) = 2939.35 (med, C-H stretching), 1760.98 (str, C=O stretching), 1471.54 (med, C-H bending), 1127.99 (str, C-O stretching), 990.31 (str, C=C bending).

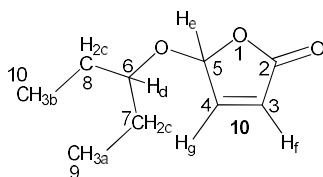


5-Isopropoxyfuran-2(5H)-one (**8**): Yellow-red liquid. UV abs, λ_{\max} : 198.1 nm. ESI-MS: $[M+CH_3]^+$, $C_8H_{13}O_3$, $m/z = 157$ (100%). ESI-MS: $[M+OH]^-$, $C_7H_{11}O_4$, $m/z = 159$ (31%). 1H -NMR (400 MHz, $CDCl_3$): δ (ppm) = 7.17 (dd, $J = 5.7, 1.0$ Hz, 1H_f), 6.19 (dd, $J = 5.7, 1.1$ Hz, 1H_c), 5.99 (s, 1H_d), 4.09 (dt, $J = 12.4, 6.2$ Hz, 1H_e), 1.26 (t, $J = 7.1$ Hz, 6H_{a/b}). ^{13}C -NMR (101 MHz, $CDCl_3$): δ (ppm) = 170.9 (C=O, C-2), 150.9 (CH, C-5), 124.8 (CH, C-3), 102.2 (CH, C-4), 73.7 (CH, C-6), 23.3 (CH₃, C-8), 22.1 (CH₃, C-7). IR (ATR): $\tilde{\nu}$ (cm^{-1}) = 2976.20 (med, C-H stretching), 1754.57 (str, C=O stretching), 1382.99 (med, C-H bending), 1111.63 (str, C-O stretching), 1008.72 (str, C=C bending), 890.89 (str, C=C bending), 684.07 (str, C=C bending).

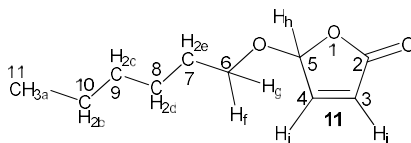


5-Butoxyfuran-2(5H)-one (**9**): Yellow-red liquid. UV abs, λ_{\max} : 198.5 nm. ESI-MS: $[M+H]^+$, $C_8H_{13}O_3$, $m/z = 157$ (100%). 1H -NMR (400 MHz, $CDCl_3$): δ (ppm) = 7.20 (dd, $J = 5.7, 1.2$ Hz, 1H_j), 6.22 (dd, $J = 5.7, 1.3$ Hz, 1H_i), 5.92 (t, $J = 1.2$ Hz, 1H_h), 3.87 (dt, $J = 9.3, 6.6$ Hz, 1H_f), 3.68 (dt, $J = 9.4, 6.7$ Hz, 1H_g), 1.61 (dd, $J = 14.7, 6.6$ Hz, 2H_{d/e}), 1.39 (dq, $J = 14.9, 7.4$

Hz, 2H_{b/c}), 0.92 (t, $J = 7.4$ Hz, 3H_a). ¹³C-NMR (101 MHz, CDCl₃): δ (ppm) = 170.7 (C=O, C-2), 150.5 (CH, C-5), 125.2 (CH, C-3), 103.5 (CH, C-4), 70.5 (CH₂, C-6), 31.6 (CH₂, C-7), 19.2 (CH₂, C-8), 13.9 (CH₃, C-9). IR (ATR): $\tilde{\nu}$ (cm⁻¹) = 2955.11 (med, C-H stretching), 1757.01 (str, C=O stretching), 1463.16 (med, C-H bending), 1122.76 (str, C-O stretching), 1015.74 (str, C=C bending), 889.60 (str, C=C bending), 685.15 (str, C=C bending).

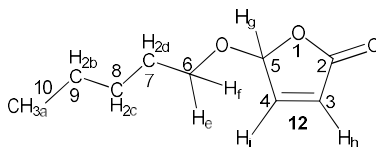


5-(Pentan-3-yloxy)furan-2(5H)-one (**10**): Orange liquid. UV abs, λ_{max} : 198.5 nm. ESI-MS: $[M+H]^+$, C₉H₁₅O₃, $m/z = 171$ (100%). ¹H-NMR (400 MHz, CDCl₃): δ (ppm) = 7.19 (dd, $J = 5.7, 1.2$ Hz, 1H_g), 6.20 (dd, $J = 5.7, 1.3$ Hz, 1H_f), 5.99 (t, $J = 1.2$ Hz, 1H_c), 3.66 (p, $J = 5.9$ Hz, 1H_d), 1.66-1.56 (m, 4H_c), 0.94 (t, $J = 5.3$ Hz, 3H_a), 0.91 (t, $J = 5.4$ Hz, 3H_b). ¹³C-NMR (101 MHz, CDCl₃): δ (ppm) = 170.9 (C=O, C-2), 150.7 (CH, C-5), 124.9 (CH, C-3), 103.2 (CH, C-4), 84.3 (CH, C-6), 27.0 (CH₂, C-7), 26.3 (CH₂, C-8), 9.6 (CH₃, C-9), 9.5 (CH₃, C-10). IR (ATR): $\tilde{\nu}$ (cm⁻¹) = 2935.48 (med, C-H stretching), 1755.18 (str, C=O stretching), 1462.25 (med, C-H bending), 1134.05 (str, C-O stretching), 1010.42 (str, C=C bending), 890.55 (str, C=C bending), 683.62 (str, C=C bending).

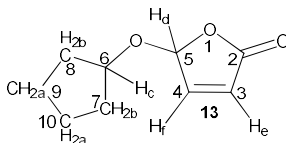


5-(Hexyloxy)furan-2(5H)-one (**11**): Yellow-red liquid. UV abs, λ_{max} : 198.5 nm. ESI-MS: $[M+H]^+$, C₁₀H₁₇O₃, $m/z = 185$ (100%). ¹H-NMR (400 MHz, CDCl₃): δ (ppm) = 7.20 (dd, $J = 5.7, 1.2$ Hz, 1H_j), 6.22 (dd, $J = 5.7, 1.3$ Hz, 1H_i), 5.91 (t, $J = 1.2$ Hz, 1H_h), 3.85 (dt, $J = 9.3, 6.7$ Hz, 1H_g), 3.71-3.62 (m, 1H_f), 1.70-1.53 (m, 4H_{e/d}), 1.37-1.20 (m, 4H_{c/b}), 0.88 (t, $J = 6.9$ Hz, 3H_a). ¹³C-NMR (101 MHz, CDCl₃): δ (ppm) = 170.7 (C=O, C-2), 150.5 (CH, C-5), 125.1 (CH, C-3), 103.5 (CH, C-4), 70.8 (CH₂, C-6), 31.6 (CH₂, C-7), 29.6 (CH₂, C-8), 25.7 (CH₂, C-9), 22.7 (CH₂, C-10), 14.1 (CH₃, C-11). IR (ATR): $\tilde{\nu}$ (cm⁻¹) = 2929.86 (med, C-H stretching), 1758.78 (str, C=O stretching), 1466.94 (med, C-H bending), 1124.76 (str, C-O stretching), 1079.05 (str, C=C bending), 889.73 (str, C=C bending), 685.51 (str, C=C bending).

Chapter 3 – Results



5-(Pentyloxy)furan-2(5H)-one (**12**): Yellow-red liquid. UV abs, λ_{\max} : 198.1 nm. ESI-MS: $[M+H]^+$, $C_9H_{15}O_3$, $m/z = 171$ (100%). 1H -NMR (400 MHz, $CDCl_3$): δ (ppm) = 7.20 (dd, $J = 5.7, 1.2$ Hz, 1H_i), 6.22 (dd, $J = 5.7, 1.3$ Hz, 1H_h), 5.92 (t, $J = 1.2$ Hz, 1H_g), 3.86 (dt, $J = 9.3, 6.7$ Hz, 1H_f), 3.67 (dt, $J = 9.3, 6.7$ Hz, 1H_e), 1.64 (dt, $J = 14.1, 7.0$ Hz, 2H_d), 1.33 (td, $J = 7.3, 3.7$ Hz, 4H_{c/b}), 0.90 (t, $J = 7.1$ Hz, 3H_a). ^{13}C -NMR (101 MHz, $CDCl_3$): δ (ppm) = 170.7 (C=O, C-2), 150.5 (CH, C-5), 125.2 (CH, C-3), 103.5 (CH, C-4), 70.8 (CH₂, C-6), 29.3 (CH₂, C-7), 28.2 (CH₂, C-8), 22.5 (CH₂, C-9), 14.1 (CH₃, C-10). IR (ATR): $\tilde{\nu}$ (cm^{-1}) = 2933.41 (med, C-H stretching), 1757.68 (str, C=O stretching), 1353.33 (med, C-H bending), 1123.69 (str, C-O stretching), 998.03 (str, C=C bending).



5-(Cyclopentyloxy)furan-2(5H)-one (**13**): Yellow-red liquid. UV abs, λ_{\max} : 199.0 nm. ESI-MS: $[M+OH]^-$, $C_9H_{13}O_4$, $m/z = 185$ (100%). ESI-MS: $[M+CH_3O]^-$, $C_{10}H_{15}O_4$, $m/z = 199$ (50%). 1H -NMR (400 MHz, $CDCl_3$): δ (ppm) = 7.16 (dd, $J = 5.7, 0.8$ Hz, 1H_f), 6.19 (ddd, $J = 5.7, 1.5, 0.8$ Hz, 1H_e), 5.96 (d, $J = 1.1$ Hz, 1H_d), 4.35-4.09 (m, 1H_c), 1.85-1.66 (m, 4H_b), 1.63-1.48 (m, 4H_a). ^{13}C -NMR (101 MHz, $CDCl_3$): δ (ppm) = 170.9 (C=O, C-2), 150.8 (CH, C-5), 124.9 (CH, C-3), 102.9 (CH, C-4), 83.2 (CH₂, C-6), 35.7 (2CH₂, C-7/8), 23.4 (2CH₂, C-9/10). IR (ATR): $\tilde{\nu}$ (cm^{-1}) = 2955.15 (med, C-H stretching), 1757.33 (str, C=O stretching), 1436.87 (med, C-H bending), 1132.72 (str, C-O stretching), 1076.11 (str, C=C bending), 991.19 (str, C=C bending), 683.89 (str, C=C bending). Indoor lamp reaction using the immersion well reactor

A conventional immersion well reactor (IW) was utilized for up-scale studies (**Figure 3.6**). The system consisted of a standard cylindrical Pyrex Schlenk reaction flask with a flat base.

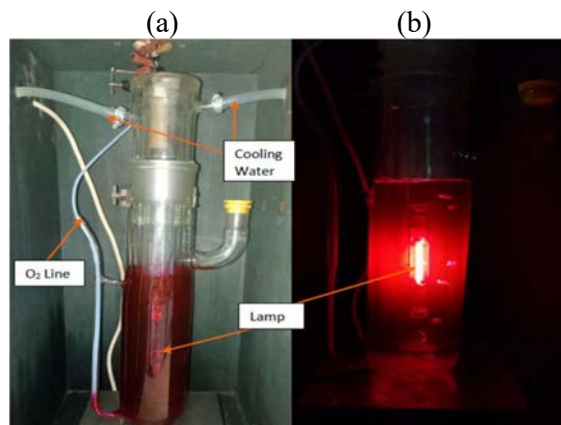


Figure 3.6: Immersion well reactor (a) prior to and (b) during early stages of irradiation.

The flask was 55 cm long and had a 45/40 top joint ($I\text{Ø} = 7$ cm). A narrow glass tube ($I\text{Ø} = 4.6$ mm) extended from the bottom of the flask upwards. An FEP tube through which oxygen was supplied was passed through this tube. A porous metal filter was attached to the end of the tube to provide agitation and gas saturation of the reacting solution. At the top of the flask was a shorter socket ($I\text{Ø} = 8.8$ mm) that was capped with a plastic stopper with a narrow hole and served as an outlet for gases and fumes. A double-walled borosilicate immersion well ($L = 42$ cm L, $O\text{Ø} = 7$ cm) was inserted into the reaction vessel. The immersion well cooler had two side arms through which chilled water was circulated to cool the reacting solution and lamp. Its walls filtered harsh wavelength and permitted transmission of light >300 nm. A 150 W medium-pressure mercury lamp (bulb $O\text{Ø} = 20$ mm) was inserted into the IW. The entire setup was placed in a wooden box ($61 \times 31 \times 31$ cm) to protect from UV-rays.

3.1.2.5. Batch synthesis of 5-Hydroxyfuran-2(5H)-one

The reaction parameters were adapted from Moradai *et al.* (2003)²⁶ and were used in several syntheses of HF. FAL, RB and MeOH were sourced in the same way as reported earlier for conversions in the smaller Rayonet reactor. Three batches of HF were synthesized, and the extent of conversions, yields of HF produced, and the selectivity of constituents were determined by ¹H-NMR analysis. The reaction parameters and subsequent yields of HF produced are shown below in **Table 3.7** and **Table 3.8**. The percentage yields of HF were derived from the theoretical mass balance and their immediate purities were determined by ¹H-NMR analysis.

The problem with isolation and purification by simple recrystallization is evident from the low yields of the desired HF. An assessment of the reaction progress was thus performed by

monitoring HF production along with the occurrences of its methoxy derivative (Table 3.9). A conversion profile of Experiment 17 is furthermore shown below in Figure 3.7.

Table 3.7: Experimental parameters for irradiations in an immersion well reactor.

Exp	MeOH (ml)	FAL			RB			HF _T Mass (g)	T _{RXN} (°C)	t _{irradiance} (min)
		Mass (g)	mmol	mM	Mass (g)	mmol	mol%			
15	250	29.61	924.16	3696.63	0.6477	0.67	0.019	120.24	21	1260
16	250	29.61	924.16	3696.63	0.744	0.76	0.033	120.24	21	2160
17	250	29.89	932.90	3731.59	0.786	0.81	0.070	121.38	21	1140

HF_T: theoretical mass of HF.

Table 3.8: Experimental results for irradiations in an immersion well reactor.

Exp	Conv (%)	Crude product					Isolated HF		
		Mass (g)	MFN (%)	MBL (%)	FAL%	HF%	Mass (g)	Yield (%)	Purity (%)
15	100	34.86	5	10	0	85	5.26	4	100
16	94	33.81	7	4	6	83	4.57	3	100
17	100	34.53	6	13	0	81	5.31	4	100

MBL: methoxybutenal; MFN: methoxyfuranone.

Table 3.9: Conversion profile of Experiment 17.

Time (hrs)	Composition (%)			
	FAL	HF	MFN	MBL
0	100	0	0	0
1	83	17	0	0
2	82	18	0	0
3	70	30	0	0
4	55	45	0	0
5	40	60	0	0
6	10	84	3	2
7	0	83	0	17
8	0	94	3	2
9	0	81	13	6

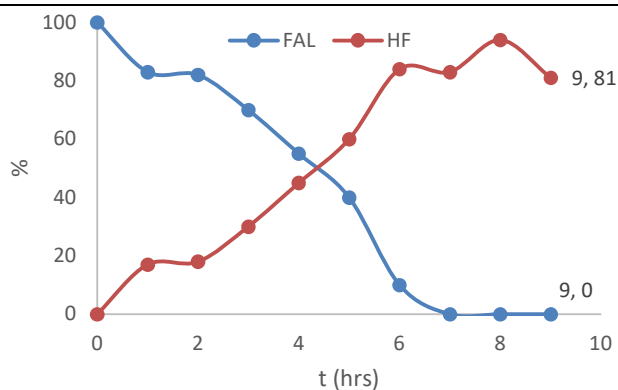


Figure 3.7: Conversion of FAL and production of HF in an IWR.

3.1.2.6. Batch synthesis of alkoxyfuranones

A Dean-Stark setup was utilized for the esterification reaction (**Figure 3.8**). The synthesis process used pure hydroxyfuranone produced by irradiation experiments and *para*-toluene sulfuric acid (*p*-TsOH) as acid catalyst. Each conversion ran for 6 hours at 60-70°C while stirring at 150 rpm in 150 ml of chloroform. The water produced was trapped and drained through the Dean-Stark attachment. The crude material was neutralized with NaHCO₃, washed with brine, dried over Na₂SO₄, and concentrated through rotary evaporation. The identities and compositions of the constituents in the crude product were determined by ¹H-NMR analyses. Subsequent isolation by flash chromatography yielded the desired alkoxy-derivatives. The experimental results are compiled in **Table 3.10** and **Table 3.11**.

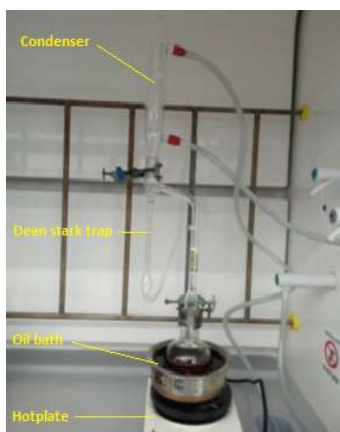


Figure 3.8: Dean-Stark setup used for batch synthesis of alkoxyfuranones.

Table 3.10: Experimental parameters of alkoxyfuranone syntheses.

Exp	^a HF			Alcohol		pTsOH (g)	T (°C)	t _{rxn} (min)	AFN _T Mass (g)
	Mass (g)	mmol	mM	Name	Vol (ml)				
18	2.15	21.48	171.87	MeOH	9.0	0.5	70	360	0.69
19	9.35	93.43	747.45	EtOH	9.0	1.5	70	360	4.30
20	2.02	20.19	161.48	n-BuOH	9.0	0.5	70	300	1.50

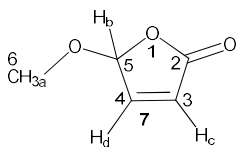
^a: Pure HF isolates from LR-9; AFN_T: theoretical yield of alkoxyfuranones.

Table 3.11: Experimental results of alkoxyfuranone syntheses.

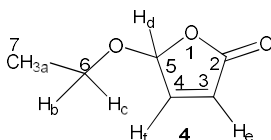
Exp	Conv (%)	Crude product					Isolated _{AFN}		
		Mass (g)	AFN (%)	HF (%)	ABL (%)	Alcohol (%)	Mass (g)	Yield (%)	Purity (%)
18	100	1.57	93	0	7	0	nd	nd	nd
^a 19	100	11.8	59	0	19	11	2.68	62	100
20	100	3.14	88	0	12	0	0.22	13	100

^a: crude contains a new diethoxy derivative with 11% composition.

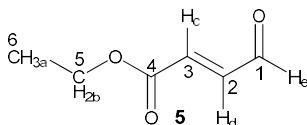
3.1.2.7. Structural characterization of alkoxyfuranones and their open analogues



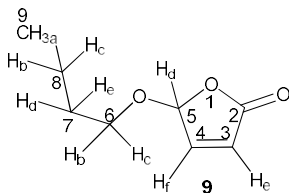
5-Methoxyfuran-2(5H)-one (**7**): Yellow-red liquid. ESI-MS: $[M+H]^+$, $C_5H_7O_3$, $m/z = 115$ (100%). 1H -NMR (400 MHz, $CDCl_3$): δ (ppm) = 7.19 (dd, $J = 5.7, 1.2$ Hz, 1H_d), 6.20 (dd, $J = 5.7, 1.2$ Hz, 1H_c), 5.83 (t, $J = 1.2$ Hz, 1H_b), 3.53 (s, 3H_a). ^{13}C -NMR (101 MHz, $CDCl_3$): δ (ppm) = 170.5, (C=O, C-2), 150.2 (CH, C-5), 125.4 (CH, C-3), 104.2 (CH, C-4), 57.2 (CH₃, C-6). IR (ATR): $\tilde{\nu}$ (cm^{-1}) = 2939.35 (med, C-H stretching), 1760.98 (str, C=O stretching), 1471.54 (med, C-H bending), 1127.99 (str, C-O stretching), 990.31 (str, C=C bending).



5-Ethoxyfuran-2(5H)-one (EFN, **4**): Yellow-red liquid. UV abs, λ_{max} : 198.5 nm. ESI-MS: $[M+H]^+$, $C_6H_9O_3$, $m/z = 129$ (100%). 1H -NMR (400 MHz, $CDCl_3$): δ (ppm) = 7.20 (dd, $J = 5.7, 1.2$ Hz, 1H_f), 6.21 (dd, $J = 5.7, 1.3$ Hz, 1H_c), 5.92 (t, $J = 1.2$ Hz, 1H_d), 3.92 (dq, $J = 9.4, 7.1$ Hz, 1H_e), 3.75 (dq, $J = 9.4, 7.1$ Hz, 1H_b), 1.27 (t, $J = 7.1$ Hz, 3H_a). ^{13}C -NMR (101 MHz, $CDCl_3$): δ (ppm) = 170.6 (C=O, C-2), 150.5 (CH, C-5), 125.1 (CH, C-3), 103.3 (CH, C-4), 66.3 (CH₂, C-6), 15.1 (CH₃, C-7). IR (ATR): $\tilde{\nu}$ (cm^{-1}) = 2980.58 (med, C-H stretching), 1755.66 (str, C=O stretching), 1348.69 (med, C-H bending), 1116.39 (str, C-O stretching), 1007.48 (str, C=C bending), 889.54 (str, C=C bending), 698.66 (str, C=C bending).

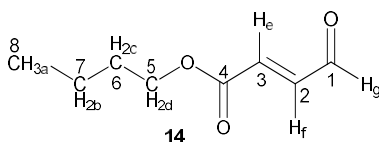


(*E*)-Ethyl 4-oxobut-2-enoate (EBL, **5**): 1H -NMR (400 MHz, $CDCl_3$): δ (ppm) = 9.76 (d, $J = 7.6$ Hz, 1H_e), 6.97 (dd, $J = 15.9, 7.6$ Hz, 1H_d), 6.72 (d, $J = 15.9$ Hz, 1H_c), 4.30 (q, $J = 7.1$ Hz, 2H_b), 1.34 (t, $J = 7.1$ Hz, 3H_a). ^{13}C -NMR (101 MHz, $CDCl_3$): δ (ppm) = 192.6 (CHO, C-1), 165.0 (O-C=O, C-4), 140.5 (C=C, C-2), 139.5 (C=C, C-3), 61.9 (C-H, C-5), 14.2 (C-H, C-5).



5-Butoxyfuran-2(5H)-one (**9**): Yellow-red liquid. 1H -NMR (400 MHz, $CDCl_3$): δ (ppm) = 7.20 (dd, $J = 5.7, 1.2$ Hz, 1H_j), 6.22 (dd, $J = 5.7, 1.3$ Hz, 1H_i), 5.92 (t, $J = 1.2$ Hz, 1H_h), 3.87 (dt, J

= 9.3, 6.6 Hz, 1H_f), 3.68 (dt, $J = 9.4, 6.7$ Hz, 1H_g), 1.61 (dd, $J = 14.7, 6.6$ Hz, 2H_{d/e}), 1.39 (dq, $J = 14.9, 7.4$ Hz, 2H_{b/c}), 0.92 (t, $J = 7.4$ Hz, 3H_a). ¹³C-NMR (101 MHz, CDCl₃): δ (ppm) = 170.7 (C=O, C-2), 150.5 (CH, C-5), 125.2 (CH, C-3), 103.5 (CH, C-4), 70.5 (CH₂, C-6), 31.6 (CH₂, C-7), 19.2 (CH₂, C-8), 13.9 (CH₃, C-9). IR (ATR): $\tilde{\nu}$ (cm⁻¹) = 2955.11 (med, C-H stretching), 1757.01 (str, C=O stretching), 1463.16 (med, C-H bending), 1122.76 (str, C-O stretching), 1015.74 (str, C=C bending), 889.60 (str, C=C bending), 685.15 (str, C=C bending).



(*E*)-Butyl 4-oxobut-2-enoate (**14**): Pale yellow liquid. ¹H-NMR (400 MHz, CDCl₃): δ (ppm) = 9.75 (d, $J = 7.6$ Hz, 1H_g), 6.95 (dd, $J = 15.9, 7.6$ Hz, 1H_f), 6.71 (d, $J = 15.9$ Hz, 1H_e), 4.23 (t, $J = 6.7$ Hz, 2H_d), 1.75-1.61 (m, 2H_c), 1.40 (dq, $J = 14.7, 7.4$ Hz, 2H_b), 0.94 (t, $J = 7.4$ Hz, 3H_a). ¹³C-NMR (101 MHz, CDCl₃): δ (ppm) = 192.6 (CHO, C-1), 165.0 (C=O, C-4), 140.4 (CH, C-2), 139.5 (CH, C-3), 65.7 (CH₂, C-6), 30.6 (CH₂, C-7), 19.2 (CH₂, C-8), 13.7 (CH₃, C-9).

Spectral analysis of ¹H-NMR (**Figure 3.9**) revealed the presence of an additional reaction product. Based on the assignments of the chemical shifts, it assigned to the acyclic acetal. The compound showed no acid or aldehyde proton at ≥ 10 ppm.

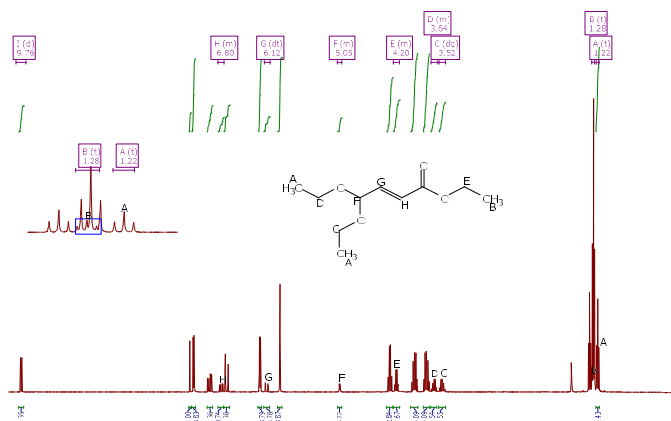
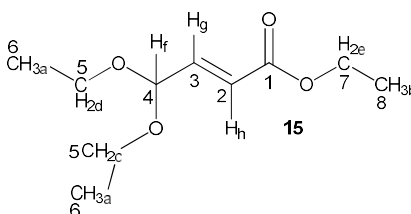


Figure 3.9: ¹H-NMR spectrum of the crude reaction mixture from Experiment 19 with assignments of the diethoxy derivative **15**.



(*E*)-4,4-Diethoxybut-2-enoic acid (**15**): $^1\text{H-NMR}$ (400 MHz, CDCl_3): δ (ppm) = 6.80 (dd, $J = 15.8, 4.2$ Hz, 1H_h), 6.12 (dd, $J = 15.8, 1.4$ Hz, 1H_g), 5.04 (dd, $J = 4.2, 1.3$ Hz, 1H_f), 4.24 (dq, 2H_e), 3.64 (dq, $J = 9.4, 7.1$ Hz, 2H_d), 3.52 (dq, $J = 9.4, 7.1$ Hz, 2H_c), 1.28 (t, $J = 7.2$ Hz, 3H_b), 1.22 (t, $J = 7.1$ Hz, 6H_a).

3.1.3. Outdoor solar experiments

All solar photochemical experiments were carried out outside the Molecular Genetics Building 20 at the James Cook University campus (latitude $19^\circ 19' 50''$ S and longitude $146^\circ 45' 33''$ E) in Townsville, Australia.

3.1.3.1. Flatbed reactor

Several direct illuminations in sunlight were performed using a 10 L capacity flatbed reactor. The reactor had an exposed surface of 2461.6 cm^2 and was fitted out with a reflective aluminium film on its back. The reactor loop incorporated an external Dimroth-condenser that was connected to the flatbed via chemically inert tubing. Circulation of the reaction medium was achieved by a rotary pump (**Figure 3.10**).

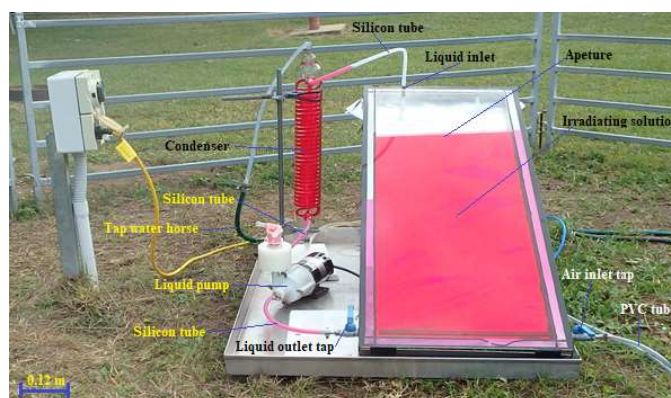


Figure 3.10: Solar flatbed reactor without aeration and circulation.

The reacting solution was contained in a rectangular box (flatbed) with an outer thickness of 3 cm. The reactor body was fabricated from thick Pyrex glass in an aluminium frame. The reactor was placed on a triangular steel frame angled at 16.84° . Teflon tubing were connected to the outlet of the flatbed reactor and its top opening. Circulation of the reaction medium through the condenser was achieved with a 15-head solvent pump, which pushed the reaction solution from the reactor into a Dimroth-condenser under tap water cooling before entering the flatbed at its top. Air was supplied at 15 LPM via a gas inlet at the bottom of the reactor. An air pump with a flow meter was connected to the gas inlet using polyvinyl tubes. The temperature of the

flatbed chamber was monitored with a mercury thermometer, which was inserted at the top of the flatbed and kept submerged throughout the reaction period.

3.1.3.2. Conversion parameters of solar batch reactions

The reaction protocol was based on the optimized reaction parameters from the indoor studies and involved a scale-up from 0.2 L to 8 L. As outdoor conditions (particularly the amount and intensity of solar light, the environmental temperature, and the atmospheric oxygen content) vary during exposure and time of day, illumination times were controlled and an effective cooling of ensured.

3.1.3.3. Monitoring of solar batch experiments

Conversion profiling helps to reveal the rate of conversion and the time when completion is reached. This strategy also helps identifying the ideal parameters for an optimized reaction. Aliquots of 2 ml reaction solution were thus sampled at specific time intervals and their chemical composition was determined by ¹H-NMR and GC-analyses. The kinetics were analysed by comparison of integrated characteristic peaks and the successive results were expressed in percent composition. **Table 3.12** shows the conversion profiles of experiments 21 – 23 under solar exposures.

Table 3.12: Composition-over-time profiles obtained by ¹H-NMR analysis.

Time (hr)	^a Exp. 21-Composition (%)				^a Exp. 22-Composition (%)				^b Exp. 23-Composition (%)			
	FAL	HF	EFN	EBL	FAL	HF	EFN	EBL	FAL	HF	EFN	EBL
0	100	0	0	0	100	0	0	0	100	0	0	0
1	-	-	-	-	7	93	0	0	8.9	88.5	2.7	0
2	-	-	-	-	0	92	0	2	4	74	2	0
3	-	-	-	-	0	97	1	1	27	71	2	0
4	-	-	-	-	9	88	3	1	1	98	1	0
5	18	80	2	0	2	94	2	2	16	83	1	0
6	-	-	-	-	4	94	2	0	1	98	1	0
7	9	89	3	0	10	90	0	0	3	95	2	0
8	-	-	-	-	2	96	2	0	10	88	2	0
9	-	-	-	-	-	-	-	-	9	89	2	0
10	7	71	20	2	-	-	-	-	100	0	0	0
11	-	-	-	-	-	-	-	-	8.9	88.5	2.7	0
12	-	-	-	-	-	-	-	-	4	74	2	0

SR: solar reaction; FAL: furfural; HF: hydroxyfuranone; EFN: ethoxyfuranone; EBL: ethoxybutenal; ^a: using 96% ethanol; ^b: using absolute ethanol.

Experiment 21 was conducted over a span of 5 hours per day for two days. Samples were retrieved with a 10 ml pipette and stored in 10 ml amber flasks for analysis. This initial batch

provided a preliminary conversion trend over time with samples taken after 0, 5, 7 and 10 hours of illumination. In contrast, Experiment 22 ran for 8 hours over two days (4 hrs/day) while Experiment 23 went for 12 hours (6 hrs/day). The collected samples were carefully concentrated by evaporation at 150 mbar at $\leq 30^\circ\text{C}$. It was found that conversion reached an optimum within the first hour as shown for Experiment 22 (93%) and Experiment 23 (91%), respectively. These promising conversion rates, however, are accompanied by varying compositions during the course of the reaction. These may have been caused by thermal decompositions during evaporation.

The kinetics of Experiment 24 were assessed by taking samples in 30 min intervals, which were then transferred to clear 10 ml vials (screw cap) and analysed by GC analysis in triplicates (**Table 3.13**). RB and 96% EtOH were occasionally added to compensate bleaching and evaporation losses, and to maintain complete solubility of the reaction mixture. The reaction temperature was recorded between 40-46°C from 09:30-15:00 hrs daily.

Table 3.13: Composition-over-time profile obtained by GC-analysis.

RXN t (min)	Concentration (mM)			
	[FAL \pm SD]	[HF \pm SD]	[EFN \pm SD]	[EBL \pm SD]
30	280.41 \pm 0.24	18.53 \pm 0.18	1.48 \pm 0.02	3.69 \pm 0.19
60	261.04 \pm 0.30	33.04 \pm 0.49	2.63 \pm 0.04	6.62 \pm 0.23
90	243.42 \pm 3.27	46.04 \pm 0.50	3.99 \pm 0.12	9.71 \pm 0.42
120	220.86 \pm 0.13	50.09 \pm 0.68	5.07 \pm 0.06	10.73 \pm 0.20
150	205.97 \pm 1.56	59.34 \pm 1.30	6.43 \pm 0.10	12.51 \pm 0.29
180	196.25 \pm 0.19	70.46 \pm 0.67	9.23 \pm 0.19	13.87 \pm 0.25
210	172.78 \pm 0.29	70.49 \pm 0.34	11.99 \pm 0.43	14.06 \pm 0.29
240	164.81 \pm 0.80	73.46 \pm 0.64	13.30 \pm 0.17	16.38 \pm 0.22
270	88.44 \pm 0.48	52.07 \pm 0.52	7.75 \pm 0.02	10.35 \pm 0.31
300	136.37 \pm 0.11	88.97 \pm 0.28	15.35 \pm 0.12	18.01 \pm 0.12
330	124.39 \pm 0.82	97.01 \pm 0.51	17.87 \pm 0.07	19.65 \pm 0.31
360	117.88 \pm 0.83	99.72 \pm 0.52	18.21 \pm 0.18	21.11 \pm 0.48
390	107.56 \pm 0.67	94.66 \pm 0.42	12.86 \pm 10.97	19.95 \pm 0.13
420	91.23 \pm 0.75	90.03 \pm 1.78	30.10 \pm 0.33	19.82 \pm 0.51
450	80.67 \pm 0.36	95.79 \pm 0.94	32.24 \pm 0.30	20.65 \pm 0.10
480	73.78 \pm 0.51	101.93 \pm 0.23	36.01 \pm 0.30	21.97 \pm 0.32
510	66.47 \pm 0.27	107.02 \pm 0.60	34.63 \pm 0.29	22.42 \pm 0.27
540	56.70 \pm 0.47	113.75 \pm 1.18	39.14 \pm 0.37	24.02 \pm 0.28
570	51.63 \pm 0.61	114.94 \pm 1.92	41.12 \pm 0.64	24.92 \pm 0.09
600	46.71 \pm 0.38	117.34 \pm 1.60	47.68 \pm 0.51	26.27 \pm 0.16
630	42.45 \pm 0.29	118.93 \pm 2.08	46.66 \pm 0.52	30.46 \pm 0.07
660	38.56 \pm 0.18	121.63 \pm 0.66	51.91 \pm 0.06	27.48 \pm 0.16
690	29.88 \pm 0.04	120.55 \pm 0.97	52.41 \pm 0.27	30.66 \pm 0.41
720	28.11 \pm 0.36	121.38 \pm 2.04	54.29 \pm 0.83	30.59 \pm 0.42

750	27.60±0.30	120.37±0.90	55.25±0.75	30.49±0.23
780	27.20±0.11	116.17±0.87	62.09±0.15	30.78±0.55
810	26.59±0.19	118.55±1.40	63.49±0.60	31.02±0.30
840	17.93±0.01	121.88±0.33	77.54±0.60	31.98±0.50
870	26.27±0.25	117.84±1.23	72.09±0.69	29.97±0.30
900	12.48±0.14	128.46±1.20	85.56±1.09	32.53±0.24

SD: standard deviation of triplicate analysis; GC systematic error = 0.2%.

3.1.3.4. Comparison of the conversions during solar exposures

Solar conversions were obtained on 7-7.9 L scales with illumination periods of 10-18 hours. The conversion profiles over time were obtained by ¹H-NMR for Experiments 21-23, while Experiment 24 was monitored by GC-analysis instead. The results are compared in **Table 3.14**. During solar illuminations, the reaction conditions naturally varied depending on weather conditions. This was especially notable for the temperature of the reaction medium, which ranged from 23-46°C. These fluctuations impacted on the conversion rates, degree of sensitizer decomposition and subsequent (thermal) conversion to the ethoxy derivative of HF. For Experiment 24, FAL conversion during illumination was slow compared to Experiments 21-23 and took three days to reach an incomplete conversion of 89%.

Table 3.14: Comparison of experimental outcomes of solar reactions.

Exp	EtOH (L)	FAL			RB			T _{RXN} (°C)	t _{illum} (min)	Conv. (%)	Composition (%)			
		Mass (g)	mmol	mM	Mass (g)	mmol	mol %				HF	EFN	EBL	FAL
21	7.00	273.6	2847.2	406.74	5.320	5.46	0.004	36-43	600	93	71	20	2	7
22	7.53	247.4	2575.3	341.95	6.144	6.31	0.005	23-33	480	98	92	2	0	2
23	7.90	260.3	2709.2	359.73	6.509	6.68	0.005	27-30	720	91	89	2	0	9
24	7.50	281.9	2933.5	389.51	10.376	10.66	0.008	33-46	1020	89	50	27	12	11

3.1.4. Workup and isolation of 5-Hydroxyfuran-2(5H)-one

The initial stage of the workup after illumination was the removal of the solvent EtOH. The crude reaction mixtures of Experiments 21-24 were carefully concentrated by rotary evaporation at 240-30 mbar at temperatures ≤30°C. Due to the large volumes of solvent and the presence of high-boiling formic acid (bp: 100.8°C) to be removed, complete evaporation and drying was time-consuming and difficult to achieve. Analysis of the dried crude product by ¹H-NMR spectroscopy revealed significant changes in the products' compositions (**Table 3.15**).

HF crystallizes at low temperatures (<0°C), but only when in a sufficient purity to achieve supersaturation. Seeding with pure HF crystals and refrigerating for 12 hours was thus

employed to initiate nucleation. Alternatively, crystallization by rapid freezing with liquid nitrogen was attempted (**Figure 3.11**). For Experiment 23, both crystallization methods failed due to the large amounts of by-products. Losses of HF were inevitable especially during filtration and washings with cold DCM during recrystallization (**Table 3.15**).

Table 3.15: Composition of dried crude materials and isolated yields of hydroxyfuranone.

Exp	HF _T (g)	Crude product					Isolated HF			Purity (%)
		Mass (g)	HF (%)	EFN (%)	EBL (%)	FAL (%)	Mass (g)	YAW (%)	LW (%)	
21	284.92	369.96	68	27	2	3	54.06	19	-49	100
22	257.71	244.67	65	23	5	8	60.66	24	-41	100
^a 23	271.10	344.77	38	32	12	18	no	nd	nd	nd
24	293.55	281.09	70	23	7	0	143.97	49	-21	100

HF_T: theoretical mass; YAW: isolated yield of HF; LW: HF lost during crystallization; ^a: no crystallization; no: not obtained; nd: not done.

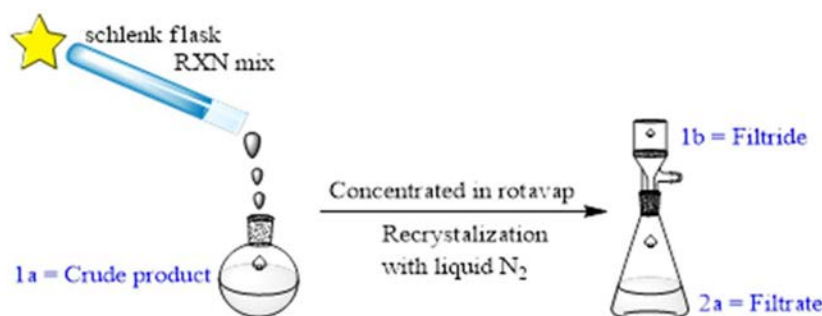


Figure 3.11: Hydroxyfuranone freeze-crystallization process.

3.1.5. Pseudo-esterification of crude residual 5-Hydroxyfuran-2(5H)-one to 5-Ethoxyfuran-2(5H)-one

The liquid filtrates collected still contained significant amounts of the desired HF, with EFN and traces of EBL as side-products. EFN was considered suitable as an easily accessible and recyclable alkoxyfuranone for successive transformations to produce further derivatives. Therefore, the remaining crude HF from the filtrates was converted to EFN in a simple acid-catalyzed esterification with ethanol. Reactions were conducted using a Dean-Stark setup to ensure that the water and the EFN produced were separated. Approximately 1.5 g of para-toluene sulfuric acid (pTsOH) were used as the acid catalyst and 150 ml of chloroform as a co-solvent. The reflux was set to 70°C for 12 hours. During this conversion, additional portions of 10 ml of chloroform were occasionally added to the reaction flask after draining off of the immiscible water condensate. The experimental parameters and outcomes are compiled in **Table 3.16** and **Table 3.17**.

Table 3.16: Pseudo-esterification parameters using crude filtrates.

Exp	CHCl ₃ (ml)	^a Crude HF filtrates		EtOH		EFN _T
		Mass (g)	HF (%)	Mass (g)	mmol	Mass (g)
25	150.0	104.91	52	29.95	650.0	67.04
26	150.0	206.78	46	44.54	966.7	132.97
^b 27	150.0	344.77	33	46.45	1008.2	389.09
28	150.0	238.22	46	50.67	1099.8	177.94

^a: Filtrate of crude product retrieved after filtering of HF crystals, ^b: Crude mass of filtrate from Experiment 23, EFN_T: Amount of crude EFN.

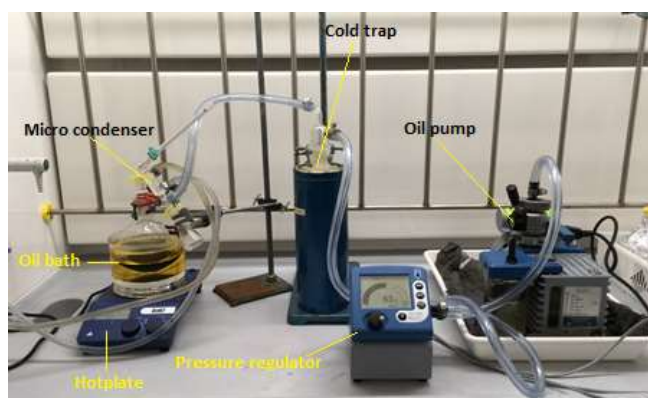
Table 3.17: Composition of refined filtrates.

Exp	^a Crude Product			
	Mass (g)	EFN (%)	EBL (%)	FAL (%)
25	67.04	76	22	2
26	132.97	58	30	12
27	389.09	48	34	18
28	177.94	83	13	0

^a: Crude product after subsequent pseudo-esterification.

3.1.6. Isolation of 5-Ethoxyfuran-2(5H)-one by microdistillation

To separate the desired EFN and EBL, the crude products from the esterification step were subjected to vacuum distillation (**Figure 3.12**). The pressure was set to 13 mbar in anticipation that EFN and EBL will separate at 101°C and 75°C, respectively. Heating was carried out using a silicon oil bath. Samples for separation were combined and transferred to a 500 ml Pyrex flask, which was lowered to partially submerge in the oil bath. The outlet of the flask was connected to a short distillation adaptor (still head, 14/23) incorporated the condenser (14 cm, length). During distillation fractions were collected at steady temperature intervals and their compositions determined by ¹H-NMR analysis. Fractions containing mixtures of EFN and EBL were combined and subjected to further separation by bulb-to-bulb vacuum distillation.

**Figure 3.12:** Micro vacuum distillation setup.

A Kugelrohr bulb-to-bulb distillation (BBD) unit was used to further separate and purify EFN and EBL at 13 mbar. Fractions VD1 and VD2 from the previous micro-distillation represented reasonable mixtures of individual constituents and were therefore subjected to BBD. Three 50 ml quick-fit bulbs were aligned in series with two bulbs in the oven whilst the third bulb was outside in an ice bath. The oven was closely monitored and controlled between 70-100°C as fractions were collected. The yields of collected fractions were somewhat unsatisfactory (**Table 3.19**), however, EFN separated well and in purities >90%, although traces of EBL were still detected.

Table 3.18: Composition of fractions obtained by micro-distillation.

VD	Exp	Mass (g)	F	Vapor T (°C)	Crude distillate					
					Mass (g)	Rec. (%)	EFN (%)	EBL (%)	FAL (%)	HF (%)
1	8	67.04	4, 6	80-110	11.43	17	77	17	6	0
2	9	132.97	4	80-110	31.68	24	50	30	20	0
3	10	389.09	8	80-110	28.69	7	79	5	16	0
4	11	177.94	3	80-110	86.80	49	78	22	0	0

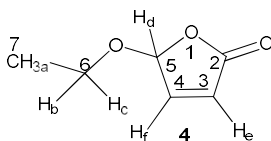
Fractions with <5% EFN or EBL were not used further; F: Exp 8-11 fractions; Rec: Recovery.

Table 3.19: Compositions of fractions from bulb-to-bulb distillation.

BBD	^a Crude distillate			^b Crude distillate					
	Sample	Mass (g)	Vapor T (°C)	Mass (g)	Rec. (%)	EFN (%)	FAL (%)	HF (%)	EBL (%)
1	VD1	11.43	90-100	3.26	28	98	0	0	2
2	VD2	31.68	90-100	4.38	14	92	0	0	8

Rec: Recovery; ^a: Most of the sample remained in the flask whilst smaller amounts were collected in the bulbs.

3.1.6.1. Structural characterization of 5-Ethoxyfuran-2(5H)-one

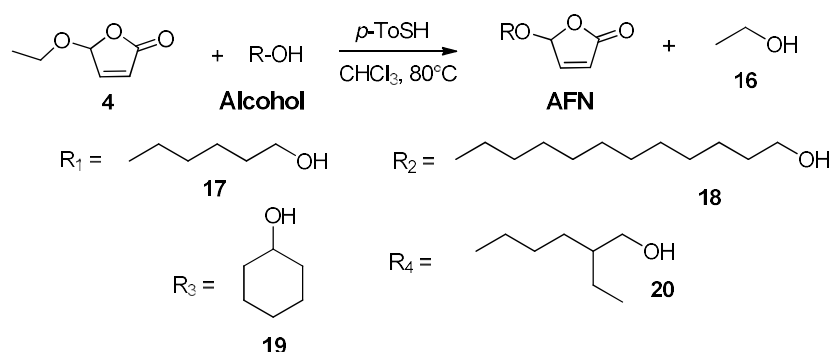


5-Ethoxyfuran-2(5H)-one (**4**): Yellow-red liquid. ΔH_{vap} 365.30 J/g. UV abs, λ_{max} : 198.5 nm.

¹H-NMR (400 MHz, CDCl₃): δ (ppm) = 7.20 (dd, ³J_{fe} = 5.7 Hz, ³J_{fd} = 1.2 Hz, 1 H, CH), 6.20 (dd, ⁴J_{cd} = 5.7 Hz, ³J_{ef} = 1.3 Hz, 1 H, CH), 5.91 (t, ³J_{df} = 1.2 Hz, ⁴J_{dc} = 1.2 Hz, 1 H, CH), 3.91 (dq, ²J_{cb} = 9.4 Hz, ³J_{ca} = 7.1 Hz, 1 H, CH₂), 3.74 (dq, ²J_{bc} = 9.4 Hz, ³J_{ba} = 7.1 Hz, 1 H, CH₂), 1.26 (t, ³J_{a(bc)}} = 7.1 Hz, 3 H, CH₃). ¹³C-NMR: δ (ppm) = 15.1 (CH₃, C-6), 66.3 (CH₂, C-5), 103.3 (C-O, C-4), 125.1 (C=C, C-3), 150.5 (C=C, C-2), 170.7 (C=O, C-1). FT-IR (ATR): $\tilde{\nu}$ (cm⁻¹) = 3101.28 (med, H-C stretching), 1756.53 (str, C=O stretching), 1374.73 (med, H-C bending), 1134.40 (str, C-O stretching), 892.24 (str, C-H bending).

3.1.7. Pseudo-transesterification of 5-Ethoxyfuran-2(5H)-one

Due to the challenging isolation of HF, pseudo-transesterification from the easier accessible EFN was investigated as an alternative access to AFN. The starting material used constitutes pure EFN, which was obtained from fractions F2-3 of VD5. Hexanol **17**, dodecanol **18**, cyclohexanol **19**, and 2-ethyl-hexanol **20** were used as alcohols for transesterification (**Scheme 3.3**). The reaction was conducted using a Dean-Stark reflux set-up, *p*-TsOH as a catalyst and chloroform as a co-solvent.



Scheme 3.3: Pseudo-transesterification of ethoxyfuranone with various alcohols.

Alkoxy substitution at C-5 of the furanone moiety was achieved within 15 hours at 80°C (**Table 3.20**). After completion, the crude reaction mixture was neutralized with NaHCO₃, washed in brine, dried over Na₂SO₄, and concentrated by rotary evaporation at 40°C and 200-40 mbar. All experiments conducted achieved complete conversions, but numerous by-products were detected (**Figure 3.13**).

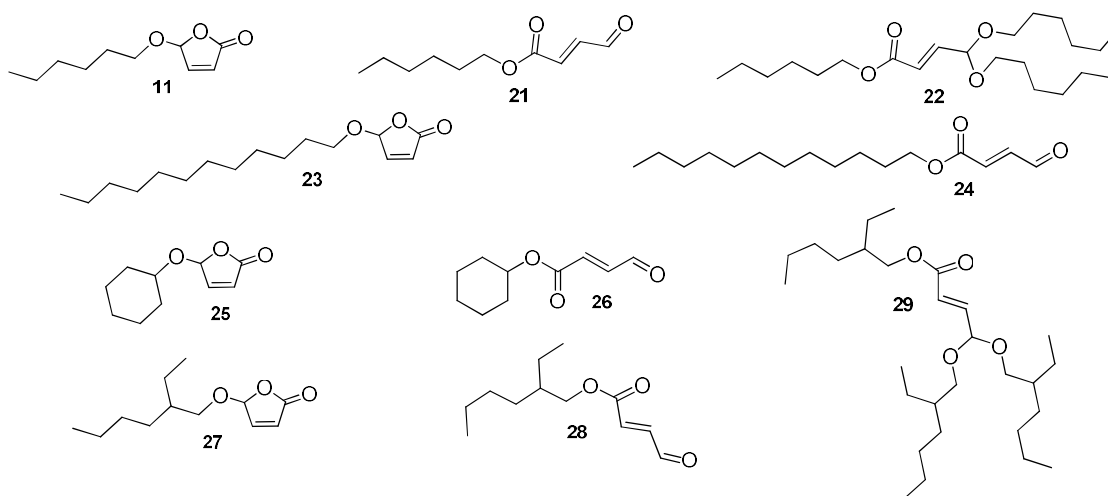


Figure 3.13: Structures of compounds identified in respective crude products.

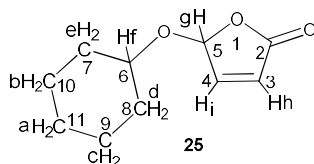
Di-alkoxylated and tri-alkoxylated products were detected in Experiment 29 and Experiment 32, while Experiments 30 and 31 primarily favoured the hydroxyfuranone parent structure.

Table 3.20: Transesterification conversion parameters.

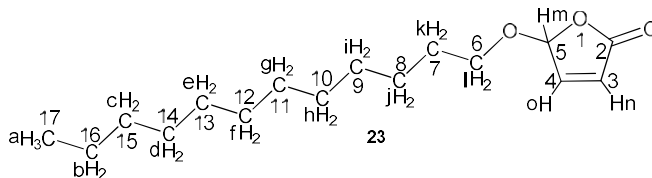
Exp	<i>p</i> TsOH		Ester		#	Alcohol		T (°C)	t (h)	RPM	Conv (%)	Compounds (%) [*]		
	Mass (g)	mmol	Mass (g)	mmol		Mass (g)	mmol					11 (43)	21 (53)	22 (4)
29	0.07	0.4	113.12	882.9	1	113.13	1107.4	~80	15	450	100	11 (43)	21 (53)	22 (4)
30	0.05	0.3	25.65	200.2	2	25.65	137.7	~80	15	450	100	23 (70)	24 (30)	NP
31	0.13	0.8	101.67	793.5	3	105.23	389.1	~80	15	450	100	25 (75)	26 (25)	NP
32	0.12	0.7	5.07	39.6	4	6.33	34.3	~80	15	450	100	28 (23)	29 (20)	20 (57)

TR: Transesterification reaction; RPM: revolutions per minute; *: composition; NP: nothing present; #: alcohol used in pseudo-transesterification.

3.1.7.1. Structural characterization of compounds **25** and **23**.



5-(Cyclohexyloxy) furan-2(5H)-one (**25**): Yellowish oil (22.1 mg). UV abs, λ_{\max} : 204 nm. ESI-MS: $[M+H]^+$, $C_{10}H_{15}O_3$, $m/z = 183$ (100%). 1H -NMR (400 MHz, $CDCl_3$): δ (ppm) = 7.18 (dd, $J = 5.7, 1.2$ Hz, 1H_i), 6.20 (dd, $J = 5.7, 1.3$ Hz, 1H_h), 6.04 (t, $J = 1.2$ Hz, 1H_g), 3.78 (ddd, $J = 13.3, 8.6, 3.9$ Hz, 1H_f), 1.99-1.93 (m, 2H_{d-e}), 1.76-1.72 (m, 2H_{c-b}), 1.58-1.53 (m, 2H_a). ^{13}C -NMR (101 MHz, $CDCl_3$): δ (ppm) = 24.1 (CH₂, C-11), 25.5 (2CH₂, C-9, C-10), 32.1 (CH₂, C-8), 33.3 (CH₂, C-7), 79.3 (CH, C-6), 102.1 (C-O, C-4), 124.9 (C=C, C-3), 150.9 (C=C, C-2), 170.9 (C=O, C-1).



5-(Dodecyloxy) furan-2(5H)-one (**23**): Colourless oily liquid (3.28 g). UV abs, λ_{\max} : 214 nm. ESI-MS: $[M+H]^+$, $C_{16}H_{29}O_3$, $m/z = 269$ (100%). ESI-MS: $[M-H]^-$, $C_{16}H_{27}O_3$, $m/z = 267$ (5%). 1H -NMR (400 MHz, $CDCl_3$): δ (ppm) = 7.44 (dd, $J = 5.7, 1.2$ Hz, 1H_o), 6.27 (dd, $J = 5.7, 1.3$ Hz, 1H_n), 6.07 (t, $J = 1.3$ Hz, 1H_m), 3.81 (dt, $J = 9.4, 6.6$ Hz, 1H_i), 3.71 (dt, $J = 9.5, 6.6$ Hz, 1H_i), 1.62 (td, $J = 13.4, 6.6$ Hz, 2H_k), 1.40 – 1.23 (m, 18H_{b-j}), 0.88 (t, $J = 6.9$ Hz, 3H_a). ^{13}C -

NMR (101 MHz, CDCl₃): δ (ppm) = 14.3 (CH₃, C-17), 22.8 (CH₂, C-16), 26.0 (CH₂, C-8), 28.6 (CH₂, C-14), 29.5 (2CH₂, C-12/13), 29.8 (2CH₂, C-10/11), 32.1 (CH₂, C-15), 66.1 (CH₂, C-7), 70.8 (CH₂, C-6), 103.5 (CH, C-2), 140.4 (=CH, C-3), 125.2 (=CH, C-3), 165.1 (C=O, C-5).

3.1.7.2. Isolation and structural characterization of (*E*)-2-Ethylhexyl 4, 4-bis ((2-ethylhexyl) oxy) but-2-enoate

3.1.7.2.1. Fraction vacuum distillation

In an attempt to isolate and verify the structure of the tri-alkoxy derivative **29**, the crude product of Experiment 32 was subjected to fractional vacuum distillation (FVD). Three fractions were collected and analysed by ¹H-NMR spectroscopy (Table 3.21). Solely Fraction 3 contained a mixture of compounds, including the desired tri-alkoxy derivative **29**.

Table 3.21: Composition of fractions obtained by vacuum distillation.

Fraction	Yield (g)	Pressure (mbar)	Temperature (°C)	RPM	Appearance	Composition
1	0.5611	4	96	250	Pale yellow oil	20 (100%)
2	0.3598	4	120	250	Pale yellow oil	20 (100%)
3	9.3365	NA	NA	250	Black swamp remains, floral scent	29 (79%), 16 (21%)

3.1.7.2.2. Further purification by solvent-solvent precipitation

Fraction 3 from the previous vacuum distillation was further purified by solvent-solvent precipitations. The crude material was treated three times with 100 ml of ethyl acetate and *n*-hexane (1:10) in an attempt to precipitate and remove the dark-coloured solid. The precipitates were removed by gravity filtration and the filtrate was concentrated under rotary evaporation, yielding 6.4624g of recovered distillation product.

3.1.7.2.3. Flash Chromatography

Flash chromatography was further employed in an attempt to separate the main constituents from Fraction 3. A 65 g cartridge was packed with 42.6744 g of silica gel (0.06-0.2 mm). About 0.4060 g of the sample was mixed with 4.2106 g of silica gel in acetone. Subsequent evaporation of acetone adsorbed the crude mixture onto the silica gel. The mobile phase employed for chromatographic separation were mixtures of ethyl acetate and *n*-hexane. In the first 7 minutes, gradient elution from 0-8% ethyl acetate was employed, followed by isocratic elution at 8% for the next 5 min, and finally ended with a gradient elution from 8-21% for

another 5 min. The flow-rate was set to 35 ml/min and fractions were selectively collected when peaks were detected by UV (200-300 nm) and evaporative light scattering (ELS) detectors. Several fractions were collected and analysed by $^1\text{H-NMR}$ spectroscopy (**Table 3.22**).

Table 3.22: Composition of fractions obtained by flash chromatography separation.

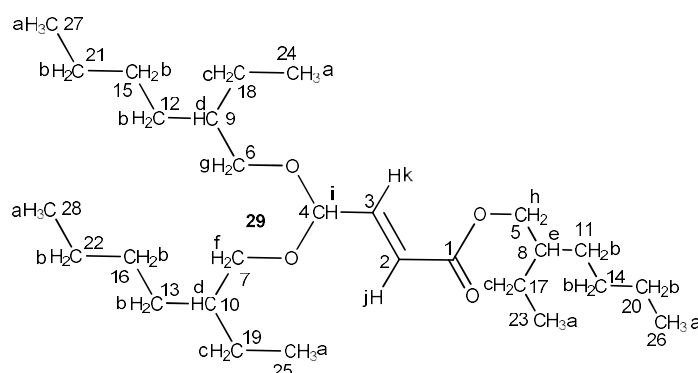
Fractions	Mass (g)	Appearance	Composition
3-6	0.1552	Golden oil	29 (88%), 28 (12%)
7-8	0.0611	Golden oil	29 (94%), 28 (6%)
9-11	0.0219	Colourless crystals	29 (92%), 28 (8%)

3.1.7.2.4. Purification by preparative HPLC

Flash chromatography enabled preconcentration of compound **29**, but the presence of residual **28** in all fractions was noted. Preparative HPLC (pHPLC) was thus conducted to compound **29** in pure form. Preparative HPLC was performed using MeOH under isocratic elution conditions at a flow of 7 ml/min. A 30 mg/ml solution of the combined Fractions 7-11 from the previous flash chromatography was prepared and 2 ml portions were injected in a series of 16 injections. **Table 3.23** gives details of the compositions of each fraction obtained from pHPLC separation.

Table 3.23: Constituents in fractions of preparative HPLC.

Fraction	Rt (min)	Mass (g)	Composition (%)					
			4	16	20	29	27	28
1	6.116	0.1255	0	0	0	92.6	0	7.4
2	8.724	0.0525	0	0	0	84.7	0	15.3
3	15.243	0.3099	0	0	0	100	0	0
4	16.099	0.1274	0	0	0	87.1	12.9	0



(E)-2-ethylhexyl 4,4-bis((2-ethylhexyl)oxy)but-2-enoate (**29**): Floral odour, yellowish oil (309.9 mg). UV abs, λ_{max} : 202 nm. ESI-MS: $[\text{M}+\text{H}]^+$, $\text{C}_{28}\text{H}_{58}\text{O}_4$, $m/z = 455$ (100%). $^1\text{H-NMR}$ (400 MHz, CDCl_3): δ (ppm) = 6.79 (ddd, $J = 15.8, 6.2, 3.0$ Hz, 1H_k), 6.12 (ddd, $J = 15.8,$

obtained from correlation of its concentration (mol.L^{-1}) and peak area ($\text{pA}\cdot\text{s}$) for triplicates of five standards. From the first calibration standard (CS1), an R_f of $33.058 \text{ pA}\cdot\text{s}\cdot\text{L}\cdot\text{mmol}^{-1}$ was calculated from $4515.84 \text{ pA}\cdot\text{s}$ produced by 13.660 mM of the IS (**Equation 3.1**).

Table 3.24: Concentration and related peak areas of the internal standard.

Analysis	^a [IS] mM	P-area				R_f ($\text{pA}\cdot\text{s}\cdot\text{L}\cdot\text{mmol}^{-1}$)
		Trial 1	Trial 2	Trial 3	Mean	
CS1	13.660	4502.4927	4545.0034	4500.0303	4515.84	33.058
CS2	27.320	8736.6768	8756.0293	8852.7217	8781.81	32.144
CS3	40.980	12908.7000	13201.2000	13107.9000	13072.60	31.899
CS4	47.810	15125.7000	15463.5000	15562.1000	15383.77	32.176
CS5	54.649	16903.1000	17199.6000	17249.3000	17117.33	31.327
Mean (\bar{x})						32.122
Standard deviation (σ)						± 0.625
Coefficient of variance (CV)						1.95%

^a: Standards prepared from 20% stock solution of 1-butanol in ethanol. Triplicate analysis with mean as true value.

$$\text{a) Internal Standard}_{\text{RF}} = \frac{\text{IS}_{\text{peak area}}}{[\text{IS}]} \quad \text{pA}\cdot\text{s}\cdot\text{L}\cdot\text{mmol}^{-1}$$

$$\text{b) } \bar{x}_{\text{Peak area}} = \frac{\sum x_c}{n}$$

$$\text{c) } \bar{x}_{\text{Rf}} = \frac{\sum x_c}{n}$$

$$\text{d) } \sigma_{\text{Rf}} = \sqrt{\frac{\sum (x - \bar{x})^2}{n}}$$

$$\text{e) } \text{CV}_{\text{Rf}} = \left(\frac{\sigma_{\text{Rf}}}{\bar{x}_{\text{Rf}}} \right) \times 100\%$$

Equation 3.1: Statistical equations used to calculate; (a) Response factor, (b) Peak area mean, (c) Response factor mean, (d) Response factor standard deviation and (e) Response factor's coefficient of variance.

A calibration curve was developed, and its slope (R_f) was then compared with the R_f of Experiment 24 to verify their similarities. The response factor of the internal standard (IS) was derived from the chromatograms of Experiment 24. In this exercise, a $35 \mu\text{L}$ aliquot of 20% n-butanol (>99%) in ethanol was mixed with $100 \mu\text{L}$ of sample in a 2 ml ambient GC vial and further dissolved with $1700 \mu\text{L}$ EtOH. Shown below is a chromatogram (**Figure 3.15**) of Experiment 24 with the main constituents being monitored.

During conversion concentration of each constituent was calculated from the quotient of the IS response factor and peak area of characteristic peaks (**Equation 3.2**).

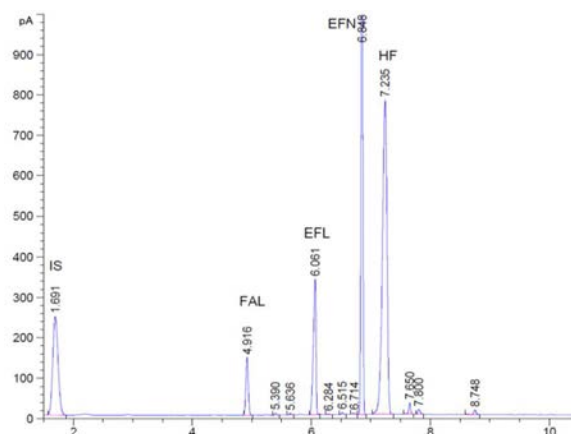


Figure 3.15: Chromatogram depicting subsequent constituents at 900th minute.

$$[\text{Constituent}] = \frac{\text{Constituent}_{\text{peak area}}}{\text{IS}_{\text{Rf}}} \quad \text{mmol.L}^{-1} = \text{mM}''$$

Equation 3.2: Equation used to calculate concentration of constituents.

3.1.8.2. Assessing of the photobleaching of rose bengal

During the solar synthesis of hydroxyfuranone, significant bleaching of the sensitizer rose Bengal (RB) was observed and as a result, additional RB had to be added occasionally. Based on this experience, a neat assessment was done in a setup where all parameters were kept constant to assess the decomposition of RB.

Approximately 0.0573 g of RB were dissolved and mixed in 100 ml of 96% EtOH and transferred to a Pyrex Schlenk flask. The flask was inserted into a Rayonet reactor, and its side arm was connected to an oxygen stream. The mixture was irradiated for 5 hours and samples were taken at the start of the reaction, after 2 and 4 hours of irradiation. Changes in sensitizer concentration ([RB]) were assessed by monitoring the UV-Vis absorbance at λ_{max} 558 nm (**Table 3.25**).

Table 3.25: Assessment of the rate of decomposition of RB over 4 hours of irradiation.

t (min)	Abs	Vol _{rxn} (ml)	mM	dt (min)	dmM
0	0.31	100	0.589	120	0.199
120	0.205	92	0.389	120	0.080
240	0.163	89	0.309	-240	0.310

3.1.8.3. Photooxygenations in EtOH, *i*-PrOH and *tert*-amyl alcohol

Earlier observations indicated that photooxygenations of furfural in ethanol were fast, but resulted in larger amounts of ethoxyfuranone due to thermal follow-up reactions, especially

during workup. Hence, it was evaluated if *i*-PrOH and *tert*-amyl alcohol (*t*-AmOH) would show lower reactivity than EtOH and would be less sensitive to subsequent pseudo-esterification. All three solvents were thus trialled on 100 ml scales and were irradiated for 10 hours at 27°C in a Rayonet reactor. The results are summarized in **Table 3.26** with description of products in **Figure 3.17**.

Table 3.26: Comparison between different alcohols and the product compositions.

Exp	FL	RB	Solvent	Conv (%)	Crude mass (g)	Composition (%)			
						HF	AFN	ABL	FAL
34	2.14	22.31	EtOH	100	1.65	2 (74)	4 (25)	5 (2)	-
35	2.12	22.05	<i>i</i> -PrOH	97	2.67	2 (86)	8 (3)	30 (3)	1 (3)
36	2.02	20.97	<i>t</i> -AmOH	79	2.22	2 (68)	-	31(11)	1 (21)

AFN: alkoxyfuranone; ABL: alkoxybutenal; HF: hydroxyfuranone.

Figure 3.16: Structures of products obtained.

3.2. Sustainable synthesis of *para*-menthane-3, 8-diol

3.2.1. Sampling and preparation of *C. citriodora* leaves

Leaves were collected at the JCU campus in Townsville at two different locations (**Figure 3.17**). Sampling was conducted in the early morning hours between 5-6 am. This was done to ensure minimum losses of volatile constituents during the harvesting process. Using a tree pruner, suitable leaves at approximately 4 m above chest height were collected in the form of small branches.



Figure 3.17: Sampling of *C. citriodora* leaves (at Site 2) and locations of sampling sites.

Collections at Site 1 (19°19'24"S, 148°45'21"E) and Site 2 (19°19'47"S, 148°45'37"E) were done at different times of year and hence varying weather conditions (**Table 3.27**). Sampled leaves were placed in baskets and immediately taken to the laboratory. The samples were then sorted to separate the damaged leaves from those with their foliage matrix intact.

Table 3.27: Details of sampling of LSG in JCU at different times.

S	Site	Weather	Date	Quantity ($\pm 0.02\text{kg}$)
S1	1	Partially cloudy, 22-25°C	04/07/18	3.56
S2	2	Partially cloudy, 22-25°C	06/07/18	3.38
S3	2	Partially cloudy, 22-25°C	19/06/19	3.69
S4	2	Clear sky, 26-27°C	28/11/19	3.72
S5	2	Clear sky, 26-27°C	03/12/19	3.35
S6	2	Partially cloudy, 24-26°C	02/07/20	3.45

S: relates to the different sampling conducted.

3.2.2. Sorting of leaves

The physical integrity of leaves selected for distillation has a direct influence on the quality of LSG oil. Particularly in the initial chemical analysis stage, this aspect is vital to establish the actual yield and representative composition of all constituents of the distilled LSG oil. Each branch was carefully spread on the bench and inspected visibly (**Figure 3.18**).

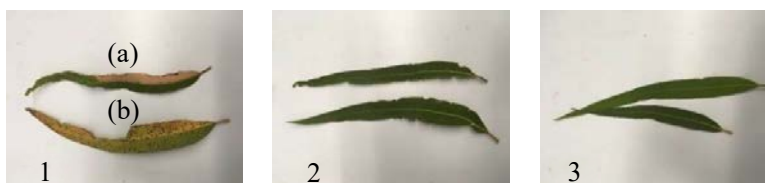


Figure 3.18: (1) Images of leaves with dead patches (a) and infectious patches (b); (2) moderately affected leaves and (3) fine leaves with physical integrity intact.

Leaves with dead or infectious patches were picked and discarded. The remaining fine leaves were picked from the stem and combined together for use in subsequent distillations.

3.2.3. Extraction of LSG oil

LSG oils from fine leaves of *C. citriodora* were primarily extracted through steam distillation (SD) and hydrodistillation (HD). Generally, leave types (species, collection conditions and quality) and their chemical compositions (water-solubles, hydrolytic stability and volatiles) determine the most suitable extraction method¹⁶⁴. In this study, both classical distillation methods were trialled in comparison to identify the highest yielding technique.

The mass of fine leaves used for each distillation method depended on the holding capacity of the distillation apparatus used. From the six samplings conducted (**Table 3.27**), twelve different distillations were carried out. Out of these, eleven used fresh leaves without any additional pre-treatment. This practice was primarily intended to ensure minimum losses of volatile components prior to distillation and to develop a simple and cost-efficient commercial process.

3.2.3.1. Hydrodistillation

Leaves collected from both sampling sites were used for the first distillations by hydrodistillation (HDg, **Figure 3.19**). Approximately 0.5-1.0 kg of fine fresh leaves were loaded into a 5 L Mowbray glass round bottom flask. The flask was placed in a 5 L heating mantle and was filled with 3 L of distilled water (DH₂O) and a few boiling chips. A distillation bridge with an incorporated Liebig condenser was placed on the flask. Its delivery adaptor was connected to a 2 L separatory funnel, which collected the distillate and allowed for its immediate removal. The distillation flask and lower part of the distillation head were covered with aluminium foil to speed up the heating-up process. The heating mantle was set to 300°C and chilled water was circulated through the condenser. Although the essential oil separated on top of the aqueous hydrosol during distillation, the separation remained incomplete and time-consuming. The collected distillates were thus transferred hourly to a secondary 1 L separating funnel. The distilled boiler water (DBW, hydrosol) was occasionally siphoned off dropwise to enable the LSG oil to accumulate in the separating funnel. After 6 hours of continuous heating, the distillation was stopped as approximately a third of the boiler water (BW) had distilled over, and most of the leaves became pale due to prolonged heating.

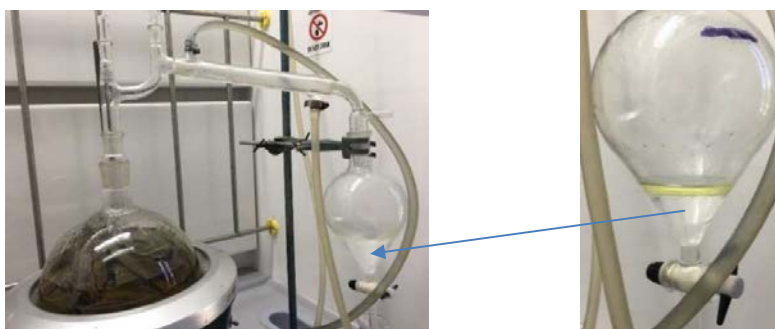


Figure 3.19: Hydrodistillation setup.

3.2.3.2. Steam distillation in a glass setup

Prolonged contact of hot water and chemical constituents of leaves may affect the composition of the essential oil extracted¹⁶⁵. In particular, polar molecules and terpene structures are readily

impacted water and heat. During steam distillation, water vapour is passed through loosely packed biomass. It is therefore less destructive to the sample matrix and selectively vaporizes volatiles.

Leaves samples were used from the same collection sites as listed in **Table 3.27**. The setup utilizes scientific-grade borosilicate glass pieces connected to give a vertical alignment of the boiler flask and distillation unit (SDg, **Figure 3.20**).



Figure 3.20: Glass-based steam distillation setup.

A 1 L flat-based boiler flask was filled with 500 ml of DH_2O to which a few boiling chips were added. The flask was placed on a hotplate and was clamped to a retort stand to keep it steady. Smaller leaves were loaded into a 5 L biomass flask that was connected to the boiler flask via a quickfit socket (19/26). A vertical distillation-bridge was attached to the larger 34/35 quickfit socket at the top of the biomass flask. This was connected to the Liebig condenser and further to a separator funnel. The funnel had an outlet, through which the hydrosol was emptied dropwise into a collecting flask. To accelerate the heat-up, the boiler flask and distillation bridge were covered with aluminium foil. The hotplate was set to 100°C , while circulating chiller water was passed through the Liebig condenser. Periodic removal of hydrosol from the separating funnel enabled the accumulation of LSG oil. At the end of distillation, the boiler water and hydrosol were siphoned off into collecting vessels.

3.2.3.3. Steam distillation in a copper setup

Copper-based distillation units are being used traditionally in contrast to ceramic, steel, and glass systems¹⁶⁶. Copper has the ability to conduct and transfer heat swiftly, which provides an advantage with respect to oil yield and distillation time¹⁶⁷. Unlike glass systems, copper is furthermore robust, easy to handle, and easy to maintain.

The copper distillation unit used was a purchased from Copper Pro[®] (SDc, **Figure 3.21**). Leaves samples were again taken from the same sites as those used in the previous glass distillations (**Table 3.27**).



Figure 3.21: Copper-based steam distillation setup.

The 5 L copper boiler was filled with 3 L of DH₂O to which a few boiling chips were added. The boiler was placed on the hotplate and a 2 L biomass column loaded with fine leaves was connected vertically to it. A second 2 L distillation unit with an attached vertical condenser as its side was mounted on it. The connections had thin rubber washers in-between and were held together with ring clamps. The hotplate was again set to 100°C, while chilled water was passed through the condenser. From the condenser an extended horizontal tube channelled the distillate into a separation funnel positioned along the distillation unit. Hydrosol from the separating funnel was drained off occasionally to accumulate the LSG oil. Hydrosol and LSG oil were separately collected in sample vials and stored in the fridge.

3.2.3.4. Continuous liquid-liquid extraction

The strong smells of the boiler water (BW) and hydrosol (DBW) recovered after each distillation suggested that these aqueous phases contained significant amounts of highly water-soluble components. Upon standing and slow evaporation of water, colourless crystals commonly formed on top of these aqueous layers. Continuous liquid-liquid extraction (solvent-solvent extraction, SSRE) was thus used to retrieve additional LSG oil constituents. The SSRE system consisted of two compartments (**Figure 3.22**), which enabled the simultaneous extraction and separate concentration of extracted organic materials. The available setup held approximately 350 ml of BW/DBW sample and approximately 100 ml of diethyl ether (Et₂O) in the extraction vessel, and both layers were separated by a perforated Teflon disc. The unit was connected to a 500 ml reservoir flask containing 250 ml of Et₂O.



Figure 3.22: Liquid-liquid extraction using boiler (left) and distilled boiler water (right).

The ether in the reservoir was heated upon homogeneous stirring at 500 rpm to 60°C using a heating mantle and the steam passed via a distillation arm to the extraction compartment. The ether condensed at the top of the extraction unit and passed through a narrow glass tube to the bottom of the extraction flask. The end of the glass tube carried a rotating glass-head that generated fine ether droplets that perled through the aqueous layer. The organic layer accumulating at the top and containing dissolved organic material overflow back into the distillation flask. Once continuous condensation of ether vapours was noted, the extraction was run for a total of 4 hours. The extracted LSG components in the reservoir flask were then recovered by careful removal of ether by rotary evaporation.

3.2.3.5. Purification and yields of LSG oils

LSG oil retrieved directly from distillation or after liquid-liquid extraction from the BW (BWO) and DBW (DBWO) were dried further to remove traces of water. All the oils were first washed twice with 20 ml of saturated NaCl solution. The aqueous NaCl layer was carefully drained off in a separation funnel. The remaining LSG oil was transferred to a 20 ml conical flask and dissolved with 15 ml of anhydrous diethyl ether. A few anhydrous Na₂SO₄ crystals were added to the conical flask to absorb residual water. The drying agent was filtered off and the LSG oil solution was collected in a pre-weighted 50 ml flask. Careful removal of the solvent by rotary evaporation (40°C, 1 atm) produced golden-like oils with a citrus aroma. The LSG oil was then transferred to glass vials that were covered in foil, capped, and stored under refrigeration. The results are summarized in **Table 3.28**.

Table 3.28: Comparison of distillation performance.

<u>Distillation</u>	<u>Sample</u>	<u>DO (g)</u>	<u>BW_v</u>	<u>BWO_m</u>	<u>DBW_v</u>	<u>DBWO_m</u>	<u>LSGO</u>	<u>Yield%</u>	
No	Type	(g)	(ml)	(g)	(ml)	(g)	(g)	(w/w)	
D1	HDg	500.0	4.4090	4800	1.106	522	0.2569	5.7714	1.15

D2	HDg	500.0	4.6513	4440	1.583	441	0.2213	6.4556	1.29
D3	SDg	502.0	5.8962	463	1.082	436	3.558	10.536	2.1
D4	SDg	302.0	1.748	510	0.252	422	0.483	2.4828	0.81
D5	SDc	1001.2	6.6461	502	0.361	1826	2.5622	9.5693	0.96
D6	HDg	100.6	1.1367	436.8	0.044	418	0.0831	1.5344	1.26
D7	SDc	1001.4	14.756	522	0.052	1750	0.7295	15.5375	1.55
D8	SDc	786.3	12.9774*	516	0.063	440	0.179	13.2194	1.68

* Used for PMD synthesis.

3.2.4. GC-analysis parameters

Qualitative and quantitative chemical profiles of LSG oils by GC-analysis have been widely reported^{97, 111, 168, 169}. Citronellal (Cal), citronellol (Col) and isopulegol (Iso) as well as other acetyls and bicyclic constituents were commonly found^{169, 170}. A frequent problem with determining the full chemical profile of LSG oil by GC-analysis was associated with the differences in retention times caused by different existing temperature programs. Three methods were thus assessed to find an improved method that would enable the separation of all constituents in a reasonable run time (**Figure 3.23**).

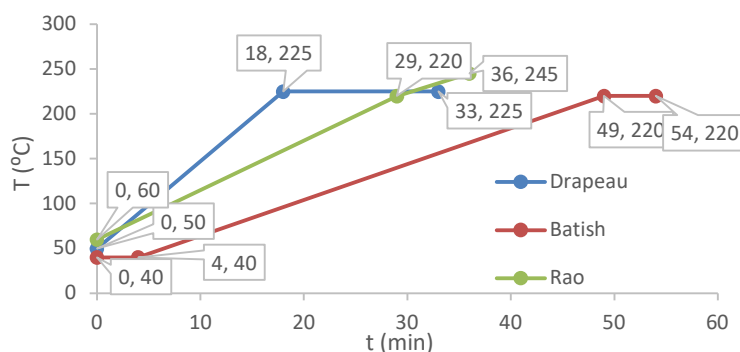


Figure 3.23: Existing GC temperature profiles used for method development.

3.2.4.1. Optimization of temperature program

The temperature program reported by Drapeau was 33 min long with a sharp gradient (10°C/min) from 60–225°C, followed by holding at 225°C for 15 min. The temperature program reported by Rao used two gradient temperature increases (5.5 and 3.5°C/min), both significantly lower than Drapeau’s method. Based on these reported methods, different temperature programs (M1-M3, **Figure 3.24**) were investigated in an attempt to reduce the run time for analysis while at the same time maintaining respectable separation of all constituents.

Chapter 3 – Results

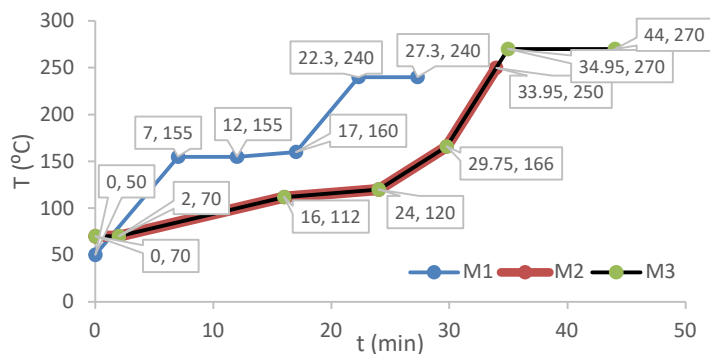


Figure 3.24: Temperature profiles of the developed in-house GC methods.

The M1 method produced congested peaks, which was attributed to the two increasing gradient and isothermal periods. For instance, the hold at 7-12 min and low ramp at 12-17 min were set to separate Cal, Col, and Iso, and later the various *para*-menthane-3, 8-diol (PMD) isomers. However, temperatures of 155-160°C were too high and subsequently increased the vapor pressure of a number of eluting components. The chromatogram (**Figure 3.25**) depicts this situation, particularly in the range of 8-10 min where Cal and the Iso appear.

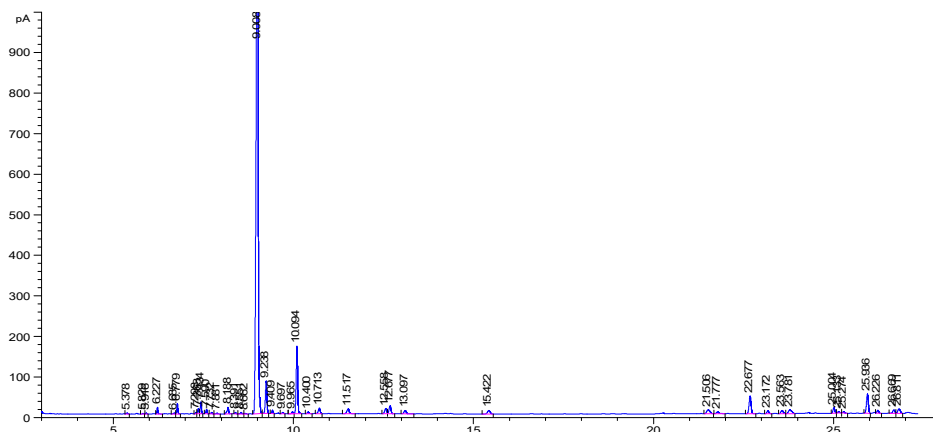


Figure 3.25: Chromatogram LSG oil analysed using M1.

Using the M2 temperature program, the separation of Cal was improved by lowering the temperature gradient between 70-120°C in conjunction with the Rao method^{169,170}. Constituents appearing within the third and fourth temperature gradient periods were few and separated well (**Figure 3.26**). Overall, method M2 enhanced Cal separation as it enabled the separation from a peak that was overlapped with the Cal peak with method M1. This peak evolving at 17.607 min (7%) using method M2 was suspected to be an Iso stereoisomer. Method M2 was used extensively to assess the chemical profiles of various commercial and extracted LSG oils.

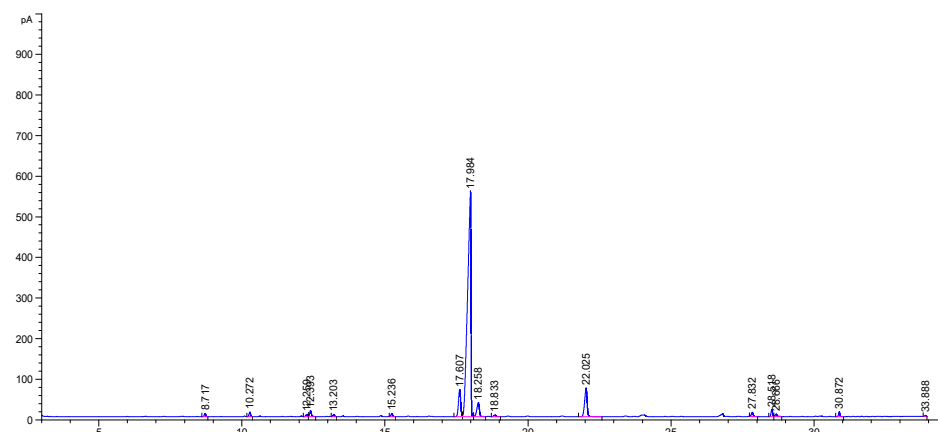


Figure 3.26: Chromatogram LSG oil analysed using M2.

LSG oils recovered from aqueous streams (BW and DBW) showed distinctive PMD peaks within 27-28 min as well as other significant peaks within the last 4 minutes of the chromatogram.

Temperature profile M3 was developed as an extension to M2 to detect compounds emerging above 250°C (>34 min). As a result, a group of compounds appeared between 36-39 min, notably peaks at 37.342 min and 37.794 min in significant amounts.

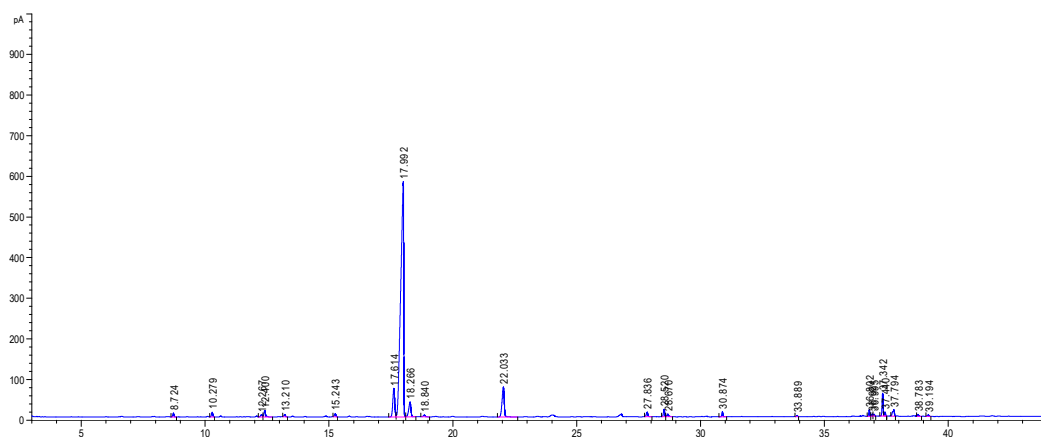


Figure 3.27: Chromatogram LSG oil analysed using M3.

3.2.4.2. Peak assignments

To determine the identity of the constituents of the LSG oils that appeared on the chromatograms, a number of reference standards were used (**Table 3.29**). The runtime (Rt) of these references were then aligned with the Rt values appearing on the respective chromatograms of the LSG oil samples. Further confirmation was achieved from retention index (RI) values calculated using the non-isothermal Kovats Retention Index equation (**Equation 3.3**).

Table 3.29: Reference standards used to assign the main compounds of LSG oils.

Compound	t _i (min)	RI _C	RI _L
Cal	17.934	1155.3	1153.7
neo-Iso	17.617 ^a	1145.8	1144.2
(-)-Iso	17.766	1148.3	1149
iso-Iso	18.241 ^a	1158.2	1159.1
cis-PMD	27.835	1342.3	NR
trans-PMD	28.521	1369.4	NR
Col	22.013	1232.6	1228.1
PMD acetal 1	37.354	1950.558	NR
PMD acetal 2	37.797	1968.843	NR

RI: Kovats retention index; NR: no records; GC parameters: M3; alkane solution: C₇-C₃₀; RI_L: literature; RI_C: experimental; Reference compounds obtained from Sigma Aldrich and Alfa Aesar; ^a: from literature.

$$I_i = 100 \left[n + \frac{(t_i) - (t_n)}{(t_{n+1}) - (t_n)} \right]$$

Equation 3.3: Non-isothermal Kovats equation.

3.2.4.3. Chemical profiles of commercial and distilled LSG oils

To identify a biomass resource with a high Cal content, a number of LSG oils were analysed by GC-analysis (**Table 3.30**). All commercial LSG oils were specified as *C. citriodora* and were obtained from local and overseas distilleries. Approximately 0.10 g of each LSG oil were transferred to 1.5 ml amber GC vials using micro syringes. The oils were diluted with 1.8 ml of anhydrous diethyl ether (DeE) and homogenized on a vortexer. These vials were then placed in the auto-sampler tray and programmed to inject in auto sequence injection mode.

Table 3.30: Comparison of the main constituents in LSG oil from several commercial products.

Compound	LSG oil composition (%)					
	EA	RE	HO	CO	NC	JCU
Cal	75.4	79.4	73.6	71.6	62.1	69.2
neo-Iso	3.3	2.8	3.2	4.6	5.4	2.8
(-)-Iso	5.9	5.9	6.3	7.3	9.9	5.8
iso-Iso	0.0	0.0	0.0	0.0	0.0	0.0
cis-PMD	0.9	0.7	0.9	1.2	1.4	1.1
trans-PMD	0.5	0.2	1.3	1.7	3.0	4.5
Col	8.5	4.8	9.9	6.1	10.1	8.4
PMD acetal 1	0.0	0.0	0.0	0.0	0.9	1.9
PMD acetal 2	0.0	0.0	0.0	0.0	0.0	0.0

EA: Essentially Australia (NSW); RE: Rare Earth oils (QLD); HO: Heritage oils (WA); CO: Ji'an Hairui Natural Plant Co (China); NC: Les Huiles Essentielles (New Caledonia); JCU: James Cook University (Townsville, QLD).

3.2.5. PMD synthesis

All conversions conducted followed the procedure developed by Drapeau⁹⁷ and incorporated green chemical principles¹⁷¹. Apart from utilizing a renewable feedstock, the robustness and durability of citric acid was also an important aspect. The procedure enabled a technically simple and financially viable process for producing PMD on larger and sustainable scales.

3.2.5.1. Laboratory-scale conversions

A series of conversions were initially carried out on a 100 ml scale utilizing materials from the commercial distillation process. The LSG oils (TLH) were obtained from Rare Earth (RE) oils distillery in Cairns. The oils were stored in two separate 1 L thermo-steel bottles. Hydrosol (BLH) from commercial distillations was furthermore received and was investigated as aqueous layer in some experiments. The 7-w% citric acid catalyst solution was prepared by dissolving 0.75 g in 10 ml of distilled water (DW) or hydrosol. The top and bottom layers of the LSG oil were furthermore assessed separately to account for density and hence composition differences within the oil (**Figure 3.28**). Upon storage a gradient in texture and thickness became clearly visible. The top portion of the LSG oil layer was thus assumed to contain lighter molecules, while denser molecules sank to the bottom. This assumption was also evident from somewhat varying Cal compositions for the top layer portion (TL, 77.6%) vs. the bottom layer (BL, 78.0%).

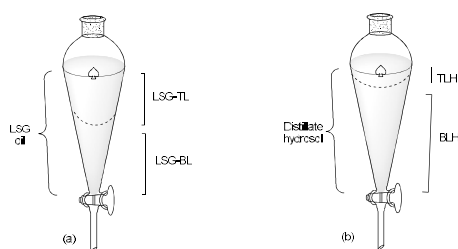


Figure 3.28: Illustration of the top (LSG-TL) and bottom (LSG-BL) LSG oil layers and, top (TLH) and bottom (BLH) layers of distillate hydrosol.

To a 250 ml Pyrex flask, approximately 7.40 g of the LSG oil were added followed by the 7-w% citric acid solution. The flask was half submerged in an oil bath, which was seated on an 800 W Heidolph stirrer-hotplate. A Graham condenser was connected to the quickfit socket of the flask to minimize evaporation losses. The solution was heated to 50-60°C for 15-28 hours while stirring at 450-600 rpm to maintain an effective emulsion. The flask was covered in aluminium foil to provide heat evenly. Different portions of LSG oil were furthermore

investigated for the synthesis of PMD. Likewise, different citric acid solvents were investigated. The experimental conditions are summarized in **Table 3.31**.

Table 3.31: Reaction parameters of waste utilization assessment.

Exp	LSG oil		Cal		7% Acid solution				RXN Condition			PMD _T		
	Type	(g)	%	(g)	mmol	S	S (g)	CA (g)	CA (mol)	T (°C)	RPM	t (h)	mmol	(g)
37	EA	7.40	77.1	5.71	36.99	DW	9.76	0.74	3.85	50	450	15	36.99	6.37
38	EA	7.44	77.1	5.74	37.19	DW	9.72	0.78	4.06	60	450	15	37.19	6.41
39	EA	7.60	77.1	5.86	37.99	DW	9.75	0.76	3.96	50	450	25	37.99	6.54
40	EA	7.33	77.1	5.65	36.64	DW	9.71	0.77	4.01	50	450	15	36.64	6.31
41	EA	7.33	77.1	5.65	36.64	DW	9.75	0.74	3.85	25	450	28	36.64	6.31
42	RE-TL	7.41	77.6	5.75	37.28	DW	9.94	0.75	3.90	50	600	15	37.28	6.42
43	RE-BL	7.46	78.0	5.82	37.72	DW	9.78	0.74	3.85	50	600	15	37.72	6.50
44	RE-TL	7.35	77.6	5.70	36.98	TLH	9.88	0.74	3.85	50	600	15	36.98	6.37
45	RE-BL	7.91	78.0	6.17	40.00	TLH	10.11	0.76	3.96	50	600	15	40.00	6.89
46	RE-BL	7.41	78.0	5.78	37.47	BLH	10.43	0.79	4.11	50	600	15	37.47	6.45
47	RE-TL	7.38	77.6	5.73	37.13	BLH	10.94	0.77	4.01	50	600	15	37.13	6.40
48	RE-TL	7.43	77.6	5.77	37.38	DW	10.17	0.75	3.90	50	600	15	37.38	6.44
49	RE-BL	7.50	78.0	5.85	37.93	DW	10.01	0.75	3.90	50	600	15	37.93	6.53

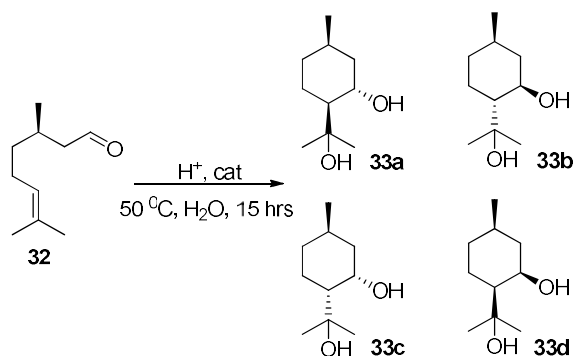
EA: Essential Australia, NSW; RE: Rear Earths oi, QLD; TLH: Top layer hydrosol; BLH: Bottom layer

hydrosol; THL: Top layer hydrosol; Cal: citronellal; PMD_T: Theoretical PMD calculations; S: acid solvent.

After each conversion, the content was transferred to a 250 ml separating funnel and allowed to rest for 30 minutes to allow for separation of the organic and aqueous layers. The aqueous layer was then drained off and the organic layer was washed twice with 60 ml of saturated NaCl. The remaining organic layer was transferred into a 250 ml conical flask. Residues on the walls of the funnel were washed with little anhydrous DeE into the flask and the collected refined oil was carefully concentrated by rotary evaporation.

Generally, the acid-catalyzed cyclization-hydration cascade furnishes a mixture of 4 stereoisomers of PMD (**Scheme 3.4**). The two main and dominant diastereoisomers were (1R, 2S, 5R)-(+/-)-*trans*-PMD (**13b**) and (1S, 2S, 5R)-(+/-)-*cis*-PMD (**13c**), respectively.

GC samples were prepared in the same way as described earlier and were analysed in single injection mode using temperature program M1. The extent of Cal conversion and selectivity for individual products were determined from the percentage integration areas of characteristic peaks in the chromatogram. Assignments were primarily conducted for the various PMD isomers, the PMD acetals, Iso, and Col apart from residual Cal (**Table 3.32**).



Scheme 3.4: Acid catalysed cyclization of citronellal to PMD.

Table 3.32: Composition of refined LSG oils.

Exp	Crude (g)	% Composition										Conv (%)	PMD _{EY}	
		Cal	Iso	Col	Acetals	PMD1	PMD2	PMD3	PMD4	PMD ₁₋₄	(g)		% (w/w)	
37	6.13	7.7	16.1	9.0	2.0	35.5	0.5	18.7	1.3	55.5	92.3	3.40	53.4	
38	7.54	7.8	20.8	8.9	2.3	32.5	0.5	17.7	1.3	51.5	92.2	3.88	60.6	
39	8.97	8.5	11.6	9.1	2.2	37.7	0.6	20.1	1.4	59.8	91.5	5.36	82.0	
40	7.35	8.4	12.4	9.0	2.1	37.4	0.5	19.7	1.3	58.9	91.6	4.33	68.6	
41	6.67	8.5	13.0	9.0	2.1	37.3	0.6	19.7	1.3	58.9	91.5	3.93	62.3	
42	7.09	13.4	11.1	8.8	1.6	32.0	0.6	21.5	1.4	55.5	84.2	3.94	61.3	
43	7.40	49.0	4.3	5.5	0.0	22.3	0.3	11.0	0.6	34.2	51.0	2.53	38.9	
44	6.90	13.4	11.7	8.6	1.5	31.5	0.6	21.1	1.4	54.6	84.2	3.77	59.1	
45	8.02	47.9	4.4	5.5	0.5	23.2	0.3	11.5	0.7	35.7	52.1	2.86	41.5	
46	8.17	11.1	8.5	5.9	2.1	38.2	0.7	24.2	1.6	64.7	88.9	5.29	81.9	
47	7.33	12.5	11.1	8.1	1.4	35.8	0.5	19.6	1.3	57.2	87.5	4.19	65.6	
48	7.57	12.7	8.4	8.1	1.4	37.3	0.6	20.4	1.4	59.7	87.3	4.52	70.2	
49	7.90	44.6	4.4	5.5	0.0	25.4	0.3	12.4	0.7	38.8	55.4	3.06	46.9	

Cal: citronellal; Col: Citronellol; Iso: Isopulegols; Acetals: PMD-acetals; PMD-1: *cis*-PMD 1; PMD-2: *cis*-PMD 2; PMD-3: *trans*-PMD 1; PMD-4: *trans*-PMD 2; PMD_{EY}: PMD experimental yield.

Generally, the conversions ranged from 51.0-92.3%, with no complete consumption of Cal achieved. All experiments with the BL oils showed very low conversions with 51.0-55.4%, except with the BLH acid solvent. Commercial EA oil gave better conversions, but these experiments showed an increase of the Iso compounds.

3.2.5.2. Demonstration-scale conversions

The transfer of the simple acid-catalyzed batch conversion to a demonstration- or semi-pilot scale was followed to develop a practical, sustainable, and reliable production protocol. Initial demonstration-scale experiments were simply based on available equipment, glassware and research environment (**Figure 3.29**).

This approach utilized LSG oil supplied by RE due to its availability in abundance and high citronellal content. A 5 L Schott Duran[®] round bottom glass was used as the reaction vessel. A

large Büchi® water bath (B480) was utilized to regulate the reaction temperature. The reaction mixture was stirred with a mechanical stirrer equipped with a Teflon-coated paddle. The 7-w% citric acid solution was prepared by dissolving 70 g of anhydrous citric acid in 930 g of aqueous medium in a 2 L conical flask and then stirred at RT for 20 minutes. In some experimental cases, the waste hydrosol from the commercial distillation stream was used to prepare the aqueous acid solvent. Approximately 700 g of RE-LSG oil was poured into the 5 L reaction vessel followed by 1 kg of the 7-w% citric acid solution.



Figure 3.29: 5 L demonstration-scale setup.

A series of five conversions was conducted (**Table 3.33**). Except for the first trial experiment, each reaction ran for 15 hours while vigorously stirring at 450 rpm at 50°C. After emptying the reaction vessel into a large separation funnel, the layers were allowed to separate. The top layer was collected as described for the laboratory-scale experiments.

Table 3.33: Conversion parameters for the 5 L scale production of PMD.

Exp	LSG oil		Cal		7% Acid solution				RXN Condition			PMD _T		
	Type	(g)	%	(g)	mol	S	S (g)	CA (g)	CA (mol)	T (°C)	RPM	t (h)	mol	(g)
50	RE	701.2	79.3	556.05	3.60	DW	932.4	69.8	0.36	50	450	20	3.60	621.00
51	RE	705.3	79.3	559.30	3.63	DW	933.1	70.3	0.37	50	450	15	3.63	624.64
52	RE	703.4	79.3	557.80	3.62	DH	931.4	70.5	0.37	50	450	15	3.62	622.95
53	RE	701.5	79.3	556.29	3.61	DW	929.4	71.1	0.37	50	450	15	3.61	621.27
54	RE	705.3	79.3	559.30	3.63	BW	930.8	70.6	0.37	50	450	15	3.63	624.64

Cal: citronellal; PMD_T: Theoretical PMD calculations; S: acid solvent; CA: Citric acid; RE: Rear Earth LSG-oil.

To monitor the reaction progress, samples were taken hourly with a 2 ml graduated pipette and transferred to a 5 ml test tube for analysis. The oil layer and the acidic aqueous layer gradually separated after standing for 20 minutes. About 0.1 g of the top oil layer was taken and prepared for GC analysis by single-mode injection as described earlier. The monitoring process revealed

changes in the quantity of constituents throughout the reaction and was used in the conversion rate assessment.

3.2.5.2.1. Initial demonstration-scale trial

Experiment 50 was performed as the initial trial to assess the performance and suitability of the setup. It utilized DW as solvent for the citric acid solution, ran for 20-hour and only three samples were taken for analysis. The first sample was taken before combining the reactants, and the other two after 15 and 20 hours of operation (**Table 3.34**). At the end of the reaction, 1 L portions of the reaction mixture were transferred to two 2 L separating funnels. The mixtures were allowed to rest for 1-2 hours to allow for the layers to separate. The crude PMD mass partially solidified during this process and the aqueous layer was carefully drained. The funnel was gently heated with a fan to liquify and remove all PMDs. The funnel was rinsed with dry DeE and the residual crude PMD recovered by rotary evaporation. A mass of 684.53 g of the crude product containing 76.8% (corresponding to 477.12 g) of PMDs was obtained. The amounts of *cis*-PMDs (43.6%) were found twice as high as of the *trans*-PMDs (26.1%).

Table 3.34: Monitoring of major constituents for the initial demonstration-scale trial.

t (hrs)	% Composition									Conv (%)	Crude (g)	PMD _{SEY}	
	Cal	Iso	Col	PMD 1	PMD 2	PMD 3	PMD 4	Acetals	PMDs			(g)	% (w/w)
0	83.6	3.7	5.4	0.8	0	0.4	0	0	1.2	0			
15	10.8	5.8	5.5	43	0.7	24.2	1.7	2.2	69.6	87.1	↓	↓	↓
20	10.6	5.2	5.5	42.9	0.7	24.3	1.8	2.3	69.7	87.3	684.53	477.12	76.8

Cal: citronellal; Col: Citronellol; Iso: Isopulegols; Acetals: PMD-acetals; PMD-1: *cis*-PMD 1; PMD-2: *cis*-PMD 2; PMD-3: *trans*-PMD 1; PMD-4: *trans*-PMD 2; PMD_{SEY}: PMD experimental yield; PMDs: all PMD isomers.

GC results (**Table 3.34**) depicted that the simple 5 L setup was able to produce acceptable amounts of PMDs if compared to the 100 ml scale synthesis. It showed a similar extent of citronellal conversion (69.7%) with a slight (2%) increase for the isopulegol isomers.

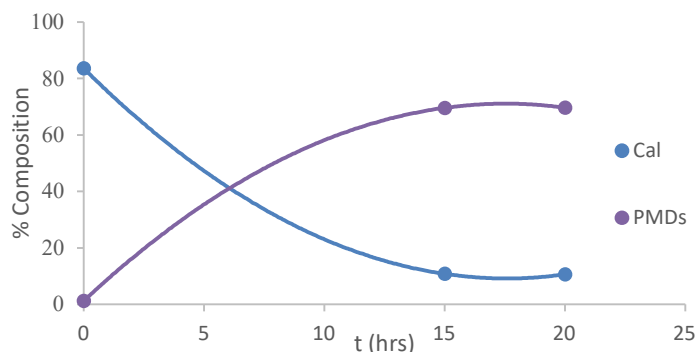


Figure 3.30: Chemical profile of PMDs vs. citronellal over time.

While a 100% conversion of Cal was not achieved according to GC-analysis, the residual amount most likely represented a co-eluting unreactive component of LSG. This mirrors similar observations made during the laboratory-scale experiments (**Table 3.32**). However, both processes differed significantly with respect to the following operation parameters:

1. Difference in the volume of the reaction mixture.
2. Difference in the heat transfer capability of the oil bath and the water bath over 15 hours.
3. Difference in the stirring output of a stirring rod under magnetic and mechanical stirring.

Notably, the Col content was not affected by the reaction, and it remained unreactive. In contrast, the Iso displayed a notable and steady increase after 12 hours before dropping by 0.5% in the last 3 hours (**Figure 3.31**). The acetals were not part of the initial LSG oil matrix, but formed during the course of the reaction. As the acetals are formed from PMD and residual citronellal, their amounts increase steadily while those of the PMD isomers drop at the same time.

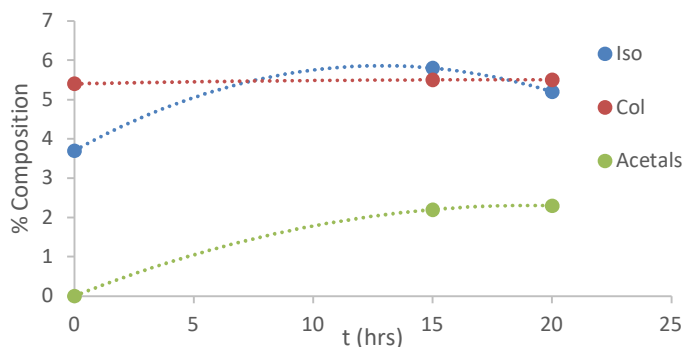


Figure 3.31: Chemical profiles of isopulegols, citronellol and PMD-acetals over time.

3.2.5.2.2. Subsequent demonstration-scale experiment with hourly monitoring

Experiment 51 was conducted as a repetition without drastic manipulation of any reaction parameters. Based on the results from the trial experiment, the reaction time was slightly reduced to 15 hours to minimize the formation of PMD-acetals. The progress of the reaction was monitored hourly by GC-analysis. The crude product was separated from the aqueous acid solution as described before. Approximately 678.21 g of crude product were obtained with slightly reduced total PMD content (74%). Similarly, the amounts of *cis*- and *trans*-PMDs

showed a small drop, probably caused by differences in the mixing efficiencies with the simple mechanical stirrer.

It was found that the reaction reached an approx. 50% conversion of Cal after 5 hours of operation and reached a stable plateau after 10 hours. The final conversion of 87% was in a similar range to that of the trial experiment (**Table 3.34**), although this may be higher due to the suspected co-eluting constituent. The steady decrease in Cal content went in line with corresponding increases in PMD contents and to a lesser extent in Iso amounts (**Figure 3.32**). The amounts of acetal follow-up products remained low with below 3.5%.

Table 3.35: Monitoring of major constituents for the repeat demonstration-scale experiment.

t (hrs)	% Composition									Conv (%)	Crude (g)	PMD _{SEY}	
	Cal	Iso	Col	PMD 1	PMD 2	PMD 3	PMD 4	Acetals	PMDs			(g)	% (w/w)
0	83.3	3.8	5.4	0.8	0.0	0.4	0.0	0.4	1.2	0.0			
1	76.5	4.0	5.4	5.2	0.0	2.7	0.0	0.4	7.9	8.2			
2	66.0	4.1	5.4	11.5	0.2	6.3	0.4	0.5	18.4	20.8			
3	55.8	4.3	5.4	17.4	0.3	9.5	0.7	0.3	27.9	33.0			
4	47.9	4.5	5.5	22.3	0.4	12.2	0.9	0.7	35.8	42.5			
5	40.1	4.7	5.5	26.6	0.4	14.6	1.0	0.6	42.6	51.9			
6	24.7	8.6	5.5	30.7	0.5	17.0	1.2	1.0	49.4	70.3			
7	18.9	9.3	5.5	33.6	0.5	18.6	1.3	1.4	54.0	77.3			
8	14.1	10.0	5.5	35.9	0.6	19.9	1.4	1.7	57.8	83.1	↓	↓	↓
9	11.3	10.2	5.5	37.3	0.6	20.7	1.5	1.9	60.1	86.4			
10	10.3	13.6	5.5	38.7	0.6	21.5	1.6	2.1	62.4	87.6			
11	10.6	10.8	5.5	40.6	0.7	22.4	1.6	2.4	65.3	87.3			
12	10.6	9.5	5.7	40.8	0.7	22.7	1.7	2.5	65.9	87.3			
13	10.7	7.5	5.5	41.2	0.7	23.0	1.6	2.6	66.5	87.2			
14	10.6	7.2	5.5	42.0	0.7	23.4	1.7	2.7	67.8	87.3			
15	10.9	6.7	5.5	42.1	0.7	23.5	1.7	2.8	68.0	86.9			
16	10.8	6.2	5.5	42.0	0.7	23.7	1.7	3.3	68.1	87.0	678.21	461.86	73.9

Cal: citronellal; Col: Citronellol; Iso: Isopulegols; Acetals: PMD-acetals; PMD-1: *cis*-PMD 1; PMD-2: *cis*-PMD 2; PMD-3: *trans*-PMD 1; PMD-4: *trans*-PMD 2; PMD_{EY}: PMD experimental yield; PMDs: combined PMD isomers.

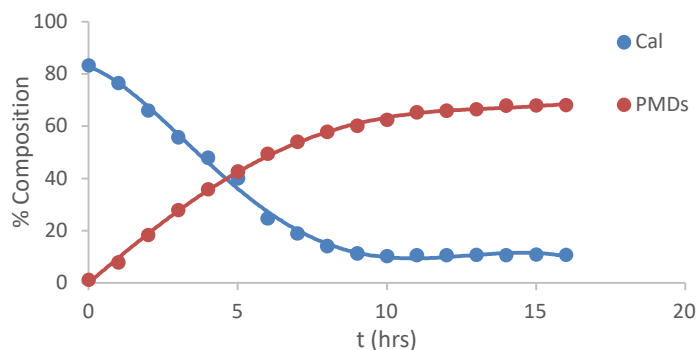


Figure 3.32: Chemical profile of PMDs vs. citronellal over time with hourly monitoring.

A similar trend in composition was observed for Col, and acetals (**Figure 3.33**), while the amounts of isopulegols peaked at 10 hours and dropped off afterwards.

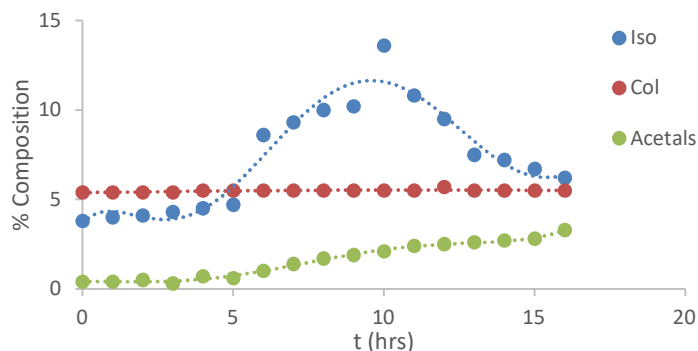


Figure 3.33: Chemical profiles of isopulegols, citronellol and PMD acetals over time.

3.2.5.2.3. Demonstration-scale experiment using hydrosol

Experiment 52 utilized hydrosol (DH) for producing the aqueous acid solution. The DH was obtained from Rare Earth. Approximately 70.5 g of citric acid was dissolved in 931.4 g of hydrosol. In comparison to the previous experiment, the reaction achieved a notably higher conversion of 98 % and additionally produced more PMDs (**Table 3.36** and **Figure 3.34**).

Table 3.36: Monitoring of the demonstration-scale experiment using hydrosol.

t (hrs)	% Composition									Conv (%)	Crude (g)	PMD _{SEY}	
	Cal	Iso	Col	PMD 1	PMD 2	PMD 3	PMD 4	Acetals	PMDs			(g)	% (w/w)
0	83.3	3.8	5.2	0.8	0.0	0.4	0.0	0.0	1.2	0.0			
1	76.5	4.0	5.2	5.2	0.0	2.7	0.0	0.0	7.9	8.2			
2	56.5	9.9	5.2	12.9	0.3	7.1	0.5	0.7	20.8	32.2			
3	44.8	13.5	5.3	19.7	0.3	10.8	0.8	0.0	31.6	46.2			
4	33.1	14.0	5.3	24.8	0.5	13.8	0.5	0.7	39.6	60.3			
5	28.6	14.6	5.3	28.5	0.4	15.8	1.1	0.9	45.8	65.7			
6	20.0	14.3	5.0	31.2	0.6	17.4	1.2	5.5	50.4	76.0			
7	16.6	15.1	5.3	35.1	0.6	19.6	1.4	1.3	56.7	80.1	↓	↓	↓
8	12.5	15.0	5.1	37.4	0.7	20.8	1.5	2.7	60.4	85.0			
9	9.0	15.3	5.2	39.2	0.7	21.9	1.5	2.8	63.3	89.2			
10	6.7	15.5	5.2	40.4	0.7	22.6	1.6	2.4	65.3	92.0			
11	4.9	15.7	5.3	41.3	0.7	23.1	1.6	2.2	66.7	94.1			
12	3.5	15.7	5.2	41.7	0.7	23.4	1.7	3.4	67.5	95.8			
13	2.5	15.5	5.1	41.6	0.7	23.3	1.7	4.9	67.3	97.0			
14	1.9	15.7	5.2	42.3	0.7	23.9	1.7	3.5	68.6	97.7			
15	1.5	15.7	5.2	42.7	0.7	23.9	1.7	3.9	69.0	98.2	688.37	474.98	76.2

Cal: citronellal; Col: Citronellol; Iso: Isopulegols; Acetals: PMD-acetals; PMD-1: *cis*-PMD 1; PMD-2: *cis*-PMD 2; PMD-3: *trans*-PMD 1; PMD-4: *trans*-PMD 2; PMD_{SEY}: PMD experimental yield; PMDs: combined PMD isomers.

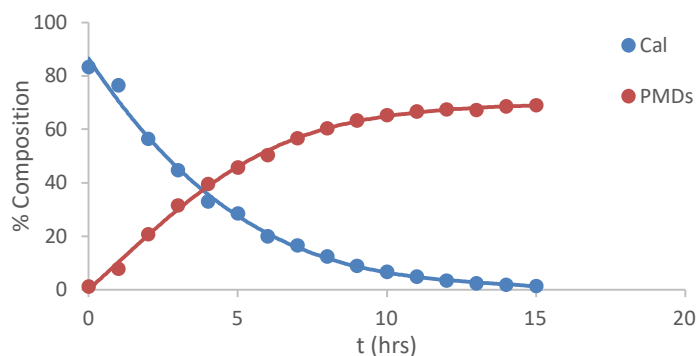


Figure 3.34: Compositions of PMDs vs. citronellal over time using hydrosol.

At the same time, the amounts of Iso and of acetals gradually increased during the course of the reaction. Initially, no acetals but smaller amounts of the Iso and Col were detected in the LSG oil used. The Iso contents rose by 11% while the acetals reached 4% at the end (**Figure 3.35**).

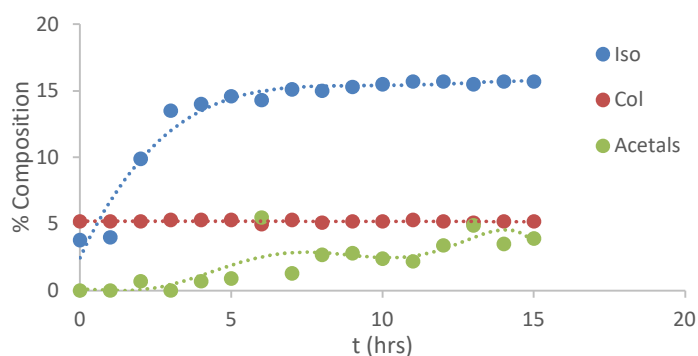


Figure 3.35: Compositions of isopulegols, citronellol and PMD-acetals over time hydrosol.

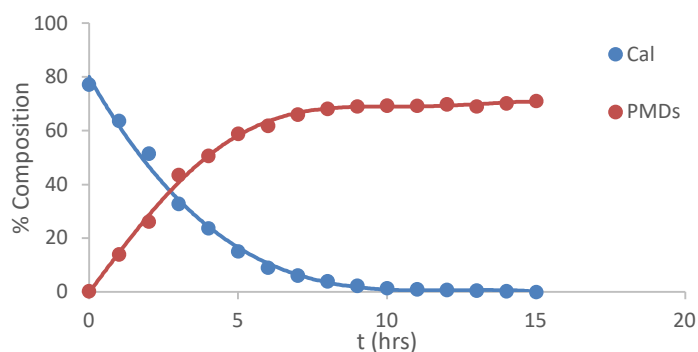
3.2.5.2.4. Demonstration-scale experiment using a recovered acid solution

Although citric acid is inexpensive, it only functions as a catalyst and is not consumed during the reaction. Likewise, PMD and other constituents are partially water-soluble and are thus removed with the aqueous waste stream. PMD-crystals indeed commonly formed on aqueous waste stored in fume cabinets. The previously used citric acid aqueous layer from the second experiment was thus used again. About 893.2 g of the waste acid stream was supplemented with 35.8 g of DW and 71.1 g of citric acid to produce the aqueous solution. Assuming that the acid was fully recovered from the previous experiment an approximately 14-w% concentration was achieved. Interestingly, Experiment 53 achieved complete conversion of citronellal to PMDs with a total PMD content of 79% (**Table 3.37** and **Figure 3.36**).

Table 3.37: Monitoring of major constituents for the demonstration-scale experiment using recovered acidic solution.

t (hrs)	% Composition									Conv (%)	Crude (g)	PMD _{SEY}	
	Cal	Iso	Col	PMD 1	PMD 2	PMD 3	PMD 4	Acetals	PMDs			(g)	% (w/w)
0	77.2	11.2	5.4	0.0	0.0	0.4	0.0	0.0	0.4	0.0			
1	63.7	11.7	5.3	9.0	0.0	4.7	0.3	0.0	14.0	17.5			
2	51.5	12.5	5.2	16.6	0.2	8.8	0.6	0.0	26.2	33.2			
3	32.8	13.8	5.2	27.4	0.4	14.8	1.0	0.0	43.6	57.5			
4	23.7	14.4	5.4	31.6	0.6	17.3	1.2	0.0	50.7	69.3			
5	15.1	15.0	5.3	36.8	0.6	20.1	1.4	0.8	58.9	80.4			
6	9.1	15.0	5.1	38.6	0.6	21.2	1.5	4.4	61.9	88.2			
7	6.2	15.6	5.3	41.1	0.7	22.7	1.6	2.1	66.1	92.0			
8	4.1	15.8	5.3	42.5	0.7	23.4	1.6	1.9	68.2	94.7			
9	2.4	15.8	5.4	43.0	0.7	23.8	1.6	2.3	69.1	96.9			
10	1.5	15.8	5.4	43.2	0.7	23.9	1.6	3.0	69.4	98.1			
11	1.0	15.6	5.4	43.2	0.7	23.8	1.6	4.0	69.3	98.7			
12	0.8	15.8	5.4	43.5	0.7	24.0	1.6	3.2	69.8	99.0			
13	0.6	15.8	5.3	43.1	0.7	23.7	1.6	4.0	69.1	99.2			
14	0.4	15.6	5.3	43.6	0.7	24.2	1.7	3.6	70.2	99.5	↓	↓	↓
15	0.0	15.7	5.4	44.2	0.7	24.5	1.7	2.9	71.1	100.0	692.41	492.30	79.2

Cal: citronellal; Col: Citronellol; Iso: Isopulegols; Acetals: PMD-acetals; PMD-1: *cis*-PMD 1; PMD-2: *cis*-PMD 2; PMD-3: *trans*-PMD 1; PMD-4: *trans*-PMD 2; PMD_{EY}: PMD experimental yield; PMDs: combined PMD isomers.

**Figure 3.36:** Chemical profile of PMDs vs. citronellal over time using recovered acidic solution.

There was also a gradual increase in the amounts of Iso and acetals observed as shown in **Figure 3.37**.

Chapter 3 – Results

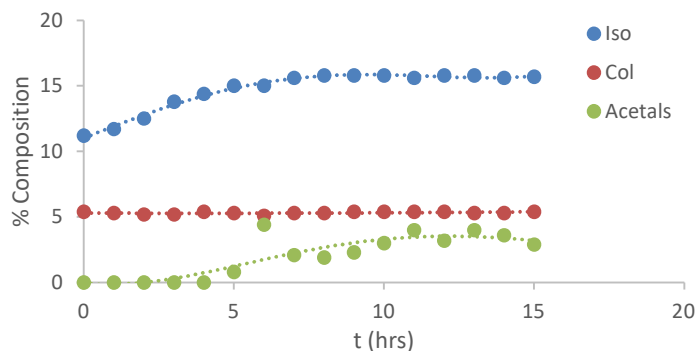


Figure 3.37: Chemical profiles of isopulegols, citronellol and PMD acetals over time using recovered acidic solution.

3.2.5.2.5. Demonstration-scale experiment using distilled boiler water

The commercial producer of LSG oil also supplied about 20 L of boiler water (DBW) from a recent harvest and distillation. This was investigated in Experiment 54 as a potential resource for the aqueous process stream.

Table 3.38: Monitoring of major constituents for the demonstration-scale experiment using distilled boiler water.

t (hrs)	% Composition									Conv (%)	Crude (g)	PMD _{SEY}	
	Cal	Iso	Col	PMD 1	PMD 2	PMD 3	PMD 4	Acetals	PMDs			(g)	(w/w)
0	73.9	11.0	4.9	0.0	0.0	0.4	0.0	4.0	0.4	0.0			
1	63.1	10.8	4.8	5.9	0.0	3.1	0.2	0.0	9.2	14.6			
2	58.5	12.5	5.2	11.8	0.2	6.4	0.4	0.0	18.8	20.8			
3	44.4	12.0	4.8	16.0	0.2	8.8	0.6	0.0	25.6	39.9			
4	39.8	13.8	5.3	22.7	0.3	12.5	0.7	0.0	36.2	46.1			
5	31.8	14.1	5.3	26.9	0.4	14.9	1.0	0.8	43.2	57.0			
6	25.0	15.5	5.3	30.6	0.6	17.0	1.2	1.0	49.4	66.2			
7	20.0	14.9	5.3	33.3	0.6	18.6	1.3	1.1	53.8	72.9			
8	15.4	15.8	5.3	35.6	0.6	19.9	1.4	1.8	57.5	79.2			
9	12.2	16.1	5.3	37.2	0.7	20.8	1.5	2.3	60.2	83.5			
10	9.9	15.6	5.5	38.2	0.7	21.4	1.5	2.4	61.8	86.6			
11	7.0	15.5	5.3	39.7	0.7	22.4	1.6	2.8	64.4	90.5			
12	5.3	15.6	5.3	40.6	0.7	22.8	1.6	3.3	65.7	92.8			
13	4.0	15.6	5.3	41.2	0.7	23.1	1.6	3.8	66.6	94.6			
14	3.1	15.7	5.3	41.6	0.7	23.4	1.7	3.8	67.4	95.8			
15	2.4	15.6	5.3	41.8	0.7	23.4	1.7	4.2	67.6	96.8	↓	↓	↓

Cal: citronellal; Col: Citronellol; Iso: Isopulegols; Acetals: PMD-acetals; PMD-1: *cis*-PMD 1; PMD-2: *cis*-PMD 2; PMD-3: *trans*-PMD 1; PMD-4: *trans*-PMD 2; PMD_{EY}: PMD experimental yield; PMDs: combined PMD isomers.

Approximately 3 L were transferred to a 5 L flask and distilled. After five hours, 2 L of clear distillate were collected and used to prepare the citric acid solution for the demonstration-scale

conversion. The experimental results and conversion profiles for selected components are shown in **Table 3.38**, **Figure 3.38** and **Figure 3.39**, respectively. Similar trends and results were observed as in previous experiments.

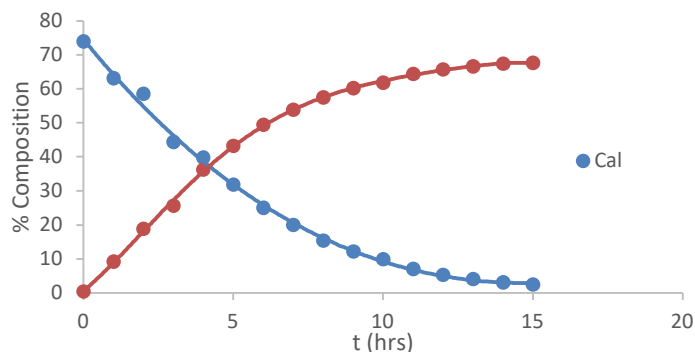


Figure 3.38: Chemical profile of PMDs vs. citronellal over time using distilled boiler water.

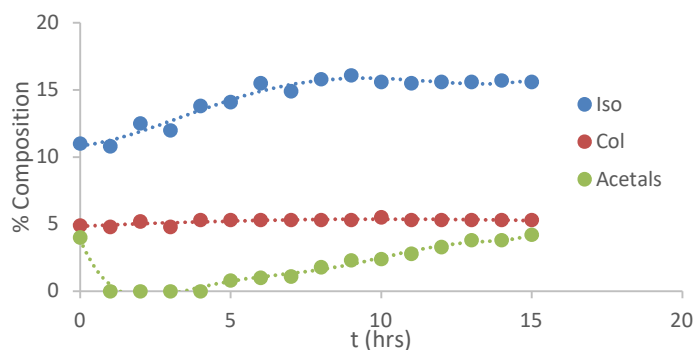
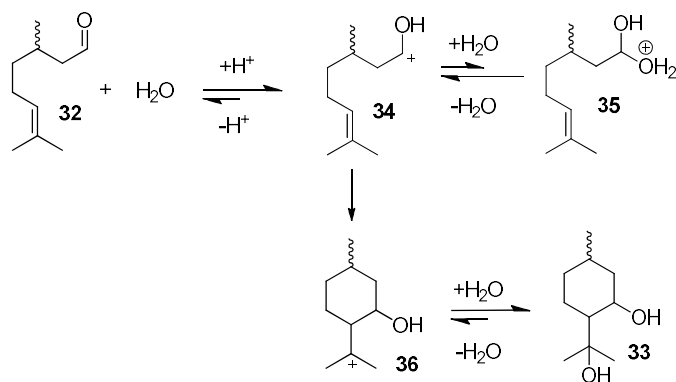


Figure 3.39: Chemical profiles of isopulegols, citronellol and PMD acetals over time using distilled boiler water.

3.2.5.3. Conversion kinetics of the demonstration-scale experiments

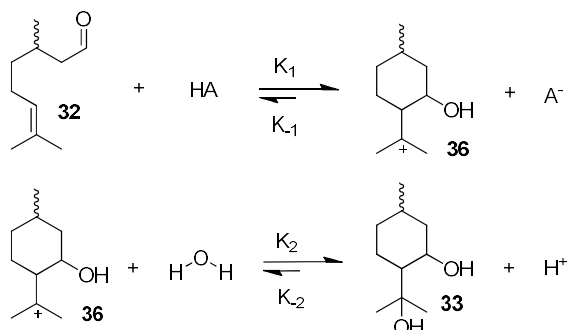
3.2.5.3.1. Deriving kinetic parameters

The transformation of Cal to PMD involves a hydration reaction incorporating a protonated intermediate (**Scheme 3.5**). Protonation and hydrolysis of the aldehyde are highly reversible due to the formed protonated geminal diol (hydrate). This is primarily due to the general instability of hydrates, which readily undergo dehydrogenation. The reformed protonated intermediate is short-lived due to its affinity to the neighbouring nucleophilic vinyl group. As shown in the mechanistic scenario below, subsequent bond formation establishes a hexacyclic carbocationic intermediate that accepts water and undergoes further deprotonation to form PMD.



Scheme 3.5: Plausible mechanism and subsequent intermediates involved in the reaction.

Acid catalyst provides sufficient hydrogen ions (H^+) that initiate swift electron withdrawal of the carbonyl carbon and a quicker transition to the primary intermediate (PI, **34**). Follow-on transition via cyclization of **34** to the more stable secondary intermediate (SI, **36**) generally occurs instantly (**Scheme 1.6** and **Scheme 3.5**).



Scheme 3.6: The two plausible rate-determining steps of the reaction.

Observation of the reaction profiles suggest that the conversion of citronellal to the various PMDs occurs quickly. This is due to the acid-catalyzed reaction and suggests that **36** is formed at the same rate as it is transformed to PMD-2 **33**. Consequently, this suggests exploring steady-state approximation.

$$\frac{d[SI]}{dt} = 0 = k_1[Cal][HA] - k_{-1}[SI][A^-] - k_2[SI][H_2O], \quad [H_2O] \text{ in excess}$$

Equation 3.4: Steady state expression of the production and loss of **12**.

$$\therefore [SI] = \frac{k_1[Cal][HA]}{k_{-1}[A^-] + k_2}$$

Equation 3.5: Rearranging to make [SI] subject.

$$\frac{d[PMD]}{dt} = k_2[SI] = k_2 \frac{k_1[Cal][HA]}{k_{-1}[A^-] + k_2}, \quad \text{assuming } k_2 \gg k_{-1}[A^-]$$

Equation 3.6: General expression of rate of synthesis of PMD.

$$\therefore \frac{d[\text{PMD}]}{dt} = k_1[\text{Cal}][\text{HA}] = -\frac{d[\text{Cal}]}{dt}$$

Equation 3.7: Expression of the rate of formation of PMD 2.

The steady-state approximation cannot be applied in deriving the reaction rates due to the use of biomass-based starting material (RE-LSG oil). Cal in LSG oils is accompanied by several other minor constituents, particularly the Iso and to a lesser extent PMDs and PMD acetals. In addition, the chemical matrix of different LSG oils varies which is a disadvantage for consistency and repeatability. The formation of different PMD isomers during the conversion and their subsequent transformations to PMD acetals adds to this complication. Due to these limitations, the general reaction kinetics is considered to determine the rate of each conversion. In fact, the reaction temperature and citric acid concentration used through all conversions are identical, which suits this change. The reaction utilizes excess water and so requires the use of a pseudo-rate constant equation. In addition, the formation of PMD acetals results in losses in the PMD produced and thus would not be reliable to determine the rate of PMD formation. Therefore, the rate for the conversion of Cal is considered instead.

$$-\frac{d[\text{Cal}]}{dt} = k[\text{Cal}]^x [\text{H}_2\text{O}]^y, \quad [\text{H}_2\text{O}] \text{ in excess}$$

Equation 3.8: Differential rate expression for the conversion of Cal.

$$-\frac{d[\text{Cal}]}{dt} = k'[\text{Cal}]^x$$

Equation 3.9: Differential rate expression with pseudo rate constant.

$$\text{a) } \ln[\text{Cal}] = \ln[\text{Cal}]_0 - k't$$

$$\text{b) } \frac{1}{[\text{Cal}]} = \frac{1}{[\text{Cal}]_0} + k't$$

Equation 3.10: Integrated first order (a) and second order (b) reactions.

3.2.5.4. Comparing the kinetics for demonstration-scale experiments

The second experiment was chosen as it was thoroughly monitored and did not introduce any organic compounds through its water source. The reaction thus serves as the reference for the other experiments. Graphs based on first and second reaction orders were constructed and assessed to determine the order of reaction with respect to Cal conversion (**Table 3.39**). The amount of citronellal used was taken from its integrated peak-area percentage as determined by hourly GC analysis.

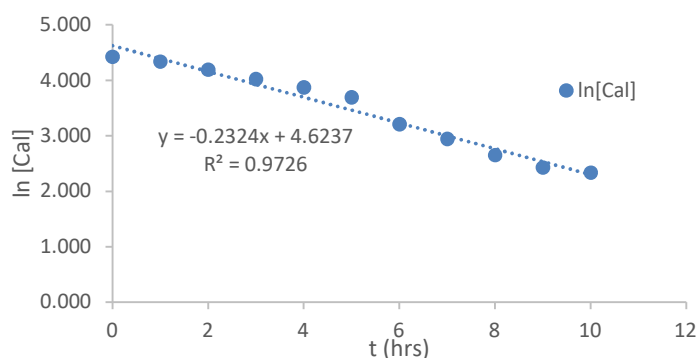
Table 3.39: Reaction order data calculations.

t (hrs)	Exp 51			Exp 52		Exp 53		Exp 54	
	Cal%	ln[Cal]	1/[Cal]	Cal%	ln[Cal]	Cal%	ln[Cal]	Cal%	ln[Cal]
0	83.3	4.422	0.012	83.3	4.422	77.2	4.346	73.9	4.303
1	76.5	4.337	0.013	76.5	4.337	63.7	4.154	63.1	4.145
2	66.0	4.190	0.015	56.5	4.034	51.5	3.942	58.5	4.070
3	55.8	4.022	0.018	44.8	3.802	32.8	3.490	44.4	3.793
4	47.9	3.869	0.021	33.1	3.500	23.7	3.165	39.8	3.684
5	40.1	3.691	0.025	28.6	3.353	15.1	2.715	31.8	3.460
6	24.7	3.207	0.040	20.0	2.996	9.1	2.208	25.0	3.219
7	18.9	2.939	0.053	16.6	2.809	6.2	1.825	20.0	2.996
8	14.1	2.646	0.071	12.5	2.526	4.1	1.411	15.4	2.734
9	11.3	2.425	0.088	9.0	2.197	2.4	0.875	12.2	2.501
10	10.3	2.332	0.097	6.7	1.902	1.5	0.405	9.9	2.293
11	10.6	2.361	0.094	4.9	1.589	1.0	0.000	7.0	1.946
12	10.6	2.361	0.094	3.5	1.253	0.8	-0.223	5.3	1.668
13	10.7	2.370	0.093	2.5	0.916	0.6	-0.511	4.0	1.386
14	10.6	2.361	0.094	1.9	0.642	0.4	-0.916	3.1	1.131
15	10.9	2.389	0.092	1.5	0.405	0.0	UD	2.4	0.875
16	10.8	2.380	0.093	ND	ND	ND	ND	ND	ND

Cal: Citronellal; ND: not done; UD: Undetermined

A plot assuming first-order kinetics (**Figure 3.40**) was derived from data obtained during the first ten hours of the reaction during which distinct changes in citronellal concentration and optimum stable were achieved. The plot of $\ln [\text{Cal}]$ vs t showed a strong relationship of change in $[\text{Cal}]$ with time. This was supported by a regression correlation value of 0.97.

The second-order plot derived from the same dataset (**Figure 3.41**) revealed a very poor correlation of $1/[\text{Cal}]$ vs t . It was observed that the data points inclined more to a quadratic expression than a linear plot. Subsequently, its poor correlation regression value of 0.89 confirmed that the reaction did not follow second-order kinetics.

**Figure 3.40:** First order plot of Experiment 51.

Chapter 3 – Results

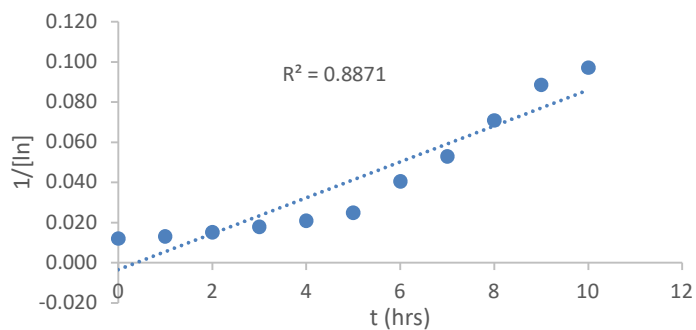


Figure 3.41: Second order plot of Experiment 51.

Based on this, all other experiments were likewise plotted as first-order kinetic plots and the resulting graphs are shown in **Figure 3.42**, **Figure 3.43** and **Figure 3.44**, respectively.

The rate constant determines the rate of each conversion. The comparison of k' -values in **Table 3.40** shows that experiment 53 has the condition kinetically favourable for laboratory-scale conversion.

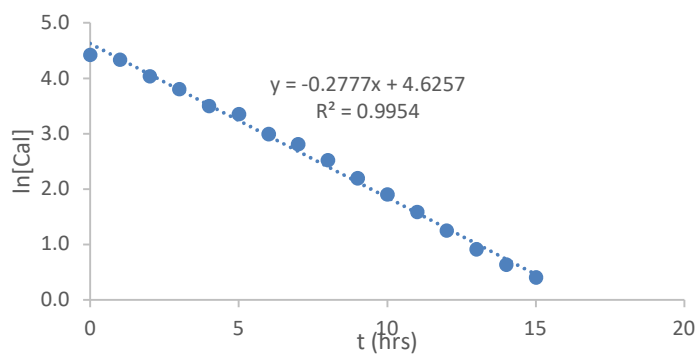


Figure 3.42: First-order plot of Experiment 52.

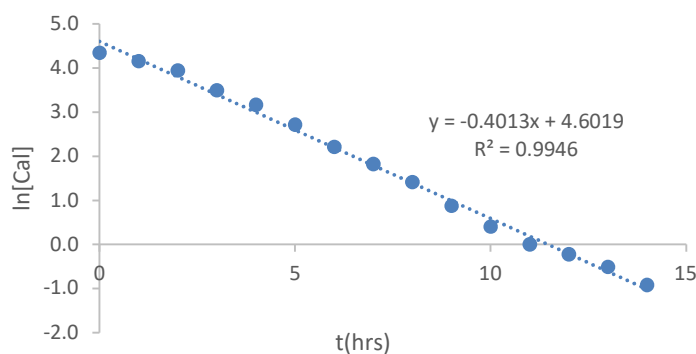


Figure 3.43: First-order plot of Experiment 53.

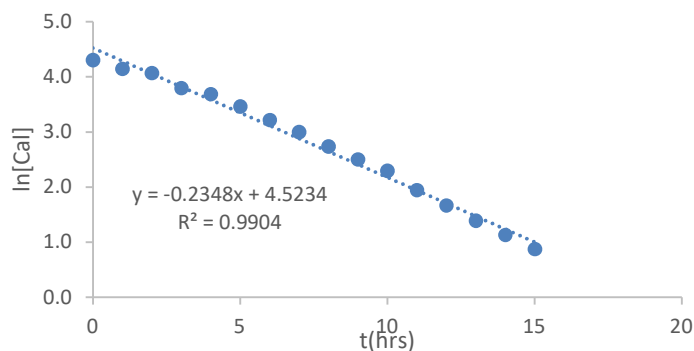


Figure 3.44: First-order plot of Experiment 54.

Table 3.40: Comparison of k' - and R^2 -values.

Constants	Experiments			
	51	52	53	54
k' (s^{-1})	0.2324	0.0439	0.4013	0.2348
R^2 (%)	97.26	99.54	99.46	99.04

3.2.5.5. Technical-scale conversions

3.2.5.5.1. Analysis of commercial LSG oil

Commercial LSG oil supplied by Rare Earth was used for technical-scale (10 L) conversions. Chemical compositions vary with each harvest and distillation. Therefore, the identity and amount of the major constituents was established by GC-analysis before any conversions were conducted (**Figure 3.45**). For earlier Experiments, the identification of individual components was based on retention times compared to reference standards. In this analysis, identification was confirmed by comparison of retention index values instead.

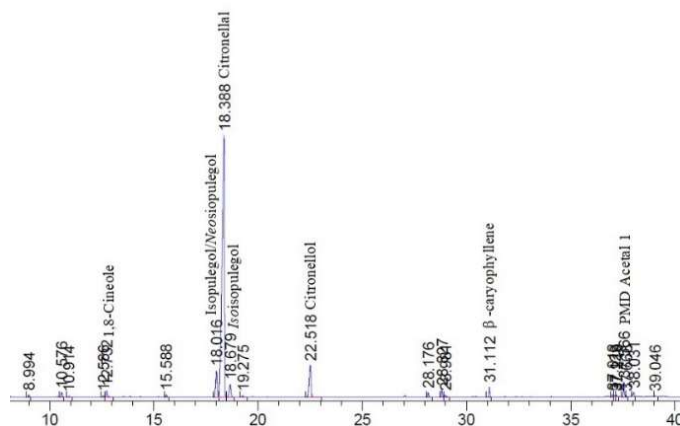


Figure 3.45: GC-chromatogram of the first batch of commercial LSG oil used for bulk synthesis.

Retention index values were calculated using **Equation 3.3**, the non-isothermal Kovats index equation. The retention times (R_t) of individual peaks of a C₈-C₂₀ alkane standard solution (Sigma) were used to calculate the RI of the major constituents of LSG oil obtained from RE (**Table 3.41**). The major constituents of interest were those with a peak area percentage of $\geq 1\%$.

Table 3.41: Assignments of main constituents in commercial LSG oil.

R_t (min)		KI (RI)		Composition (%)		Compound
1	2	1	2	1	2	
12.73	12.70	1035.20	1034.45	1.11	1.06	1,8-Cineole ^a
18.01	17.97	1147.83	1146.90	4.96	5.30	Neo-Iso
18.39	18.33	1155.15	1153.79	74.81	72.91	Cal
18.68	18.63	1160.69	1159.51	2.75	3.07	Iso-Iso ^a
22.52	22.46	1230.42	1229.30	6.78	5.79	Col
31.11	37.55	1436.82	1959.57	1.03	2.26	β -Caryophyllene ^a
37.57	38.74	1961.63	N/A	1.55	2.54	PMD Acetal 1 ^b

R_t: Run time; RI: Retention index; ^aPartially identified by literature and reference material based on R_t/RI¹⁷²;

^bIdentified by synthesized in-house reference; KI: Kovats retention index (RI).

3.2.5.5.2. Reaction parameters and reactor setup

A commercial benchtop Brunswick BioFlo[®] 310 fermenter with a vessel capacity of 14 L was used as the reactor. The sparger and harvest tube were connected to the head plate through their specific ports. A steel agitation drive shaft with two six-plate impellers was mounted onto the head plate. A metal baffle accessory was placed inside the reaction vessel. The head plate was held with screw bolts. The reaction temperature was monitored with a temperature probe inserted through the head plate's thermowell/RTD port. All connecting cables were attached to the main control unit at the back cabinet rear panel.

The 7-w% citric acid solution and LSG oil for subsequent conversion were prepared separately. The citric acid solution was prepared by dissolving 329 g of citric acid in three parts in 1.5 kg of DW each. This mixture was stirred in a 2 L conical flask at 40-50°C to achieve thorough acid dissolution. Approximately 3.7 kg of commercial LSG oil and 4.7 kg of citric acid solution were used, resulting in a total mass input of 8.0 kg. A total of three technical-scale reactions were completed (**Table 3.42**).

A funnel was inserted into the reaction vessel's head plate via the harvest port. The LSG oil was then poured into the reaction vessel followed by the combined 7-w%-citric acid solution. The funnel was then removed, and an exhaust condenser was connected to the exhaust port to minimize evaporation losses during operation. Due to the immiscibility of the liquids and the

mass of the mixture, the agitation speed was set at 1000 rpm to maintain a stable emulsion (**Figure 3.46**).

Table 3.42: Reaction parameters of the technical-scale conversions.

Exp	LSG oil		Cal		7-w% Acid solution			RXN Condition			PMD _T			
	Type	(kg)	%	(kg)	mol	S	S (kg)	CA (kg)	CA (mol)	T (°C)	rpm	t (hrs)	mol	(kg)
55	RE	3.67	72.19	2.65	17.16	DW	4.51	0.34	1.76	50	1000	15	17.16	2.96
56	RE	3.67	73.51	2.70	17.47	DW	4.84	0.36	1.89	50	1000	15	17.47	3.01
57	RE	3.61	73.04	2.64	17.11	DW	4.77	0.36	1.87	50	1000	15	17.11	2.95
Mean		3.65	72.91	2.66	17.25		4.71	0.35	1.84	50	100	15	17.25	2.97

Cal: citronellal; PMD_T: Theoretical PMD calculations; S: acid solvent; CA: Citric acid; RE: Rear Earth LSG-oil.



Figure 3.46: Initial LSG oil-water layers and generation of a stable emulsion.

The reaction temperature was set at 50°C. The conversions of all three reactions were monitored by GC-analysis over a period of 15 hours. The theoretical yield of PMD by mass was calculated based on the reaction stoichiometry and initial amount of citronellal in the LSG oil used.

3.2.5.5.3. Conversion profiles and reaction kinetics

GC-analysis showed similar trends to those observed for the corresponding demonstration-scale experiments (Experiments 50-54). The conversion of citronellal to PMDs was fluent in Experiment 55 (**Table 3.43** and **Figure 3.47**) and reached a high value of 99.4% and an experimental yield of PMD of 92.7%.

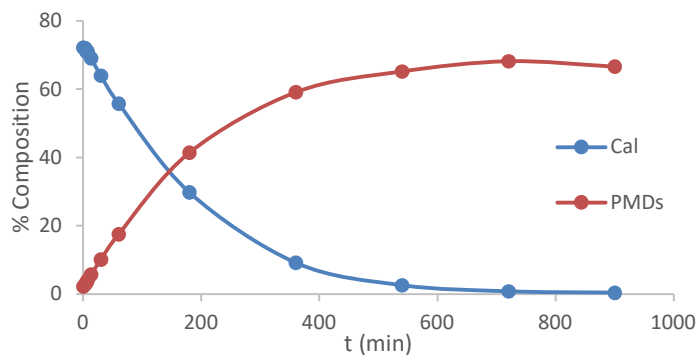
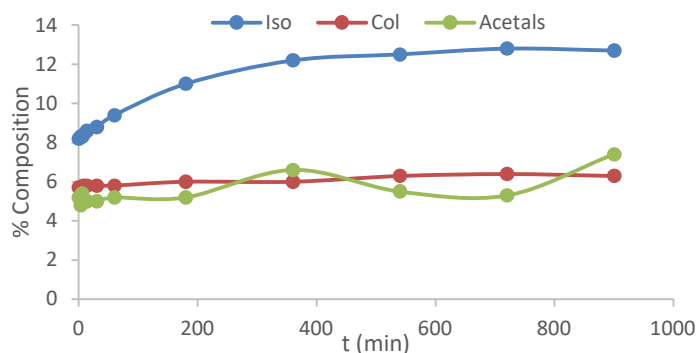
There was a gradual increase in the composition of Iso from 8.2% to 12.7% during the reaction (**Figure 3.48**). The amount of Col also increased slightly from 5.7% to 6.3% , suggesting concentration effects by evaporation. The amounts of PMD acetals increased slightly from 5.2% to 7.4%.

A perfect fit for a first-order reaction was obtained from the analytical data (**Figure 3.49**).

Table 3.43: Monitoring of major constituents for technical-scale Experiment 55.

t (min)	Composition (% , ±0.2)									Conv (%)	Crude (kg)	PMD _{SEY}	
	Cal	Iso	Col	PMD 1	PMD 2	PMD 3	PMD 4	Acetals	PMDs			(kg)	% (w/w)
0	72.2	8.2	5.7	0.8	0.0	1.0	0.4	5.2	2.2	0.0	↓	↓	↓
3.5	72.0	8.3	5.7	1.2	0.0	1.0	0.7	4.8	2.9	0.3			
5.5	70.9	8.3	5.7	1.5	0.0	1.0	0.9	5.4	3.4	1.8			
7.5	71.0	8.4	5.8	2.0	0.0	1.0	1.1	5.0	4.1	1.7			
13.5	69.1	8.6	5.8	3.0	0.0	1.0	1.7	5.0	5.7	4.3			
30	64.0	8.8	5.8	5.7	1.0	3.2	0.2	5.0	10.1	11.4			
60	55.8	9.4	5.8	10.3	1.0	5.8	0.4	5.2	17.5	22.7			
180	29.8	11.0	6.0	24.9	1.4	14.1	1.0	5.2	41.4	58.7			
360	9.2	12.2	6.0	35.8	1.6	20.2	1.5	6.6	59.1	87.3			
540	2.6	12.5	6.3	39.6	1.6	22.4	1.6	5.5	65.2	96.4			
720	0.8	12.8	6.4	41.4	1.7	23.4	1.7	5.3	68.2	98.9			
900	0.4	12.7	6.3	40.4	1.7	22.8	1.7	7.4	66.6	99.4	4.118	2.74	92.7

Cal: citronellal; Col: Citronellol; Iso: Isopulegols; Acetals: PMD-acetals; PMD-1: *cis*-PMD 1; PMD-2: *cis*-PMD 2; PMD-3: *trans*-PMD 1; PMD-4: *trans*-PMD 2; PMD_{EY}: PMD experimental yield; PMDs: combined PMD isomers.

**Figure 3.47:** Chemical profile of PMDs and citronellal in Experiment 55.**Figure 3.48:** Profile of the isopulegols, citronellol and PMD acetals during Experiment 55.

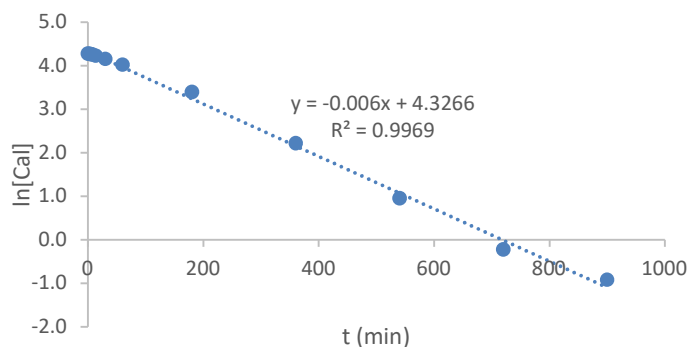


Figure 3.49: First order plot of Experiment 55.

Likewise, the conversion of Cal to the desired PMD isomers went smoothly in Experiment 56. Under identical conditions, the reaction achieved a high conversion of 99.5% and an experimental yield of PMD of 92.7% (**Table 3.44**).

Table 3.44: Monitoring of major constituents for technical-scale Experiment 56.

t (min)	Composition (% , ±0.2)									Conv (%)	Crude (kg)	PMD _{EY}	
	Cal	Iso	Col	PMD 1	PMD 2	PMD 3	PMD 4	Acetals	PMDs			(kg)	% (w/w)
0	73.5	8.4	5.9	0.7	0.0	1.0	0.4	4.0	2.1	0.0			
3.5	71.2	8.3	5.7	1.3	0.0	1.0	0.8	4.7	3.1	3.1			
7.5	70.0	8.3	5.8	2.0	0.0	1.0	1.2	4.9	4.2	4.8			
13.5	68.2	8.5	5.7	3.0	0.0	1.0	1.7	5.5	5.7	7.2			
30	64.0	8.9	5.8	5.7	1.0	3.2	0.2	5.9	10.1	12.9			
60	55.7	9.4	5.8	10.3	1.2	5.8	0.4	4.7	17.7	24.2	↓	↓	↓
180	29.4	10.8	6.0	24.7	1.4	13.9	1.0	5.0	41.0	60.0			
360	9.3	13.9	6.2	35.7	1.6	20.2	1.5	5.7	59.0	87.3			
540	2.8	12.7	6.5	40.5	1.7	22.9	1.7	5.2	66.8	96.2			
720	0.9	12.8	6.5	41.6	1.7	23.5	1.7	5.3	68.5	98.8			
900	0.4	12.9	6.4	40.7	1.6	23.0	1.7	5.9	67.0	99.5	3.924	2.63	87.3

Cal: citronellal; Col: Citronellol; Iso: Isopulegols; Acetals: PMD-acetals; PMD-1: *cis*-PMD 1; PMD-2: *cis*-PMD 2; PMD-3: *trans*-PMD 1; PMD-4: *trans*-PMD 2; PMD_{EY}: PMD experimental yield; PMDs: combined PMD isomers.

The conversion profiles of starting material, product and the main constituents (**Figure 3.50** and **Figure 3.51**) and the kinetic profile for Cal conversion (**Figure 3.52**) behaved similarly.

Analysis of the GC-data from additional repetition runs (Experiments 57 and 58) revealed similar trends to those observed before. The conversion rate for Cal to PMDs was again high for Experiment 57 with a value of 99.4%, with an experimental yield of PMD of 92.7% (**Table 3.45**). The changes in compositions for citronellal, the PMD isomers and the other main constituents (**Figure 3.53** and **Figure 3.54**) as well as the kinetic profile (**Figure 3.55**) behaved similarly.

Chapter 3 – Results

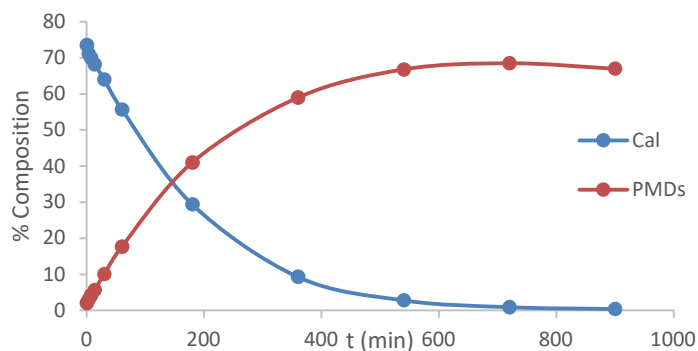


Figure 3.50: Chemical profile of PMDs and citronellal in Experiment 56.

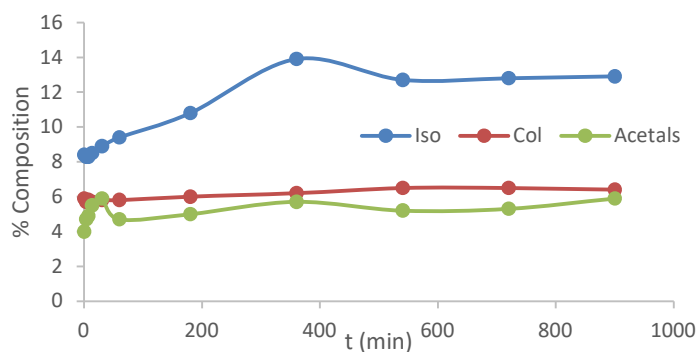


Figure 3.51: Profile of the isopulegols, citronellol and PMD-acetals during Experiment 56.

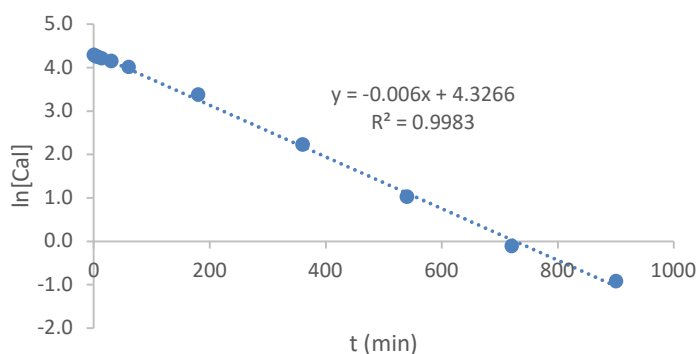


Figure 3.52: First order plot for Experiment 56.

Table 3.45: Monitoring of major constituents for technical-scale Experiment 57.

t (min)	Composition (% , ±0.2)									Conv (%)	Crude (kg)	PMD _{SEY}	
	Cal	Iso	Col	PMD 1	PMD 2	PMD 3	PMD 4	Acetals	PMDs			(kg)	% (w/w)
0	73.0	8.4	5.8	0.8	0.0	1.0	0.4	5.3	2.2	0.0			
3.5	71.9	8.3	5.8	1.3	0.0	1.0	0.8	4.4	3.1	1.5			
7.5	70.4	8.4	5.8	2.0	0.0	1.0	1.2	5.0	4.2	3.6			
13.5	68.5	8.5	5.8	3.0	0.0	1.0	1.8	4.9	5.8	6.2	↓	↓	↓
30	63.5	8.8	5.8	5.8	1.0	3.3	0.2	5.3	10.3	13.0			
60	55.6	9.4	5.9	10.5	1.2	6.0	0.4	4.7	18.1	23.8			

Chapter 3 – Results

180	29.1	10.9	5.9	25.0	1.4	14.1	1.0	5.6	41.5	60.1			
360	9.3	12.6	6.2	37.0	1.6	20.9	1.6	4.7	61.1	87.3			
540	2.5	12.6	6.3	39.5	1.7	22.4	1.6	6.5	65.2	96.6			
720	0.9	12.8	6.6	40.8	1.7	23.0	1.7	5.3	67.2	98.8			
900	0.4	12.8	6.4	41.0	1.7	23.2	1.7	5.4	67.6	99.5	4.657	3.15	104.6

Cal: citronellal; Col: Citronellol; Iso: Isopulegols; Acetals: PMD-acetals; PMD-1: *cis*-PMD 1; PMD-2: *cis*-PMD 2; PMD-3: *trans*-PMD 1; PMD-4: *trans*-PMD 2; PMD_{EY}: PMD experimental yield; PMDs: combined PMD isomers.

A comparison of the rate constant (k') for all three technical-scale conversions is shown in **Table 3.46**.

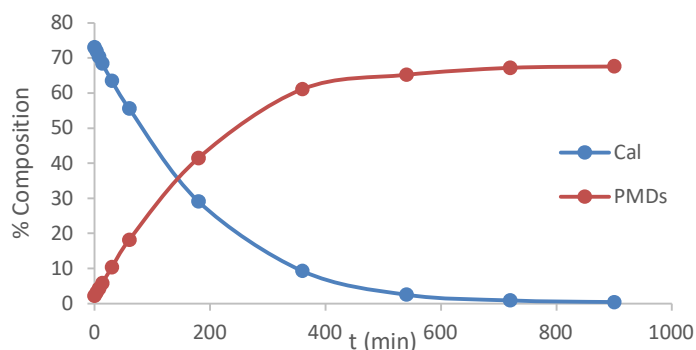


Figure 3.53: Chemical profile of PMDs and citronellal in Experiment 57.

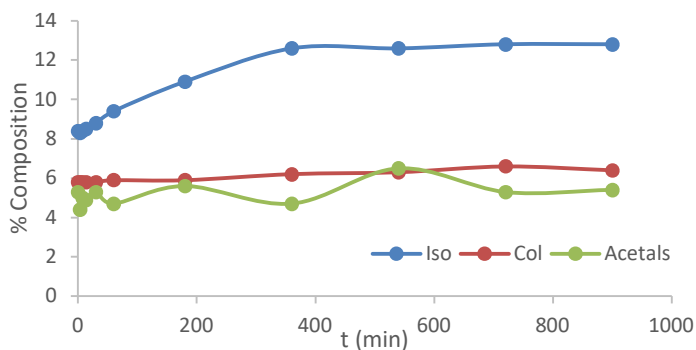


Figure 3.54: Profile of the isopulegols, citronellol and PMD acetals during Experiment 57.

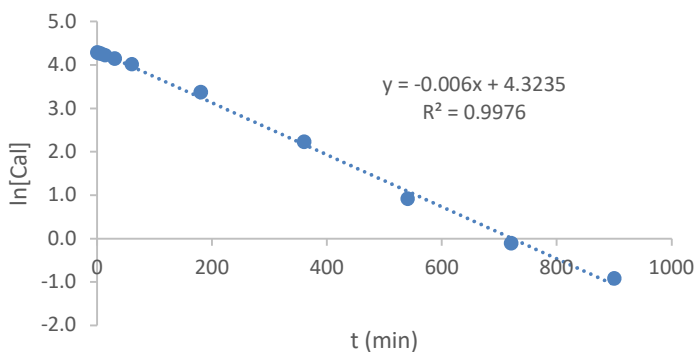


Figure 3.55: First order plot of Experiment 57.

Table 3.46: Comparison of k' and R^2 -values for Experiments 55-57.

Constants	Experiments		
	55	56	57
k' (s^{-1})	0.0060	0.0060	0.0060
R^2 (%)	99.69	99.83	99.76

3.2.6. Separation of PMD stereoisomers

The isolating of all four stereoisomers of PMD from the crude product was challenging due to the presence of Iso, PMD-acetals, and other minor constituents. All GC-analyses revealed two major PMD-stereoisomers (**Figure 3.56**), accompanied by two minor ones. Each of these minor compounds appeared approx. 0.3 min after the respective major peaks and were thus suspected to represent their respective diastereoisomer. Nevertheless, the two dominant diastereoisomers were readily isolated by recrystallization followed by vacuum distillation.

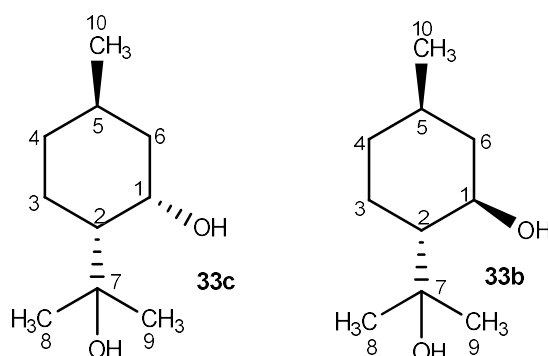


Figure 3.56: Structures of main isomers of PMD, (1S, 2S, 5R)-(+/-)-*cis*-PMD (**33c**) and (1R, 2S, 5R)-(+/-)-*trans*-PMD (**33b**).

3.2.6.1. Recrystallization

3.2.6.1.1. PMD synthesis using neat citronellal

To avoid the presence of interfering components and hence increase the chances of isolating pure fractions of the major *cis*- and *trans*-PMD isomers, a batch of PMD was synthesized using synthetic Cal with >90% purity (**Table 3.47**). To achieve this, an emulsion of 45.012 g of Cal and 64.019 g of 7-w% citric acid solution was stirred at 750 rpm at 50°C for 16 hours. The organic layer was separated and washed twice with 40 ml of brine solution. The organic material was dissolved in 100 ml DeE and dried with anhydrous Na_2SO_4 , followed by rotary evaporation to give 45.554 g of crude product.

GC-analysis of the product revealed a conversion of 96.9% and an 80.82% composition of total PMDs (Table 3.48).

Table 3.47: Reaction parameters for PMD synthesis from synthetic citronellal.

Exp	Cal (g)	Cal composition			7% Acid solution				RXN Condition			PMD _T	
		%	(g)	mol	S	S (g)	CA (g)	CA (mol)	T (°C)	RPM	t (hrs)	mol	(g)
58	45.01	90	40.51	0.26	DW	59.54	4.48	0.02	50	750	16	0.26	44.79

Cal: citronellal; PMD_T: Theoretical PMD calculations; S: acid solvent; CA: Citric acid.

Table 3.48: Conversion profile for the neat PMD synthesis from synthetic citronellal.

t (hrs)	Composition (%±0.2)									Conv (%)	Crude (g)	PMD _{SEY}	
	Cal	Iso	nIso	iIso	PMD 1	PMD 2	PMD 3	PMD 4	PMDs			(g)	% (w/w)
0	90.2	2.9	2.4	1.1	0.0	0.0	0.0	0.0	0.0	0.0	↓	↓	↓
16	2.8	2.0	5.7	2.6	49.6	0.8	29.3	2.1	81.8	96.9	45.6	37.3	83.3

Cal: citronellal; Iso: isopulegol; nIso: *neo*-isopulegol; iIso: *iso*-isopulegol; PMD-1: *cis*-PMD 1; PMD-2: *cis*-PMD 2; PMD-3: *trans*-PMD 1; PMD-4: *trans*-PMD 2; PMD_{SEY}: PMD experimental yield; PMDs: combined PMD isomers.

3.2.6.2. Diastereoisomeric recrystallization

The crude PMD mass was dissolved in 150 ml of *n*-heptane and then transferred to a 500 ml conical flask, seeded with small amounts of crystalline *cis*-PMD (93%) and stored at 2°C for 72 hours. A significant amount of colourless, thin and short crystals was formed. The solution was filtered, washed with little cold *n*-heptane and dried to yield 13.234 g of colourless crystals. GC-analysis confirmed the isolation of the major *cis*-PMD in 94% purity. The structure of *cis*-PMD was furthermore confirmed by ¹H- and ¹³C-NMR-analysis (Figure 3.57 and Figure 3.58) and in comparison with literature data (Table 3.49).

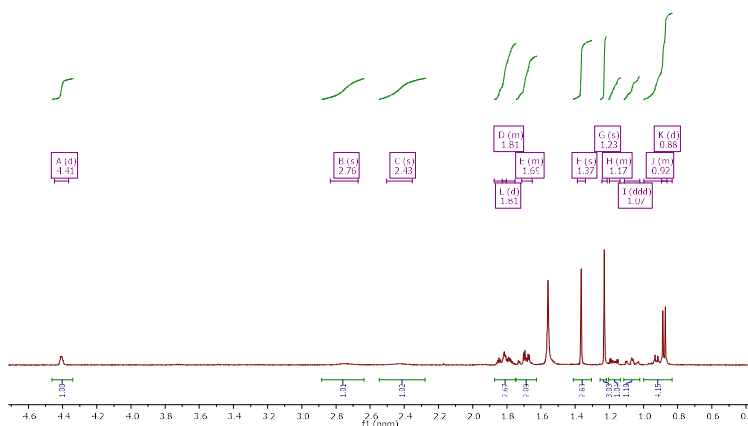


Figure 3.57: ¹H-NMR spectrum of *cis*-PMD (33c) in CDCl₃.

Various filtrates from previous filtrations were combined, seeded with pure crystalline *trans*-PMD and refrigerated for another 72 hours. Filtration and careful washing gave 4.426 g of

colourless crystals. GC-analysis revealed that the *trans*-PMD (**33b**) isomer was obtained in 95% purity. The structure of *trans*-PMD was again confirmed by NMR-analysis (**Figure 3.59** and **Figure 3.60**) and in comparison with literature data (**Table 3.50**).

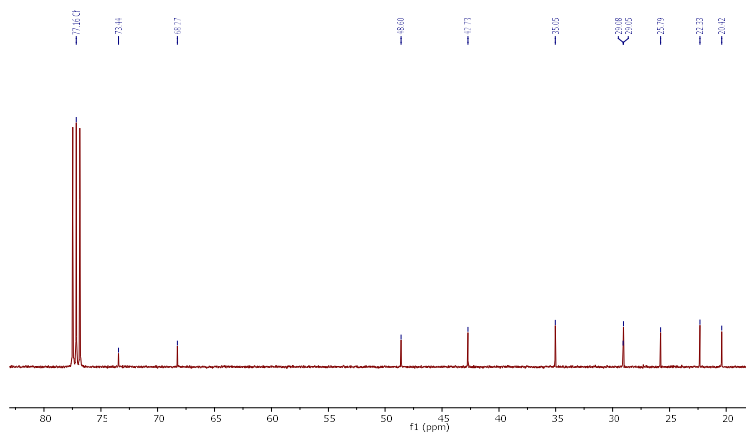


Figure 3.58: ^{13}C -NMR spectrum of *cis*-PMD (**33c**) in CDCl_3 .

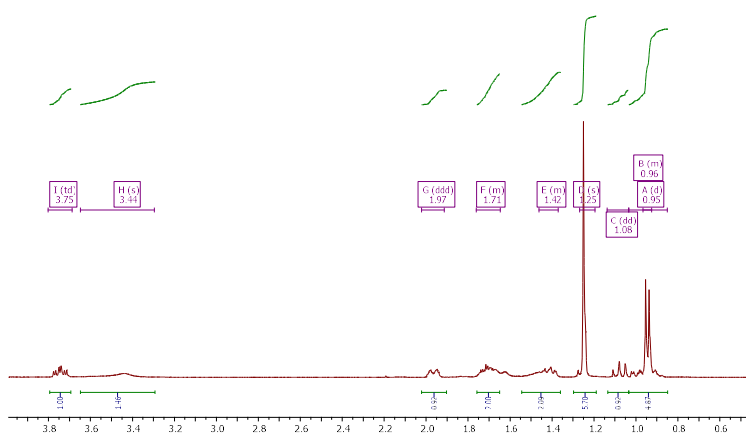


Figure 3.59: ^1H -NMR spectrum of *trans*-PMD (**33b**) in CDCl_3 .

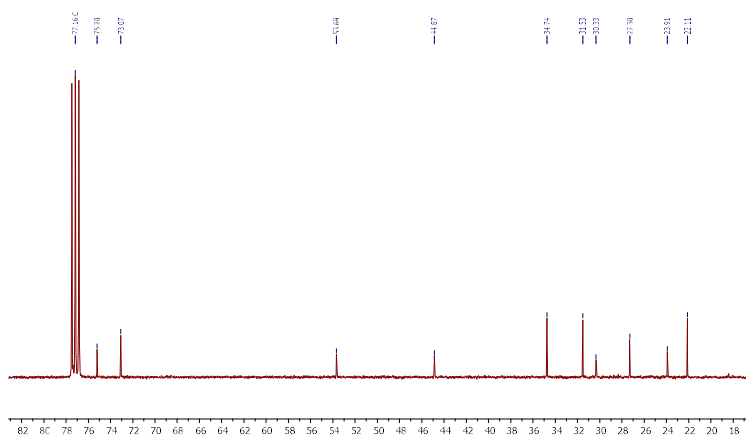


Figure 3.60: ^{13}C -NMR spectrum of *trans*-PMD (**33b**) in CDCl_3 .

Table 3.49: Comparison of recorded chemical shifts for *cis*-PMD (**33c**) with literature values.

Atom(s)	Yuasa <i>et al.</i> ^{a 77}		Lemaire <i>et al.</i> ^{b 173}		this study	
	¹³ C	¹ H	¹³ C	¹ H	¹³ C	¹ H
1	34.9	1.64-1.86 (m, 2H)	36.1	1.71-1.67 (m, 2H)	35.1	1.71-1.65 (m, 1H)
2	20.3	0.86-0.96 (m, 1H) 1.05 (t, 9 Hz, 1H,)	21.6	0.97-0.91 (m, 1H) 1.10-1.04 (m, 1H)	20.4	1.00-0.83 (m, 1H) 1.07 (ddd, <i>J</i> = 15.2, 12.7, 2.3 Hz, 1H)
3	48.3	1.64-1.86 (m, 1H)	49.9	1.83-1.74 (m, 1H)	48.7	1.81 (d, <i>J</i> = 2.3 Hz, 1H)
4	67.9	4.40 (brs, 1H)	68.8	4.35 (dd, <i>J</i> = 3.0 and 5.4 Hz, 1H)	68.3	4.41 (d, <i>J</i> = 2.4 Hz, 1H)
5	42.5	1.64-1.86 (m, 2H)	43.7	1.83-1.74 (m, 2H)	42.7	1.87-1.75 (m, 3H)
6	25.6	1.13-1.18 (m, 1H)	26.8	1.22-1.19 (m, 1H)	25.8	1.20-1.14 (m, 1H)
7	22.2	0.87 (d, <i>J</i>) 6 Hz, 3H, CH ₃)	22.7	0.87 (d, <i>J</i> = 6.4 Hz, 3H)	22.3	0.88 (d, <i>J</i> = 6.2 Hz, 3H)
8	-	3.25 (d, <i>J</i>) 2 Hz, 1H, OH)	-	3.26 (d, <i>J</i>) 2 Hz, 1H,)	-	2.76 (s, 1H)
9	73.2	-	74.0	-	73.4	-
10	28.7	1.22 (s, 3H, CH ₃)	28.5	1.22-1.19 (m, 3H)	29.1	1.23 (s, 3H)
11	28.9	1.36 (s, 3H, CH ₃)	28.9	1.31 (s, 3H)	29.1	1.37 (s, 3H)
12	-	3.25 (d, <i>J</i>) 2 Hz, 1H, OH)	-	3.26 (d, <i>J</i>) 2 Hz, 1H,)	-	2.43 (s, 1H)

^a: ¹H- and ¹³C-NMR determined at 400 and 100 MHz in CDCl₃ with TMS as internal standard; ^b: ¹H- and ¹³C-NMR determined at 500 and 125 MHz in CDCl₃ with TMS internal standard.

Table 3.50: Comparison of recorded chemical shifts for *trans*-PMD (**33b**) with literature values.

Atom(s)	Yuasa <i>et al.</i> ^{a 77}		Lemaire <i>et al.</i> ^{b 173}		this study	
	¹³ C	¹ H	¹³ C	¹ H	¹³ C	¹ H
1	34.5	1.35-1.49 (m, 2H)	35.9	1.49-1.41 (m, 1H) 1.35 (ddd, <i>J</i> = 3.3, 10.1 and 12.1 Hz, 1H)	34.7	1.46-1.37 (m, 2H)
2	26.9	0.84-0.98 (m, 2H)	28.0	1.05-0.97 (m, 2H)	27.3	1.03-0.85 (m, 2H)
3	53.0	1.92-1.97 (m, 1H)	54.4	1.92-1.88 (m, 1H)	53.7	1.97 (ddd, <i>J</i> = 12.2, 5.8, 3.9 Hz, 1H)
4	72.6	4.21 (d, <i>J</i>) 3 Hz, 1H)	73.9	3.69 (td, <i>J</i> = 4.2 and 10.5 Hz, 1H)	73.1	3.75 (td, <i>J</i> = 10.5, 4.3 Hz, 1H)
5	44.4	1.63-1.73 (m, 2H)	45.7	1.75-1.71 (m, 1H) 1.70-1.66 (m, 1H)	44.9	1.76-1.65 (m, 2H)
6	31.2	1.04 (q, <i>J</i>) 11, 24 Hz, 1H)	32.7	0.95-0.85 (m, 1H)	31.5	1.08 (dd, <i>J</i> = 13.8, 9.2 Hz, 1H)
7	21.9	0.92 (d, <i>J</i>) 6.5 Hz, 3H, CH ₃)	22.6	0.95-0.85 (m, 3H)	22.1	0.95 (d, <i>J</i> = 6.6 Hz, 3H)
8	-	3.95 (s, 1H, OH)	-	3.26 (s, 1H)	-	3.44 (s, 1H)
9	74.8	-	75.6	-	75.2	-
10	23.5	1.22 (s, 6H, 2CH ₃)	24.3	1.20 (s, 3H)	23.9	1.25 (s, 6H)
11	29.7	1.22 (s, 6H, 2CH ₃)	29.8	1.18 (s, 3H)		
12	-	3.71 (s, 1H, OH)	-	3.26 (s, 1H)	-	3.44 (s, 1H)

^a: ¹H- and ¹³C-NMR determined at 400 and 101 MHz in CDCl₃ with TMS as internal standard; ^b: ¹H- and ¹³C-NMR determined at 500 and 125 MHz in CDCl₃ with TMS internal standard.

After the second filtration, the excess heptane was removed by rotary evaporation to give 26.564 g of a solid residue. $^1\text{H-NMR}$ analysis of this material showed a mixture of residual PMDs, Iso and Cal. No attempts were made to further isolate or purify any compounds from this mass.

3.2.6.2.1. Vacuum distillation of diastereoisomer mixture

While recrystallization successfully produced portions of *cis*- and *trans*-PMD, this process came with significant losses. Vacuum distillation was thus investigated as an alternative purification method (**Figure 3.61**). A 500 ml flask containing crude PMD was partially submerged in an oil bath. A Vigreux column was attached to improve the separation of compounds. A distillation bridge was subsequently placed on the column. Several clean and pre-weighed collecting flasks were attached at the vacuum receiver at the end of the Liebig-bridge. The crude product was stirred at 250 rpm and carefully heated at <1 mbar pressure. Condensing fractions were collected at steady temperature intervals and analysed by GC- (**Table 3.51**) and $^1\text{H-NMR}$ analyses.



Figure 3.61: Fractional vacuum distillation setup.

The first fraction (F1) of a colourless viscous liquid was collected at 70°C (<1 mbar) and weighed 11.29 g. At 80°C (<1 mbar), a second fraction (F2) of 3.53 g with the same appearance as F1 was collected. Following this, a small fraction (F3) of 1.13 g of a viscous liquid was collected at 90°C (<1 mbar). A final fourth fraction (F4) was slowly collected at 110°C (<1 mbar) and weighed 58.11 g. After reaching 130°C (<1 mbar), the distillation process was stopped. A viscous mass of 5.32 g remained in the crude product flask while a total distillate of 74.00 g (86% recovery) was collected. GC-analyses revealed that F1 composed mainly of 1.4% of PMD isomers and 71.8% Iso, F2 of 5.5% PMD isomers and 68.7% Iso, and F3 of

10.8% of PMD isomers and 33.1% of Iso, respectively. F4, which was collected over a period of 60 minutes, accounted to 91.4% (53.1 g) of total PMDs and contained 3.4% of Iso.

Table 3.51: Composition of main constituents in fractions obtained by vacuum distillation.

F	T (°C)	Mass (g)	Composition (%)									Total PMDs	
			Cal	<i>n</i> Iso	Iso	<i>i</i> Iso	Col	PMD1	PMD2	PMD3	PMD4	%	Mass (g)
1	70	11.3	5.4	46.2	0.0	25.6	3.0	1.2	0.2	0.0	0.0	1.4	0.2
2	80	3.5	1.4	50.9	0.0	17.8	11.5	4.6	0.2	0.0	0.9	5.7	0.2
3	90	1.1	1.4	27.3	0.0	5.8	37.3	10.4	0.4	0.0	2.0	12.8	0.1
4	110	58.1	0.6	2.0	0.0	1.4	4.6	64.0	1.1	24.7	1.6	91.4	53.1

Cal: citronellal; Col: citronellol; Iso: isopulegol; *n*Iso: *neo*-isopulegol; *i*Iso: *iso*-isopulegol; PMD-1: *cis*-PMD 1; PMD-2: *cis*-PMD 2; PMD-3: *trans*-PMD 1; PMD-4: *trans*-PMD 2.

Comparison of characteristic $^1\text{H-NMR}$ signals of F4 (**Figure 3.62** and **Figure 3.63**) confirmed an abundance of *cis*-PMD and *trans*-PMD, followed by minor amounts of Col, *n*Iso, and *i*Iso.

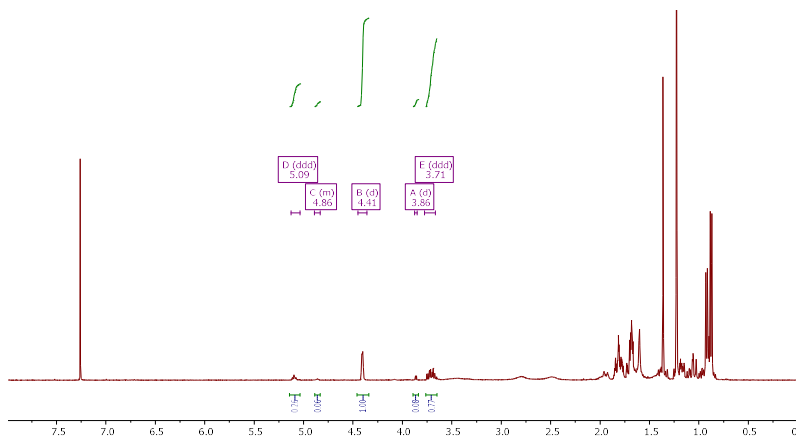


Figure 3.62: $^1\text{H-NMR}$ spectrum of fraction F4 obtained by vacuum distillation.

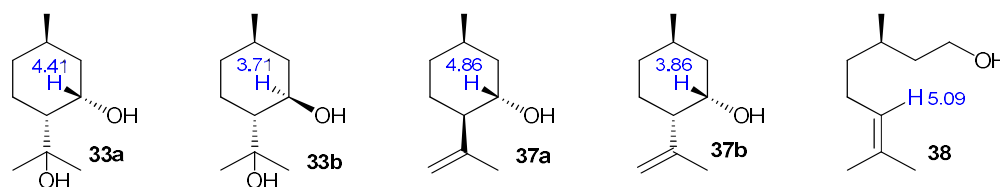


Figure 3.63: Characteristic $^1\text{H-NMR}$ signals of the main constituents in fraction F4.

3.2.6.2.2. Further purification by recrystallization

Similar to the initial separation, fraction F4 was subjected to recrystallization from *n*-heptane in an attempt to separate the *cis*-PMD and *trans*-PMD. The material was thus dissolved in 175 ml of *n*-heptane under gentle heating and then transferred to a clean 250 ml conical flask and stored in a refrigerator at 2°C. After hours, substantial amounts of colourless, thin and short crystals had formed. Filtration and careful washing gave 41.05 g of these crystals (RC1). The

filtrate was evaporated to dryness and gave 15.77 g of a viscous clear liquid. The crystalline material was analysed by GC- (Table 3.52) and ¹H-NMR analyses.

GC-analysis showed that the crystals contained 67.1% of *cis*-PMD, 28.0% of *trans*-PMD, and 2.1% of the minor PMD isomers. *Neo*-isopulegol (1.1%), *iso*-isopulegol (0.8%) and Col (0.6%) were furthermore detected as trace impurities. ¹H-NMR analysis also confirmed the dominant presence the main PMD isomers (Figure 3.64). The residue from the filtrate contained 68.6% of combined PMDs with significantly more impurities.

Table 3.52: Changes in the composition of fraction F4 during successive recrystallizations.

RC	T (°C)	Mass (g)	Composition (%)										Total PMDs	
			Cal	<i>n</i> Iso	Iso	<i>i</i> Iso	Col	PMD1	PMD2	PMD3	PMD4	%	Mass (g)	
1	2	41.1	0.3	1.1	0.0	0.8	0.6	67.1	0.4	28.0	1.7	97.2	39.9	
2	2	31.3	0.0	0.0	0.0	0.0	0.0	84.0	0.0	15.1	0.9	100.0	31.3	

RC: Recrystallization experiment, Cal: citronellal, Col: citronellol, Iso: (-)-isopulegol, *n*Iso: *neo*-isopulegol, *i*Iso: *iso*-isopulegol, PMD-1: *cis*-PMD 1, PMD-2: *cis*-PMD 2, PMD-3: *trans*-PMD 1, PMD-4: *trans*-PMD 2.

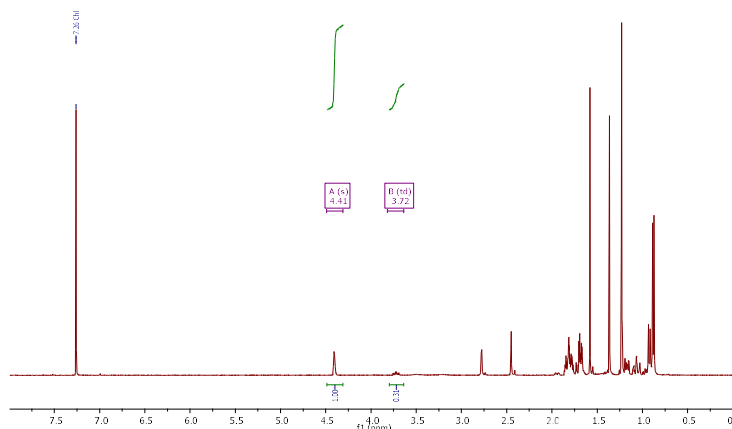


Figure 3.64: ¹H-NMR spectrum of fraction RC1 after initial recrystallization.

In an attempt to improve the purity of *cis*-PMD, the crystals recovered as RC1 were subjected to a second recrystallization process. Following the same protocol as before, 31.32 g of colourless, thin and short crystals were obtained (RC2) and analysed (Table 3.52). Evaporation of the filtrate solution furnished 6.04 g of a colourless viscous oil.

The GC-chromatogram of RC2 revealed a mixture of 84.0% of *cis*-PMD and 15.1% of *trans*-PMD. This was confirmed by ¹H-NMR spectroscopic analysis, which gave a ratio of 86.2% of *cis*-PMD vs. 13.8% of *trans*-PMD by integration (Figure 3.65).

3.2.6.3. Synthesis of PMD-acetals

The so-called PMD-acetals have been commonly found as by-products during the PMD synthesis. Typically, the amounts of acetals conditions increased by approximately 2%. Due to the acidic conditions of the reaction medium, these compounds are formed by acetalization of PMD with residual Cal, especially at the end of the reaction when larger amounts of PMD were formed^{106, 108}.

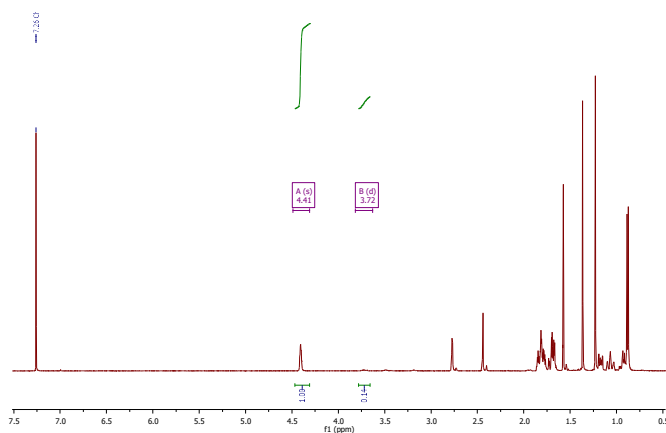
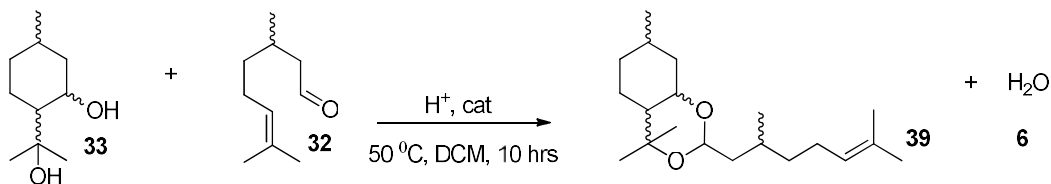


Figure 3.65: ¹H-NMR spectrum of fraction RC2 after successive recrystallization.

3.2.6.3.1. Synthesis of PMD-acetals from citronellal and PMD

Following a general procedure for acetalization (**Scheme 3.7**), three experiments were conducted (**Table 3.53**).



Scheme 3.7: Synthesis of PMD acetals.

In a 50 ml flask, approximately 2.00 g (11.6 mmol) of PMD (RC2) and 2.04 ml of 90% Cal (10.1 mmol) were added. The mixture was then dissolved in 25 ml dichloromethane (DCM) and. To this solution, approximately 0.10 ml of 2 M aqueous H₂SO₄ (0.2 mmol) were added dropwise, and the reaction mixture was refluxed at 60°C. After 10 hours, the reaction solution was washed twice with cold water and twice with brine solution. The organic layer was then dried over Na₂SO₄ and filtered. After evaporating, the crude material was dried and analysed by GC and ¹H-NMR for its PMD-acetal content (**Table 3.54**).

Table 3.53: Reaction conditions for acetalization.

Exp	Cal (ml)	Cal composition			PMD (g)	PMD composition			RXN Condition			PMD-Acetal _T	
		%	(ml)	mmol		%	(g)	mmol	T (°C)	rpm	t (hrs)	mol	(g)
60-62	2.04	89.5	1.6	10.1	0.10	100.0	0.1	0.6	50	1000	10	0.01	3.69

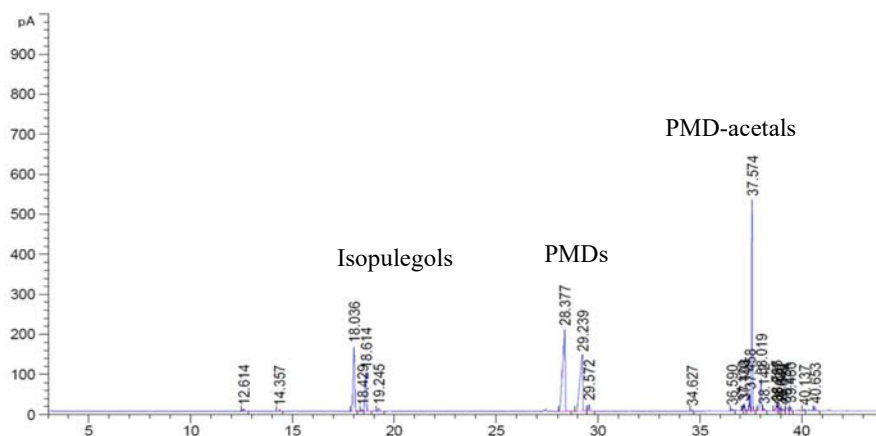
Cal: citronellal; PMD: PMD from standard reagent; PMD-Acetal_T: Theoretical PMD-acetal calculations.

Table 3.54: Constituents and composition of the PMD-acetals.

Exp	% Composition (±0.2)												Crude		
	Cal	<i>n</i> Iso	<i>i</i> Iso	Iso	1 ^a	2 ^a	3 ^a	4 ^a	1 ^b	2 ^b	Σ ^b	Σ ^a	(g)	EY ^b (g)	% (w/w)
60	0.0	11.8	6.9	0.3	24.2	0.0	18.2	0.9	23.3	4.9	28.2	43.3	2.8	0.8	21.9
61	0.0	11.1	7.5	0.4	30.1	0.0	5.7	0.3	31.5	2.1	33.6	36.1	2.8	0.9	26.5
62	0.0	17.5	7.9	0.4	3.0	0.0	42.9	2.0	2.6	13.8	16.4	47.9	2.6	0.4	12.0

Cal: citronellal; Iso: isopulegol; *n*Iso: *neo*-isopulegol; *i*Iso: *iso*-isopulegol; 1^a: *cis*-PMD 1; 2^a: *cis*-PMD 2; 3^a: *trans*-PMD 1; 4^a: *trans*-PMD 2; 1^b: *cis*-PMD acetal; 2^b: *trans*-PMD acetal; Σ^a: Sum of combined PMDs; Σ^b: Sum of combined PMD acetals; EY^b: Experimental yield of PMD acetals.

The GC chromatogram of Experiment 60 is exemplarily shown in **Figure 3.66**. While it showed a noticeable absence of Cal and hence confirmed complete conversion, the crude reaction mixture predominantly contained unreacted PMD isomers. Nevertheless, the partial formation of PMD-acetals was confirmed. Likewise, Experiments 61 and 62 also gave large amounts of PMDs.

**Figure 3.66:** GC-chromatogram of Experiment 60.

Characteristic ¹H-NMR peaks detected at 5.10 and 4.08 ppm confirmed the presence of the desired PMD-acetal compounds (**Figure 3.67**). Significant quantities of PMD were again found as indicated by the characteristic peaks of *cis* and *trans*-PMD at 4.40 and 3.72 ppm, respectively. No characteristic aldehyde peak for citronellal at 9.74 ppm (CHO) was detected, thus confirming that it was consumed during the reaction or removed during workup.

In comparison with literature data (**Figure 3.68**), the dominant PMD-acetal was assigned to the *cis*-isomer. The broad triplet at 5.10 ppm corresponds to the methine proton at C6' and the doublet of doublets at 4.86 and 4.08 ppm represent the protons at C1' and C1, respectively. The characteristic peaks of *neo*-isopulegol were found at 4.95 (m, C1'), 4.79 (s, C1') and 3.99 ppm (dd, C1), respectively. The corresponding protons of *iso*-isopulegol exhibited signals at 4.90 (dq, C1'), 4.88 (d, C1') and 3.46 ppm (m, C1) instead.

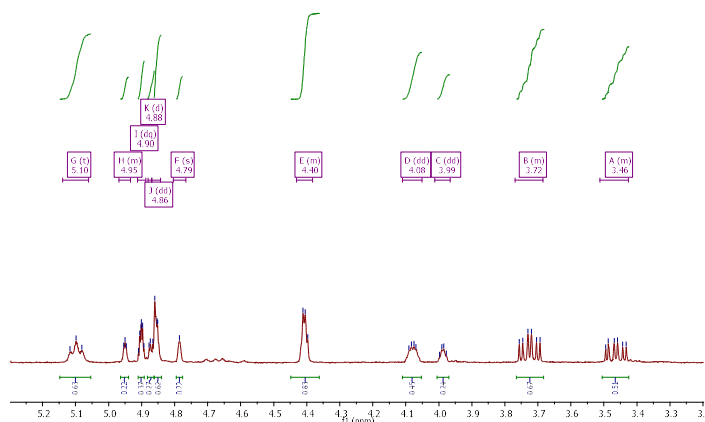


Figure 3.67: Expanded ^1H -NMR-spectrum of the crude product of Experiment 60.

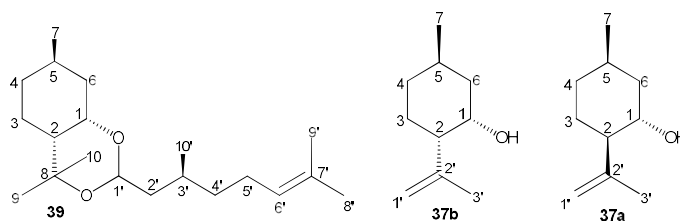


Figure 3.68: Characteristic ^1H -NMR signals of *cis*-PMD acetal (**39a**), *neo*-isopulegol (**37b**) and *iso*-isopulegol (**37a**).

3.2.6.3.2. Isolation of PMD-acetals by column chromatography

TLC trials were conducted to establish the separation parameters for column chromatographic separation of the crude reaction mixture obtained during acetalization. A solvent system of ethyl acetate and hexane at 1:10 offered suitable separation, as confirmed by staining with KMnO_4 solution. Using this mobile phase, the PMD acetals showed a higher affinity for the solvent system ($R_f = 0.6$), followed by the isopulegols ($R_f = 0.3$) and PMDs ($R_f = 0.2$).

A chromatography column (35 × 2 cm) equipped with a sintered glass frit was prepared with 6.0 g of silica gel. A concentrated solution of 2.8 g of the crude product from Experiment 62 in the mobile phase was adsorbed onto and a layer of sand laid on top of the silica. A total of

twenty-four 10 ml-fractions were collected. TLC spot-tests revealed that the PMD-acetals were present in fractions 7-13. These fractions were combined and concentrated by rotary evaporation to yield 0.78 g of crude acetals.

GC-analysis of the combined fractions showed high a high proportion *cis*-PMD acetal (72.0%), followed by *trans*-PMD acetal (15.2%) and traces of other constituents including Iso and *trans*-PMD (Figure 3.69).

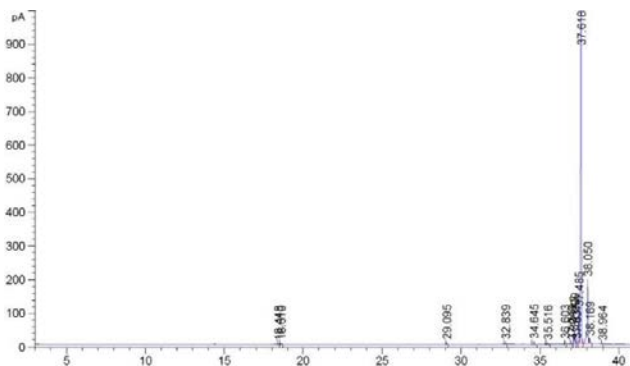


Figure 3.69: GC chromatogram of crude PMD-acetals obtained after column chromatography.

3.2.6.3.3. Attempted purification of crude PMD-acetals by recrystallization

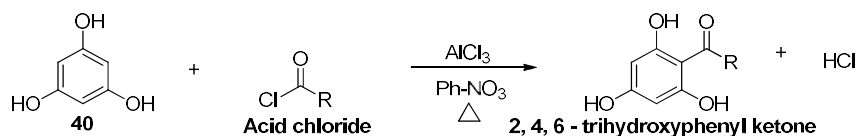
In an attempt to further purify *cis*-PMD acetal and separate it from its *trans*-isomer, the crude concentrate was dissolved in 2 ml of *n*-heptane and refrigerated at 2°C overnight. As no precipitation was observed, the solution was evaporated to dryness, dried, and analysed by ¹H-NMR spectroscopy. The composition of the recovered crude PMD-acetals was similar to the one determined by GC-analysis with *cis*-PMD acetal as the major component (75.8%).

3.3. β-Triketone syntheses and isolation

To expand the study of biological activity of β-triketones and conduct a more detailed structure-activity-relationship study, several synthetic analogues were produced via a two-step thermal synthesis process.

3.3.1. Syntheses of 2, 4, 6-trihydroxyphenyl ketones (acetyl phloroglucinols)

Initially, 2, 4, 6-trihydroxyphenyl ketones was prepared by Friedel-Crafts acylation of phloroglucinol (40) following a protocol described by Jonathan *et al.* (Scheme 3.8)¹⁷⁴.



Scheme 3.8: Acetylation of phloroglucinol.

Following this procedure, 100 ml of nitrobenzene were added to a 500 ml flask that was partially submerged in an oil bath seated on a stirrer hotplate (**Figure 3.70**).

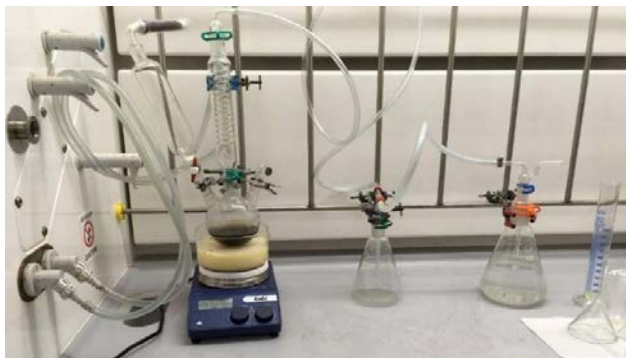


Figure 3.70: Reaction setup for the Friedel-Crafts' acetylation of phloroglucinols.

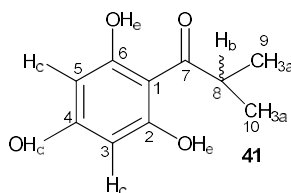
Approximately 10.0 g (1 equ.) of phloroglucinol was added and stirred at room temperature for 30 minutes. To this solution, 42.2 g (4 equ.) of aluminium trichloride were added slowly in three portions. Finally, 1.2 equ. of the respective acid chloride were added slowly under nitrogen and the reaction mixture was further stirred at 65°C for 18 hours. At the end of the reaction, the solution was cooled down, poured into 300 ml of ice-cold water and extracted three times with 100 ml of ethyl acetate (EtOAc). The combined organic layers were dried over Na₂SO₄, filtered, and concentrated to dryness in vacuo. TLC-analysis of the crude product on silica gel plates identified a 1:1-mixture of EtOAc and *n*-hexane as a suitable mobile phase for monitoring. The crude extract was subjected to flash chromatography elution using a 0-30% EtOAc in *n*-hexane gradient to isolate the desired 2, 4, 6-trihydroxyphenyl ketones. The corresponding fractions were collected and concentrated in vacuo to give orange-like viscous pastes. The identity and purity of the structures was determined by ¹H-NMR analysis using the characteristic peak at 5.93 ppm (s) of the unsubstituted aromatic methine protons. Further singlets at 9.17 ppm for the *para*-hydroxyl proton and at 11.73 ppm for the *ortho*-hydroxyl protons further structural confirmation. The experimental conditions and results of the acylation reactions are compiled in **Table 3.55**.

Table 3.55: Reaction parameters for the synthesis of β -triketone precursors.

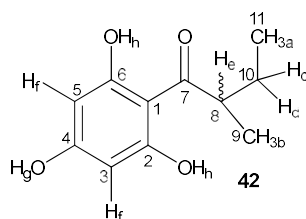
Exp	Acylchloride		Phloroglucinol		AlCl ₃		Theoretical		Crude (g)	Mass (g)	Yield (%)	Purity (%) ^a	
	Name	Mass (g)	mmol	mmol	Mass (g)	Mass (g)	mmol	mmol					
63	Isobutyryl	8.60	81	80	10.11	36.25	272	80	15.73	6.35	6.31	40.1	100
64	2-Methylbutyryl	4.99	41	38	4.75	19.91	149	38	7.92	6.62	6.59	83.2	100
65	Benzoyl	5.04	36	46	5.75	21.58	162	46	10.49	3.60	1.69	16.1	100
66	Propionyl	4.05	44	40	5.00	21.33	160	40	7.22	4.70	4.40	60.9	100
67	Isovaleryl	10.00	83	93	11.77	45.62	342	93	19.61	9.85	9.76	49.8	100
68	Valeroyl	10.56	88	99	12.43	48.18	361	99	20.72	6.44	6.40	30.8	100
69	Butyryl	9.32	87	98	12.41	48.09	361	98	19.30	6.28	5.98	31.0	100
70	Hexanoyl	11.76	87	98	12.39	48.05	360	98	22.04	7.82	7.73	35.1	100
71	Nonanoyl	15.41	87	98	12.37	47.96	360	98	26.13	7.88	7.83	30.0	100
72	Octanoyl	14.15	87	98	12.34	47.85	359	98	24.70	4.92	3.81	15.4	100
73	Heptanoyl	15.00	101	114	14.32	55.51	416	114	27.05	3.68	3.16	11.7	100
74	Acetyl	10.00	127	143	18.08	70.08	526	143	24.10	0.65	0.30	1.2	100
75	Cyclohexanecarbonyl	15.00	102	115	14.52	56.27	422	115	27.19	2.93	2.55	9.4	100

^a: Determined by ¹H-NMR analysis.

3.3.2. Characterization of the 2, 4, 6-trihydroxyphenyl ketones

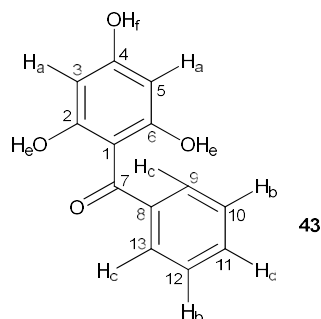


2-Methyl-1-(2, 4, 6-trihydroxyphenyl) propan-1-one (**41**): light-orange solid cluster. $R_f = 0.70$. UV abs, λ_{\max} : 283.0 nm. M.pt: 141°C. ESI-MS: $[M-H]^-$, $C_{10}H_{11}O_4$, $m/z = 195$ (100%). ESI-MS: $[M+H]^+$, $C_{10}H_{13}O_4$, $m/z = 197$ (100%). 1H -NMR (400 MHz, acetone- d_6): δ (ppm) = 11.73 (s, 2H_e), 9.17 (s, 1H_d), 5.93 (s, 2H_c), 4.08-3.88 (m, 1H_b), 1.13 (d, $J = 6.7$ Hz, 6H_a). ^{13}C -NMR (101 MHz, acetone- d_6): δ (ppm) = 212.2-209.3 (C=O, C-7), 186.3 (C-OH, C-4), 172.1 (2C-OH, C-6/C-2), 103.0 (C=C, C-1), 95.3 (2HC=C, C-3/C-5), 39.0 (HC-C, C-8), 18.6 (2CH₃, C-9/C-10). IR (ATR): $\tilde{\nu}$ (cm^{-1}) = 3277.08 (br, O-H stretching), 2968.25 (med, C-H stretching), 1700.47 (wk, bending C=O), 1624.09 (str, C=C stretching), 1594.53 (med, C=C stretching), 1451.07 (med, O-H stretching), 1365.39 (str, C-O stretching), 1215.11 (str, C-O stretching) 1155.04 (str, C-O stretching) and 822.99 (med, C=C bending).

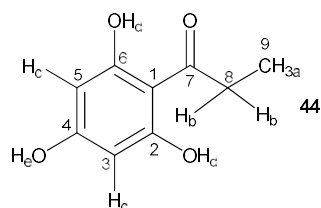


2-Methyl-1-(2, 4, 6-trihydroxyphenyl) butan-1-one (**42**): Yellow-red viscous liquid. $R_f = 0.68$. UV abs, λ_{\max} : 287.0 nm. ESI-MS: $[M-H]^-$, $C_{11}H_{13}O_4$, $m/z = 209$ (100%). ESI-MS: $[M+H]^+$, $C_{11}H_{15}O_4$, $m/z = 211$ (100%). 1H -NMR (400 MHz, acetone- d_6): δ (ppm) = 11.82 (s, 2H_h), 9.28 (s, 1H_g), 5.93 (s, 2H_f), 3.90-3.80 (m, 1H_e), 1.82 (ddd, $J = 13.7, 7.4, 6.4$ Hz, 1H_d), 1.43-1.31 (m, 1H_c), 1.12 (d, $J = 6.8$ Hz, 3H_b), 0.88 (t, $J = 7.4$ Hz, 3H_a). ^{13}C -NMR (101 MHz, acetone- d_6): δ (ppm) = 210.5 (C=O, C-7), 165.5 (C-OH, C-4), 165.1 (2C-OH, C-6/C-2), 105.0 (C=C, C-1), 96.0 (2HC=C, C-3/C-5), 46.3 (HC-C, C-8), 27.7 (H₂C-C, C-10), 17.0 (CH₃-C, C-9) and 12.3 (CH₃-C, C-11). IR (ATR): $\tilde{\nu}$ (cm^{-1}) = 3290.18 (br, O-H stretching), 2965.13 (med, C-H stretching), 1702.96 (wk, C=O bending), 1624.30 (str, C=C stretching), 1595.70 (med, C=C stretching), 1453.37 and 1374.35 (med, O-H bending), 1215.92 (str, C-O stretching), 1156.95 (str, C-O stretching) and 824.37 (med, C=C bending).

Chapter 3 – Results

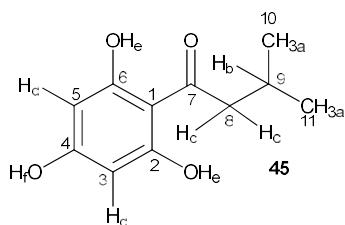


Phenyl (2, 4, 6-trihydroxyphenyl)methanone (**43**): Colourless clustered solid. $R_f = 0.82$. UV abs, λ_{\max} : 293.0 nm. M.pt: 166°C. ESI-MS: $[M-H]^-$, $C_{13}H_9O_4$, $m/z = 333$ (100%). ESI-MS: $[M+H]^+$, $C_{13}H_{11}O_4$, $m/z = 335$ (80%). 1H -NMR (400 MHz, acetone- d_6): δ (ppm) = 13.19 (s, 2H_e), 11.07 (s, 1H_f), 7.70-7.65 (m, 2H_b), 7.55-7.50 (m, 2H_c), 7.46-7.41 (m, H_d), 6.06 (s, 2H_a). ^{13}C -NMR (101 MHz, acetone- d_6): δ (ppm) = 199.4 (C=O, C-7), 167.1 (C-OH, C-4), 166.7 (2C-OH, C-6/C-2), 141.8 (C=C, C-8), 132.4 (HC=C, C-11), 130.0 (2HC=C, C-9/ C-13), 128.7 and 130.0 (2HC=C, C-10/C-12), 105.3 (C=C, C-1), 96.0 (2HC=C, C-3/C-5). IR (ATR): $\tilde{\nu}$ (cm^{-1}) = 3246.41 (br, O-H stretching), 2914.01 (med, C-H stretching), 1738.33 (wk, C=O bending), 1568.48 (med, C=C stretching), 1472.46 (med, O-H bending), 1303.52 (str, C-O stretching), 1198.20 (str, C-O stretching), 1096.61 (str, C-O stretching), 987.05 (str, C=C bending), 684.83 (str, C=C bending).

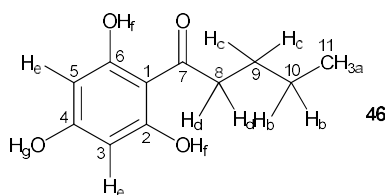


1-(2, 4, 6-Trihydroxyphenyl)propan-1-one (**44**): Colourless clustered solid. $R_f = 0.58$. UV abs, λ_{\max} : 283.0 nm. M.pt: 177°C. ESI-MS: $[M-H]^-$, $C_9H_9O_4$, $m/z = 181$ (100%). 1H -NMR (400 MHz, CD_3CN): δ (ppm) = 10.92 (s, 2H_d), 7.72 (s, 1H_e), 5.85 (s, 2H_c), 3.04 (q, $J = 7.2$ Hz, 2H_b), 1.09 (t, $J = 7.2$ Hz, 3H_a). ^{13}C -NMR (101 MHz, acetone- d_6): δ (ppm) = 206.9 (C=O, C-7), 165.4 (C-OH, C-4), 165.1 (2C-OH, C-6/C-2), 95.8 (2HC=C, C-3/ C-5), 37.6 (H_2C -C, C-8), 8.9 (H_3C -C, C-9). IR (ATR): $\tilde{\nu}$ (cm^{-1}) = 3261.97 (br, O-H stretching), 2978.05 (med, C-H stretching), 1738.12 (wk, C=O bending), 1601.19 (med, C=C stretching), 1449.19 (med, O-H bending), 1217.13 (str, C-O stretching), 1158.24 (str, C-O stretching), 1077.90 (str, C-O stretching), 730.06 (str, C=C bending).

Chapter 3 – Results

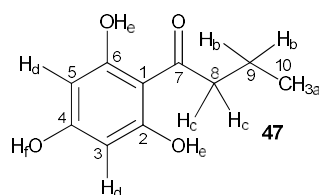


3-Methyl-1-(2, 4, 6-trihydroxyphenyl)butan-1-one (**45**): Colourless clustered solid. $R_f = 0.51$. UV abs, λ_{\max} : 283.0 nm. M.pt: 143°C. ESI-MS: $[M-H]^-$, $C_{11}H_{13}O_4$, $m/z = 209$ (100%). ESI-MS: $[M+H]^+$, $C_{11}H_{15}O_4$, $m/z = 211$ (75%). 1H -NMR (400 MHz, acetone- d_6): δ (ppm) = δ 11.72 (s, 2H_e), 9.16 (s, 1H_f), 5.92 (s, 2H_d), 2.94 (d, $J = 6.7$ Hz, 2H_c), 2.24 (dt, $J = 13.3, 6.6$ Hz, 1H_b), 0.95 (d, $J = 6.7$ Hz, 6H_a). ^{13}C -NMR (101 MHz, acetone- d_6): δ (ppm) = 206.1 (C=O, C-7), 165.5 (C-OH, C-4), 165.2 (2C-OH, C-6/C-2), 105.5 (C=C, C-1), 95.9 (2HC=C, C-3/ C-5), 53.3 (H₂C-C, C-8), 26.0 (HC-C, C-9), 23.1 (H₃C-C, C-10/C-11). IR (ATR): $\tilde{\nu}$ (cm⁻¹) = 3261.96 (br, O-H stretching), 2958.22 (med, C-H stretching), 1738.02 (wk, C=O bending), 1599.89 (med, C=C stretching), 1458.23 (med, O-H bending), 1282.37 (str, C-O stretching), 1158.66 (str, C-O stretching), 1077.49 (str, C-O stretching), 813.25 (str, C=C bending), 662.49 (str, C=C bending).

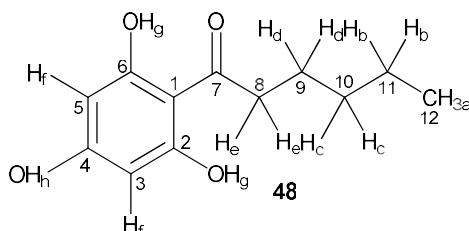


1-(2, 4, 6-Trihydroxyphenyl)pentan-1-one (**46**): Colourless clustered solid. $R_f = 0.49$. UV abs, λ_{\max} : 281.0 nm. M.pt: 140°C. ESI-MS: $[M-H]^-$, $C_{11}H_{13}O_4$, $m/z = 209$ (100%). ESI-MS: $[M+H]^+$, $C_{11}H_{15}O_4$, $m/z = 211$ (75%). 1H -NMR (400 MHz, CD₃CN): δ (ppm) = 10.96 (s, 2H_f), 7.79 (s, 1H_g), 5.85 (s, 2H_e), 3.10-2.94 (m, 2H_d), 1.61 (ddd, $J = 18.7, 8.5, 6.4$ Hz, 2H_c), 1.44-1.29 (m, 2H_b), 0.92 (t, $J = 7.3$ Hz, 3H_a). ^{13}C -NMR (101 MHz, acetone- d_6): δ (ppm) = 189.1 (C=O, C-7), 165.2 (C-OH, C-4), 164.7 (2C-OH, C-6/C-2), 105.4 (C=C, C-1), 95.9 (2HC=C, C-3/C-5), 44.3 (H₂C-C, C-8), 27.7 (H₂C-C, C-9), 23.3 (H₂C-C, C-10), 14.3 (H₃C-C, C-11). IR (ATR): $\tilde{\nu}$ (cm⁻¹) = 3266.85 (br, O-H stretching), 2946.23 (med, C-H stretching), ~1660.00 (str, C=O bending), 1449.76 (med, O-H bending), 1216.43 (str, C-O stretching), 1156.97 (str, C-O stretching), 1012.63 (str, C-O stretching), 818.32 (str, C=C bending), 645.78 (str, C=C bending).

Chapter 3 – Results

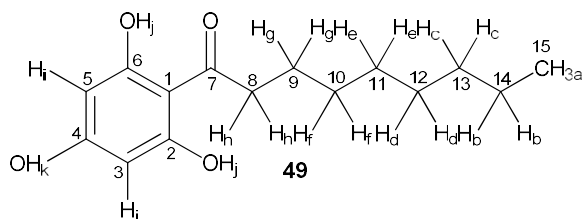


1-(2, 4, 6-Trihydroxyphenyl)butan-1-one (**47**): Colourless clustered solid. $R_f = 0.64$. UV abs, λ_{\max} : 282.0 nm. M.pt: 182°C. ESI-MS: $[M-H]^-$, $C_{10}H_{11}O_4$, $m/z = 195$ (100%). ESI-MS: $[M+H]^+$, $C_{10}H_{13}O_4$, $m/z = 197$ (100%). 1H -NMR (400 MHz, acetone- d_6): δ (ppm) = 11.77 (d, $J = 42.1$ Hz, 2H_e), 9.17 (s, 1H_f), 5.92 (d, $J = 1.6$ Hz, 2H_d), 3.04 (t, $J = 7.3$ Hz, 2H_c), 1.75-1.62 (m, 2H_b), 0.95 (t, $J = 7.4$ Hz, 3H_a). ^{13}C -NMR (101 MHz, acetone- d_6): δ (ppm) = 187.6 (C=O, C-7), 165.3 (C-OH, C-4), 164.8 (2C-OH, C-6/C-2), 105.4 (C=C, C-1), 95.9 (2HC=C, C-3/C-5), 44.3 (H₂C-C, C-8), 23.3 (H₂C-C, C-9), 14.3 (H₃C-C, C-9). IR (ATR): $\tilde{\nu}$ (cm^{-1}) = 3169.11 (br, O-H stretching), 2966.03 (med, C-H stretching), 1738.49 (wk, C=O bending), 1599.56 (med, C=C stretching), 1457.45 (med, O-H bending), 1285.77 (str, C-O stretching), 1201.80 (str, C-O stretching), 1070.94 (str, C-O stretching), 824.53 (str, C=C bending).

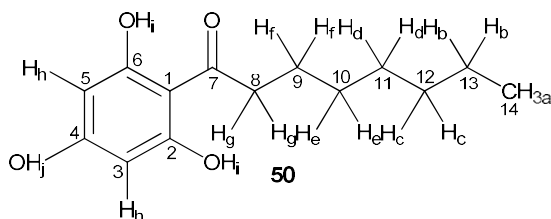


1-(2, 4, 6-Trihydroxyphenyl)hexan-1-one (**48**): Colourless clustered solid. $R_f = 0.44$. UV abs, λ_{\max} : 283.0 nm. M.pt: 127°C. ESI-MS: $[M-H]^-$, $C_{12}H_{15}O_4$, $m/z = 223$ (100%). ESI-MS: $[M+H]^+$, $C_{12}H_{17}O_4$, $m/z = 225$ (100%). 1H -NMR (400 MHz, CD₃CN): δ (ppm) = 10.96 (s, 2H_g), 7.79 (s, 1H_h), 5.85 (s, 2H_f), 3.10-2.91 (m, 2H_e), 1.70-1.56 (m, 2H_d), 1.38-1.27 (m, 4H_{c/b}), 0.90 (ddd, $J = 4.7, 4.3, 1.8$ Hz, 3H_a). ^{13}C -NMR (101 MHz, CD₃CN): δ (ppm) = 196.6 (C=O, C-7), 165.2 (C-OH, C-4), 164.7 (2C-OH, C-6/C-2), 105.4 (C=C, C-1), 95.8 (2HC=C, C-3/ C-5), 44.6 (H₂C-C, C-8), 32.4 (H₂C-C, C-9), 25.2 (H₂C-C, C-10), 23.3 (H₂C-C, C-11), 14.3 (H₃C-C, C-12). IR (ATR): $\tilde{\nu}$ (cm^{-1}) = 3251.10 (br, O-H stretching), 2954.54 (med, C-H stretching), 1738.74 (wk, C=O bending), 1617.00 (med, C=C stretching), 1466.88 (med, O-H bending), 1200.00 (str, C-O stretching), 1070.30 (str, C-O stretching), 808.30 (str, C=C bending).

Chapter 3 – Results

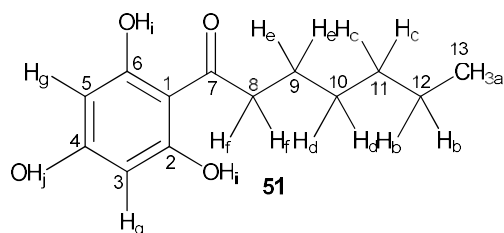


1-(2, 4, 6-Trihydroxyphenyl) nonan-1-one (**49**): Colourless clustered solid. $R_f = 0.54$. UV abs, λ_{\max} : 282.0 nm. M.pt: 114°C. ESI-MS: $[M-H]^-$, $C_{15}H_{21}O_4$, $m/z = 265$ (100%). ESI-MS: $[M+H]^+$, $C_{15}H_{23}O_4$, $m/z = 267$ (100%). 1H -NMR (400 MHz, DMSO- d_6): δ (ppm) = δ 12.17 (s, 2H_j), 10.28 (s, 1H_k), 5.73 (d, $J = 2.3$ Hz, 2H_i), 2.97-2.79 (m, 2H_h), 1.49 (dd, $J = 14.2, 7.0$ Hz, 2H_g), 1.29-1.09 (m, 10H_{f-b}), 0.79 (t, $J = 6.9$ Hz, 3H_a). ^{13}C -NMR (101 MHz, DMSO- d_6): δ (ppm) = 193.6 (C=O, C-7), 164.5 (C-OH, C-4), 164.2 (2C-OH, C-6/C-2), 103.8 (C=C, C-1), 94.7 (2HC=C, C-3/C-5), 43.1 (H₂C-C, C-8), 31.3 (H₂C-C, C-9), 28.9 (H₂C-C, C-10/C-11), 28.6 (H₂C-C, C-12), 24.5 (H₂C-C, C-13), 22.1 (H₂C-C, C-14), 14.0 (H₃C-C, C-15). IR (ATR): $\tilde{\nu}$ (cm^{-1}) = 3250.04 (br, O-H stretching), 2921.51 (med, C-H stretching), 1738.09 (wk, C=O bending), 1589.73 (med, C=C stretching), 1466.26 (med, O-H bending), 1226.73 (str, C-O stretching), 1189.77 (str, C-O stretching), 812.44 (str, C=C bending).

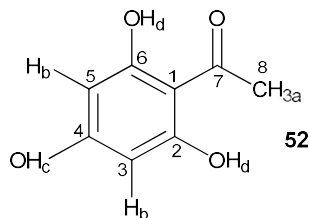


1-(2, 4, 6-Trihydroxyphenyl) octan-1-one (**50**): Colourless clustered solid. $R_f = 0.53$. UV abs, λ_{\max} : 282.0 nm. M.pt: 128°C. ESI-MS: $[M-H]^-$, $C_{14}H_{19}O_4$, $m/z = 251$ (100%). ESI-MS: $[M+H]^+$, $C_{14}H_{21}O_4$, $m/z = 253$ (45%). 1H -NMR (400 MHz, DMSO- d_6): δ (ppm) = 12.23 (s, 2H_i), 10.34 (s, 1H_j), 5.79 (s, 2H_h), 3.04-2.86 (m, 2H_g), 1.62-1.51 (m, 2H_f), 1.25 (dt, $J = 12.8, 7.4$ Hz, 8H_{e-b}), 0.85 (t, $J = 6.9$ Hz, 3H_a). ^{13}C -NMR (101 MHz, DMSO- d_6): δ (ppm) = 167.0 (C=O, C-7), 164.5 (C-OH, C-4), 164.2 (2C-OH, C-6/C-2), 103.8 (C=C, C-1), 94.7 (2HC=C, C-3/C-5), 43.1 (H₂C-C, C-8), 31.2 (H₂C-C, C-9), 28.9 (H₂C-C, C-10), 28.6 (H₂C-C, C-11), 24.5 (H₂C-C, C-12), 22.1 (H₂C-C, C-13), 14.0 (H₃C-C, C-14). IR (ATR): $\tilde{\nu}$ (cm^{-1}) = 3254.43 (br, O-H stretching), 2925.49 (med, C-H stretching), 1738.67 (med, C=O bending), 1605.19 (med, C=C stretching), 1467.62 (med, O-H bending), 1366.96 (med, O-H bending), 1191.48 (str, C-O stretching), 1069.95 (str, C-O stretching), 812.70 (str, C=C bending).

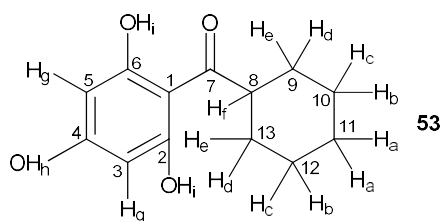
Chapter 3 – Results



1-(2, 4, 6-Trihydroxyphenyl)heptan-1-one (**51**): Colourless clustered solid. $R_f = 0.55$. UV abs, λ_{\max} : 282.0 nm. M.pt: 110°C. ESI-MS: $[M-H]^-$, $C_{13}H_{17}O_4$, $m/z = 237$ (100%). ESI-MS: $[M+H]^+$, $C_{13}H_{19}O_4$, $m/z = 239$ (62%). 1H -NMR (400 MHz, acetone- d_6): δ (ppm) = 11.74 (s, 2H_i), 9.20 (s, 1H_j), 5.92 (s, 2H_g), 3.12-2.96 (m, 2H_f), 1.66 (dt, $J = 14.9, 7.5$ Hz, 2H_e), 1.46-1.18 (m, 6H_{d-b}), 0.88 (t, $J = 6.9$ Hz, 3H_a). ^{13}C -NMR (101 MHz, acetone- d_6): δ (ppm) = 206.6 (C=O, C-7), 165.4 (C-OH, C-4), 165.2 (2C-OH, C-6/C-2), 105.2 (C=C, C-1), 95.8 (2HC=C, C-3/C-5), 44.5 (H₂C-C, C-8), 32.5 (H₂C-C, C-9), 29.9 (H₂C-C, C-10), 25.5 (H₂C-C, C-11), 23.3 (H₂C-C, C-12), 14.3 (H₃C-C, C-13). IR (ATR): $\tilde{\nu}$ (cm^{-1}) = 3258.93 (br, O-H stretching), 2916.30 (med, C-H stretching), 1738.20 (wk, C=O bending), 1568.15 (med, C=C stretching), 1466.50 (med, O-H bending), 1200.17 (med, O-H bending), 1169.92 (str, C-O stretching), 1068.17 (str, C-O stretching), 792.12 (str, C=C bending).



1-(2, 4, 6-Trihydroxyphenyl)ethanone (**52**): Yellowish clustered solid. $R_f = 0.54$. UV abs, λ_{\max} : 282.0 nm. M.pt: 216°C. ESI-MS: $[M-H]^-$, $C_8H_7O_4$, $m/z = 167$ (70%). ESI-MS: $[M+H]^+$, $C_8H_9O_4$, $m/z = 169$ (100%). 1H -NMR (400 MHz, acetone- d_6): δ (ppm) = 11.72 (s, 2H_d), 9.33 (s, 1H_c), 5.92 (s, 2H_b), 2.59 (s, 3H_a). ^{13}C -NMR (101 MHz, acetone- d_6): δ (ppm) = 206.7 (C=O, C-7), 165.5 (C-OH, C-4), 165.4 (2C-OH, C-6/C-2), 105.4 (C=C, C-1), 95.7 (2HC=C, C-3/C-5), 32.7 (H₃C-C, C-13). IR (ATR): $\tilde{\nu}$ (cm^{-1}) = 3105.41 (br, O-H stretching), 2358.98 (med, C-H stretching), 1738.52 (str, C=O bending), 1621.86 (med, C=C stretching), 1361.58 (med, O-H bending), 1279.21 (med, O-H bending), 1164.80 (str, C-O stretching), 1064.16 (str, C-O stretching), 811.33 (str, C=C bending).

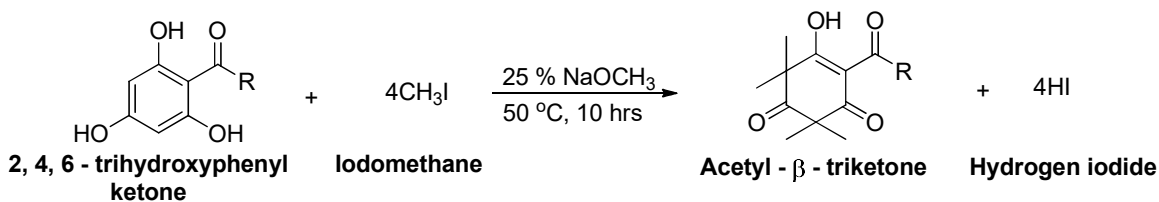


Cyclohexyl (2, 4, 6-trihydroxyphenyl)methanone (**53**): Colourless clustered solid. $R_f = 0.68$. UV abs, λ_{\max} : 283.0 nm. M.pt: 109°C. ESI-MS: $[M-H]^-$, $C_{13}H_{15}O_4$, $m/z = 235$ (100%). ESI-MS: $[M+H]^+$, $C_{13}H_{17}O_4$, $m/z = 237$ (35%). 1H -NMR (400 MHz, acetone- d_6): δ (ppm) = 11.84 (s, 2H_i), 9.33 (s, 1H_h), 5.92 (s, 2H_g), 3.69 (ddd, $J = 11.0, 7.0, 3.0$ Hz, 1H_f), 1.95-1.64 (m, 4H_{e-d}), 1.48-1.17 (m, 6H_{a-c}). ^{13}C -NMR (101 MHz, acetone- d_6): δ (ppm) = 183.4 (C=O, C-7), 165.5 (C-OH, C-4), 165.2 (2C-OH, C-6/C-2), 104.5 (C=C, C-1), 96.0 (2HC=C, C-3/C-5), 50.1 (C=C, C-8), 30.3 (2H₂C-C, C-9/C-13), 26.9 (2H₂C-C, C-10/C-12), 26.9 (2H₂C-C, C-11). IR (ATR): $\tilde{\nu}$ (cm^{-1}) = 3217.65 (br, O-H stretching), 2919.71 (med, C-H stretching), 1738.45 (med, C=O bending), 1596.41 (med, C=C stretching), 1447.29 (med, O-H bending), 1374.72 (str, C-O stretching), 1211.13 (str, C-O stretching), 1073.98 (str, C-O stretching), 971.50 (str, C=C bending), 822.29 (str, C=C bending).

3.3.3. Syntheses of β -triketones (acetyl- β -triketones)

The 2, 4, 6-trihydroxyphenyl ketones synthesized were subsequently used for the generation of the corresponding β -triketone analogues (**Scheme 3.9**). Following a protocol described by Wolfgang *et al.*, the trihydroxyphenyl ketones were subjected to exhaustive methylation with excess amounts of iodomethane¹⁷⁵.

To a 250 ml flask (**Figure 3.71**), approximately 25 ml of 25% methanolic NaOCH₃ (3 equ) was added, followed by a solution of the β -triketone precursors (1 equ) in methanol. The mixture was stirred at room temperature for 10 minutes and then iodomethane (11 equ) was added dropwise under N₂ gas. The reacting solution was then stirred at 50°C for 10 hours.



Scheme 3.9: Exhaustive methylation of acylphloroglucinols.



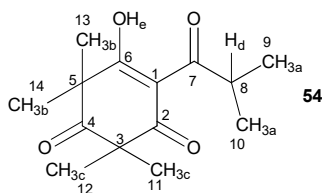
Figure 3.71: Reaction setup for the exhaustive methylation of acylphloroglucinols.

At the end of the reaction, the solution was concentrated by rotary evaporation, and the crude product was acidified with 50 ml of 2M aqueous HCl. This solution was then extracted three times with 50 ml of diethyl ether (DeE). The combined organic layers were treated twice with 100 ml of 5% aqueous Na_2CO_3 . The combined aqueous extract was then neutralized with 2M HCl, extracted three times with 60 ml of DeE and dried over anhydrous Na_2SO_4 . The filtered solution was concentrated in vacuo to give yellowish oils. These oils were subsequently purified by bulb-to-bulb high vacuum distillation. Pure β -triketone fractions were identified by characteristic $^1\text{H-NMR}$ signals of the dimethyl pairs at 1.37 (s) and 1.45 ppm (s), and of the single hydroxyl proton at 18.45 ppm (s), respectively. The experimental conditions and results of the methylation reactions are compiled in **Table 3.56**.

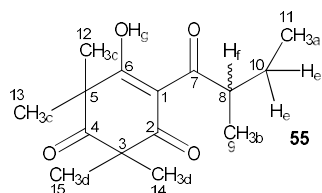
Table 3.56: Reaction parameters for the exhaustive methylation of acylphloroglucinols.

Exp	Precursors ^a			25% MeONa		MeI		Theoretical			Experimental				
	No	Mass (g)	mmol	Mass (g)	Vol (ml)	mmol	Mass (g)	Vol (ml)	mmol	Mass (g)	Crude (g)	Isolated (g)	mmol	Yield (%)	Purity (%)
76	54	6.31	32	19.84	25.07	353	50.18	22.01	30	8.11	2.81	1.06	4.20	13.1	100
77	55	6.59	31	19.36	24.92	345	48.95	21.47	30	8.35	2.42	0.90	3.38	10.8	100
78	56	1.69	7	4.53	20.24	81	11.45	5.02	10	1.95	1.57	0.25	0.87	12.8	100
79	57	4.40	24	14.90	23.51	266	37.69	16.53	20	6.43	2.77	0.83	3.48	12.9	100
80	58	9.76	46	28.66	27.86	511	72.47	31.79	50	12.36	6.15	4.40	16.5	35.6	100
81	59	6.40	30	18.78	24.74	335	47.50	20.84	30	8.10	4.16	2.21	27.2	27.3	100
82	60	5.98	30	18.73	24.72	334	47.38	20.78	30	8.08	2.56	0.91	11.3	11.3	100
83	61	7.73	34	21.27	25.52	379	53.79	23.59	30	9.18	3.11	1.26	13.7	13.7	100
84	62	7.83	29	18.15	24.54	323	45.91	20.14	30	7.83	0.84	0.11	1.4	1.4	100
85	63	3.81	15	9.32	21.75	166	23.56	10.33	20	4.02	2.60	1.49	37.1	37.1	100
86	64	3.16	13	8.18	21.39	146	20.69	9.07	10	3.53	2.21	0.78	22.1	22.1	100
87	65	0.30	2	1.10	19.15	20	2.79	1.22	2	0.48	1.19	0.26	1.16	54.2	100
88	66	2.55	11	6.67	20.91	119	16.86	7.39	10	2.88	1.80	1.13	39.2	39.2	100

^a: Acetyl phloroglucinols or trihydroxyphenyl ketone

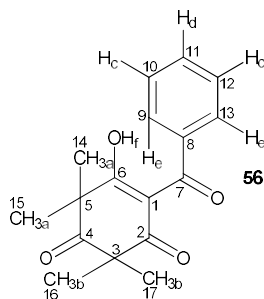
3.3.4. Characterization of the β -triketones

5-Hydroxy-4-isobutyryl-2, 2, 6, 6-tetramethylcyclohex-4-ene-1, 3-dione (**54**): Yellow oily liquid. UV abs, λ_{\max} : 281.0 nm. ESI-MS: $[M+H]^+$, $C_{14}H_{21}O_4$, $m/z = 253$ (5%). 1H -NMR (400 MHz, $CDCl_3$): δ (ppm) = 18.45 (s, 1H_e), 3.80 (dt, $J = 13.6, 6.8$ Hz, 1H_d), 1.45 (s, 6H_b), 1.37 (s, 6H_b), 1.18 (d, $J = 6.8$ Hz, 6H_a). ^{13}C -NMR (101 MHz, $CDCl_3$): δ (ppm) = 210.1 (C=O, C-4), 208.8 (C=O, C-7), 199.5 (C=O, C-2), 197.0 (C-OH, C-6), 108.4 (C=C, C-1), 57.1 (C-C, C-5), 52.4 (C-C, C-3), 35.3 (C-C, C-8), 24.4 (H₃C-C, C-13/ C-14), 24.0 (H₃C-C, C-11/C-12), 19.2 (H₃C-C, C-9/C-10). IR (ATR): $\tilde{\nu}$ (cm^{-1}) = 2978.25 (wk/br, O-H stretching), 2937.75 (med, C-H stretching), 1722.38 (str, bending C=O), 1668.39 (str, C=O stretching), 1544.54 (str, C=C bending), 1458.99 (med, C-H bending) 1381.36 (med, O-H bending), 1228.91 (str, C-O stretching), 1045.85 (str, C-O stretching), 936.44 (str, C=C bending), 854.29 (str, C=C bending).

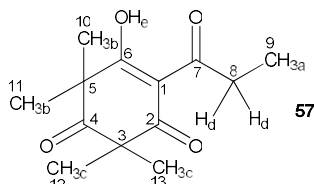


5-Hydroxy-2, 2, 6, 6-tetramethyl-4-(2-methylbutanoyl) cyclohex-4-ene-1, 3-dione (**55**): Yellow oily liquid. UV abs, λ_{\max} : 280.0 nm. ESI-MS: $[M-H]^-$, $C_{15}H_{21}O_4$, $m/z = 265$ (100%). ESI-MS: $[M+H]^+$, $C_{15}H_{23}O_4$, $m/z = 267$ (25%). 1H -NMR (400 MHz, $CDCl_3$): δ (ppm) = 18.43 (s, 1H_g), 3.62 (h, $J = 6.8$ Hz, 1H_f), 1.76 (tt, $J = 14.4, 7.4$ Hz, 2H_e), 1.44 (d, $J = 3.5$ Hz, 6H_d), 1.36 (d, $J = 2.6$ Hz, 6H_c), 1.17 (d, $J = 6.8$ Hz, 3H_b), 0.91 (t, $J = 7.4$ Hz, 3H_a). ^{13}C -NMR (101 MHz, $CDCl_3$): δ (ppm) = 210.0 (C=O, C-4), 207.9 (C=O, C-7), 199.7 (C=O, C-2), 197.2 (C-OH, C-6), 109.1 (C=C, C-1), 57.1 (C-C, C-3), 52.7 (C-C, C-5), 41.6 (HC-C, C-8), 27.0 (H₂C-C, C-10), 24.7 (H₃C-C, C-14/C-15), 23.9 (H₃C-C, C-12/C-13), 17.0 (H₃C-C, C-9), 11.9 (H₃C-C, C-11). IR (ATR): $\tilde{\nu}$ (cm^{-1}) = 2971.30 (wk/br, O-H stretching), 2936.19 (med, C-H stretching), 1721.66 (str, C=O bending), 1669.53 (str, C=O stretching), 1545.26 (str, C=C bending), 1458.95 (med, C-H bending) 1380.65 (med, O-H bending), 1228.03 (str, C-O stretching), 1046.33 (str, C-O stretching), 966.05 (str, C=C bending), 871.16 (str, C=C bending).

Chapter 3 – Results

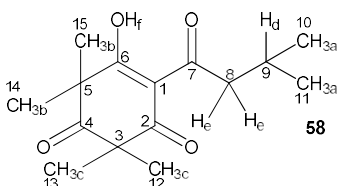


4-Benzoyl-5-hydroxy-2,2,6,6-tetramethylcyclohex-4-ene-1,3-dione (**56**): Yellow oily liquid. UV abs, λ_{max} : 277.0 nm. ESI-MS: $[M-H]^-$, $C_{17}H_{18}O_4$, $m/z = 265$ (100%). ESI-MS: $[M+H]^+$, $C_{17}H_{18}O_4$, $m/z = 267$ (100%). $^1\text{H-NMR}$ (400 MHz, CDCl_3): δ (ppm) = 17.54 (s, 1H_f), 7.56-7.49 (m, 2H_c), 7.48 (t, $J = 1.9$ Hz, 1H_d), 7.45-7.40 (m, 2H_c), 1.51 (s, 6H_b), 1.44 (s, 6H_a). $^{13}\text{C-NMR}$ (101 MHz, CDCl_3): δ (ppm) = 210.1 (C=O, C-4), 197.4 (C=O, C-7), 196.7 (C=O, C-2), 196.6 (C-OH, C-6), 136.9 (C=C, C-1), 132.4 (C=C, C-8), 128.2 (HC=C, C-9/C-13), 128.0 (HC=C, C-10/C-12), 109.6 (HC-C, C-11), 56.8 (C-C, C-3), 52.1 (C-C, C-5), 24.3 (H₃C-C, C-16/C-17), 24.0 (H₃C-C, C-14/C-15). IR (ATR): $\tilde{\nu}$ (cm^{-1}) = 2976.78 (wk/br, O-H stretching), 2943.01 (med, C-H stretching), 1678.76 (str, C=O stretching), 1583.26 (str, C=C bending), 1452.77 (med, C-H bending), 1417.05 (med, C-H bending), 1378.71 (med, O-H bending), 1284.77 (str, C-O stretching), 1025.99 (str, C-O stretching), 931.05 (str, C=C bending), 807.51 (str, C=C bending).

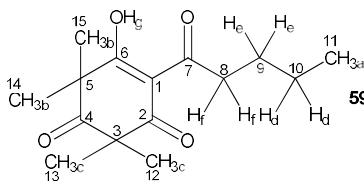


5-Hydroxy-2,2,6,6-tetramethyl-4-propionylcyclohex-4-ene-1,3-dione (**57**): Yellow oily liquid. UV abs, λ_{max} : 280.0 nm. ESI-MS: $[M-H]^-$, $C_{13}H_{18}O_4$, $m/z = 237$ (100%). ESI-MS: $[M+H]^+$, $C_{13}H_{18}O_4$, $m/z = 239$ (25%). $^1\text{H-NMR}$ (400 MHz, CDCl_3): δ (ppm) = 18.35 (s, 1H_e), 3.03 (q, $J = 7.3$ Hz, 2H_d), 1.46 (s, 6H_c), 1.36 (s, 6H_b), 1.18 (t, $J = 7.3$ Hz, 3H_a). $^{13}\text{C-NMR}$ (101 MHz, CDCl_3): δ (ppm) = 210.2 (C=O, C-4), 205.9 (C=O, C-7), 198.6 (C=O, C-2), 196.9 (C-OH, C-6), 109.1 (C=C, C-1), 57.0 (C-C, C-3), 51.9 (C-C, C-5), 33.2 (H₂C-C, C-8), 24.6 (H₃C-C, C-12/C-13), 24.0 (H₃C-C, C-10/C-11), 8.9 (H₃C-C, C-9). IR (ATR): $\tilde{\nu}$ (cm^{-1}) = 2979.94 (wk/br, O-H stretching), 939.98 (med, C-H stretching), 1718.67 (str, C=O bending), 1665.86 (str, C=O stretching), 1549.75 (str, C=C bending), 1458.95 (med, C-H bending), 1419.37 (med, C-H bending), 1380.36 (med, O-H bending), 1228.40 (str, C-O stretching), 1044.75 (str, C-O stretching), 998.77 (str, C=C bending), 861.89 (str, C=C bending).

Chapter 3 – Results

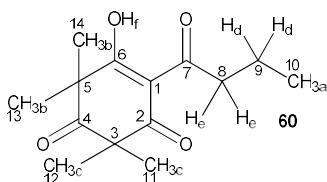


5-Hydroxy-2, 2, 6, 6-tetramethyl-4-(3-methylbutanoyl) cyclohex-4-ene-1, 3-dione (**58**): Yellow oily liquid. UV abs, λ_{\max} : 279.0 nm. ESI-MS: $[M-H]^-$, $C_{15}H_{21}O_4$, $m/z = 265$ (100%). ESI-MS: $[M+H]^+$, $C_{15}H_{23}O_4$, $m/z = 267$ (20%). 1H -NMR (400 MHz, $CDCl_3$): δ (ppm) = 18.36 (s, 1H_f), 2.87 (d, $J = 7.0$ Hz, 2H_e), 2.17 (dp, $J = 13.5, 6.8$ Hz, 1H_d), 1.44 (s, 6H_c), 1.35 (s, 6H_b), 0.98 (d, $J = 6.7$ Hz, 6H_a). ^{13}C -NMR (101 MHz, $CDCl_3$): δ (ppm) = 210.1 (C=O, C-4), 203.8 (C=O, C-7), 199.7 (C=O, C-2), 197.0 (C-OH, C-6), 109.6 (C=C, C-1), 57.0 (C-C, C-3), 52.5 (C-C, C-5), 47.3 (H₂C-C, C-8), 26.2 (HC-C, C-9), 24.4 (H₃C-C, C-12/C-13), 24.0 (H₃C-C, C-14/C-15) 22.8 (H₃C-C, C-10/C-11). IR (ATR): $\tilde{\nu}$ (cm^{-1}) = 2958.76 (wk/br, O-H stretching), 2872.17 (med, C-H stretching), 1722.00 (str, C=O bending), 1667.56 (str, C=O stretching), 1540.89 (str, C=C bending), 1462.80 (med, C-H bending), 1380.04 (med, O-H bending), 1218.05 (str, C-O stretching), 1045.96 (str, C-O stretching), 969.32 (str, C=C bending), 870.55 (str, C=C bending).

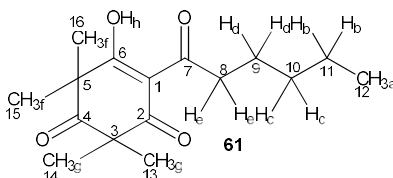


5-Hydroxy-2, 2, 6, 6-tetramethyl-4-pentanoylcyclohex-4-ene-1, 3-dione (**59**): Yellow oily liquid. UV abs, λ_{\max} : 280.0 nm. ESI-MS: $[M-H]^-$, $C_{15}H_{21}O_4$, $m/z = 265$ (100%). ESI-MS: $[M+H]^+$, $C_{15}H_{23}O_4$, $m/z = 267$ (20%). 1H -NMR (400 MHz, $CDCl_3$): δ (ppm) = 18.34 (s, 1H_g), 3.01-2.95 (m, 2H_f), 1.69-1.58 (m, 2H_e), 1.44 (s, 6H_c), 1.39 (dd, $J = 8.5, 6.2$ Hz, 2H_d), 1.36 (s, 6H_b), 0.94 (t, $J = 7.3$ Hz, 3H_a). ^{13}C -NMR (101 MHz, $CDCl_3$): δ (ppm) = 210.2 (C=O, C-4), 204.9 (C=O, C-7), 199.2 (C=O, C-2), 196.9 (C-OH, C-6), 109.2 (C=C, C-1), 57.0 (C-C, C-3), 52.2 (C-C, C-5), 39.0 (H₂C-C, C-8), 39.0 (H₂C-C, C-9), 27.4 (H₃C-C, C-12/C-13), 24.4 (H₃C-C, C-14/C-15), 24.0 (H₃C-C, C-10/C-11), 22.6 (H₂C-C, C-10), 14.0 (H₃C-C, C-11). IR (ATR): $\tilde{\nu}$ (cm^{-1}) = 2936.17 (wk/br, O-H stretching), 2873.06 (med, C-H stretching), 1720.52 (str, C=O bending), 1667.54 (str, C=O stretching), 1549.09 (str, C=C bending), 1466.74 (med, C-H bending), 1380.94 (med, O-H bending), 1204.32 (str, C-O stretching), 1046.29 (str, C-O stretching), 962.57 (str, C=C bending), 844.70 (str, C=C bending).

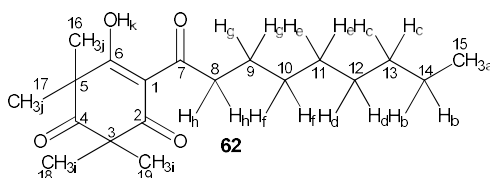
Chapter 3 – Results



4-Butyryl-5-hydroxy-2, 2, 6, 6-tetramethylcyclohex-4-ene-1, 3-dione (**60**): Yellow oily liquid. UV abs, λ_{\max} : 279.0 nm. ESI-MS: $[M-H]^-$, $C_{14}H_{20}O_4$, $m/z = 251$ (100%). ESI-MS: $[M+H]^+$, $C_{14}H_{20}O_4$, $m/z = 253$ (100%). 1H -NMR (400 MHz, $CDCl_3$): δ (ppm) = 18.34 (s, 1H_f), 3.07-2.87 (m, 2H_e), 1.79-1.60 (m, 2H_d), 1.45 (s, 6H_c), 1.36 (s, 6H_b), 1.00 (t, $J = 7.4$ Hz, 3H_a). ^{13}C -NMR (101 MHz, $CDCl_3$): δ (ppm) = 210.2 (C=O, C-4), 204.7 (C=O, C-7), 199.2 (C=O, C-2), 196.9 (C-OH, C-6), 109.3 (C=C, C-1), 57.0 (C-C, C-3), 52.2 (C-C, C-5), 41.2 (H₂C-C, C-8), 24.5 (H₃C-C, C-11/C-12), 24.0 (H₃C-C, C-13/C-14), 18.7 (H₂C-C, C-9) 14.0 (H₃C-C, C-10). IR (ATR): $\tilde{\nu}$ (cm^{-1}) = 2934.55 (wk/br, O-H stretching), 2872.24 (med, C-H stretching), 1720.90 (str, C=O bending), 1667.75 (str, C=O stretching), 1548.26 (str, C=C bending), 1462.62 (med, C-H bending), 1381.07 (med, O-H bending), 1217.41 (str, C-O stretching), 1047.05 (str, C-O stretching), 963.26 (str, C=C bending), 866.11 (str, C=C bending).



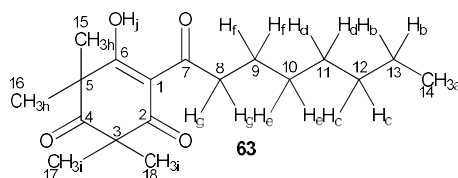
4-Hexanoyl-5-hydroxy-2, 2, 6, 6-tetramethylcyclohex-4-ene-1,3-dione (**61**): Yellow oily liquid. UV abs, λ_{\max} : 280.0 nm. ESI-MS: $[M-H]^-$, $C_{16}H_{23}O_4$, $m/z = 279$ (100%). ESI-MS: $[M+H]^+$, $C_{16}H_{25}O_4$, $m/z = 281$ (100%). 1H -NMR (400 MHz, $CDCl_3$): δ (ppm) = 18.34 (s, 1H_h), 3.00-2.95 (m, 2H_e), 1.71-1.60 (m, 2H_d), 1.44 (s, 6H_g), 1.39-1.33 (m, 4H_{b-c}), 1.36 (s, 6H_f), 0.90 (t, $J = 7.1$ Hz, 3H_a). ^{13}C -NMR (101 MHz, $CDCl_3$): δ (ppm) = 210.2 (C=O, C-4), 204.9 (C=O, C-7), 199.2 (C=O, C-2), 197.0 (C-OH, C-6), 109.2 (C=C, C-1), 57.0 (C-C, C-3), 52.3 (C-C, C-5), 39.3 (H₂C-C, C-8), 31.6 (H₂C-C, C-9), 25.0 (H₂C-C, C-10), 24.5 (H₃C-C, C-13/C-14), 24.0 (H₃C-C, C-15/C-16), 22.6 (H₂C-C, C-11), 14.1 (H₃C-C, C-12).



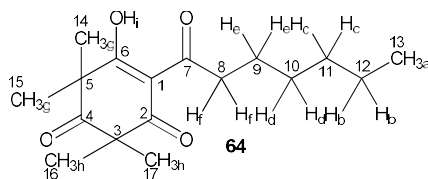
5-Hydroxy-2, 2, 6, 6-tetramethyl-4-nonanoylcyclohex-4-ene-1, 3-dione (**62**): Yellow oily liquid. UV abs, λ_{\max} : 281.0 nm. ESI-MS: $[M-H]^-$, $C_{19}H_{29}O_4$, $m/z = 321$ (100%). ESI-MS: $[M+H]^+$, $C_{19}H_{30}O_4$, $m/z = 323$ (30%). 1H -NMR (400 MHz, $CDCl_3$): δ (ppm) = 18.35 (s, 1H_k), 3.12-2.85 (m, 2H_h), 2.35 (t, $J = 7.5$ Hz, 2H_g), 1.67-1.60 (m, 4H_{e-f}), 1.45 (s, 6H_i), 1.39 (d, $J =$

Chapter 3 – Results

4.5 Hz, 2H_d), 1.36 (s, 6H_j), 1.28 (dd, $J = 5.6, 3.4$ Hz, 4H_{b-c}), 0.88 (t, $J = 6.9$ Hz, 3H_a). ¹³C-NMR (101 MHz, CDCl₃): δ (ppm) = 210.2 (C=O, C-4), 204.8 (C=O, C-7), 199.2 (C=O, C-2), 196.9 (C-OH, C-6), 109.2 (C=C, C-1), 57.0 (C-C, C-3), 52.2 (C-C, C-5), 39.3 (H₂C-C, C-8), 31.6 (H₂C-C, C-9), 25.0 (H₂C-C, C-10), 24.5 (H₃C-C, C-13/C-14), 24.0 (H₃C-C, C-15/C-16), 22.6 (H₂C-C, C-11), 14.0 (H₃C-C, C-12). IR (ATR): $\tilde{\nu}$ (cm⁻¹) = 2982.67 (wk/br, O-H stretching), 2937.57 (med, C-H stretching), 1708.33 (str, C=O bending), 1592.13 (str, C=O stretching), 1537.98 (str, C=C bending), 1471.52 (med, C-H bending), 1389.41 (med, O-H bending), 1247.77 (str, C-O stretching), 1177.96 (str, C-O stretching), 1041.97 (med, C=C bending), 860.16 (med, C=C bending).

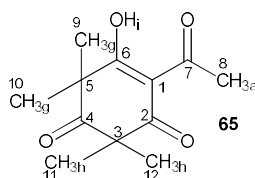


5-Hydroxy-2, 2, 6, 6-tetramethyl-4-octanoylcyclohex-4-ene-1, 3-dione (**63**): Yellow oily liquid. UV abs, λ_{\max} : 279.0 nm. ESI-MS: $[M+H]^+$, C₁₈H₂₉O₄, $m/z = 309$ (100%). ¹H-NMR (400 MHz, CDCl₃): δ (ppm) = 18.33 (s, 1H_j), 2.98-2.94 (m, 2H_g), 1.64 (dd, $J = 14.5, 7.6$ Hz, 2H_f), 1.43 (s, 6H_i), 1.39 (d, $J = 13.6$ Hz, 2H_e), 1.34 (s, 6H_h), 1.32-1.17 (m, 6H_{b-d}), 0.86 (t, $J = 6.5$ Hz, 3H_a). ¹³C-NMR (101 MHz, CDCl₃): δ (ppm) = 210.2 (C=O, C-4), 204.9 (C=O, C-7), 199.2 (C=O, C-2), 196.9 (C-OH, C-6), 109.2 (C=C, C-1), 57.0 (C-C, C-3), 52.2 (C-C, C-5), 39.3 (H₂C-C, C-8), 31.8 (H₂C-C, C-9), 29.5 (H₂C-C, C-10), 29.2 (H₂C-C, C-11), 25.3 (H₂C-C, C-12), 24.5 (H₃C-C, C-17/C-18), 24.0 (H₃C-C, C-15/C-16), 22.7 (H₂C-C, C-13), 24.0 (H₃C-C, C-14). IR (ATR): $\tilde{\nu}$ (cm⁻¹) = 2928.28 (wk/br, O-H stretching), 2856.68 (med, C-H stretching), 1721.99 (str, C=O bending), 1668.45 (str, C=O stretching), 1549.07 (str, C=C bending), 1458.23 (med, C-H bending), 1380.33 (med, O-H bending), 1216.78 (str, C-O stretching), 1047.49 (med, C=C bending), 875.09 (med, C=C bending).

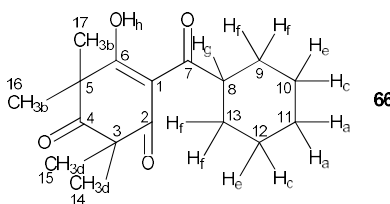


4-Heptanoyl-5-hydroxy-2, 2, 6, 6-tetramethylcyclohex-4-ene-1, 3-dione (**64**): Yellow oily liquid. UV abs, λ_{\max} : 279.0 nm. ESI-MS: $[M+H]^+$, C₁₇H₂₆O₄, $m/z = 295$ (100%). ¹H-NMR (400 MHz, CDCl₃): δ (ppm) = 18.34 (s, 1H_i), 3.00-2.95 (m, 2H_f), 1.68-1.61 (m, 2H_e), 1.44 (s, 6H_h), 1.39 (dd, $J = 10.9, 5.1$ Hz, 2H_d), 1.36 (s, 6H_g), 1.32-1.28 (m, 4H_{b-c}), 0.88 (t, $J = 7.0$ Hz, 3H_a). ¹³C-NMR (101 MHz, CDCl₃): δ (ppm) = 210.2 (C=O, C-4), 204.9 (C=O, C-7), 199.2 (C=O, C-2), 196.9 (C-OH, C-6), 109.2 (C=C, C-1), 57.0 (C-C, C-3), 52.2 (C-C, C-5), 39.3 (H₂C-C, C-

8), 31.7 (H₂C-C, C-9), 29.2 (H₂C-C, C-10), 25.3 (H₂C-C, C-11), 24.5 (H₃C-C, C-14/C-15), 24.0 (H₃C-C, C-16/C-17), 22.6 (H₂C-C, C-12), 14.2 (H₃C-C, C-13). IR (ATR): $\tilde{\nu}$ (cm⁻¹) = 2931.38 (wk/br, O-H stretching), 2859.28 (med, C-H stretching), 1721.19 (str, C=O bending), 1668.39 (str, C=O stretching), 1549.13 (str, C=C bending), 1458.47 (med, C-H bending), 1380.59 (med, O-H bending), 1216.46 (str, C-O stretching), 1047.20 (med, C=C bending), 874.87 (med, C=C bending).



4-Acetyl-5-hydroxy-2,2,6,6-tetramethylcyclohex-4-ene-1,3-dione (**65**): Yellow oily liquid. UV abs, λ_{\max} : 277.0 nm. ESI-MS: $[M+H]^+$, C₁₂H₁₇O₄, m/z = 225 (100%). ¹H-NMR (400 MHz, CDCl₃): δ (ppm) = 18.19 (s, 1H_i), 2.58 (s, 3H_a), 1.43 (s, 6H_h), 1.34 (s, 6H_g). ¹³C-NMR (101 MHz, CDCl₃): δ (ppm) = 210.1 (C=O, C-4), 201.8 (C=O, C-7), 199.3 (C=O, C-2), 196.9 (C-OH, C-6), 109.5 (C=C, C-1), 56.9 (C-C, C-3), 52.1 (C-C, C-5), 27.5 (H₃C-C, C-8), 24.4 (H₃C-C, C-11/C-12), 24.0 (H₃C-C, C-9/C-10). IR (ATR): $\tilde{\nu}$ (cm⁻¹) = 2994.00 (wk/br, O-H stretching), 2943.91 (med, C-H stretching), 1716.03 (str, C=O bending), 1659.49 (str, C=O stretching), 1540.99 (str, C=C bending), 1424.96 (med, C-H bending), 1362.36 (med, O-H bending), 1171.80 (med, C-O stretching), 1048.38 (med, C=C bending), 872.16 (med, C=C bending).



4-(Cyclohexane carbonyl)-5-hydroxy-2,2,6,6-tetramethylcyclohex-4-ene-1,3-dione (**66**): Yellow oily liquid. UV abs, λ_{\max} : 281.0 nm. ESI-MS: $[M-H]^-$, C₁₇H₂₄O₄, m/z = 321 (100%). ESI-MS: $[M+H]^+$, C₁₇H₂₄O₄, m/z = 323 (30%). ¹H-NMR (400 MHz, CDCl₃): δ (ppm) = 18.53 (s, 1H_h), 3.50 (ddd, J = 10.9, 6.6, 2.5 Hz, 1H_g), 1.83-1.69 (m, 4H_f), 1.51-1.45 (m, 2H_e), 1.42 (d, J = 0.8 Hz, 6H_d), 1.41-1.36 (m, 2H_c), 1.35 (d, J = 0.8 Hz, 6H_b), 1.28-1.16 (m, 2H_a). ¹³C-NMR (101 MHz, CDCl₃): δ (ppm) = 210.1 (C=O, C-4), 207.5 (C=O, C-7), 200.0 (C=O, C-2), 197.0 (C-OH, C-6), 108.4 (C=C, C-1), 57.1 (C-C, C-3), 52.5 (C-C, C-5), 45.2 (HC-C, C-8), 29.4 (H₃C-C, C-14/C-15), 26.0 (H₂C-C, C-11), 25.8 (H₃C-C, C-16/C-17), 24.4 (H₂C-C, C-9/C-13), 24.0 (H₂C-C, C-10/C-12). IR (ATR): $\tilde{\nu}$ (cm⁻¹) = 2930.27 (wk/br, O-H stretching), 2854.31 (med, C-H stretching), 1721.94 (str, C=O bending), 1667.43 (str, C=O stretching), 1541.52 (str,

C=C bending), 1448.47 (med, C-H bending), 1380.17 (med, O-H bending), 1217.50 (med, C-O stretching), 1046.90 (med, C=C bending), 887.62 (med, C=C bending).

3.3.5. Photolysis of β -triketones

β -Triketones absorb light within 270-290 nm and therefore are susceptible to photolysis¹⁷⁶. Photodegradations have been reported for aqueous solutions of sulcotrione and mesotrione at various pH under UV-B and solar simulator irradiation conditions¹⁷⁷. The photolytic mechanisms was suggested to involve Norrish-type reactions. The β -triketones also carry acidic protons that produce anionic intermediates for pH-induced keto-enol tautomerisation¹⁷⁸. This feature may also enable photochemical tautomerizations. Based on these reports, several of the synthesised β -triketones were dissolved in acetonitrile (MeCN) and subjected to UV-B irradiation. Approximately 0.032 g of a β -triketone were dissolved in MeCN. The solutions were transferred to either a Pyrex or Quartz Schlenk flask and irradiated in a Rayonet reactor equipped with UV-B fluorescent tubes for 2-5 hours (**Table 3.57**). Selected reactions were carried out in deuterated acetonitrile in Pyrex NMR tubes instead.

Table 3.57: Reaction parameters for the photolysis of selected β -triketones.

Exp	β -Triketone ^b			RXN Vessel						RXN _t (hr)
	No	Mass (g)	Vol (ml)	Vol (ml)	Tube	ID (cm)	OD (cm)	L (cm)	T (cm)	
89	54	0.0267	100	50	Pyrex	2.3	2.35	15.3	0.12	2
90	54	0.0321	25	20	Quartz	2.9	3.1	15.3	0.10	5
91	54	0.0189	25	20	Quartz	2.9	3.1	15.3	0.10	5
92	54	0.0469	25	20	Quartz	2.9	3.1	31.25	0.10	3
93	54	0.018	10	5	Pyrex	2.3	2.35	15.3	0.10	3
94 ^a	55	0.013	0.8	0.8	NMR	0.415	0.494	17.76	0.10	3
95 ^a	57	0.011	0.8	0.8	NMR	0.415	0.494	17.76	0.10	3
96 ^a	60	0.013	0.8	0.8	NMR	0.415	0.494	17.76	0.10	3

^a: Deuterated acetonitrile used as solvent; ^b: Stock solutions of different acetyl- β -triketones prepared; ID: inner diameter; OD: outer diameter; L: length; T: thickness.

After each reaction, the product was analysed by GC- and ¹H-NMR analyses to determine the extent of photolysis. For the reactions conducted in Schlenk tubes, about 2 ml volumes of the solution were transferred to GC vials for GC analysis. For NMR analysis, the reaction mixture was concentrated by rotary evaporation before a small amount of the crude product was used for ¹H-NMR analysis. Reactions conducted in NMR tubes were directly analysed by ¹H-NMR.

3.3.6. Photooxidation of flavasone

Under environmental conditions, photooxidation reactions can contribute to degradation processes. The photooxygenation of a selected triketone was thus investigated (**Table 3.58**). A

solution of 6.63 mM flavesone **54** in acetonitrile was prepared and transferred to a Pyrex Schlenk tube. An oxygen stream was passed through the solution while it is irradiated with visible light emitted from fluorescent lamps ($16 \times 8W$).

Table 3.58: Reaction parameters for the photooxidation of flavesone.

Exp	β -Triketone			RXN _t (hrs)	RXN Vessel					
	No	Mass (g)	MeCN (ml)		Tube	ID (cm)	OD (cm)	Length (cm)	Thickness (cm)	Vol (ml)
97	54	0.032	25	10	Pyrex	2.3	2.35	15.3	0.10	50

RXN_t: Reaction time; ID: inner diameter; OD: outer diameter.

3.3.7. Exploring Myrtaceae species for β -triketones

3.3.7.1. Sampling

Leaves were collected at Tolga (27 Equestrian Drive) in Queensland (**Figure 3.72**). Sampling was done in the early morning before sunrise between 6-9 am. This strategy minimized losses of volatile constituents. A tree pruner was used so collect suitable branches at approx. 4-10 m above chest height.



Figure 3.72: Sampling of *X. chrysanthus* in Tolga (QLD).

Collections were conducted at different times of year and under different weather conditions (**Table 3.59**). The collected branches and leaves were placed in sampling bags and immediately taken to the laboratory in Townsville. The samples were then sorted as described earlier to remove damaged leaves from the foliage.

3.3.8. Extraction of essential oils

Essential oil from intact leaves of each collection were extracted by different distillation methods using a Clevenger apparatus. Oil from *E. cloeziana* was obtained by steam distillation

(SD), while the oils of *Xanthostemon* were extracted via continuous hydrodistillation (HD). The biomass used depended on the sample holding capacity of the distillation apparatus utilized.

Table 3.59: Details of leaves collected for distillation.

No.	Coordinates	Plant name	Date	Quantity (±0.02kg)
S7	-19.3289094, 146.760361	<i>X. chrysanthus</i>	10/07/21	3.80
S8	17°11'48"S, 145°27'17"E	<i>X. chrysanthus</i>	06/06/22	3.20
S9	17°11'47"S, 145°27'16"E	<i>X. umbrosus</i>	06/06/22	3.30
S10	17°11'47"S, 145°27'16"E	<i>X. verticillatus</i>	06/06/22	3.20
S11	17°11'47"S, 145°27'15"E	<i>X. verticillatus/X. chrysanthus (hybrid)</i>	06/06/22	3.40
S12	-19.330404, 146.756458	<i>E. cloeziana</i>	27/10/22	0.50
S13	NA	<i>Leptospermum scoparium</i>		0.01 ^a

S: relates to the different sampling conducted; Coordinates obtained from Google Maps; ^a: Commercial Manuka oil obtained from Plant Essentials® retail.

3.3.8.1. Steam distillation

The steam distillation setup and operation procedure were the same as described earlier in section 3.2.3.2. Approximately 0.30 kg of *E. cloeziana* leaves from S12 (**Table 3.59**) were used. The hydrosol was further extracted by continuous liquid-liquid extraction.

3.3.8.2. Continuous hydrodistillations

Approximately 0.5-1.0 kg of healthy and fresh leaves (S7-S11, **Table 3.59**) were loaded into a 5 L flask (**Figure 3.73**). The flask was placed in a heating mantle and 3 L of distilled water, and a few boiling chips were added. A Clevenger apparatus and a Graham condenser were attached. The flask and distillation bridge were covered with aluminium foil to create a rapid reflux.



Figure 3.73: Hydrodistillation setup.

The heating mantle was set at <300°C as chilled water was circulated through the condenser at 21°C. After 8 hours, the distillation was stopped, and after complete separation of the layers, the essential oil was siphoned off into a clean and dry glass vial. The hydrosols were furthermore subjected to continuous liquid-liquid extraction.

3.3.8.3. Outcomes of distillations

The operation parameters and experimental results from both distillation processes and all liquid-liquid extractions are compiled in (Table 3.60). Preliminary GC-FID analysis of the oils was conducted to identify possible major constituents (Table 3.61). Approximately 12 mg of each oil was transferred to a GC vial (2 ml) to which 50 μ L of *n*-hexane (98%) was added as internal standard followed by 1.75 ml of anhydrous DeE as solvent. GC-FID analysis of *E. cloeziana* oil showed a distinct presence of tasmanone in 88.9% of the composition. Its identity was verified by comparison with literature RI values and NMR spectral analysis. Similarly, the presence of flavesone (5.3%), leptospermone (17.5%), and isoleptospermone (3.8%) in Manuka oil was confirmed by GC-FID.

Table 3.60: Distillation and extraction parameters and results.

Sample Name	Distillation			Time (hrs)	T (°C)	Oil (g)			Yield (%)	Appearance
	Qty (g)	Type	Water (L)			Distilled	SSE	Total		
<i>E. cloeziana</i>	352.12	gSD	1	5	120	1.34	0.01	1.35	0.38	yellowish green
<i>X. chrysanthus</i>	507.77	cHD	2	8	200	0.12	0.02	0.14	0.03	greenish yellow
<i>X. chrysanthus</i>	530.57	cHD	2	8	200	0.05	0.04	0.09	0.02	greenish yellow
<i>X. umbrosus</i>	500.01	cHD	1	8	200	0.92	0.02	0.93	0.19	greenish yellow
<i>X. verticillatus</i>	500.02	cHD	1	8	200	2.91	0.01	2.92	0.58	cloudy colourless
Hybrid ^a	502.10	cHD	1	8	200	0.23	0.02	0.24	0.05	golden brown

^a: *X. verticillatus*/*X. chrysanthus*; gSD: Glass steam distillation setup; cHD: continuous hydrodistillation in a glass setup; SSE: Solvent-solvent extract obtained by extracting remnants of oil in the hydrosol and boiler water.

Table 3.61: Characterization of major peaks from the Myrtaceae essential oils.

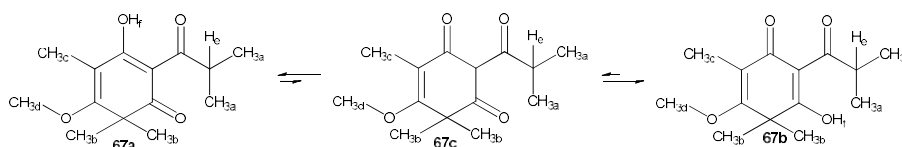
Plant	Constituent(s)				Identification
	Rt	%	KI	KI ^c	
<i>E. cloeziana</i>	26.41	88.87	1719.59	1698 ¹⁷⁹	Tasmanone 67
<i>X. chrysanthus 1</i>	28.09	21.70	1807.83	1805 ^{143,180}	Isotorquatone 68
	30.77	18.23	1957.20	NI	NI
<i>X. chrysanthus 2</i>	28.17	84.60	1812.21	1805 ^{143,180}	Isotorquatone 68
<i>X. umbrosus</i>	27.26	63.52	1763.89	1760 ¹⁸¹	Cyclocolorenone 69
<i>X. verticillatus</i>	19.63	94.04	1399.71	1400 ¹⁴³	1, 3-Dimethoxy-5-isopropylbenzene 70
	19.53	18.19	1395.50	1400 ¹⁴³	1, 3-Dimethoxy-5-isopropylbenzene 70
Hybrid ^a	21.26	10.45	1472.17	1472 ¹⁸²	β -Cadinene 71
	24.45	13.17	1621.54	1622 ^b	Isoleptospermone 55
	24.30	4.10	1621.54	1622 ^b	Isoleptospermone 55
<i>L. scoparium</i>	24.51	16.83	1624.52	1624 ^b	Leptospermone 58
	22.71	3.14	1538.70	1538 ^b	Flavesone 54

^a: Hybrid of *X. chrysanthus* and *X. verticillatus*; KI: Calculated Kovats retention index values; NI: Subsequent compounds not identified; ^b: Internal standard prepared in-house; ^c: Literature KI values.

3.3.9. Separation and characterization of major β -triketone constituents

3.3.9.1. Extraction of flavesone from *E. cloeziana* oil

About 1.348 g of *E. cloeziana* oil was dissolved in 20 ml of diethyl ether (DeE). This solution was transferred to a separating funnel and extracted twice with 15 ml of aqueous 0.623 M Na_2CO_3 . The alkaline extract was acidified with 20 ml of aqueous 2 M HCl to give a milky solution, which was then extracted three times with 15 ml of DeE. The combined organic layer was washed with saturated NaCl solution and dried over anhydrous MgSO_4 . The filtrate was subsequently concentrated by rotary evaporation at 40°C and 1000-40 mbar to give 0.213 g of a golden oil. GC-FID analysis of the *E. cloeziana* oil showed a dominant peak for tasmanone (79), which is known to exist in different tautomeric forms in solution (**Scheme 3.10**).



Scheme 3.10: Equilibrium of the tasmanone tautomers.

$^1\text{H-NMR}$ spectroscopy of the treated *E. cloeziana* extract confirmed that tasmanone is present in two dominant tautomeric forms (**Figure 3.74** and **Table 3.62**). The signals marked in blue and green represent the chemical shifts for the minor and major tautomer, respectively.

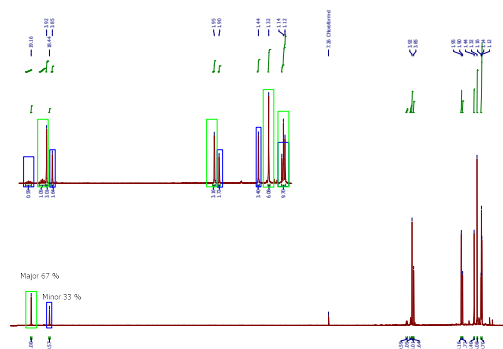


Figure 3.74: $^1\text{H-NMR}$ spectrum of tasmanone in CDCl_3 .

Table 3.62: $^1\text{H-NMR}$ assignments of the two major tautomeric forms of tasmanone

$^1\text{H-NMR}$	δ (400 MHz, CDCl_3 , ppm)	
	67a	67b
6 CH_{3a}	1.14 (t, $J = 7.2$ Hz, 1H)	1.14 (t, $J = 7.2$ Hz, 1H)
6 CH_{3b}	1.32 (s, 1H)	1.44 (s, 1H)
CH_{3c}	1.95 (s, 1H)	1.90 (s, 1H)
CH_{3d}	3.92 (s, 1H)	3.85 (s, 1H)
CH_e	3.97 (dt, $J = 13.6, 6.8$ Hz, 1H)	4.13 (dt, $J = 13.5, 6.7$ Hz, 1H)
OH_f	19.16 (s, 1H)	18.44 (s, 1H)

3.3.9.2. Isolation of flavesone, leptospermone and isoleptospermone from Manuka oil

About 10.3724 g of Manuka oil were dissolved in 80 ml of DeE. This solution was transferred to a separating funnel and extracted four times with 20 ml of 0.623 M aqueous Na₂CO₃. The alkaline aqueous layer was acidified with 80 ml of 2 M aqueous HCl to give a cloudy solution, which was extracted four times with 50 ml of DeE each. The combined organic layers were washed with saturated NaCl-solution and dried over anhydrous MgSO₄. After filtration the filtrate was concentrated to dryness by rotary evaporation at 40°C and 1000-40 mbar to give 3.4408 g of a golden-like oil. ¹H-NMR and GC-FID analyses confirmed the presence of triketones in 97% purity. The crude extract was further purified by bulb-to-bulb distillation to give three fractions, collected in three separate bulbs (**Table 3.63**). GC-analysis was conducted to determine their compositions.

Table 3.63: β-Triketones of Manuka oil fractions.

Fraction ^a	Mass (g)	Composition (%)				Appearance
		54	55	58	others	
Crude ^b	3.4408	16.85	17.60	63.30	2.25	golden oil
1	0.1802	19.60	12.56	67.84	0.00	clear oil
2	1.4710	25.18	18.45	56.37	0.00	clear oil
3		empty				
4	0.7082	45.20	13.12	29.01	12.67	clustered white solids

^a: Fractions 1 to 4 collected in bulbs 1 to 4; ^b: Crude obtained by acid-base extraction.

Fractions 1 and 2 contained β-triketones in high purities, but in different compositions compared to the crude product. As an example, Fraction 2 (**Figure 3.75**) contained flavesone (22.712 min), isoleptospermone (24.297 min), and leptospermone (24.511 min).

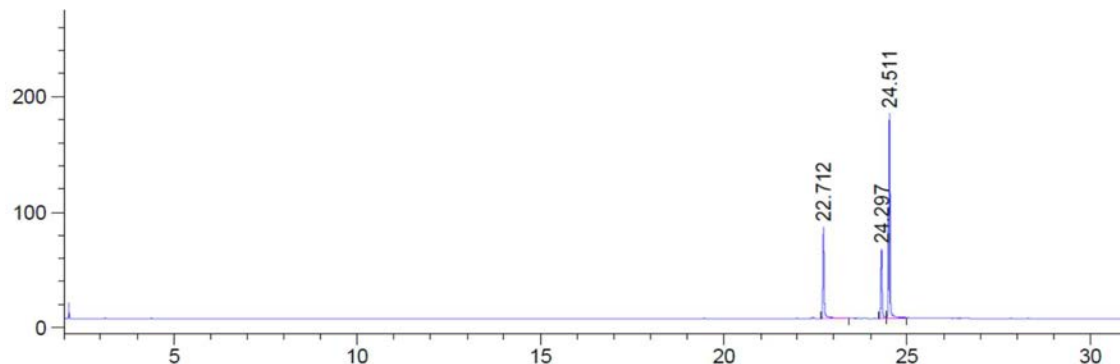


Figure 3.75: GC-chromatogram of Fraction 2 from bulb-to-bulb purification.

3.3.10. Isolation and identification of cyclocolorenone from *X. umbrosus* oil

According to **Table 3.61**, the RI value determined for the major constituent in *X. umbrosus* oil corresponded to cyclocolorenone (**69**, **Figure 3.76**). To verify this assumption, this constituent

The corresponding HSQC and HMBC spectra were used to unambiguously confirm the structure of **69**. Given below in **Table 3.64** are the assigned single and multiple H-C correlations.

Table 3.64: HMBC and HSQC ^1H - ^{13}C -correlations of cyclocolorenone.

C	δ (ppm)			
	^{13}C	^1H - 1J (HSQC)	^1H - 2J (gHMBC)	^1H - 3,4J (gHMBC)
4	31.8	2.02-1.98 (m, 1H)	0.79 (d, $J = 6.9$ Hz, 1H), 2.04 (d, $J = 2.5$ Hz, 1H), 2.08 (d, $J = 2.9$ Hz, 1H), 1.41 (dt, $J = 13.2, 3.1$ Hz, 1H).	1.60 (ddd, $J = 8.2, 5.6, 3.1$ Hz, 1H), 1.98-1.94 (m, 1H), 2.49 (dd, $J = 18.5, 6.6$ Hz, 1H)
3	32.4	2.08 (d, $J = 2.9$ Hz, 1H), 1.41 (dt, $J = 13.2, 3.1$ Hz, 1H).	1.60 (ddd, $J = 8.2, 5.6, 3.1$ Hz, 1H), 1.98-1.94 (m, 1H), 2.02-1.98 (m, 1H)	0.79 (d, $J = 6.9$ Hz, 3H), 2.08 (d, $J = 2.9$ Hz, 1H)
2	21.3	1.60 (ddd, $J = 8.2, 5.6, 3.1$ Hz, 1H), 1.98-1.94 (m, 1H)	2.08 (d, $J = 2.9$ Hz, 1H), 1.41 (dt, $J = 13.2, 3.1$ Hz, 1H).	1.46 (t, $J = 5.9$ Hz, 1H), 0.79 (d, $J = 6.9$ Hz, 3H), 1.01 (s, 3H), 1.23 (s, 3H)
1a	32.6	1.28-1.26 (m, 1H)	1.98-1.94 (m, 1H)	1.41 (dt, $J = 13.2, 3.1$ Hz, 1H), 1.01 (s, 3H), 1.23 (s, 3H), 2.02-1.98 (m, 1H)
7b	28.7	1.46 (t, $J = 5.9$ Hz, 1H)	1.72 (d, $J = 1.9$ Hz, 3H)	1.41 (dt, $J = 13.2, 3.1$ Hz, 1H), 1.01 (s, 3H), 1.23 (s, 3H), 1.98-1.94 (m, 1H), 2.95 (d, $J = 2.1$ Hz, 1H)
7a	140.5	-	1.46 (t, $J = 5.9$ Hz, 1H)	1.72 (d, $J = 1.9$ Hz, 3H)
4a	42.6	2.95 (d, $J = 2.1$ Hz, 1H)	2.49 (dd, $J = 18.5, 6.6$ Hz, 1H), 2.04 (d, $J = 2.5$ Hz, 1H)	0.79 (d, $J = 6.9$ Hz, 3H), 1.46 (t, $J = 5.9$ Hz, 1H), 2.08 (d, $J = 2.9$ Hz, 1H)
1	26.1	-	1.46 (t, $J = 5.9$ Hz, 1H), 1.23 (s, 3H), 1.01 (s, 3H), 1.28-1.26 (m, 1H)	1.98-1.94 (m, 1H), 2.08 (d, $J = 2.9$ Hz, 1H)
8	29.6	1.23 (s, 3H)	-	1.46 (t, $J = 5.9$ Hz, 1H), 1.01 (s, 3H), 1.28-1.26 (m, 1H), 1.98-1.94 (m, 1H)
9	16.6	1.01 (s, 3H)	-	1.46 (t, $J = 5.9$ Hz, 1H), 1.23 (s, 3H), 1.28-1.26 (m, 1H), 1.98-1.94 (m, 1H)
7	176.6	-	1.72 (d, $J = 1.9$ Hz, 3H)	2.49 (dd, $J = 18.5, 6.6$ Hz, 1H), 2.04 (d, $J = 2.5$ Hz, 1H), 2.95 (d, $J = 2.1$ Hz, 1H)
6	208.4	-	2.49 (dd, $J = 18.5, 6.6$ Hz, 1H), 2.04 (d, $J = 2.5$ Hz, 1H)	1.72 (d, $J = 1.9$ Hz, 3H), 2.02-1.98 (m, 1H)
5	40.3	2.49 (dd, $J = 18.5, 6.6$ Hz, 1H), 2.04 (d, $J = 2.5$ Hz, 1H)	2.95 (d, $J = 2.1$ Hz, 1H)	2.02-1.98 (m, 1H), 2.08 (d, $J = 2.9$ Hz, 1H), 1.41 (dt, $J = 13.2, 3.1$ Hz, 1H), 1.46 (t, $J = 5.9$ Hz, 1H), 1.72 (d, $J = 1.9$ Hz, 3H)
10	17.6	0.79 (d, $J = 6.9$ Hz, 3H)	2.02-1.98 (m, 1H)	2.08 (d, $J = 2.9$ Hz, 1H), 1.41 (dt, $J = 13.2, 3.1$ Hz, 1H), 2.49 (dd, $J = 18.5, 6.6$ Hz, 1H), 2.04 (d, $J = 2.5$ Hz, 1H)
11	8.4	1.72 (d, $J = 1.9$ Hz, 3H)	-	2.49 (dd, $J = 18.5, 6.6$ Hz, 1H), 2.04 (d, $J = 2.5$ Hz, 1H), 1.46 (t, $J = 5.9$ Hz, 1H), 2.95 (d, $J = 2.1$ Hz, 1H)

The lJ correlation of ^{13}C to ^1H was established by ^1H -NMR and ^{13}C -NMR, and further confirmed with 2D-HSQC. Subsequent ^1H at $>^lJ$ were derived from 2D-HMBC.

3.3.11. Identification of 1, 3-dimethoxy-5-isopropylbenzene from *X. verticillatus* oil

The oil obtained from *X. verticillatus* revealed the presence of 1, 3-dimethoxy-5-isopropylbenzene (**70**, **Figure 3.79**) in 94.4% by RI value comparison (**Table 3.61**). It was also the major constituent in the oil from the hybrid *Xanthostemon* species.

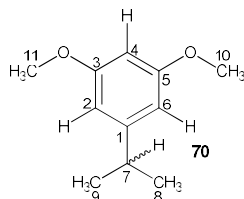


Figure 3.79: Structure of 1, 3-dimethoxy-5-isopropylbenzene (**70**).

Due to its already high 1, 3-dimethoxy-5-isopropylbenzene content, the *X. verticillatus* oil was directly subjected to 2D-NMR assessment without any purification. The $^1\text{H-NMR}$ spectrum of the oil depicts all characteristic peaks of compound **70** (**Figure 3.80**).

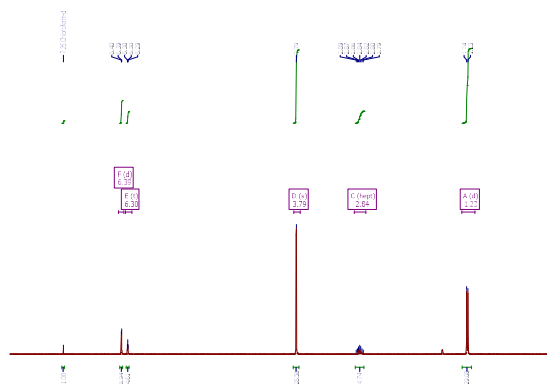


Figure 3.80: $^1\text{H-NMR}$ spectrum of 1, 3-dimethoxy-5-isopropylbenzene (**70**).

Analysis of proton and carbon correlations (J -couplings) using HSQC- and HMBC-techniques further confirmed the structure **70** (**Table 3.65**).

3.3.12. GC-MS characterization of other constituents in the essential oils

A comprehensive identification of other constituents present in the distilled essential oils was conducted by extensive GC-MS analysis. The identity of these constituents was determined by calculating the KI-values for each peak from the corresponding retention time of the spectrum and comparison with known KI-values of compounds from the NIST GC-MS library and Wiley GC-MS library (**Table 3.66**), respectively.

Table 3.65: HMBC and HSQC ^1H - ^{13}C -correlations of 1, 3-dimethoxy-5-isopropylbenzene.

C	δ (ppm)			
	^{13}C	^1H - 1J (HSQC)	^1H - 2J (gHMBC)	^1H - ^3-7J (gHMBC)
1	151.7	-	2.84 (hept, $J = 6.9$ Hz, 1H)	1.24 (d, $J = 6.9$ Hz, 3H)
2	104.8	6.40 (d, $J = 2.2$ Hz, 1H)	-	6.30 (t, $J = 2.3$ Hz, 1H), 2.84 (hept, $J = 6.9$ Hz, 1H)
3	160.9	-	6.40 (d, $J = 2.2$ Hz, 1H), 6.30 (t, $J = 2.3$ Hz, 1H)	3.79 (s, 3H)
4	97.6	6.30 (t, $J = 2.3$ Hz, 1H)	-	6.40 (d, $J = 2.2$ Hz, 1H), 1.24 (d, $J = 6.9$ Hz, 3H)
5	160.9	-	6.40 (d, $J = 2.2$ Hz, 1H), 6.30 (t, $J = 2.3$ Hz, 1H)	3.79 (s, 3H)
6	104.8	6.40 (d, $J = 2.2$ Hz, 1H)	-	6.30 (t, $J = 2.3$ Hz, 1H), 2.84 (hept, $J = 6.9$ Hz, 1H)
7	34.6	2.84 (hept, $J = 6.9$ Hz, 1H)	1.24 (d, $J = 6.9$ Hz, 3H)	6.40 (d, $J = 2.2$ Hz, 1H), 3.79 (s, 3H)
8/9	24.0	1.24 (d, $J = 6.9$ Hz, 3H)	2.84 (hept, $J = 6.9$ Hz, 1H)	3.79 (s, 3H)
9	24.0	1.24 (d, $J = 6.9$ Hz, 3H)	2.84 (hept, $J = 6.9$ Hz, 1H)	3.79 (s, 3H)
10/11	55.4	3.79 (s, 3H)	-	1.24 (d, $J = 6.9$ Hz, 3H)

The 1J correlation of ^{13}C to ^1H was established by ^1H -NMR and ^{13}C -NMR, and further confirmed with 2D-HSQC. Subsequent ^1H at $>^1J$ were derived from 2D-HMBC.

3.3.13. Biological activity testing

β -Triketones isolated from natural sources are known for their diverse biological properties. Therefore, a biological activity assessment of the synthesized β -triketone precursors, actual β -triketones, and Myrtaceae extracts was carried out on indicator microorganisms to determine their antimicrobial activities. Insecticidal activity screening was also conducted on larval and adult *A. aegypti*.

3.3.13.1. Antimicrobial activity

Antibacterial activity testing of the essential oil extracts and synthetic compounds was performed on gram positive *Staphylococcus epidermidis*, gram negative *Escherichia coli* and, fungi *Candida albicans*, respectively. Growth inhibition of these microorganisms confirms the antibacterial potency of the molecule or extract tested.

Chapter 3 – Results

Table 3.66: Identified constituents of the isolated essential oils based on MS (m/z) and KI (RI) values.

No	Compound		XC1	XU	XCV	XC2	XV	EC	MO _r	MO-1	MO-2
	Name	KI Lit, KI									
72	α -Pinen	934 934	-	-	-	-	-	-	1.3	2.4	-
73	NI (MW 113)	945	-	-	-	-	-	<0.1	-	-	-
74	β -Pinene	980 980	-	-	-	-	-	-	0.1	-	-
75	β -Myrcene	991 991	-	-	-	-	-	-	0.1	-	-
76	NI (MW 136)	1006	-	-	-	-	-	-	<0.1	-	-
77	<i>m</i> -Cymene	1027 1025	-	-	-	-	-	-	0.2	-	-
78	Limonene	1032 1032	-	-	-	-	-	-	0.1	-	-
79	Eucalyptol	1035 1035	-	-	-	-	-	<0.1	0.1	-	-
80	NI (MW 218)	1051 -	-	0.8	-	-	-	-	-	-	-
81	γ -Terpinene	1060 1060	-	-	-	-	-	-	0.1	-	-
82	1, 3-Heptanedione-2, 6-dimethyl	1075 1076	-	-	-	-	-	0.4	-	-	-
83	α -Terpinolene	1088 1088	-	-	-	-	-	-	<0.1	-	-
84	Linalol	1101 1101	-	-	-	-	-	-	0.1	-	-
85	Isoamylisovaterate	1107 1105	-	-	-	-	-	-	0.1	-	-
86	NI (MW 85)	1116	-	-	-	-	-	-	0.2	-	-
87	NI (MW 170)	1148	-	-	-	-	-	-	<0.1	-	-
88	Terpinene-4-ol	1183 1184	-	-	-	-	-	-	<0.1	-	-
89	NI (MW 102)	1194	-	-	-	-	-	-	0.1	-	-
90	α -Terpineol	1197 1197	-	-	-	-	-	-	<0.1	-	-
91	NI (MW 101)	1200	-	-	-	-	-	-	0.1	-	-
92	Benzoic acid	1205 1210	1.3	-	-	-	-	-	-	-	-
93	3-Phenyl-2-butanone	1243 1243	-	-	2.4	5	-	-	-	-	-
94	NI (MW 168)	1243	-	-	-	-	-	-	0.1	-	-
95	Benzylacetone	1247 1253	11.9	-	-	-	-	-	-	-	-
96	NI (MW 191)	1249	-	-	-	-	-	<0.1	-	-	-

Chapter 3 – Results

97	NI (MW 168)	1276	-	-	-	-	-	-	<0.1	-	-	
98	NI (MW 209)	1320	-	-	-	-	-	0.2	-	-	-	
99	NI (MW 170)	1327	-	-	-	-	-	0.1	-	-	-	
100	NI (MW 214)	1342	-	-	-	-	-	0.6	-	-	-	
101	α -Cubebene	1350	1351	-	-	0.4	-	-	-	4.2	7.2	1
102	Benzalacetone	1360	1356	1.2	-	-	-	-	-	-	-	-
103	α -Cupaene	1380	1380	-	-	-	-	-	-	4.5	7.6	1.2
104	β -Elemene	1393	1389	-	2.8	-	-	-	-	1.4	2.8	0.3
105	NI (MW 105)	1393	-	-	-	-	-	<0.1	-	-	-	-
106	Eugenol	1397	1389	-	-	-	-	-	-	-	-	0.2
70	1,3-Dimethoxy-5-isopropylbenzene	1397	1397	-	-	-	-	95.9	-	-	-	-
107	NI (MW 208)	1401	-	-	-	-	-	<0.1	-	-	-	-
108	NI (MW 166)	1407	-	-	20	-	-	-	-	-	-	-
109	NI (MW 204)	1408	-	-	-	-	-	0.8	-	-	-	-
110	α -Gurgenene	1412	1412	-	5.7	-	-	-	-	0.9	2.1	0.2
111	NI (MW 183)	1420	-	-	-	-	-	-	-	-	-	-
112	α -Santalene	1426	1424	-	-	3	-	-	-	-	-	-
113	β -Caryophyllene	1428	1428	-	-	-	-	-	-	1.9	4	0.5
114	NI (MW 184)	1432	-	-	-	-	-	-	-	-	-	-
115	NI (MW 152)	1438	-	-	0.8	-	-	-	-	-	-	-
116	Alloaromadendrene	1443	1442	-	4.1	-	-	-	-	-	4.6	0.3
117	Aromadendrene	1447	1449	-	-	-	-	-	-	1.4	-	-
118	Naphthalene	1454	1458	-	-	-	-	-	-	-	-	1.5
119	epi-Bicyclosesquiphellandrene	1457	1452	-	-	-	-	-	-	-	5.6	-
120	NI (MW 204)	1457	-	-	-	-	-	-	-	2.4	-	-
121	NI	1460	-	-	-	1.7	-	-	-	-	-	-
122	Humulene	1462	1462	-	-	-	-	-	-	-	0.7	-
123	NI (MW 190)	1464	-	-	-	-	-	-	0.1	-	-	-
124	NI (MW 194)	1471	-	-	-	-	-	0.6	-	-	-	-

Chapter 3 – Results

71	β -Cadinene	1474	1471	-	-	-	-	-	-	2.8	3.8	0.8
125	NI (MW 194)	1476		-	-	-	-	1.1	-	-	-	-
126	Patchoulene	1477	1484	-	1.2	-	-	-	-	-	-	-
127	β -Cadinene	1479	1472	-	-	-	-	-	-	2.8	-	-
128	α -Curcumene	1482	1482	-	-	-	-	-	-	-	-	-
129	NI (MW 69)	1484		-	-	15.2	-	-	-	-	-	-
130	Germacrene D	1485	1484	-	-	-	-	-	-	-	-	-
131	NI (MW 218)	1489		-	-	10.2	-	-	-	-	-	-
132	δ -Selinene	1494	1493	-	-	-	-	-	-	-	-	0.8
133	Virdiforene	1496	1496	-	1.3	-	-	-	-	-	-	0.3
134	Eremophilene	1499	1498	-	-	-	-	-	-	-	5.7	-
135	NI (MW 226)	1499		-	-	-	-	-	0.2	-	-	-
136	NI (MW 204)	1499		-	-	-	-	-	-	4.4	-	-
137	β -Guaiene	1501	1500	-	-	0.9	-	-	-	-	-	-
138	α -Seliene	1501	1498	-	-	-	-	-	-	-	-	0.8
139	Dibunol	1505	1504	11.4	-	-	2.8	-	-	-	7.4	-
140	β -Bisabolene	1509	1509	-	-	1.4	-	-	-	-	-	-
141	γ -Cadinene	1517	1517	-	0.7	-	-	-	-	-	-	0.2
142	δ -Cadinene	1522	1522	-	-	1.3	-	-	-	-	-	-
143	(-)- α -Panasinsene	1524	1527	-	-	-	-	-	-	-	-	-
144	Calamenene	1528	1528	-	-	1.5	-	-	-	-	-	3.1
145	<i>cis</i> -Calamene	1537	1537	-	-	-	-	-	-	22.7	18.1	-
54	Flavesone	1541	1546	-	-	1.3	-	-	0.2	-	-	15.8
146	α -Cubenene	1544	1345	-	-	-	-	-	-	-	9.6	-
147	NI (MW 254)	1547		-	-	-	-	-	-	11.1	-	-
148	Calacorene	1549	1546	-	-	-	-	-	-	-	1.7	-
149	α -Calacorene	1552	1548	-	-	-	-	-	-	0.8	-	-
150	<i>cis</i> -Nerolidol	1568	1565	1.1	-	0.9	-	-	-	-	-	-
151	Palustrol	1571	1581	-	7.9	-	-	-	-	-	-	-

Chapter 3 – Results

152	Caryophyllene oxide	1581	1581	-	-	-	-	-	-	1.2	1.4	-
153	Spathulenol	1584	1584	-	1.1	-	-	-	0.1	-	-	-
154	Espatulenol	1585	1585	-	-	-	-	-	-	-	1.8	-
155	NI	1588		-	0.7	-	-	-	-	-	-	-
156	Globulol	1591	1590	-	2.3	-	-	-	0.1	-	0.9	-
157	Spirijatamol	1592	1592	-	-	1.4	-	-	-	-	-	-
158	δ -Viridiflorol	1599	1595	-	-	-	-	-	-	-	-	-
159	Guaiol	1602	1600	-	-	-	-	-	-	-	-	0.1
160	Viridiflorol	1603	1604	-	5.7	-	-	-	0.7	0.4	1.6	-
161	NI (MW 266)	1612		-	-	-	-	-	0.2	-	-	-
162	Ledol	1615	1608	-	8.2	-	-	-	-	-	-	-
163	Isoleptospermone	1622	1622	21	-	13.2	-	-	-	5.3	1.2	8.2
164	Epicubenol	1632	1632	-	-	-	-	-	-	-	1.6	-
165	Isospathulenol	1639	1639	-	0.5	-	-	-	-	-	-	-
58	Leptospermone	1640	1640	-	-	-	-	-	-	22.4	-	64.5
166	Cubenol	1641	1641	-	-	3.3	-	-	-	-	2.9	-
167	NI (MW 238)	1642		-	-	-	-	-	0.8	-	-	-
168	α -Muurolol	1648	1645	-	-	-	-	-	-	-	-	-
169	τ -Muurolol	1649	1650	-	1.6	1.9	-	-	-	-	-	-
170	γ -Cadinol	1661	1658	-	-	-	-	-	-	-	-	-
171	α -Cadinol	1662	1662	-	2	-	-	-	-	1.9	-	-
172	NI	1663	-	-	-	-	-	-	-	-	0.9	-
173	Juniper camphor	1666	1675	-	1.5	-	-	-	-	-	0.7	-
174	NI (MW 218)	1666		-	-	-	-	-	-	0.7	-	-
175	NI	1677		-	-	-	2	-	-	-	-	-
176	Eudesma-4-(15)-7-diene-1b-ol	1679	1685	0.7	-	-	-	-	-	-	0.9	-
177	NI	1680		-	-	1.6	-	-	-	-	-	-
178	NI (MW 220)	1681		-	-	-	-	-	-	0.5	-	-
179	NI	1687		-	-	-	-	-	-	-	0.8	-

Chapter 3 – Results

180	NI (MW 220)	1689		-	-	-	-	-	-	0.6	-	-
181	α -Bisabolol	1692	1691	-	-	0.4	-	-	-	-	-	-
182	NI (MW 238)	1694		-	-	-	-	-	1.1	-	-	-
183	Farnesol	1711	1713	4	1.6	3.6	-	-	-	-	-	-
184	(2Z, 6E)-Farnesol	1723	1722	1.2	-	2.7	-	-	-	-	-	-
185	NI (MW 206)	1736		-	-	-	-	-	-	0.3	-	-
186	(E, E)-Farnesal	1739	1738	2.4	-	5.7	-	-	-	-	-	-
67	Tasmanone (MW 252)	1744		-	-	-	-	-	93.6	-	-	-
187	NI (MW 266)	1753		-	-	-	-	-	-	<0.1	-	-
69	Cyclocolorenone	1756	1758	-	-	2.6	0.9	0.9	-	-	-	-
188	NI (MW 220)	1758		-	-	-	-	-	-	0.2	-	-
189	Benzyl benzoate	1770	1769	-	-	-	1.2	-	-	-	-	-
190	Aristolone	1780	1787	-	35.3	-	-	-	-	-	-	-
191	Papuanone	1788	1787	-	-	-	-	-	-	-	-	-
192	NI (MW 266)	1794		-	-	-	-	-	1	-	-	-
193	NI	1796		-	-	1.3	-	-	-	-	-	-
194	NI (MW 238)	1799		-	-	-	-	-	-	0.3	-	-
195	NI	1805		-	-	1	-	-	-	-	-	-
196	NI (MW 266)	1805		-	-	-	-	-	0.7	-	-	-
197	5-Hydroxy-calamenene	1805	1801	-	-	-	-	-	-	0.1	-	-
198	NI (MW 236)	1818		-	-	-	-	-	-	0.1	-	-
199	Farnesoic acid	1829	1824	35	11.2	-	28	-	2.1	-	-	-
200	NI (MW 236)	1837		-	-	-	-	-	-	0.1	-	-
201	Baeckeol	1859	1861	-	-	2.3	-	-	-	-	-	-
202	NI (MW 268)	1859		-	-	-	-	-	0.4	-	-	-
203	5-Hexenoic acid	1871	1885	-	-	-	26.2	-	-	-	-	-
204	NI (MW 300)	1873		-	-	-	-	-	0.3	-	-	-
205	Benzyl salicylate	1877	1868	-	-	-	3.8	-	-	-	-	-
206	NI	1905	-	-	2.8	-	-	-	-	-	-	-

Chapter 3 – Results

207	Palmitic acid	1925	1927	-	-	-	-	-	0.5	-	-	-
208	Isophytol	1948	1948	1	-	-	6.2	-	-	-	-	-
209	Hexadecanoic acid	1988	1984	-	-	-	3.1	-	-	-	2	-
210	Kaurene	2058	2043	6.1	-	0.4	13.7	-	-	-	-	-
211	<i>trans</i> -Phytol	2115	2111	1.6	-	-	4.9	-	-	-	-	-
212	Supraene	2808	2808	0.4	-	-	-	-	-	-	-	-

NI: Not identified; KI: Kovats index; XC1: *X. chrysanthus 1*; XC2: *X. chrysanthus 2*; XU: *X. umbrosus*; XCV: *X. chrysanthus/X. verticillatus* hybrid; XV: *X. verticillatus*; EC: *E. cloeziana*; MOr: Untreated Manuka oil; MO-1: neutral fraction of Manuka oil; MO-2: acetic fraction of Manuka oil.

About 1 ml of 100 µg/ml solutions of each antimicrobial sample was transferred to culture tubes containing the medium inoculated with the respective microorganism. The treated culture tubes were subsequently incubated at 35°C for 12 hours. The tubes were vortexed and certain volumes were transferred to glass cuvettes for analysis using a UV-Vis spectrometer. A decrease in transmittance correlates with an increase of microbial growth and vice versa. Experiments were performed once and the average OD₆₀₀ of three replicates for each sample was derived. The growth inhibition was calculated relative to the growth rate of the bacteria alone (**Table 3.67**).

Table 3.67: Mean values of antimicrobial growth inhibitions expressed by selected 2, 4, 6-trihydroxyphenyl ketones, acetyl-β-triketones and Myrtaceae essential oils.

Antimicrobial sample	Growth inhibition (%)		
	<i>S. epidermidis</i>	<i>E. coli</i>	<i>C. albicans</i>
^a 54	84.70	3.67	2.66
^b 41	96.81	6.27	0.54
^b 42	96.87	28.44	1.66
^a 58	85.81	1.40	5.45
^b 44	22.20	22.96	5.30
^a 57	27.25	6.24	2.03
^b 45	13.74	2.98	1.95
^a 55	84.58	9.31	2.24
XC-1	2.98	9.21	2.95
XU	1.00	6.50	2.49
XV	0.72	7.23	2.34
XCV	40.21	3.04	0.31
XC-2	4.87	4.87	4.51
EC	14.96	7.56	3.19
MO-1	3.03	3.03	0.23
MOr	31.43	1.54	1.36
MO-2	81.33	6.03	2.03
STD	80.94	78.69	76.04

STD: Gentamicine; ^a: synthetic acetyl-β-triketone; ^b: synthetic 2, 4, 6 – trihydroxyphenyl ketones; XC-1: *X. chrysanthus 1*; XU: *X. umbrosus*; XV: *X. verticillatus*; XCV: *X. chrysanthus/X. verticillatus* hybrid; XC-2: *X. chrysanthus 1*; EC: *E. cloeziana*; MO-1: neutral fraction of Manuka oil; MOr: untreated Manuka oil; MO-2: acetic fraction of Manuka oil.

3.3.13.2. Larvicidal activity

Larvicidal activities of the essential oil extracts and synthesized compounds were evaluated against young L3 and L4 stage larvae of *A. aegypti*. The toxicity of the samples on the larvae was deduced from the mortality of the larvae in each well. A 24-well plate system seeded with medium was inoculated with six larvae each (**Figure 3.81**). The potential anti-larval agents were added as a single dose of 200 µg/ml. A total of 15 samples were inoculated into 4 wells (a-d) and incubated for 24 hours. In general, a 3×24-well plate system was used, each containing four samples for anti-larval evaluation and a 1% absolute ethanol (Tem) control.



Figure 3.81: Larvicidal test setup using 24-well plates containing seeded larvae.

The screening was done in duplicate and the larvicidal toxicity of individual samples were recorded as percent mortality from the mean of the 4 replicates. For each sample tested, the 95% confidence intervals were also calculated at $n = 48$ larvae per compound. **Table 3.68** below summarises the results of the antilarval screening.

Table 3.68: Anti-larval activity of selected 2, 4, 6-trihydroxyphenyl ketones, acetyl- β -triketones and Myrtaceae essential oils.

Compound	Dead larvae after 24 hrs		Mortality at 24hrs (%)				95% CI ($\pm\%$)
	AS 1	AS 2	AS 1	AS 2	Mean	SD ($\pm\%$)	
EtOH	0	0	0.00	0.00	0.00	0.000	0.000
^b 42	0	2	0.00	8.33	4.17	5.893	1.667
^a 57	24	25	100.00	100.00	100.00	0.000	0.000
^b 44	0	0	0.00	0.00	0.00	0.000	0.000
^a 57	24	23	100.00	100.00	100.00	0.000	0.000
^b 45	0	1	00.00	4.17	2.08	2.946	0.834
^a 55	24	25	100.00	100.00	100.00	0.000	0.000
XC-1	24	25	100.00	100.00	100.00	0.000	0.000
XU	24	24	100.00	100.00	100.00	0.000	0.000
XV	24	24	100.00	100.00	100.00	0.000	0.000
XCV	24	23	100.00	92.00	96.00	5.657	1.600
EC	23	23	95.83	100.00	97.92	2.946	0.834
MO-1	12	9	50.00	37.50	43.75	8.839	2.501
MOr	24	15	100.00	62.50	81.25	26.517	7.502
MO-2	24	26	100.00	100.00	100.00	0.000	0.000

AS: Antilarval screening; EtOH: Ethanol control is marked as “Tem” on the well plate; ^a: synthetic acetyl- β -triketone; ^b: synthetic 2, 4, 6 – trihydroxyphenyl ketones; XC-1: *X. chrysanthus 1*; XU: *X. umbrosus*; XV: *X. verticillatus*; XCV: *X. chrysanthus/X. verticillatus* hybrid; XC-2: *X. chrysanthus 1*; EC: *E. cloeziana*; MO-1: neutral fraction of Manuka oil; MOr: untreated Manuka oil; MO-2: acetic fraction of Manuka oil.

3.3.13.3. Adulticidal activity

The adulticidal activity of Manuka oil extract (MOr) was tested against adult *A. aegypti* mosquitoes. Various concentrations of the oil were exposed to a population of mosquitoes and those that were knocked down (KD) were determined over a period of one hour and after two hours, respectively.

Chapter 3 – Results

WHO bioassay tubes were used to determine the susceptibility of Manuka oil extract against adult mosquitoes (**Figure 3.82**). The setup is composed of an observation tube and a control tube. The mosquitoes are passed through a trap door and were exposed to MOr samples for a total of 2 hours. The experiment was performed once and for each concentration, 3 batches of 25 adult female mosquitoes were tested.

The number and percentages of mosquitoes knocked down based on the concentration of MOr are given in **Table 3.69** and **Table 3.70**, respectively. The mortality rates of adult mosquitoes after 24 hours were additionally determined (see **Table 3.71** and **Table 3.72**).

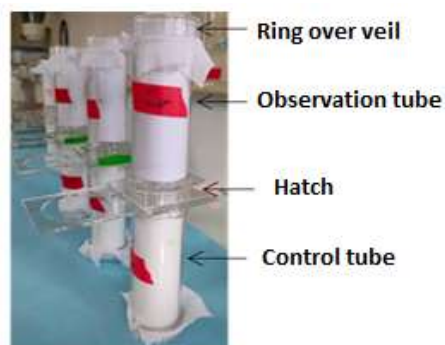


Figure 3.82: WHO tubes infused with adult *A. aegypti*.

Chapter 3 – Results

Table 3.69: Total number of adult mosquitoes knocked down by MOr.

t (min)	Number of adult mosquitoes KD																				EtOH			
	1000 µg/L				1500 µg/L				3000 µg/L				6000 µg/L				9000 µg/L				0 µg/L ^a			
	B1	B2	B3	TKD	B1	B2	B3	TKD	B1	B2	B3	TKD	B1	B2	B3	TKD	B1	B2	B3	TKD	B1	B2	B3	TKD
0	0	0	0	0	0	0	0	0	0	0	0	0	0	0	0	0	0	0	0	0	0	0	0	0
3	0	0	0	0	0	0	0	0	0	0	0	0	1	0	0	1	24	24	25	73	0	0	0	0
6	0	0	0	0	0	0	0	0	0	0	0	0	22	23	24	69	24	24	25	73	0	0	0	0
9	0	0	0	0	0	0	0	0	0	0	0	0	25	25	25	75	24	24	25	73	0	0	0	0
12	0	0	0	0	0	0	0	0	0	0	0	0	25	25	25	75	24	24	25	73	0	0	0	0
15	0	0	0	0	0	0	0	0	1	0	0	1	25	25	25	75	24	24	25	73	0	0	0	0
18	0	0	0	0	0	0	0	0	4	1	0	5	25	25	25	75	24	24	25	73	0	0	0	0
21	0	0	0	0	0	0	0	0	6	4	0	10	25	25	25	75	24	24	25	73	0	0	0	0
25	0	0	0	0	1	1	1	3	8	5	1	14	25	25	25	75	24	24	25	73	0	0	0	0
30	0	0	0	0	2	2	1	5	22	5	4	31	25	25	25	75	24	24	25	73	0	0	0	0
40	0	0	0	0	4	2	2	8	22	9	7	38	25	25	25	75	24	24	25	73	0	0	0	0
50	0	0	0	0	8	5	8	21	24	10	9	43	25	25	25	75	24	24	25	73	0	0	0	0
60	1	0	0	1	8	5	8	21	25	10	10	45	25	25	25	75	24	24	25	73	1	0	0	1
120	5	2	2	9	17	11	8	36	10	6	7	23	25	25	25	75	24	24	25	73	0	0	0	0
TM	25	26	25	76	25	25	25	75	25	25	25	75	25	25	25	75	24	24	25	73	25	25	23	73

B1-3: Bioassay replicates for each MOr concentration tested; TKD: Total number of mosquitoes knocked down at specific time intervals from B1-3; TM: Total number of mosquitoes passed through each WHO bioassay tube during B1-3; ^a: Tests with WHO tubes treated with pure EtOH solvent.

Chapter 3 – Results

Table 3.70: Percentages (%) of adult mosquitoes knocked down by MOr.

t (min)	Treatment Manuka oil										EtOH	
	1 ppm		1.5 ppm		3 ppm		6 ppm		9 ppm		0 ppm	
	$\Sigma(76)$	%	$\Sigma(75)$	%	$\Sigma(75)$	%	$\Sigma(75)$	%	$\Sigma(73)$	%	$\Sigma(73)$	%
0	0	0	0	0	0	0	0	0	0	0	0	0
3	0	0	0	0	0	0	1	1.3	73	100	0	0
6	0	0	0	0	0	0	69	92	73	100	0	0
9	0	0	0	0	0	0	75	100	73	100	0	0
12	0	0	0	0	0	0	75	100	73	100	0	0
15	0	0	0	0	1	1.3	75	100	73	100	0	0
18	0	0	0	0	5	6.7	75	100	73	100	0	0
21	0	0	0	0	10	13.3	75	100	73	100	0	0
25	0	0	3	4	14	18.7	75	100	73	100	0	0
30	0	0	5	6.7	31	41.3	75	100	73	100	0	0
40	0	0	8	10.7	38	50.7	75	100	73	100	0	0
50	0	0	21	28	43	57.3	75	100	73	100	0	0
60	1	1.3	21	28	45	60	75	100	73	100	1	1.4

Chapter 3 – Results

Table 3.71: Percentage mortality (\bar{x}) of adult female mosquitoes after 24 hrs.

AS	% Mortality																	
	1000 µg/L						1500 µg/L						3000 µg/L					
	B1	B2	B3	\bar{x}	SD	95% CI	B1	B2	B3	\bar{x}	SD	95 CI	B1	B2	B3	\bar{x}	SD	95% CI
1	4.00	0.00	0.00	1.33	1.89	2.13	8.00	0.00	0.00	8.00	4.62	5.23	nd					
1	nd						nd						4.00	0.00	0.00	4.00	3.27	2.61
2	nd						nd						8.00	8.00	4.00	-	-	-

AS: Adulticidal screening; B1-3: Bioassay replicates for each Manuka oil concentration tested; SD: Standard Deviation; nd: Not done.

Table 3.72: Percentage mortality (\bar{x}) of adult female mosquitoes after 24 hrs.

AS	% Mortality																	
	6000 µg/L						9000 µg/L						0 µg/L ^a					
	B1	B2	B3	\bar{x}	SD	95% CI	B1	B2	B3	\bar{x}	SD	95% CI	B1	B2	B3	\bar{x}	SD	95% CI
1	nd						nd						4.00	0.00	0.00	5.90	6.77	4.42
1	68.00	68.00	72.00	81.33	12.58	10.07	100.00	100.00	100.00	100.00	0.00	0.00	20.80	8.30	8.00			
2	100.00	92.00	88.00				100.00	100.00	100.00				0.00	12.00	0.00			

AS: Adulticidal screening; B1-3: Bioassay replicates for each Manuka oil concentration tested; SD: Standard Deviation; nd: Not done; ^a: Tests with WHO tubes treated with pure EtOH solvent.

CHAPTER 4: DISUSSION

4. Discussion

4.1. Synthesis of 5-Hydroxy-2(5H)-furanone and its alkoxy-derivatives

4.1.1. Purification of furan-2-carbaldehyde

The purity of FAL was essential to establish accurate stoichiometric and conversion parameters during the optimization studies. Likewise, the dark colourization of technical grade furfural impacts transparency and hence light absorption. Therefore, a controlled distillation was conducted. During distillation, the vapor temperature remained consistently stable at 161°C and more than 95% of the technical-grade FAL were distilled at this vapor temperature. This high recovery suggests a rather small number of impurities.

A light-yellow oil with an almond-like smell was obtained as the distillate compared to the brown technical-grade material. ¹H-NMR analysis of the distillate revealed a downfield doublet at 9.45 ppm for the aldehyde proton. A doublet at 7.35 ppm and two subsequent doublet of doublets at 7.10 and 6.42 ppm represented the three vinyl protons respectively. ¹³C-NMR signals between 112.4 and 147.9 ppm accounted for the heteroaromatic carbons, while a signal at 152.6 ppm represented the aldehyde carbon. The IR-spectrum revealed C=C and aldehyde groups through a strong signal at 1666.98 cm⁻¹ and a medium signal at 1391.93 cm⁻¹, respectively. Fraction FD1 was subsequently used for all conversions using artificial light, while fractions FD2-5 were used for outdoor solar reactions.

4.1.2. Photooxygenations with artificial light

4.1.2.1. Photooxygenation studies in a Rayonet reactor

Reactions conducted using the Rayonet chamber reactor generally gave high conversions ranging from 73-100%. The yield of isolated HF, however, dropped to 30-52% after workup and recrystallization (**Figure 4.1**).

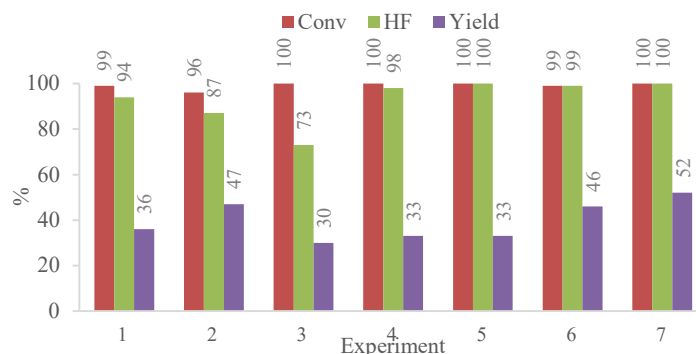


Figure 4.1: Comparison of conversions, isolated yields and purities.

Ethoxy derivatives and residual FAL were only observed in Experiments 1-3. In contrast, Experiments 4-7 showed complete conversions with negligible amounts of the ethoxy derivatives, affording HF in high purity of 98-100%. Considerable amounts of product were lost during (re)crystallization, which impacts any future commercialization. From the outcome of Experiment 1, the presence of by-products and residual FAL (<30%) does not necessarily affect crystal formation. However, while successful crystallization was initially achieved, subsequent recrystallization caused significant losses.

Experiment 1 and 3 followed the Esser *et al.* method, Experiments 4-6 the Huan *et al.* protocol, and Experiments 2 and 7 the Oelgemöller *et al.* reaction conditions^{4,62,67}. Experiment 5 gave complete conversion and 100% selectivity towards HF within an hour of irradiation (**Figure 4.2**). Even with increased amounts of FAL and RB as in the case of Experiments 2 and 7, complete conversion was achieved within 2 hours.

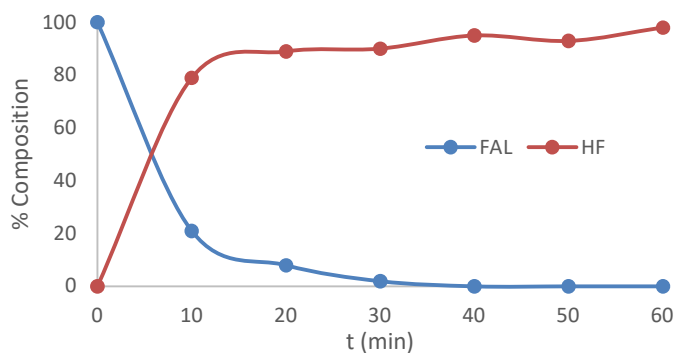


Figure 4.2: Reaction profile of Experiment 5.

4.1.2.2. Syntheses and characterization of alkoxy-furanones

Six different AFN were satisfactorily produced by formic acid-catalyzed esterification reactions with arrange of C1, C3, C4 and C5 alcohols (**Figure 4.3**).

Of these, methanol worked best, as excess amounts of alcohol could be separated from the crude by direct rotary evaporation. In contrast, the less volatile C4-C5 alcohols persisted removal even at increased temperatures and pressures. To overcome this, the alcohols were removed as azeotropes from heterogeneous mixtures of the crude product and water.

Experiment 8 achieved complete conversion, but produced only 12% (5 mg) of pure MFN (7). This significant loss in material was likely caused by the ternary azeotrope of water, methanol and MFN (7). The ¹H-NMR spectrum revealed a singlet at 3.58 ppm and a triplet at 5.86 ppm, which confirms the presence of the methoxy group and the methine proton at C-5, respectively.

Both, ^{13}C -NMR and IR confirmed the presence of the methoxy-group as signals at 57.2 ppm or 1471.54 cm^{-1} , respectively.

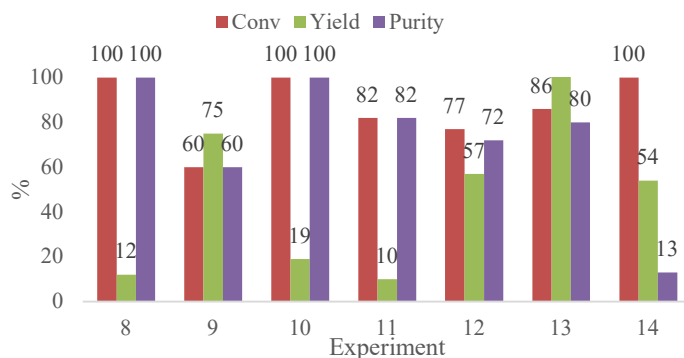


Figure 4.3: Conversion rates, selectivity and yields of alkoxyfuranones.

Experiment 9 reached only 60% conversion and offered a crude yield of 75%. The product comprised of 60% *i*-PrFN (**8**), corresponding to a yield of 45%. The residual mass of the crude was primarily residual isopropanol. The ^1H -NMR spectrum of *i*-PrFN (**8**) showed a complex signal at 4.09 ppm due to coupling of the C-6 proton with the adjacent methyl protons at C-7 and C-8. The integration of the triplet at 1.26 ppm corresponded to the six equivalent protons of the methyl groups. The C-6 carbon resonated at 73.7 ppm, depicting a gem-dimethyl group, which also corresponded to the IR signal at 1111.63 cm^{-1} .

Experiment 10 reached 100% conversion, but resulted in a crude yield of just 19%. However, the crude product constituted 65 mg of pure BFN (**9**). The by ^1H -NMR spectral conformation of BFN (**9**) was primarily done via the butoxy moiety. The doublet of triplets at 3.87 and 3.68 ppm was caused by 2J couplings of the two protons at C-6 (H_g and H_f) and 3J couplings with their two neighbouring protons at C-7. At 1.61 ppm, a triplet of triplet with 3J couplings to the adjacent C-6 and C-8 protons was assigned to the respective protons ($\text{H}_{e,d}$) at C-7. The triplet of quartet at 1.39 ppm with a 3J splitting to the C-8 protons ($\text{H}_{b,c}$) and the C-9 methyl protons corresponded to the protons at C-7. The IR vibration at 1463.16 cm^{-1} also confirmed the presence of methylene groups.

Experiment 11 gave a conversion of 82% with a crude yield of 10%. The crude mixture contained 82% of *i*-PeFN (**10**) and 18% of its acyclic analogue *iso*-pentoxybutenal (*i*-PeBL). Confirmation of the isopentyl substituent was achieved by ^1H -NMR via a quintet at 3.66 ppm with 3J -couplings to the individual methylene protons at C-7 and C-8, respectively. The later methylene protons exhibited adjacent 2J couplings as well as 3J coupling with the methyl protons at C-9/10 and the lone proton at C-6, and hence gave a multiplet at 1.31 ppm. The gem-

dimethyl carbon at C-6 was characterized by a ^{13}C -NMR signal at 84.3 ppm and verified by an IR signal at 1134.05 cm^{-1} .

Experiment 12 had an overall conversion of 77% with a subsequent crude yield of 57%. It was determined that 23% of the crude was hexanol, 5% was the acyclic form hexanoylbutenal (HBL, **21**) and the rest was hexoxy-furanone (HFN, **11**) with 72%. This composition accounted for a 41% yield of HFN (**11**). The hexoxy-moiety, especially the methylene carbons and the C-6 component, were evident from the ^1H -NMR spectrum. Signals at 3.85 (dt) and 3.67 ppm (m) represented the C-6 protons H_g and H_f with couplings to each other and the two C-7 protons. The methylene protons at C-7 and C-8 were observed at 1.62 ppm (m) with an integration of 4H, similarly for C-9 and C-10 at 1.29 ppm (m). The methyl protons at C-11 appeared at 0.88 ppm (t). The ^{13}C -NMR signal at 70.8 represented the C-6 carbon, while the preceding signals at 31.6-22.7 accounted for the methylene protons at C-7 to C-10. The IR signals at 1466.94 cm^{-1} and 1124.76 cm^{-1} were indicative of the methylene groups and the C-O carbon at C-6.

Experiment 13 achieved a conversion of 86% with an >100% crude yield. The crude product contained 80% of pentoxy-furanone (PeFN, **12**), 6% of its acyclic form and 14% of residual pentanol. A yield of 85% (487 mg) of PeFN (**12**) was hence attained in 80% purity. Structural confirmation of the pentoxy-moiety was evident from ^1H -NMR signals at 3.86 ppm (dt, H_f) and 3.67 ppm (dt, H_e), showing 2J couplings of the adjacent protons at C-6 and unequal couplings with the methylene protons at C-7. Additional signals at 1.64 (2H_d) and 1.33 ppm ($4\text{H}_{b/c}$) belonged to the methylene protons at C-7 to C-9. IR signals at 1353.33 and 1123.69 cm^{-1} furthermore indicated methylene groups as well as the C-O carbon at C-6, the later further confirmed by a ^{13}C -NMR signal at 70.9 ppm.

Experiment 14 gave complete conversion to cyclopentoxy-furanone (cPeFN, **13**) in a crude yield of 54%. The bulk of the crude product comprised of cyclopentanol, with only 13% composition of cPeFN (**13**), resulting in a yield of just 7%. The pentacyclic moiety was confirmed by ^1H -NMR, having signals at 4.35-4.09 ppm that represent the lone proton at C-6 with 3J -couplings to its neighbouring methylene protons. The subsequent methylene protons at C-7 and C-8 were observed at 1.85-1.66 (m) and 1.63-1.48 ppm (m) for the C-9 and C-10 protons, respectively. The ^{13}C -NMR signals of these methylene carbons were observed at 83.2 and 35.7 ppm, while the C-O carbon at C-6 was found at 83.2 ppm. IR peaks at 1436.87 cm^{-1} and 1132.72 cm^{-1} furthermore corresponded to the methylene groups and the ether group.

4.1.3. Photooxygenation studies in an Immersion Well Reactor

The immersion-well reactor utilized a reaction vessel of 250 ml capacity. It was observed that the reaction temperature was similar to that in the Rayonet reactor and remained at approx. 21°C. Despite the stronger lamp power and hence heat generation, the advanced design of the immersion well cooler allowed for effective cooling. Due to the larger scale, it took at least 6 hours to reach high conversions, compared to 1 hour in the smaller Rayonet device.

4.1.3.1. 5-Hydroxy-2(5H)-furanone synthesis

Experiments 15 and 17 reached complete consumption of starting material, while Experiment 16 achieved a 94% conversion with 6% of residual FAL. The reaction conditions and parameters of Experiment 16 were similar for all reactions and hence, a consistent O₂ stream and sufficient irradiation from the lamp were provided throughout the course of irradiation. Differences in performances could thus arise from undissolved or impure furfural, a lower light transmittance due to impurities or insufficient production of ¹O₂ caused by sensitizer bleaching. Nevertheless, a 28% yield of crude product was obtained which constituted 83% of HF (**2**). Workup of the crude product yielded 3% (4.57 g) of pure HF (**2**), which accounted for an 84% loss during the isolation process. Experiment 15 had a 29% yield of the crude product with 85% of HF (**2**), 10% MBL, and 5% of MFN (**7**). Subsequent workup of the crude resulted in a low yield of 4% (5.26 g) of pure hydroxyfuranone crystals, corresponding to an 82% loss during purification. Experiment LR8 showed a similar trend with a 28% crude yield, containing 81% of HF (**2**). However, due to a loss of 81% of material during workup, only 4% (5.31 g) of pure HF crystals were obtained.

The difficulty of obtaining crystalline HF (**2**) is well known. Several methods such as freezing out with liquid nitrogen or sublimation have been proposed but these are time- or resource-demanding. Crude HF (**2**) of decent purity may thus be converted directly without purification. Despite the low yields, the immersion well setup generated multi-gram amounts of pure HF (**2**) due to its larger size and more powerful lamp.

4.1.3.2. Syntheses of alkoxy-furanones

Experiments 18-20 all achieved complete conversions with crude yields of 64, 99 and 99%, respectively. However, their crude constituents varied in composition but in particular the ratios of the ring-chain tautomers ABL and AFN. Experiment 18 was not subjected to isolation, as it constitutes MFN (**7**) in 93% purity. Experiment 16 contained 19% of EBL (**5**) and 11% of residual EtOH. It was further purified by flash chromatography and rendered 61 mg of EBL (**5**)

and 2.68 g of EFN (**4**). The crude product of Experiment 20 contained 12% of BBL (**14**) and 88% of BFN (**9**), which were separated by flash chromatography to yield 33 mg of BBL (**14**) and 0.23 g of BFN (**9**), respectively.

4.1.3.2.1. Isolation and identification of dialkoxy-derivatives

A diethoxy derivative (DiE) was identified in the crude product of Experiment 19 with close resemblance to the acyclic tautomer. In the $^1\text{H-NMR}$ spectrum, it gave a characteristic doublet of doublet at 5.03 ppm through the coupling of the C2 proton with adjacent groups. The two distinctive protons of the π -system at C3-C4 were identified by doublets of doublets at 6.09 and 6.83 ppm with a *trans*- 3J -coupling of 15.8 Hz. **Figure 4.4** below gives three possible structures with a diethoxy moiety.

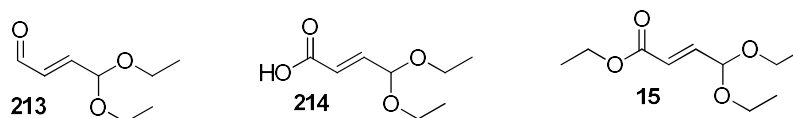


Figure 4.4: Three possible structures of the polyethoxy-derivative.

It is assumed that structures **213** and **214** would differ primarily in their downfield $^1\text{H-NMR}$ profile. However, no characteristic signals supporting an aldehyde or acid derivative were observed. Instead, the spectrum showed three distinctive signals that are characteristic of structure **15**. Firstly, the methylene protons of both ethoxy groups are in two different chemical environments, as confirmed by peaks at 6.12 (dd) and 6.80 ppm (dd), respectively. Secondly, the singlet at 6.21 ppm is representative of the methine proton. Finally, the two methyl groups appeared as a triplet at 1.22 ppm. Based on these findings, structure **15** was assigned to the triethoxy derivative isolated from Experiment 23.

4.1.4. Photooxygenations with natural sunlight

4.1.4.1. Flatbed design

The reactor's design was simple but suboptimal. The frame was angled at approx. 17° to achieve effective solar exposure during illumination. The fixed frame did not allow for further adjustment of the tilting angles. As a rule of thumb, static solar reactors are typically tilted at the latitude angle of their location (here: ca. 19°) to allow for maximum harvest of sunlight. Due to its fixed construction, the tilting angle was slightly lower. This, however, minimized the pressure on the flatbed's seals caused by the weight of the reaction mixture and reduced the risk of leakage. The low tilting angle did not allow for effective saturation with air as the injected bubbles immediately rose to the top side of the reactor. The back side of the reaction mixture

was thus less saturated with oxygen. The recirculating solvent pump also had to be positioned higher than the reactor's outlet, resulting in a weak circulating flow rate. As the pump's head had to be filled with liquid in order to operate, a lower positioning might have achieved an easier operation and higher flow rates. Despite these limitations, extended exposure times achieved continuous conversion rates regardless of the intensity and quantity of sunlight during illuminations.

4.1.4.2. Illumination efficiency

The solar spectrum consists of ultraviolet, visible and infrared radiation. Of the light that reaches the Earth's surface, infrared radiation makes up 49.4%, visible light 42.3% and ultraviolet radiation just over 8%, respectively. Generally, the 97.5 cm × 35.2 cm aperture can only harvest the 42-43% of visible light to facilitate photosensitization and subsequent photooxygenation. This amount of usable radiation is further reduced by the absorption spectrum of the sensitizer. While the UV-fraction is largely filtered by the glass, the weak IR-radiation does not enable excitation but contributes to warm-up effects of the solution. As a result, the reactor's cleanliness, especially of its glass surfaces, elevation angle, and horizontal positioning to the sun all contribute to optimum illumination. Due to its static and simple design, changes during operation such as manual sun tracking were not possible. To somewhat compensate for these suboptimal features, a reflective aluminium sheet was placed directly under the reactor's body. As aluminium reflects light above 275 nm with efficiencies of >50%, it enabled an improved utilization of the solar radiation. Sunlight that is passing through the flatbed's body is hence largely redirected back into the solution, improving photon utilization.

4.1.4.3. Cooling and oxygen supply

Simple water cooling was supplied through garden hosing from an outdoor tap at the Molecular Genetics Laboratory. The tap water temperature varied depending on the daytime and position of the sun between 15-21°C. The water was passed in the upward direction through the mantle of a large external Dimroth-condenser, while the reaction mixture passed through the cooling coil. The usage of unchilled cooling water and the need for direct exposure to sunlight resulted in an ineffective cooling of the reaction solution inside the flatbed, which reached 34°C on average (21-46°C) for most part of the day. The elevated temperature in combination with air purging resulted in notable evaporation losses of the solvent. Heating effects may have also contributed to unwanted decomposition, side- or follow-up reactions. A more suitable cooling system using a recirculating chiller and/or cooling coils inside the flatbed's body are thus desirable for future solar studies.

Natural air constituting approx. 21% of oxygen was pumped into the reaction chamber at 15 LPM via a metal pipe with several outlet holes. While the large sizes of the bubbles achieved a less optimal saturation of the solution, the somewhat violent air-stream promoted circulation of the reaction solution. While natural air represents a readily available and cheap oxygen-supply, its temperature and composition depend largely on the surrounding environmental conditions. Compressed air or oxygen provided from a cylinder, gas cooling and gas spargers may provide more efficient conditions for optimal $^1\text{O}_2$ generation.

4.1.4.4. Conversion assessment of solar batch reactions

A series of four solar illumination experiments was conducted and their experimental performances depended on the reaction and exposure conditions (Error! Reference source not found.). The concentration of furfural was kept similar and ranged from approx. 340-400 mM in ethanol. The amount of sensitizer differed more significantly and changed from 0.004-0.008 mol%.

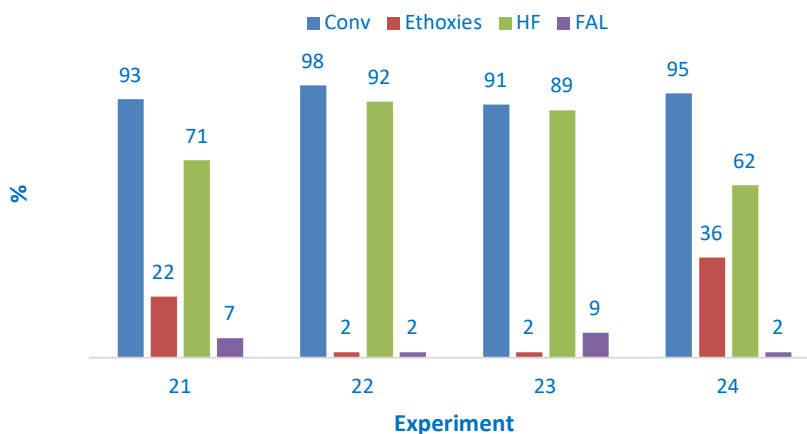


Figure 4.5: Conversions and product compositions of solar photooxygenations.

Experiment 21 used the least amounts of RB and EtOH of 0.004 mol% and 7 L, respectively, but the highest amount of FAL of approx. 400 mM. The solar reaction ran for 10 hours on a hot day with temperatures in the reaction chamber reaching 36-43°C. A conversion of 93% was achieved, but the elevated temperatures had caused partial thermal conversion to the corresponding EFN (4) in 22%. The amount of hydroxyfuranone was found satisfactory with 71%.

Experiment 22 had the least amount of FAL of approx. 340 mM. With a sensitizer loading of 0.005 mol%, the highest conversion of all solar exposures was readily achieved. The reaction ran for the shortest exposure time of 8 hours on a cooler day, resulting in reaction temperatures

ranging from 23-33°C. An almost complete conversion of 98% was achieved with 92% of HF (**2**) and only 2% of EFN (**4**). This improved selectivity confirms the importance of heat management to minimize thermal follow-up reactions.

Experiment 23 was carried out in the largest volume of EtOH of approx. 8 L, a furfural concentration of ca. 260 mM and 0.005 mol% of RB. The reaction ran over two days with six hours per day and under milder temperature conditions. The later naturally resulted in lower reaction temperatures of 27-30°C. At the end of the illumination, conversion had reached about 91% with 89% of HF (**2**) and just 2% of EFN (**4**) produced.

Experiment 24 was conducted over 3 days with a maximum of 6 hours of exposure per day. This reaction accounted for the largest concentration of furfural at approx. 280 mM and RB at 0.008 mol%. About 89% of furfural were converted, but the extremer temperature conditions resulted in reaction temperature of 33-46°C. Consequently, pseudo-esterification was dominant and resulted in the formation of 27% of EFN (**4**) and 12% of EBL (**5**), respectively. Only 50% of the crude reaction mixture consisted of HF (**2**).

Of all solar reactions, Experiment 24 demanded an extended exposure time of 17 hours over three days but still resulted in an incomplete conversion of 89%. Suboptimal solar and operation conditions may have contributed to the poorer performance. For example, the increased concentration of FAL (**1**) may have increased the turbidity of the solution, thus reducing light efficiency through scattering. Its distinct colour may have likewise caused light-filtering effects. This, in combination with the increased concentration of RB might have reduced light transparency.

Experiments conducted during more extreme temperature conditions produced larger amounts of thermal follow-up products (**Figure 4.6**), thus clearly demonstrating the importance of effective heat management for HF (**2**) synthesis. At an average temperature of 29°C and a reaction time of 12 hours, Experiment 23 showed a high conversion of 91% with high selectivity of 89% towards HF (**2**). With an exposure time of 8 hours at an average temperature of 28°C, Experiment 22 recorded the highest conversion of 98% with excellent HF (**2**) selectivity of 92%. Hence, the thermal follow-up reactions are minimized below 28°C. Experiments 21 and 24 occurred at average temperatures of 39°C within 10- and 17-hour periods, respectively. Despite their satisfactory conversion rates of 93% and 89%, significant pseudo-esterification reactions had occurred at the elevated temperatures. However, prolonged and controlled solar-thermal reactions, especially at temperatures above 30°C, may enable the deliberate production of AFNs instead.

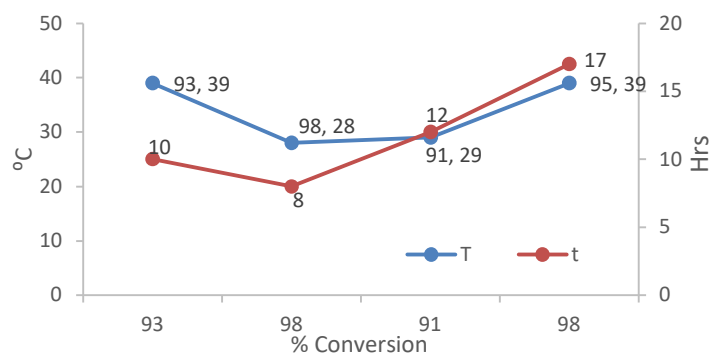


Figure 4.6: Temperature-and exposure time-dependences on furfural conversion.

4.1.4.5. Kinetic assessment of solar reactions

The four solar experiments were routinely sampled and analysed to determine their FAL (1) conversions and hence reaction progress. $^1\text{H-NMR}$ analysis was found time-consuming and unreliable. This sampling method demanded thermal evaporation to dryness prior to analysis, which may have caused thermal degradation or follow-up reactions or evaporation of volatile compounds. Removing false analytical data points, the corrected conversion-over-time profiles are depicted in **Figure 4.7**.

Experiment 21 proceeded with an incremental conversion at a rate of $16.6\%.\text{hr}^{-1}$ in the first five hours and continued at $1.5\%.\text{hr}^{-1}$ until it reached a conversion of 93% after 10 hours of exposure. Experiment 24 displayed a similar conversion pattern, however, at a much slower rate. It reached a conversion of 84% at a rate of $9.3\%.\text{hr}^{-1}$ after 10 hours, and extended to a peak of 93% at $0.33\%.\text{hr}^{-1}$ after a further 5 hours of illumination. In contrast to Experiments 21 and 24, Experiments 22 and 23 exhibited faster transformations and achieved high conversions of 93% and 91% within an hour.

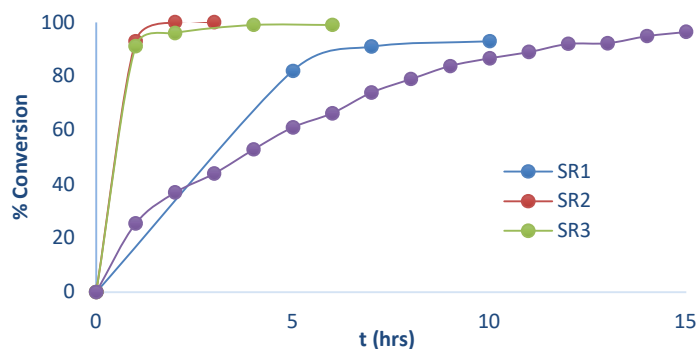


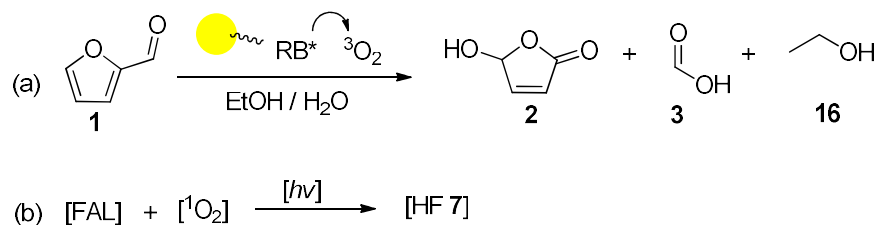
Figure 4.7: Corrected conversion over time profile during solar exposures.

The different performances of the solar reactions may result from various experimental and environmental factors. Naturally, the different solar light conditions impact significantly on the

conversion rates. Clearer and sunnier weather conditions give faster conversion rates and hence yields. Additionally, different concentrations of reagents and sensitizers impact on the transparency of the reaction mixture. This, as well as varying oxygen saturation conditions alter singlet oxygen production.

The failure to reach completion for Experiment 24 was possibly due to a lack of visible light under the specific solar conditions. Additionally, the higher concentration of sensitizer may have reduced the light transparency of the reaction mixture. Likewise, enhanced sensitizer bleaching over time may have decreased light penetration due to the formation of degradants.

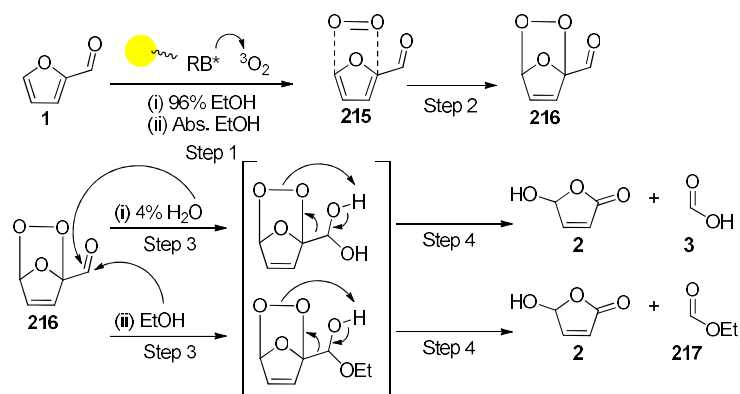
The rate of conversion is primarily facilitated by the amount and intensity of irradiation as well as $[^1\text{O}_2]$ (**Scheme 4.1**). $[\text{RB}]$ and $[\text{FAL}]$ can be monitored and controlled, whereas $[h\nu]$, I_x and $[^1\text{O}_2]$ cannot be monitored easily. These three factors dictate the rate and hence the extent of conversion. The kinetic efficiency was found to decrease in the order Experiment 22>23>21>24, and a similar trend is hence assumed for $[h\nu]$, I_x and $[^1\text{O}_2]$ during solar exposure. Solar irradiation data would be helpful to evaluate the influence of $[h\nu]$ and I_x but could not be obtained.



Scheme 4.1: (a) Reaction scheme. (b) Crucial kinetic parameters.

4.1.4.6. Photooxygenation mechanisms

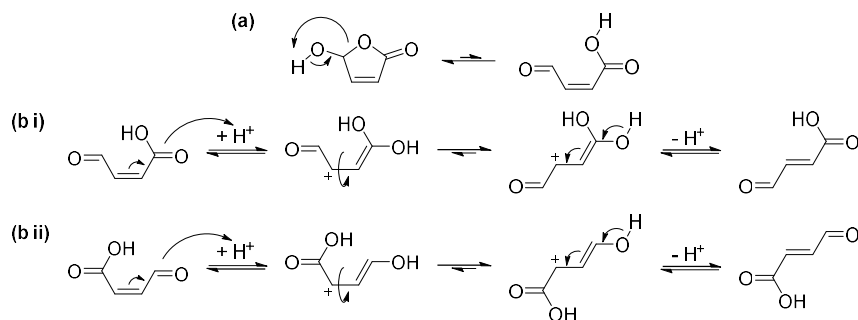
The water-content of ethanol plays an important role in the reaction. According to the generally accepted reaction mechanism (**Scheme 4.2**), a furfural- $^1\text{O}_2$ complex (**215**) is initially formed (**Step 1**). Singlet oxygen subsequently adds to the C-2 and C-5 positions of FAL (**1**) to the endoperoxide intermediate **216** (**Step 2**). Nucleophilic attack by water or ethanol at the exposed carbonyl group generates an unstable hydrate or hemiacetal intermediate (**Steps 3**), respectively. Collapse of these intermediates (**Step 4**) leads to HF (**2**) via ring opening of the peroxide-bridge and proton-rearrangement. Formic acid (**3**) or its ethyl-ester (**217**) are formed as additional decomposition products. As water is about 100-times more nucleophilic than alcohol, the presence of water is beneficial for the formation of **7**.



Scheme 4.2: Reaction mechanism for the conversion of furfural.

The presence or absence of water indeed had a noticeable effect on the performance of the solar photooxygenations. Experiments 22 and 23 were conducted at similar FAL (1) and identical RB concentrations. However, Experiment 23 used absolute ethanol, while Experiment 22 utilized technical (96%) ethanol instead. The exposure in the absence of water required a prolonged illumination time (12 vs. 8 hours) and gave a lower conversion (91 vs. 98%). The presence of water may likewise aid the solubility of the sensitizer salt and therefore improve the transparency of the solution. However, the acidic nature of formic acid (3) and the more drastic evaporation conditions for the removal of water contribute to follow-up reactions, especially pseudo-esterification at elevated temperatures.

HF (2) potentially exists in an equilibrium of ring-chain tautomers with the ring form being the most stable and hence dominant structure (**Scheme 4.3a**). Upon acid-catalysis, further isomerization can shift this equilibrium towards the corresponding open *trans*-isomer (**Scheme 4.3b**). Protonation at either carbonyl-group and relocation of the C=C-double bond electrons generates a carbocationic intermediate, which can undergo rotation towards its more stable transoid structure. Subsequent deprotonation and relocation of π -electrons yields *trans*-4-oxo-2-butenic acid.



Scheme 4.3: (a) Ring-chain tautomerization of hydroxyfuranone and (b) possible *cis-trans* isomerizations to open *trans*-isomer.

4.1.4.7. Formation of ethoxy-derivatives

Generally, the production of the ethoxy-derivatives is impacted by the reaction temperature and the presence of acid. The production of the two main ethoxy derivatives can be contained at temperatures below 28°C as demonstrated by Experiments 22 (SR2) and 23 (SR3) in **Figure 4.8**. In contrast, solar light, oxygen saturation and sensitization conditions have no impact on pseudo-esterification reactions.

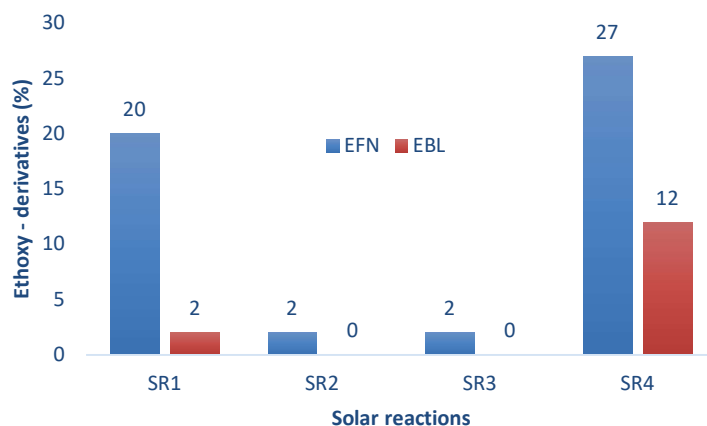


Figure 4.8: Composition of the ethoxy-derivatives during solar experiments.

The temperature range of Experiment 21 was 36-43°C and this facilitated the production of EFN **4** (20%) and EBL **5** (2%). More ethoxy derivatives were produced in Experiment 24, which operated at an average temperature of 40°C. In contrast, Experiments 22 and 23 occurred within average temperatures of 28-29°C and solely accounted for 2% of EFN (**4**). This confirms that the production of EFN (**4**) is spontaneous at temperatures beyond 28°C, while EBL (**5**) is likely produced beyond 33°C.

Experiment 24 gave the highest amounts of ethoxy-derivatives, but their formation may have been influenced by the chosen analytical technique, *i.e.* GC-analysis. In particular, the inlet and oven temperatures may have caused partial esterification and ring-opening during analysis. As a result, the amounts of EFN and EBL may have been overexpressed. This affect may be verified by parallel monitoring by GC and ¹H-NMR. However, NMR-analysis also demands evaporation of the solvent which might also initiate thermal follow-up reactions. Signal overlap and detection limits also impact on product analysis by ¹H-NMR.

A possible mechanism for the formation of EBN (**5**) is shown in **Scheme 4.4a**. Protonation of the carbonyl-group initiates ring-opening to a resonance-stabilized carbocationic intermediate. Subsequent addition of ethanol and proton-transfer, followed by ring-closure, elimination of

indicates that the raw material of Experiment 21 was concentrated under the least thermally stressed conditions.

Experiment 22 showed an increase of 26% in the ethoxy derivatives while losing 27% of HF (2). This observation indicates that the evaporation conditions were suited for pseudo-esterification. As a result, only 68% of its HF (2) content remained in the crude product. Efforts to crystallize HF (2) from this crude matrix were thus laborious, but ended with approx. 61 g of pure HF (2).

Experiment 23 experienced the highest drop in HF (2) content of 51%, of which 42% were converted to the ethoxy derivatives during evaporation. The acidic environment and poor heat management during evaporation must have favoured spontaneous pseudo-esterification of HF (2). As the heating baths of the evaporators were not calibrated or simply set based on the indicators on the dial, precise temperature control may have not been guaranteed.

Surprisingly, the composition of the crude product from Experiment 24 changed opposite to those observed for Experiments 21-23. The amount of EFN (4) had dropped by 4% and that of EFL (4) by 5%, while the amount of HF (2) increased by 20%. This finding confirms that GC-analysis may give unreliable product compositions due to thermal reactions inside the instrument, *i.e.* injector and oven. Hence, alternative GC-parameters of less thermally stressful analytical techniques such as HPLC should be considered for future process monitoring.

While composition changes due to evaporation losses cannot be ruled out under the high vacuum conditions, all constituents have high boiling points that would require excessive heating of <40°C even at 10 mbar. However, the formation of azeotropes for any of the components cannot be ruled out.

4.1.6. Crystallization efficiencies

The amounts of HF (2) obtained from the solar conversion after evaporation varied between 39-70%. Isolation of crystalline HF (2) from these mixtures, however, resulted in dramatic losses of material (**Figure 4.10**). The rather complex composition obtained from Experiment 23 completely prevented any crystallization. Different methods such as rapid freezing with liquid nitrogen or seeding with pure HF (2) were tried with varying success. Most losses occurred during repeated washing of the collected crystals.

Experiment 21 produced an acceptable amount of HF (2) of 68% in the crude product. However, during crystallization, only 19% (54.063 g) of pure HF (2) were recovered, while 49% were lost during isolation.

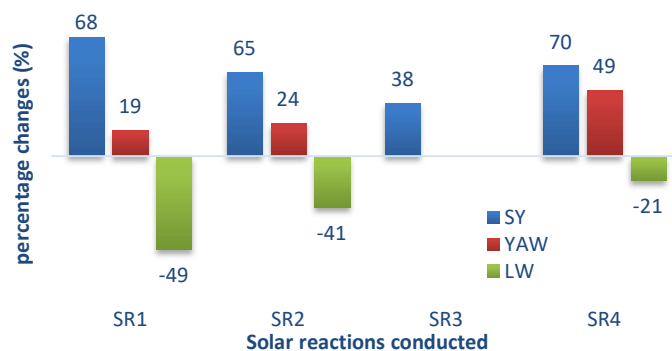


Figure 4.10: Percentage of hydroxyfuranone in the crude product (SY), isolated yields (YAW) and losses (LW).

Experiment 22 gave a decent amount of HF (**2**) of 65%, but 41% were lost during crystallization and washing. As a result, only 24% (60.675 g) of pure HF (**2**) were obtained.

The crude product of Experiment 23 contained only 38% of HF (**2**), which was insufficient to achieve supersaturation for crystal formation. Due to the large quantity of material, alternative resource-demanding isolation methods such as column chromatography were not attempted.

Experiment 24 furnished the highest amount of HF (**2**) with 70% and gave the least losses of material of 21% during crystallization. Consequently, an acceptable amount of crystalline HF (**2**) of 49% (143.968 g) was obtained.

These results indicate that the purity of the crude material has a significant impact on the success of crystallization. Any larger amounts of by-product prevent nucleation and stacking of the individual molecules or require excessive washings. These limitations demand alternative isolation or purification methods, for example, after further deliberate transformation into more stable compounds. Direct solar-thermally induced pseudo-esterification of the reaction mixture prior to evaporation or during solar exposure may offer such an opportunity.

4.1.7. Pseudo-esterifications using recovered materials

Experiment 27 used the recovered material of solar Experiment 23 that was unable to reach supersaturation during crystallization. After enforced pseudo-esterification, the refined material consisted of 48% of EFN and 34% of EBL with no residual hydroxyfuranone detected. The changes in composition for this experiment are illustrated in **Figure 4.11**.

The other filtrates collected after the recovery of HF (**2**) crystals contained significant amounts of residual HF (**2**) in 46-52%. These were thus subjected to pseudo-esterification to enforce complete transformation of all HF (**2**). All experiments showed complete conversions. Residual

FAL (1) present in the recovered materials was largely unaffected by the pseudo-esterification conditions.



Figure 4.11: Composition changes during pseudo-esterification in Experiment 27.

The refined product of Experiment 25 (using the filtrate of Experiment 21) contained 76% of EFN (4) and 22% of EBL (5), while Experiment 26 (using the filtrate of Experiment 22) furnished a final composition of 58% of EFN (4) and 30% of EBL (5). Experiment 28 (using the filtrate of Experiment 24) resulted in a mixture containing 83% of EFN (4) and 13% of EBL (5).

These results clearly show that further utilization of waste streams from the isolation process is feasible. However, selectivities towards EFN production remained somewhat unsatisfactory. Further transformation into the open EBL compound could not be prevented. Future studies may attempt to enforce complete conversion to EBL under more extreme conditions or using extended reaction times.

4.1.7.1. Isolation of 5-Ethoxyfuran-2(5H)-one by fractional distillations

The crude products of Experiments 25-28 were initially subjected to vacuum microdistillation to separate EFN (4) from the crude matrix. At 13 mbar, FAL (1) and EBL (5) were expected to be collected at 44°C and 75°C, and EFN (4) at 101°C, respectively. However, material recoveries remained low with 7-49% and all fractions collected contained mixtures of EFN (4) and EBL (5). The desired EFN (5) was obtained as the main constituent in 50-79%.

The combined fractions for VD1 resulted in a recovery of just 17% and contained EFN (4) in 77%. The fraction obtained from VD2 showed a recovery of 24% with just 50% of EFN (4), 30% of EBL (5) and 20% of residual FAL (1). Isolation VD3 gave the lowest recovery of 7% but furnished a fraction containing 79% of EFN (4). Finally, VD4 furnished 49% recovery and

gave a distillate containing 78% EFN (**4**). The simple microdistillation setup was thus not able to effectively separate the individual components and only achieved preconcentration of ethoxyfuranone. The fractions obtained from VD1 and VD2 were subjected to further bulb-to-bulb distillation. Recovery rates were again low with 28% and 14%, respectively. However, this advanced distillation process was capable in producing EFN (**4**) in high purities of 98% and 98%, respectively.

Distillation was thus found to be very inefficient in product isolation. The extreme heating conditions may have favoured thermal polymerization and degradation reactions to non-volatile compounds. Future studies should thus evaluate more effective and less destructive purification methods.

4.1.8. Pseudo-transesterification of ethoxyfuranone

The transesterification of EFN (**4**) to alternative AFN was partially successful under the chosen reaction conditions. In all cases, complete conversions were achieved. However, selectivities were somewhat poor, and several compounds were obtained (**Figure 4.12** and **Figure 4.13**).

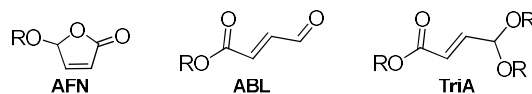


Figure 4.12: Generic general structures of pseudo-transesterification products.

The desired AFNs were formed in variable compositions of 23-75%. Tautomerization and isomerization caused the generation of ABL derivatives. The later pathway was observed for all conversions in 20-53%. Tri-alkoxylation to the corresponding acetals (TriA) was only observed with hexanol and 2-ethylhexanol in amounts of 4% and 57% (see **Appendix 73** and **Appendix 59**), respectively. These TriA-compounds were formed from the open ABL derivatives through subsequent acetalization.

The results somewhat mirror those of the pseudo-esterification reactions of HF (**5**). While different nucleophilicities and steric effects of the various alcohols may impact on the product composition, no clear trends were notable. The secondary alcohol cyclohexanol (Experiment 31) gave the largest amount of alkoxyfuranone (cHFN, **43**) with 75%. The linear dodecanol (Experiment 30) also produced predominantly its corresponding alkoxy-analogue DFN (**23**) in 70%. While all transformations were complete, the extended reaction time in combination with continuous heating may have enforced follow-up reactions. Future studies should thus aim at finding milder conditions and should also include process monitoring.

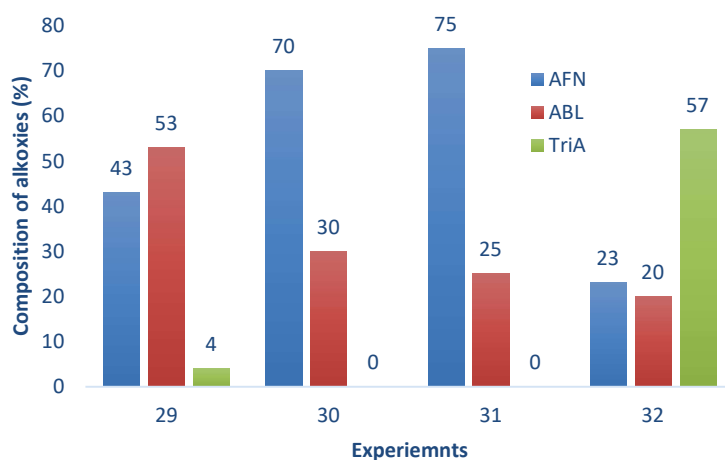


Figure 4.13: Product compositions of transesterification reactions.

4.1.9. Additional assessments

4.1.9.1. Reproducibility of reaction monitoring

Reproducibility of the analytical method used to monitor solar Experiments 21-24 was established by a linear regression of a calibration plot. This was also essential to validate the accuracy and reveal the ideal analysis parameters for monitoring conversions. The approach included defining the sampling technique, sample storage, sample preparation, and setting instrumental analysis parameters. The calibration plot in **Figure 4.14** below showed a strong and consistent positive correlation ($R^2 = 0.9995$) between the concentration [IS] and their subsequent peak areas for CS1-CS5. The regression complimented well with the σ value (± 0.625). This illustrates that the analysis was highly reproducible under the immediate analytical parameters.

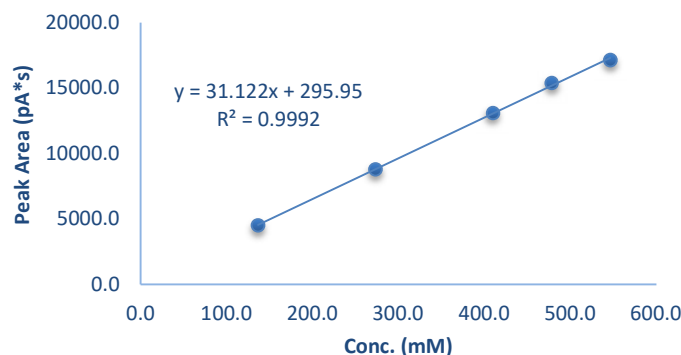


Figure 4.14: Calibration curve of the IS "*n*-butanol" used to verify the response factor (R_f).

The plot demonstrates that the *mM* vs *pA* regression model has low to nil variability with a positive correlation ($R^2 = 0.9992$). Furthermore, its slope of $31.22 \text{ pA} \cdot \text{mM}^{-1}$ corresponds well with the R_f of $32.279 \text{ pA} \cdot \text{mM}^{-1}$ generated by standard addition assessment in Experiment 24.

These two validation methods offset by $\pm 1.157 \text{ pA} \cdot \text{mM}^{-1}$, which is sufficiently low to assume that both methods demonstrate similar trends in conversion and analytical repeatability. The repeatability assessment accounts for correction of GC runtime drifts and composition variations caused by multiple sequence injections. Hence, this improves the accuracy of the quantitative analysis.

4.1.9.2. Limitations of solar illuminations

While solarchemical synthesis represents an attractive and sustainable approach, careful reaction planning is essential to achieve optimal results. In the case of the chosen HF (2) synthesis, attention must be given to select the most suitable solvent. While ethanol was found efficient, it caused subsequent thermal follow-up reactions that were difficult to control. Also, evaporation and recovery of the large volumes was found challenging. Naturally, optimal illumination and weather conditions should be chosen with clear sunny skies, low humidity, and temperatures of $< 28^\circ\text{C}$. Under these conditions, effective solar photooxygenations may operate with negligible thermal pseudo-esterification.

Monitoring of the reaction process by either NMR- or GC-analysis was found equally challenging. GC avoided the need for time-consuming and material-demanding rotary evaporation. However, changes through pseudo-esterification inside the GC-instrument were observed and produced “false” compositions. Mass spectrometric analysis may have allowed rapid identification and structure determination of individual constituents. Instead, NMR required larger amounts of samples. The complexity of some crude reaction mixtures also made the identification and quantification of individual compounds difficult.

4.1.10. Rose Bengal decomposition with artificial light

During the irradiation and illumination reactions, decomposition of the sensitizer rose Bengal (RB) was noted. The stability of the photosensitizer was thus examined by UV-Vis monitoring over 4 hours (**Figure 4.15**). The loss of [RB] occurred at a rate of $0.001 \text{ mM} \cdot \text{min}^{-1}$. At this rate, most RB would thus, have decomposed after 589 minutes.

It is assumed that the decomposition of RB is mainly induced by physiochemical stressors such as temperature (recorded at $27\text{-}28^\circ\text{C}$) and light intensity (I_x , recorded at 924.19 Wm^{-2}). Hence, the rate of decomposition is thus proportional to the change in temperature of the system and the light intensity. As the rise in temperature is mainly caused by continuous irradiation at a particular light intensity, bleaching of RB as well as thermal pseudo-esterifications of HF (2)

are difficult to contain. Due to the continuous formation of formic acid as a by-product, further acid-induced decompositions cannot be ruled out either.

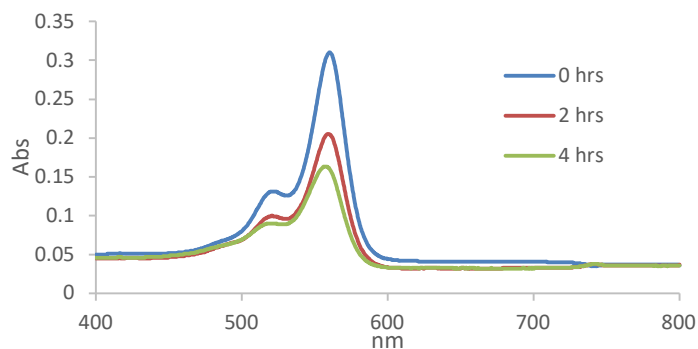


Figure 4.15: The gradual change in [RB] under visible light for 4 hours.

4.1.11. Assessment of pseudo-esterification in different alcohols

Photooxygenation in EtOH achieved high to complete conversions but commonly furnished pseudo-esterification and partial isomerization the ethoxy-derivatives. Alternative alcohols were thus trialled to investigate the nucleophilicity of the solvent (**Figure 4.16**). *Iso*-propanol was chosen as a readily available secondary and *tert*-amyl alcohol as a tertiary alcohol, respectively. Under identical irradiation conditions, the choice of solvent impacted significantly on the conversion rates and product compositions.

With ethanol, complete conversion was obtained but 25% of AFN and 2% of ABL were detected. The reaction in *i*-PrOH had reached near completion with 97% and furnished only small amounts of the corresponding alkoxy-derivatives of 3% each. Using *tert*-amyl alcohol the lowest conversion of only 79% was obtained with only 11% of the corresponding ABL product formed. The choice of solvent changed the optical and physicochemical properties of the solution. In particular, the light transmittance and oxygen solubility decreases in the order EtOH > *i*-PrOH > *tert*-amyl-OH. Therefore, the best kinetic performance was found in ethanol. In contrast, however, EtOH showed the lowest selectivity towards the desired HF (**2**) synthesis. This observation aligns with the steric hindrance of the selected alcohols, which increases in the order EtOH < *i*-PrOH < *tert*-amyl-OH. The absence of any AFN in case of *tert*-amyl alcohol suggests that ring-opening might be favoured for sterically demanding alkoxy-groups. However, since isopropanol and *tert*-amyl alcohol show higher boiling points of approx. 83°C and 101°C, the need for higher temperature for their removal may reduce the observed selectivities.

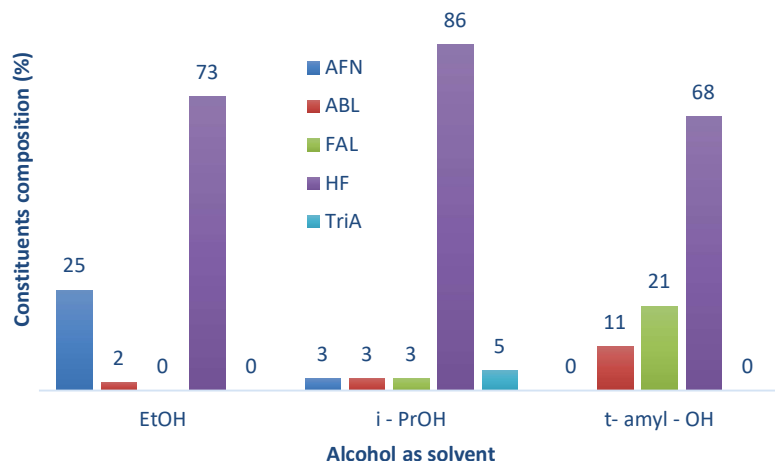


Figure 4.16: Pseudo-esterification with different alcohols.

4.2. Sustainable synthesis of *para*-menthane-3, 8-diol

4.2.1. Assessment of LSG distillation methods

To develop a sustainable PMD (**33**) production, this investigation first looked at establishing a reliable resource of Cal (**32**) from natural biomass. Two isolated *C. citriodora* trees on the JCU campus were evaluated. This very small population does not supply any significant material for commercialization but enable the investigation of leave sampling and laboratory-scale distillations methods. Subsequently, the oil yields and chemical profiles were assessed from these collections and were compared to literature and commercially sourced LSG oils.

Eight distillations (D1-D8) were conducted using three different distillation setups (**Table 4.1**). These included hydrodistillation (HDg) and steam distillation (SDg) in glass devices, and a steam distillation in a copper apparatus. (SDc).

It was observed that steam distillation furnished slightly higher average oil yields of 1.4-1.46%, compared to 1.23% for hydrodistillation. However, HDg produced more consistent oil yields with ± 0.07 SD, followed by SDg (± 0.38) and SDc (± 0.91). The hydrodistillation setup provided a shorter path for the steam with fewer connecting joints. As a result, HDg can provide more steam, which results in fewer losses in vaporized constituents. In contrast, the general design of a steam distil involves longer passageways with additional joints. The later may cause pressure drops during operation and hence unstable distillations. Additional joints and attachments also increase the risk of steam or vapor leaks.

During hydrodistillation, the biomass is directly heated in boiling water, thus allowing a more rapid and constant evaporation. In contrast, the steam during steam distillation has to pass through a bed of leaves. The density of the biomass packing may also vary between operations. Denser packing prevents passage of steam, while a looser packing enables better penetration of steam vapours through the entire biomaterial. Despite this, steam distillation is considered a softer extraction method. During hydrodistillation, the biomass sample is heated at or above the boiling point of water. The composition of the boiler water also changes more drastically during the distillation process and may involve accumulation of acidic or basic compounds. These experimental conditions may cause thermal changes of individual chemical constituents. As a result, initially non-volatile ingredients may convert into more volatile compounds or vice versa. In contrast, the biomass during steam distillation is exposed to steam of $\leq 100^{\circ}\text{C}$, which somewhat minimizes thermally induced chemical changes. Hence, volatilization by SD is considered more selective and induces less thermal stress on the samples' constituents. To somewhat evaluate potential changes in the chemical profile of the samples, the boiler water (BW) and hydrosol (DBW) from all distillations were subjected to continuous liquid-liquid extraction. **Figure 4.17** shows the normalized mass distribution of all the oil fractions obtained. Since the removal of the diethyl ether used for continuous extraction had to be performed carefully to minimize evaporation of dissolved volatiles, the amounts of boiler water (BWO) and hydrosol oils (DBWO) may contain residual solvent and have thus to be interpreted with care.

Table 4.1: Comparison of distillation yields

DT	SN	DN	T ($^{\circ}\text{C}$)	Yield (w/w)%			Cal%
				Individual	Mean	SD (\pm)	
SDg	3	D3	100	2.1	1.46	0.91	59.54
	4	D4		0.81			60.83
	5	D5		0.96			67.66
SDc	6	D7	100	1.55	1.40	0.38	68.79
	6	D8		1.68			60.17
	1	D1		1.15			36.83
HDg	2	D2	300	1.29	1.23	0.07	36.76
	5	D6		1.26			36.33

DT: Type of distillation, SN: Sampling number, DN: Distillation number, SD: Standard deviation, Cal: Citronellal, SDg: Steam distillation in glass setup, SDc: Steam distillation in copper setup, HDg: Hydro distillation in glass setup.

The hydrodistillations (D1, D2, and D6) had 72-90w% of distilled essential oil (DO) collected. For two of these distillations (D1 and D2), larger fractions of boiler water oils (BWO) of 19.2w% and 24.5w%, respectively, were furthermore obtained by liquid-liquid extraction. This

finding suggests that the direct heating during hydrodistillation may indeed induce hydrolysis or hydration reactions to less volatile and more water-soluble compounds. In contrast, the oil obtained through extraction of the collected hydrosol (DBWO) furnished only smaller amounts of material with 3.4-6.6w%. This implies that only small amounts of water-soluble volatiles were distilled off.

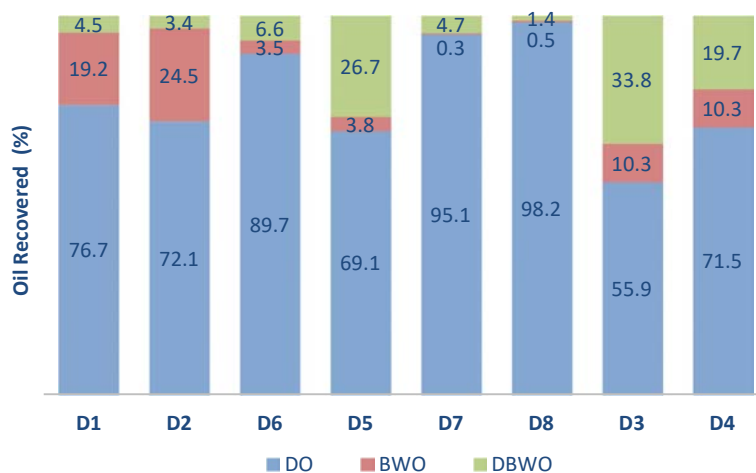


Figure 4.17: Normalized mass distribution for all oil fractions.

Two of the steam distillations conducted in the copper distil (D7 and D8) produced the highest weight-percentages of distilled oil with 95.1w% and 98.2w%, respectively. In all cases, solvent extractions of the residual boiler water produced only small quantities of BWO of 0.3-3.8w%. From D5, an unusually large quantity of DBWO of 26.7w% was extracted from the hydrosol, which may suggest significant amounts of residual solvent due to incomplete evaporation. All steam distillations in the copper distil produced only small amounts of boiler water oils with 0.3-3.8w%. In comparison, the two hydrodistillations conducted in the glass apparatus (D3 and D4) produced fewer quantities of essential oil of 55.9w% and 71.5w%, and showed considerable amounts of BWO and DBWO after liquid-liquid extraction. The different performances of the steam distils may have been caused by their different designs. The glass setup had a narrow connection between boiling and biomass flask, and the biomass flask provided a wider surface area. These features may have favoured condensation of steam and volatiles, which resulted in accumulation of chemical constituents in the boiler water. In contrast, the wide, cylindrical and compact design of the copper apparatus provided an even upwards flow for the steam and volatiles and minimized condensation. The improved heat conductivity of copper may have further contributed to an improved transfer of all vapours.

4.2.2. GC-FID method development

Numerous chemical profiles of LSG oil have been determined by GC-analysis^{97,111,168}. Due to its naturally complex composition, most of the reported GC-chromatograms show crowded and overlapping peaks. This is especially problematic when determining the amounts of crucial constituents such as Cal (**32**) and in particular the stereoisomers of PMD (**33**), Iso (**37**) and the PMD acetals (**39**). Generally, volatile monoterpenes, particularly olefinic and aliphatic structures, produce earlier peaks, followed by oxygenated monoterpenes, sesquiterpenes, and acetals.

For the crucial monitoring of Cal (**32**), many of the reported GC-methods showed overlap of the Cal (**32**) peak with other constituents. The development of a GC-method with baseline-separated peaks was thus essential.

Using the initial temperature program M1, crowded peaks were observed due to the extremer ramp of $15^{\circ}\text{C}\cdot\text{min}^{-1}$ for the first 7 minutes (**Figure 4.18a**). This cluster of peaks also caused overlapping of the essential Cal (**32**) peak with components of similar mass and polarity, presumably *i*Iso (**37a**). The modified method M2 had the slower ramp of $3^{\circ}\text{C}\cdot\text{min}^{-1}$ for the first 16 minutes and this efficiently separated all volatile monoterpenes. It then ramped at $1^{\circ}\text{C}\cdot\text{min}^{-1}$ for the next 8 minutes and successfully separated Cal (**32**) from *i*Iso (**37a**) (**Figure 4.18b**). However, the slow ramp caused a significant extension of the total run time.

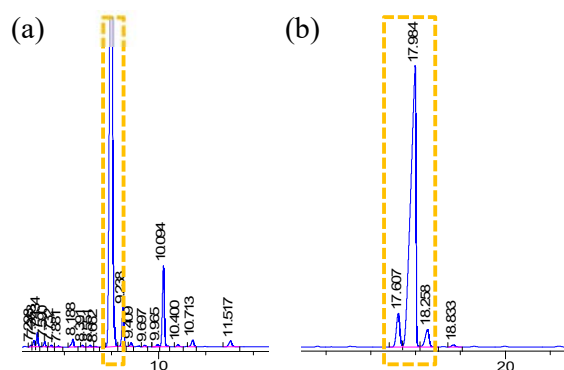


Figure 4.18: GC-chromatogram with (a) crowded and overlapping peaks and (b) resolved peaks.

The resolution of the various PMD-stereoisomers was also improved using the revised temperature program. While the chromatogram from the initial M1-method was able to separate the major *cis*- (**33c**, 12.677 min) and *trans*-PMD (**33b**, 13.097 min) peaks, the *cis*-isomer partially overlapped with another compound, affecting its integration (**Figure 4.19a**). Elution of the same peaks using method M2 improved baseline-separation of all peaks (**Figure 4.19a**).

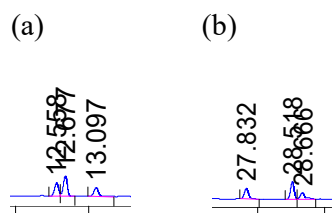


Figure 4.19: (a) Initial and (b) improved resolution of PMD peaks.

High molecular weight compounds, in particular the PMD-acetals (**39**), could not be detected by the improved temperature program M2. Quantification of these materials is essential as they are generated by follow-up reactions between residual Cal (**32**) and the respective PMD-isomer. Analysis method M3 was able to rectify this detection limit by extending the improved method M2. As shown in **Figure 4.20a**, the chromatogram obtained using M2 showed only two peaks towards its end. In contrast, the chromatogram obtained with the extended method M3 (**Figure 4.20b**) revealed eight additional peaks including those of *cis*- (**33c**, 37.342 min) and *trans*-PMD acetal (**33b**, 37.794 min).

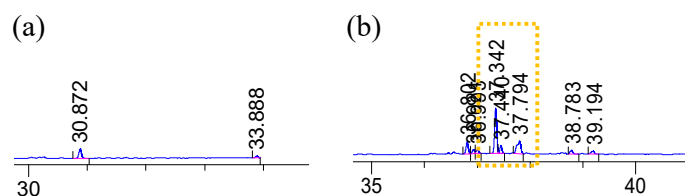


Figure 4.20: (a) Absent and (b) observed PMD-acetal

peaks.

4.2.3. Citronellal content of commercial LSG oils

In the search to identify a commercial and hence reliable source of LSG oil with a high Cal (**32**) content, several commercial oils were assessed and compared to the oil obtained at JCU (**Figure 4.21**). In line with the literature, typical other major constituents were Col (**38**) and the various isopulegol isomers, while the stereoisomers of PMD and its acetals were only present in trace amounts or entirely absent.

The oil produced at JCU, and all commercial LSG oil products investigated contained Cal (**32**) as the dominant constituent in >62%. The products with the highest amount of Cal (**32**) of >70% were from Australian producers (EA, RE, and HO). In contrast, the oil obtained from New Caledonia had a rather low Cal (**32**) content of approx. 62%. Of all the commercial products, the local RE material showed the highest Cal (**32**) content of >79% and is thus recommended for use in the production of PMD (**33**).

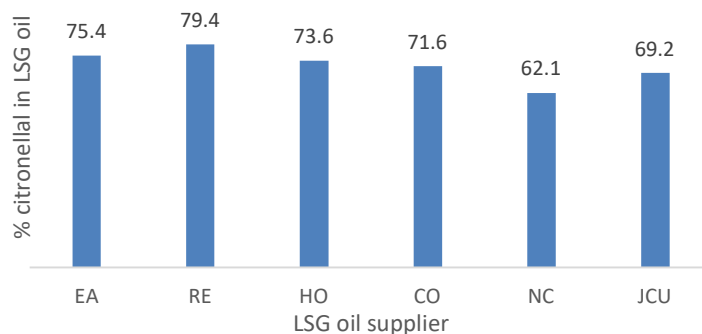


Figure 4.21: Citronellal content of various commercial LSG oil.

4.2.4. Laboratory-scale conversions

Thirteen preliminary experiments were performed on a 100 ml laboratory scale and utilizing different raw materials. In almost all cases examined, high conversion rates of citronellal and good selectivities towards the desired PMD-mixture were achieved (**Figure 4.22**). The simplified setup and small scale may have impacted on the effectiveness of the transformation. Especially the need to create a stable emulsion may not be reproducibly achieved by simple magnetic stirring.

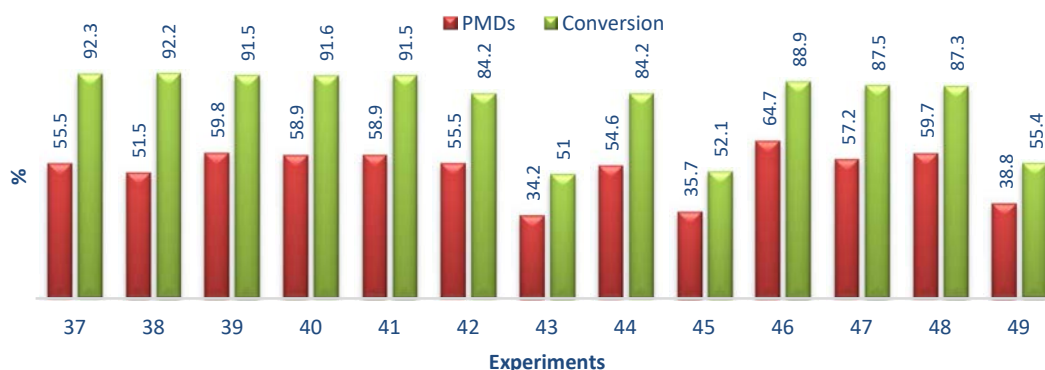


Figure 4.22: Citronellal conversions and PMD contents of laboratory-scale experiments.

Experiments 37-41 used the LSG oil sourced from EA in combination with acid solutions prepared with purified water (DW). Under these conditions, high citronellal conversions of 91.8% on average were achieved. Experiments 43, 45 and 49 employed the bottom layer of the LSG oil sourced from RE (RE-BL) and gave the lowest conversions as well as the least amounts of PMDs produced. Interestingly, Experiment 46 used the same type of RE-BL oil but the bottom layer of recovered hydrosol (BLH) and achieved a conversion of 88.9% with the highest quantity of PMDs produced with approx. 65%. Dissolved components, *i.e.* organic acids, in the hydrosol may have thus assisted the conversion process. Alternatively, initially dissolved PMD from the hydrosol was released into the essential oil during the experiment. Experiments 42,

44, 47 and 48 used the top layer of the LSG oil of RE (RE-TL) in combination with various aqueous acid solutions. In these cases, citronellal conversions ranged between 84.2-88.9%, while the quantities of PMDs produced varied from 54.6-64.7%.

These results suggest that the materials used for conversions have a noticeable impact on their performances and outcomes. When commercial LSG oil is received in large containers, vigorous mixing is recommended to provide a homogenous composition and prevent concentration gradients of constituents. Reusage of aqueous waste streams from the essential oil distillation process also impact on the performances of PMD production. To achieve reproducibility of a future standard operation procedure (SOP), these material parameters must be considered.

4.2.5. Demonstration-scale conversions

The demonstration-scale setup was different in scale (5 L compared to 100 ml) and type of stirring. The chosen setup utilized mechanical stirring with an impeller, which achieved constant and efficient mixing and hence creation of a stable emulsion throughout the experimental phase. Two settings of 300 and 450 rpm were trialed. Five different reactions were carried out with essential oil sourced from RE and distilled water (DW), hydrosol (DH), recovered citric acid solution and distilled boiling water (DBW) as resources for the preparation of the aqueous acid solution. All experiments consistently gave good to high conversions of citronellal and high proportions of the desired PMD isomers (**Figure 4.23**).

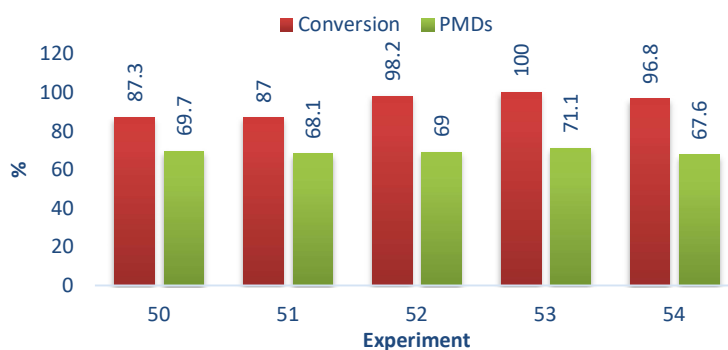


Figure 4.23: Citronellal conversions and PMD contents of demonstration-scale experiments.

Experiments 50 and 51 conducted using DW at 300 rpm achieved comparable levels of citronellal conversion of approx. 87% and similar amounts of PMDs of approx. 68-69%. Experiments 52-54 utilized various aqueous waste streams at 450 rpm and reached very high citronellal conversions of 97-100% with comparable amounts of PMDs of approx. 68-71%. The

stirring speed had a significant impact on the conversion rate. As the reaction is conducted in an emulsion, rapid stirring provides a superior contact between the reagents. In contrast to the laboratory-scale reactions that utilized magnetic stirring, mechanical stirring allows for more reproducible and stable conditions. In contrast, the nature of the aqueous matrix had no pronounced influence on conversion or PMD contents, at least not under rapid stirring conditions.

The stirring speed also had a notable effect on the quantities of the various Iso (**37**) isomers (**Figure 4.24**). At 300 rpm, Iso (**37**) were formed in 5.2 and 6.2%. These values increased to 15.6-15.7% at 400 rpm. The rise in Iso (**37**) content correlated well with the increase in Cal (**32**) conversion. In contrast, the amounts of Col (**38**) and PMD-acetals (**39**) remained almost constant at around 5.4% or similar at 2.3-4.2%, respectively.

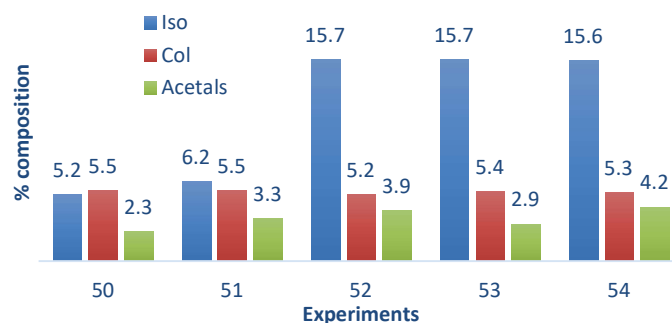
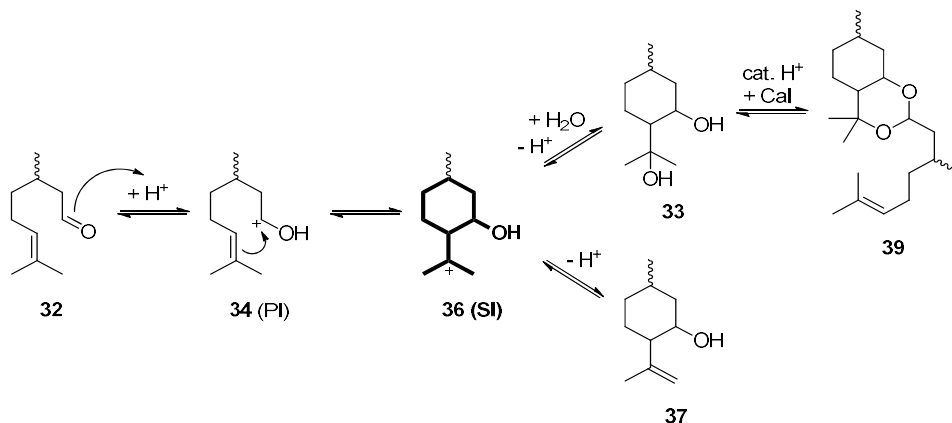


Figure 4.24: Isopulegol, citronellol and PMD-acetal contents of demonstration-scale experiments.

The formation of the Iso (**37**) – isomers and PMD (**33**) – isomers occurs via the common intermediate SI (**36**) (**Scheme 4.5**). Activation by acid-catalysis generates the initial carbocationic intermediate PI (**34**). Subsequent nucleophilic attack of the remote C=C-bond yields the cyclic intermediate SI (**36**). Addition of water followed by deprotonation furnishes PMD (**33**), while deprotonation alone produces Iso (**37**) instead. PMD subsequently reacts with residual Cal (**32**) in an acid-catalyzed acetalization to the PMD-acetals (**39**). From Experiments 50-54, the average quantities of the PMDs (**33**), Iso (**37**) and PMD-acetals (**39**) were 68%, 5% and 3.2%, respectively. Hence, the formation of the PMDs (**33**) was 21-times and that of the isopulegols 2-times more favoured than that of the acetals.

According to the mechanistic scheme below, water is essential for PMD and subsequent acetal production from intermediate SI (**36**). This intermolecular process competes with the intramolecular deprotonation step. The kinetics of the reaction was assessed based on the

conversion of citronellal, the key step influencing the conversion rate is thus the cyclization of intermediates PI (34) to SI (36).



Scheme 4.5: Reaction mechanism of PMD, isopulegol and PMD-acetal formation.

Figure 4.25 shows that conversion in Experiment 53 occurred at a rate 1.5-1.8-times faster than in Experiments 51, 52 and 54, respectively. Likewise, it also accounted for complete consumption of Cal (32) and the highest percentage of PMDs (33) produced with approx. 71%. This experiment utilized a recovered citric acid solution from a previous experiment that was supplemented with additional solid acetic acid. Hence, the acceleration was solely caused by the higher acid concentration of approx. 14-w%.

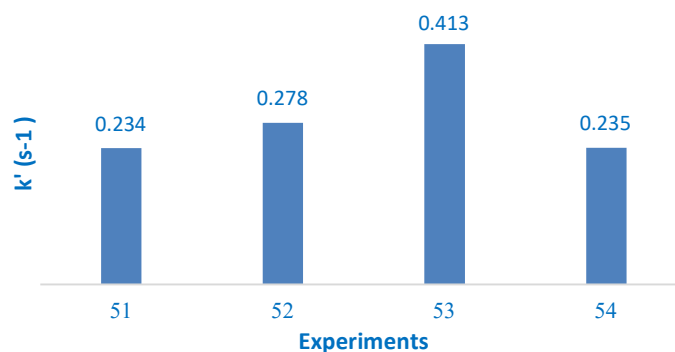


Figure 4.25: Rate constants for citronellal conversions.

4.2.6. Technical-scale conversions

The demonstration-scale reactor assembled glassware and equipment from a typical research laboratory. Its design and setup were thus rather primitive and, for example, did not allow for monitoring of process parameters such as stirring speed and temperature. As these features had an impact on the conversion and selectivity and thus have to be controlled precisely. The need for reproducible and controlled reaction conditions was in particular visible from the

laboratory-scale experiments, which gave the most fluctuating results. Hence, an advanced and automated bioreactor system was selected for technical-scale reactions. Three reactions were conducted on a total volume of 10-L each and using LSG oil obtained from RE and DW for the acidic aqueous layer. As visible from **Figure 4.26**, all three reactions achieved near complete conversions and produced comparable amounts of the PMD isomers of approx. 67%. The advanced reactor system thus gives reliable results and reproducible performances. It has been subsequently used to produce several batches of PMDRBO for an external collaborator.

The importance of the reactor design is also visible when comparing the average conversion rates of the laboratory-, demonstration- and technical-scale experiments. These increased steadily from 81% to 94% and finally 100% with each reactor advancement. In addition, the average percentage of PMDs (**33**) produced also increased from 53% for the laboratory setup to 67-69% for the advanced tank reactors.

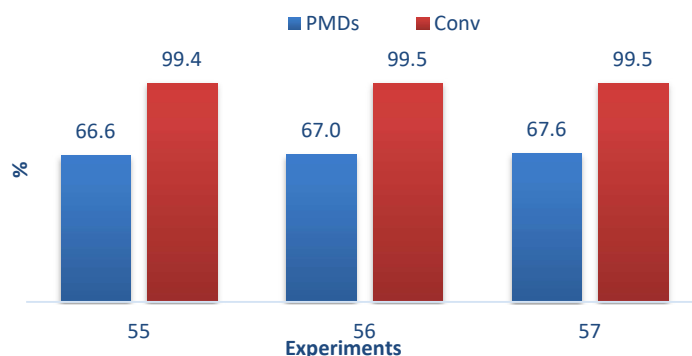


Figure 4.26: Citronellal conversions and PMD contents of technical-scale experiments.

The amounts of isopulegols and PMD-acetals (**39**) were also highly reproducible in the advanced bioreactor. The average quantity of isopulegols was similar to the simpler demonstration-scale system with 12.8% vs. 11.7%, although the later varied significantly with the stirring speed. In contrast, the average PMD-acetal (**39**) composition was almost doubled in the bioreactor with 6.2%, compared to 3.3% in the basic demonstration-scale device. The bioreactor achieved impressive stirring speeds of 1000 rpm and incorporated baffle elements, which enabled highly effective mixing of the immiscible layers. While this improved the consumption of Cal (**32**), it causes competitive reactions with PMD (**33**) at higher conversions.

On average, the technical-scale reactor produced 64.9% of PMDs, 1.4% of PMD acetals and 4.5% of isopulegols. Consequently, the formation of the PMDs was 46-times and that of the Iso (**37**) 3-times favoured over the acetals. This represents more than a doubling in PMD-preference compared to the demonstration-scale system.

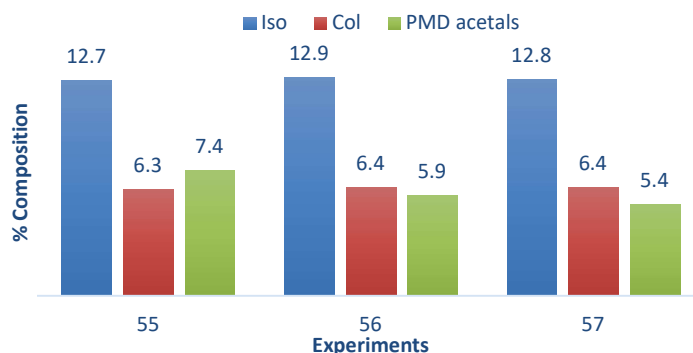


Figure 4.27: Isopulegol, citronellol and PMD-acetal contents of technical-scale experiments.

For all three experiments conducted in the advanced bioreactor, the rate of conversion followed first order kinetics and was highly consistent at 0.006 s^{-1} with an average 99.8% linear regression (**Figure 4.28**). However, this was significantly lower compared to the corresponding Experiment 51 in the simpler demonstration-scale reactor with 0.234 s^{-1} . This finding may be attributed to the type of reaction vessel, the rate of stirring, differences in heat distribution and the reaction scale.

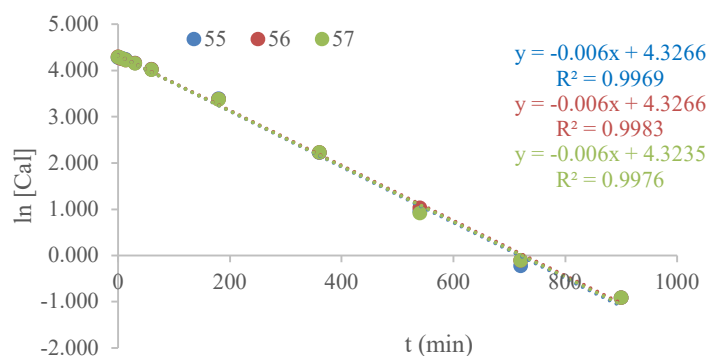


Figure 4.28: First-order comparison of citronellal conversion.

4.2.7. Separation of PMD-stereoisomers by recrystallization

Experiment 58 was conducted to isolate the dominant PMD-isomers (**33a/b**) in high purity. The reaction thus utilized neat citronellal with >96% purity and was performed on a 250 ml laboratory-scale. The crude product was extracted with diethyl ether and gave 45.6 g of a clear oily liquid with a menthol-like odour. The crude product contained about 3% of residual Cal (**32**), approx. 10% of the Iso (**37**) and ca. 82% of the isomeric PMDs (**Figure 4.29**).

The crude mass was repeatedly recrystallized from n-heptane to produce 13.2 g (58.5% yield) of 94% pure *cis*-PMD (**33a**). The filtrate was then used to obtain *trans*-PMD (**33b**). After repetitive recrystallization and seeding with pure stock *trans*-PMD (**33b**), approximately 4.42 g of *trans*-PMD (**33b**) in a purity of 95% were obtained. The purity and identity of each isomer

were confirmed by $^1\text{H-NMR}$ and $^{13}\text{C-NMR}$ in comparison with literature data (**Table 4.2**). Characteristic signals were found for the chiral positions 3 and 4. The $^1\text{H-NMR}$ revealed distinctive signals for the hydroxy-groups at C-1 and C7, respectively.

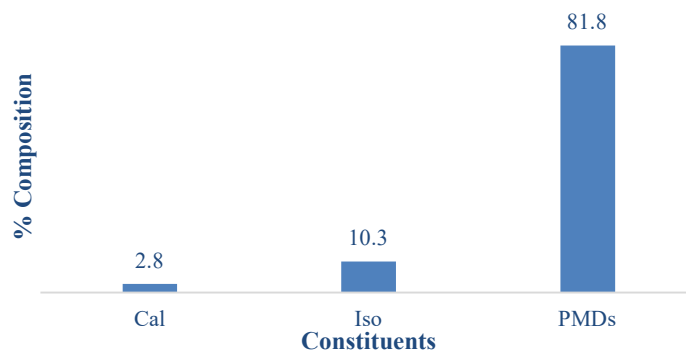


Figure 4.29: Composition of crude product from neat citronellal.

Table 4.2: Main NMR assignments of *cis*- and *trans*-PMD.

C No.	<i>trans</i> -PMD (33b)		<i>cis</i> -PMD (33a)	
	^{13}C	^1H	^{13}C	^1H
3	53.7	1.97 (ddd, $J = 12.2, 5.8, 3.9$ Hz, 1H)	48.7	1.81 (d, $J = 2.3$ Hz, 1H)
4	73.1	3.75 (td, $J = 10.5, 4.3$ Hz, 1H)	68.3	4.41 (d, $J = 2.4$ Hz, 1H)
6	31.5	1.08 (dd, $J = 13.8, 9.2$ Hz, 1H)	25.8	1.20-1.14 (m, 1H)
7	22.1	0.95 (d, $J = 6.6$ Hz, 3H)	22.3	0.88 (d, $J = 6.2$ Hz, 3H)
8	-	3.44 (s, 1H)	-	2.76 (s, 1H)
12	-	3.44 (s, 1H)	-	2.43 (s, 1H)

4.2.8. Separation of PMD stereoisomers by fractional distillation

Experiment 59 was again conducted to obtain the pure stereoisomers of PMD (**33**) but utilized RE-LSG oil and operated on a 500 ml scale. The same workup process was followed and 85.58 g of a clear oily liquid with a menthol-like odour were obtained. The reaction achieved almost completion with 72.3% of the PMD isomers (**33**) in the crude product (**Figure 4.30**).

The PMDs (**33**) in the crude product were then separated from other constituents by vacuum fractional distillation, which yielded various fractions. Fraction 4 collected at 110°C gave 58.1 g of oil that contained 65.1% of *cis*- (**33a**) and 26.3% of *trans*-PMDs (**33b**). $^1\text{H-NMR}$ analysis (**Figure 4.31a**) furthermore revealed the presence of traces of Col **38** (5.09 ppm), *n*Iso **37b** (4.86 ppm) and *i*Iso **37a** (3.86 ppm), respectively. The material was subjected to repeated recrystallization from *n*-heptane twice and yielded 31.1 g of the pure PMD isomers in a *cis:trans* ratio of 84:16 (**Figure 4.31b**).

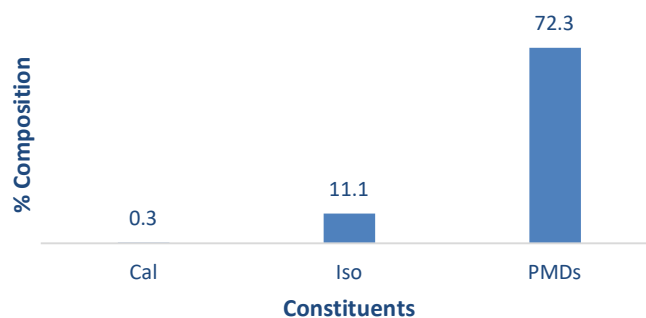


Figure 4.30: Composition of crude product from RE-LSG oil.

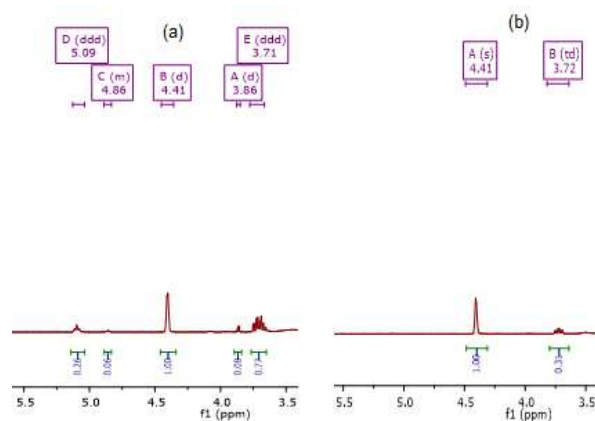


Figure 4.31: Partial ^1H -NMR spectra of (a) crude and (b) recrystallized Fraction 4 material.

4.2.9. Synthesis of PMD-acetals

The isomeric PMD-acetals (**39**) were the dominant follow-up products during all PMD syntheses. These compounds are proposed to form through acetalization of unreacted Cal (**32**) with the corresponding PMD isomer. Three experiments were thus conducted to confirm this assumption. In all cases, complete consumption of Cal (**32**) was achieved. However, selectivities towards PMD-acetal (**39**) production were low with approx. 16-34% (Figure 4.32).

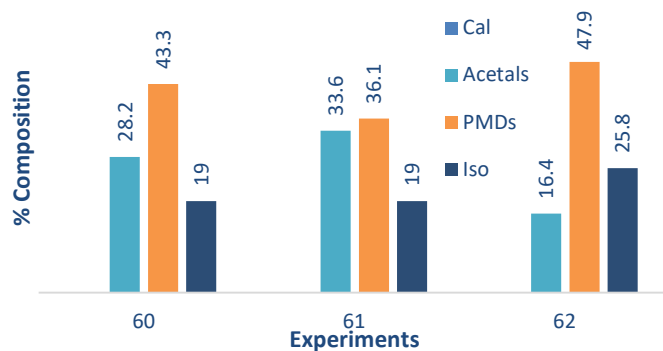


Figure 4.32: Composition of crude acetalization products.

The crude product obtained from Experiment 60 contained twice as much PMDs (**33**) than PMD-acetals (**39**). A similar outcome was observed for Experiment 61. Experiment 62 gave the lowest quantity of PMD-acetals (**39**) with just 16.4%, while the amounts of the PMDs (**33**) and Iso (**37**) dominated with 47.9% and 25.8%, respectively.

The consumption of citronellal and the dominance of the PMDs (**33**) and Iso (**37**) suggested that the intramolecular cyclization of Cal (**32**) dominated the course of the reaction (**Scheme 4.5**). The bimolecular reaction of PMD (**33**) with Cal (**32**) could not compete. Further optimization of the reaction conditions is thus required in future studies. Column chromatography separation of the crude product from Experiment 61 gave sufficiently pure PMD-acetals. The clear oily liquid consisting of 72.0% of *cis*- and 15.2% of *trans*-PMD acetal (**39a/b**), respectively. Structural identification and assignment were achieved by comparison with literature NMR-data.

4.3. β -Triketone syntheses and isolation

4.3.1. Synthesis of 2, 4, 6-trihydroxyphenyl ketones

The 2, 4, 6-trihydroxyphenyl ketones were prepared by AlCl₃-assisted Friedel-Crafts acylation of phloroglucinol (**40**). Although the synthesis of 15 trihydroxyphenyl ketones was attempted, only 11 compounds were successfully produced. Their yields ranged widely, but all compounds were isolated in excellent purities (**Figure 4.33**). The lowest yield was recorded for 1-(2, 4, 6-trihydroxyphenyl) ethanone (**65**, Experiment 74) with just 1.2%. Most of these losses occurred during repeated extraction of the trihydroxyphenyl ketones. Purification of impure crude products via flash chromatography contributed to further losses.

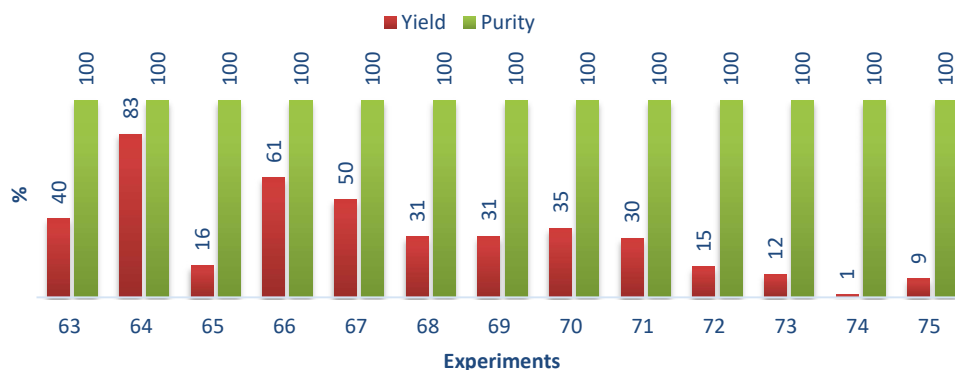


Figure 4.33: Yields and purities of acyl phloroglucinols.

All analogues possessed the 2, 4, 6-trihydroxyphenyl ketone moiety. This is characterized by an UV-absorbance at 282-287 nm characteristic for the $n \rightarrow \pi^*$ transition of the carbonyl group.

The ^1H -NMR singlet at 5.90 and 11.70 ppm were attributed to the chemically equivalent HC_{arom} - and HO-protons, respectively. The carbonyl carbon showed a characteristic ^{13}C -NMR signal at 210.5 ppm and the stretching vibration of the C=O bond and IR-signal at 1730.0 cm^{-1} .

4.3.2. Synthesis of acetyl- β -triketones

Exhaustive methylation of the 2, 4, 6-trihydroxyphenyl-ring occurred swiftly to give the desired β -triketones. As depicted below in **Figure 4.34**, the yields of the purified compounds were poor to moderate with 1-54%. These losses were again encountered during workup and purification by bulb-to-bulb distillation. Despite this, a total of 11 acetyl- β -triketones were successfully obtained in excellent purity.

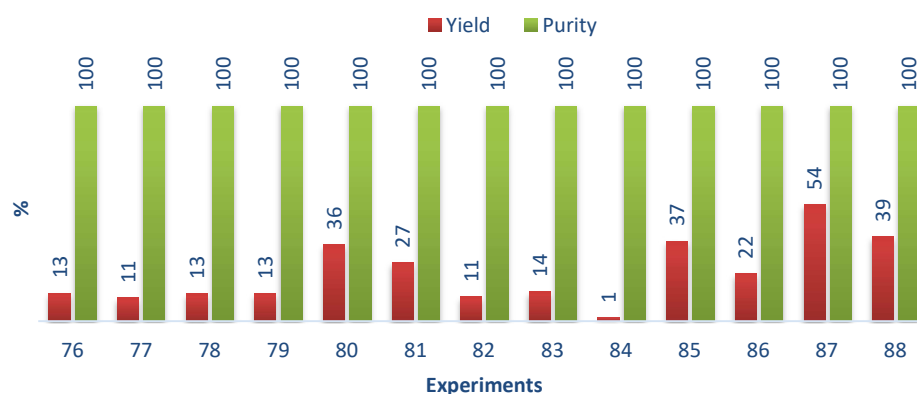


Figure 4.34: Yields and purities of acetyl- β -triketones.

All compounds were identified by spectral assessment of their 5-hydroxy-2, 2, 6, 6-tetramethylcyclohex-4-ene-1, 3-dione moiety. This group showed characteristic downfield ^1H -NMR singlet at 18.0-19.0 ppm for the hydroxyl protons at C-5, which were locked in an intramolecular hydrogen-bond with the carbonyls of the neighbouring acetyl-group. The pairs of methyl-substituents at C-2 and C-6 were characterized by equatorial ^1H -singlets between 1.30-1.50 ppm and ^{13}C -signals at 24.2 and 23.9 ppm, respectively. The adjacent carbonyl groups in the ring exhibited strong to weak IR carbonyl vibrations at $1670\text{-}1730\text{ cm}^{-1}$.

4-(*sec*-Butyl)-5-hydroxy-2, 2, 6, 6-tetramethylcyclohex-4-ene-1, 3-dione (**55**) was the only product present as a racemic mixture due to the presence of a chiral centre in its side-chain (**Figure 4.35**). ^1H -NMR revealed two sets of signals in a ratio of approx. 95:5, suggesting the existence of possible rotamers or conformers.

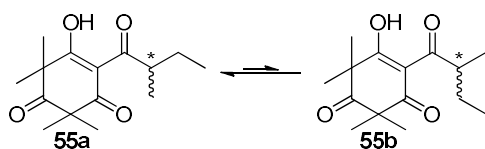


Figure 4.35: Structure of penitential rotamers of 4-(*sec*-butyl)-5-hydroxy-2, 2, 6, 6-tetramethylcyclohex-4-ene-1, 3-dione (**55**).

4.3.3. Photolytic stability testing

Acetyl- β -triketones show strong absorptions in the UVA-range due to the presence of carbonyl-groups. They may thus undergo all typical photochemical transformations of carbonyl-compounds, in particular Norrish-type cleavage reactions (**Figure 4.36**). A series of eight reactions were thus conducted to determine the stability of the acetyl- β -triketones towards photolysis. The reactions were performed in MeCN under UV-B irradiation for 2-5 hours using Pyrex and Quartz Schlenck flasks as well as NMR tubes.

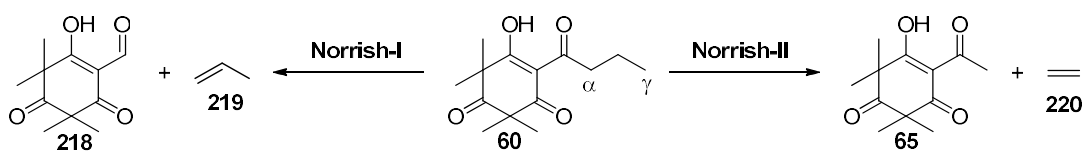


Figure 4.36: Possible Norrish-type cleavages of acetyl- β -triketones.

Five experiments utilized flavesone (**54**) incorporating an ⁱPr-group, which can only undergo Norrish-I type cleavages due to the absence of a γ -CH group. Under all irradiation conditions, compound **54** remained entirely stable over 2-5 hours of exposure to UV-B light. Subsequent irradiation experiments for 3 hours were conducted in an NMR-tube with acetyl- β -triketones **55** (^sBu), **57** (Et) and **60** (ⁿPr), respectively. Of these, compounds **55** and **60** are potentially capable of Norrish-II cleavage reactions. However, none of these molecules expressed any photochemical changes. It is assumed that the acetyl- β -triketones may undergo a deactivating and thus protective photo-keto-enol tautomerization (**Figure 4.37**), as known for 2-hydroxybenzophenone derivatives. The pseudo-6-membered ring structure due to the strong intramolecular hydrogen-bond may favour this pathway over alternative Norrish-reactions that require conformational changes.

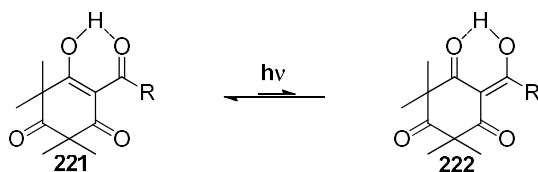


Figure 4.37: Possible photo-keto-enol tautomerization of acetyl- β -triketones.

4.3.4. Photooxidative stability testing

The stability of flavesone (**54**) towards photooxidation in visible light was furthermore investigated. After irradiation for 10 hours with oxygen-purging and hourly monitoring, GC-analysis showed no changes and flavesone remained entirely stable. In contrast, irradiation of **54** at pH 3 or 7 in water with simulated sunlight (290-429 nm) was reported to result in slow oxidation (**Figure 4.38**).

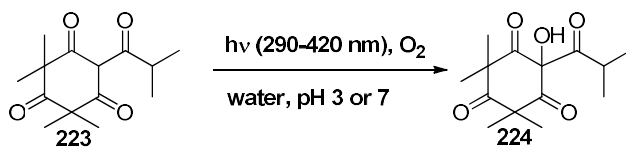


Figure 4.38: Reported slow photooxidation of flavesone.

The literature study differed significantly as it simulated environmental conditions. For the photochemical laboratory study, visible light emitted from fluorescent tubes (>400 nm) was used. Due to the poor absorption of flavesone (**54**) in this emission range, self-sensitization, $^1\text{O}_2$ -sensitization or light-induced autooxidation processes can be ruled out. In polar aprotic solvents such as acetonitrile, acetyl- β -triketones are also more likely to exist in their tautomeric enol-forms.

4.3.5. Exploring Myrtaceae species as potential β -triketone resources

4.3.5.1. Sampling

A total of six sampling trips were conducted between in the Far-North QLD region. The first batches of *X. chrysanthus* and *E. cloeziana* were collected on the Townsville JCU campus, whilst the second batches of *X. chrysanthus* and other Xanthostemon species were obtained from Tolga. Manuka oil distilled from *L. scoparium* leaves was sourced from Plant Essentials[®].

4.3.5.2. Distillation of essential oils

Six steam or hydrodistillations were conducted using variable amounts of biomass and hence produced different quantities of essential oils. The distillation method and setup depended on the available amounts and the presence or absence of a notable scent of the biomass. *E. cloeziana* leaves produced a strong scent indicating volatiles and were thus subjected to steam distillation. About 350 g of leaves were distilled in a glass setup and 1.35 g (0.38%) of a yellowish-green oil were obtained. Of the Xanthostemon species, >500 g of leave material was used. The *X. verticillatus* leaves exhibited a noticeable aromatic scent, while those of *X. chrysanthus*, *X. umbrosus* and the hybrid species lacked any distinct odour. These materials

were subjected to continuous hydrodistillation with recycling of the distillate in order to concentrate the essential oil constituents. Oil yields varied depending on distillation method and plant species and ranged between 0.02-0.58% (**Figure 4.39**).

Consistent with its distinct odour, *X. verticillatus* offered the highest yield at 0.58% (2.92 g). *X. umbrosus* also presented a reasonable amount of 0.93 g (0.19%) of a greenish-yellow oil. The hybride and *X. chrysanthus* species gave low amounts of 0.09-0.24 g (0.02%-0.05%), particularly the *X. chrysanthus* material from Tolga.

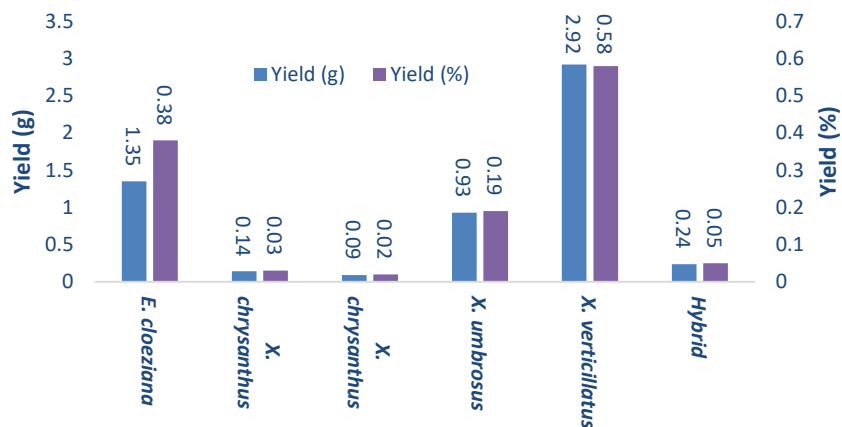


Figure 4.39: Difference between the percent yield and actual mass of oil.

4.3.5.3. Identification of major constituents of Myrtaceae essential oils

GC-analysis of the essential oils obtained and KI value comparison with literature data revealed that the high-oil yield producing plants contained one major constituent (**Figure 4.40**). In particular, the main ingredient of *X. verticillatus* essential oil was 1, 3-dimethoxy-5-isopropylbenzene (**70**) with 94%. Likewise, *E. cloeziana* oil contained 89% of tasmanone (**67**), while *X. umbrosus* oil composed of 64% of cyclocolorenone (**69**).

The major constituent in *X. chrysanthus* appeared in both species collected in Townsville and Tolga. Correlation of its KI value suggested isotorquatone (**68**) as structure. While both plant materials gave low oil yields, the amount of isotorquatone (**68**) varied significantly with sampling location with 85% and 22%, respectively. Both locations are separated by over 350 km and thus consist of isolated populations. Local soil chemistry, climatic conditions and natural hybridization thus affect the chemical profiles differently.

Three dominant compounds were present in the essential oil of the hybrid species; β -cadinene (**106**, 10%), isoleptospermone (**55**, 13%) and 1, 3-dimethoxy-5-isopropylbenzene (**70**, 18%).

Noticeable β -triketones identified in the *L. scoparium* essential oil were leptospermone (**58**, 17%), isoleptospermone (**55**, 4%) and flavesone (**54**, 3%).

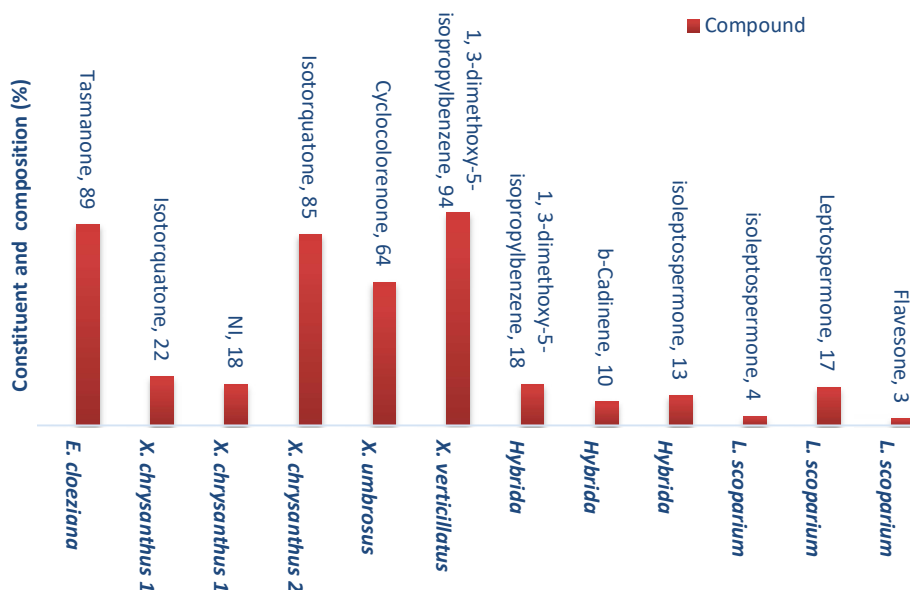


Figure 4.40: Major constituents of the essential oils.

4.3.6. Isolation and structural characterization of tasmanone

E. cloeziana has been reported to contain >90% of tasmanone (**67**)¹⁶⁰, which correlates well with the amount of 89% from this study. To further separate tasmanone from the residual non-polar organic constituents, it was firstly transferred through deprotonation with Na_2CO_3 into the aqueous layer. Reprotonation of the tasmanone-anion and extraction with ether recovered approx. 16% of pure **67** as a golden-like oil. The existence of two major keto-enol tautomers in a 33% to 67% ratio was confirmed by $^1\text{H-NMR}$ analysis.

4.3.7. Extraction of flavesone, leptospermone and isoleptospermone from Manuka oil

Manuka oil from *L. scoparium* is known for its insecticidal properties due to its β -triketone constituents. These acetyl- β -triketones are structurally related to tasmanone and likewise possess an acidic hydroxyl-group that enables separation by acid-base extraction. Following this approach, Manuka oil produced a golden oil with 33.2% recovery of material. This refined oil consisted of 16.9% of flavesone (**54**), 17.6% of isoleptospermone (**55**), 63.3% of leptospermone (**58**) and only 2.2% of other constituents. This result confirms the effectiveness of acid-base extraction for the isolation of acetyl- β -triketones. The material was further purified

by bulb-to-bulb distillation and gave two fractions with pure mixtures of the acetyl- β -triketones (Figure 4.41).

Fraction 1 and 2 purely composed of the acetyl- β -triketone mixtures with a combined yield of 1.7 g (50%). Leptospermone (**58**) was the major component of these fractions with >55%. The other compounds largely remained in the residual Fraction 4. Hence, small-scale bulb-to-bulb distillation can be used to successfully enrich and purify the naturally occurring acetyl- β -triketones.

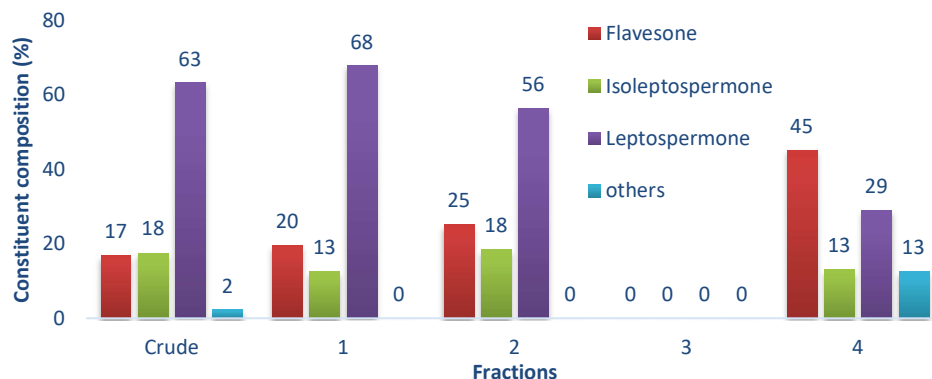


Figure 4.41: Composition of refined Manuka oil prior and after bulb-to-bulb purification.

4.3.8. Isolation and identification of cyclocolorenone from *X. umbrosus* oil

Cyclocolorenone (**69**) was successfully isolated from the *X. umbrosus* oil matrix by combi flash column chromatography using gradient elution of 0-10% EtOAc in *n*-hexane. A reasonable yield of 0.21 g (42%) of pure **69** was obtained after workup. The structural identity was verified by ^1H -, ^{13}C -, HSQC- and HMBC-NMR analyses. A comparison of the experimental ^1H - and ^{13}C -NMR chemical shifts with those calculated using ChemDraw showed good correlation and hence supported the structure of **69** (Table 4.3).

Table 4.3: Comparison of experimental and calculated chemical shifts of cyclocolorenone.

C-No	^{13}C -NMR (ppm)		^1H -NMR (ppm)	
	Experiment	ChemDraw®	Experiment	ChemDraw®
4	31.8	34.9	2.02-1.98	1.68
3	32.4	33.3	2.08, 1.41	1.26, 1.24
2	21.2	21.5	1.60, 1.98-1.94	1.38, 1.13
1a	32.6	32.8	1.28-1.26	0.22
7b	28.6	28.9	1.46	0.87
7a	140.4	140.5	-	-
4a	42.6	42.8	2.95	2.38
1	26.1	26.1	-	-
8	29.6	22.7	1.23	0.99
9	16.6	22.7	1.01	0.99

7	176.5	175.8	-	-
6	208.4	207.5	-	-
5	40.3	42.8	2.49, 2.04	3.06, 2.81
10	17.5	15.7	0.79	0.96
11	8.3	10.0	1.72	2.43

4.3.9. Isolation and identification of 1, 3-dimethoxy-5-isopropylbenzene from *X. verticillatus* oil

X. verticillatus oil was composed in 94.4% of 1, 3-dimethoxy-5-isopropylbenzene (**70**). Due to its already high purity and to avoid material losses, no further purification was attempted. The structure of **70** was again confirmed by advanced NMR-analyses. The good correlation of experimental and calculated NMR-data further supported the identity of 1, 3-dimethoxy-5-isopropylbenzene **70** (Table 4.4).

Table 4.4: Comparison of experimental and calculated chemical shifts of 1, 3-dimethoxy-5-isopropylbenzene.

C-No	¹³ C-NMR (ppm)		¹ H-NMR (ppm)	
	70	ChemDraw®	70	ChemDraw®
1	151.6	150.4	-	-
2	104.8	104.6	6.40	6.64
3	160.8	161.3	-	-
4	97.6	97.6	6.30	6.19
5	160.8	161.3	-	-
6	104.8	104.6	6.40	6.64
7	34.6	33.8	2.84	2.87
8	24.0	23.3	1.24	1.20
9	24.0	23.3	1.24	1.20
10	55.3	55.8	3.79	3.83
11	55.3	55.8	3.79	3.83

4.3.10. Identification of other constituents in the essential oils by GC-analyses

The experimental KI values obtained through extensive GC-assessment of the essential oils of *X. chrysanthus 1*, *X. chrysanthus 2*, *X. umbrosus* and the hybrid species, as well as the extracted Manuka oil (Manuka 2), and the remains of the Manuka oil extract (Manuka 1) were compared to documented KI values in the NIST and/or Wiley databases. Following this approach, several constituents in these oils and extracts could be successfully assigned. Figure 4.42 shows selected examples of these compounds.

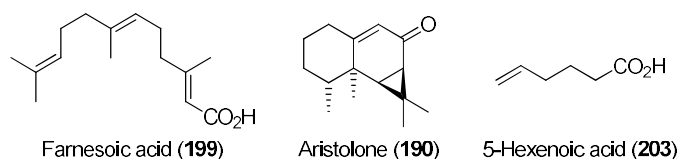


Figure 4.42: Chemical structures of selected constituents (>20%) of the essential oils.

The chemical composition of the *X. chrysanthus* species again depended somewhat on their sampling location. The oil obtained from the Townsville location revealed a total of 14 constituents identified (**Table 4.5**). Farnesoic acid (**199**) was found as a major component in 35%.

Table 4.5: Constituents identified from *X. chrysanthus* oil from the Townsville region.

No	Compound	Exp KI	Lit KI	%
92	Benzoic acid	1205	1210	1.3
95	Benzylacetone	1247	1253	11.9
139	Dibunol	1505	1504	11.4
150	<i>cis</i> -Nerolidol	1568	1565	1.1
55	Isoleptospermone	1622	1622	21.0
176	Eudesma-4-(15)-7-diene-1b-ol	1679	1685	0.7
183	Farnesol	1711	1713	4.0
184	(2 <i>Z</i> , 6 <i>E</i>)-Farnesol	1723	1722	1.2
186	(<i>E</i> , <i>E</i>)-Farnesal	1739	1738	2.4
199	Farnesoic acid	1829	1824	35.0
208	Isophytol	1948	1948	1.0
210	Kaurene	2058	2043	6.1
211	<i>trans</i> -Phytol	2115	2111	1.6
212	Supraene	2808	2808	0.4

In contrast, the chemical profile of the isolated oil from the Tolga location contained 13 additional components, of which 11 could be identified based on their KI values (**Table 4.6**). Farnesoic acid (**199**) and 5-Hexenoic acid (**203**) were confirmed as major constituents in 28% and 26.2%, respectively.

Table 4.6: Constituents identified from *X. chrysanthus* oil from the Tolga region.

No	Compound	Exp KI	Lit KI	%
93	3-Phenyl-2-butanone	1243	1243	5.0
121	NI	1460	-	1.7
139	Dibunol	1505	1504	2.8
175	NI	1677	-	2.0
69	Cyclocolorenone	1756	1758	0.9
189	Benzyl benzoate	1770	1769	1.2
199	Farnesoic acid	1829	1824	28.0
203	5-Hexenoic acid	1871	1885	26.2

205	Benzyl salicylate	1877	1868	3.8
208	Isophytol	1948	1948	6.2
209	Hexadecanoic acid	1988	1984	3.1
210	Kaurene	2058	2043	13.7
211	<i>trans</i> -Phytol	2115	2111	4.9

Analysis of *X. umbrosus* essential oil revealed 21 additional compounds, of which 18 could be assigned by comparison of their respective KI values (**Table 4.7**). The major constituent aristolone (**190**) was found in 35%. Aristolone (**190**) is structurally related to cyclocolorenone (**69**).

Table 4.7: Constituents identified from *X. umbrosus* oil from the Tolga region.

No	Compound	Exp KI	Lit KI	%
80	NI	1051	-	0.8
104	β -Elemene	1393	1389	2.8
110	α -Gurgenene	1412	1412	5.7
116	Alloaromadenrene	1443	1442	4.1
126	Patchoulene	1477	1484	1.2
133	Viridiforene	1496	1496	1.3
141	γ -Cadinene	1517	1517	0.7
151	Palustrol	1571	1581	7.9
153	Spathulenol	1584	1584	1.1
155	NI	1588	-	0.7
156	Globulol	1591	1590	2.3
160	Viridiflorol	1603	1604	5.7
162	Ledol	1615	1608	8.2
165	Isospathulenol	1639	1639	0.5
169	τ -Muurolol	1649	1650	1.6
171	α -Cadinol	1662	1662	2
173	Juniper camphor	1666	1675	1.5
183	Farnesol	1711	1713	1.6
190	Aristolone	1780	1787	35.3
199	Farnesoic acid	1829	1824	11.2
206	NI	1905	-	2.8

As depicted below in **Table 4.8**, the oil from the *X. chrysanthus* and *X. verticillatus* hybrid species contained 27 compounds, of which only 20 could be determined. Next to three unknown compounds in a total amount of 45.2%, isoleptospermone (**55**) was confirmed as a major component with 13.2%.

Table 4.8: Constituents identified from *X. chrysanthus* and *X. verticillatus* hybrid oil from the Tolga region.

No	Compound	Exp KI	Lit KI	%
93	3-Phenyl-2-butanone	1243	1243	2.4
101	α -Cubebene	1350	1351	0.4

Chapter 4 – Discussion

108	NI	1407	-	20.0
112	α -Santalene	1426	1424	3.0
115	NI (MW 152)	1438	-	0.8
129	NI (MW 69)	1484	-	15.2
131	NI (MW 218)	1489	-	10.2
137	β -Guaiene	1501	1500	0.9
140	β -Bisabolene	1509	1509	1.4
142	δ -Cadinene	1522	1522	1.3
144	Calamenene	1528	1528	1.5
54	Flavesone	1541	1546	1.3
150	<i>cis</i> -Nerolidol	1568	1565	0.9
157	Spirijatamol	1592	1592	1.4
55	Isoleptospermone	1622	1622	13.2
166	Cubenol	1641	1641	3.3
169	τ -Muurolol	1649	1650	1.9
177	NI	1680	-	1.6
181	α -Bisabolol	1692	1691	0.4
183	Farnesol	1711	1713	3.6
184	(2 <i>Z</i> , 6 <i>E</i>)-Farnesol	1723	1722	2.7
186	(<i>E</i> , <i>E</i>)-Farnesal	1739	1738	5.7
69	Cyclocolorenone	1756	1758	2.6
193	NI	1796	-	1.3
195	NI	1805	-	1.0
201	Baeckeol	1859	1861	2.3
210	Kaurene	2058	2043	0.4

The oil from *X. verticillatus* was found to contain only 6 compounds and, only two of these compounds were fully identified (**Table 4.9**). Molar mass of the unidentified compounds from MS is provided and this will aid in the identification these compounds in the future. The major compound was identified to be 1, 3 - dimethoxy - 5 - isopropylbenzene (**70**, 95.9%).

Table 4.9: Constituents identified from *X. verticillatus* oil from the Tolga region.

No	Compound	KI	Lit, KI	%
105	NI (MW 105)	1393		<0.1
70	1,3-Dimethoxy-5-isopropylbenzene	1397	1397	95.9
109	NI (MW 204)	1408		0.8
124	NI (MW 194)	1471		0.6
125	NI (MW 194)	1476		1.1
69	Cyclocolorenone	1756	1758	0.9

E. cloeziana oil offered 24 compounds, of which 15 were not identified while 9 were identified (**Table 4.10**). Despite the reasonable number of constituents the general composition was >1%. Tasmanone (**67**) was however, the dominant constituent with 93.6% composition. The MS data for the unknown compounds were determined and will be used as leads for their identification.

Table 4.10: Constituents identified from *E. cloeziana* oil from the Townsville region.

No	Compound	KI	Lit, KI	%
73	NI (MW 113)	945		<0.1
79	Eucalyptol	1035	1035	<0.1
82	1, 3-Heptanedione-2, 6-dimethyl	1075	1076	0.4
96	NI (MW 191)	1249		<0.1
98	NI (MW 209)	1320		0.2
99	NI (MW 170)	1327		0.1
100	NI (MW 214)	1342		0.6
107	NI (MW 208)	1401		<0.1
123	NI (MW 190)	1464		0.1
135	NI (MW 226)	1499		0.2
54	Flavesone	1541	1546	0.2
153	Spathulenol	1584	1584	0.1
156	Globulol	1591	1590	0.1
160	Viridiflorol	1603	1604	0.7
161	NI (MW 266)	1612		0.2
167	NI (MW 238)	1642		0.8
182	NI (MW 238)	1694		1.1
67	Tasmanone (MW 252)	1744		93.6
192	NI (MW 266)	1794		1
196	NI (MW 266)	1805		0.7
199	Farnesoic acid	1829	1824	2.1
202	NI (MW 268)	1859		0.4
204	NI (MW 300)	1873		0.3
207	Palmitic acid	1925	1927	0.5

Table 4.11 shows that the untreated Manuka oil (MOr) contains 47 compounds, of which 28 were identified and 19 were not identified. *Cis*-Calamene (**145**, 22.7%), leptospermone (**58**, 22.4%) and isoleptospermone (**55**, 5.3%) were the known major constituents. The MS data for the unknown compounds were determined and will be used as leads for their identification.

Table 4.11: Constituents identified from the organic fraction of Manuka oil.

No	Compound	KI	Lit, KI	%
72	α -Pinene	934	934	1.3
74	β -Pinene	980	980	0.1
75	β -Myrcene	991	991	0.1
76	NI (MW 136)	1006		<0.1
77	m-Cymene	1027	1025	0.2
78	Limonene	1032	1032	0.1
79	Eucalyptol	1035	1035	0.1
81	γ -Terpinene	1060	1060	0.1
83	α -Terpinolene	1088	1088	<0.1
84	Linalol	1101	1101	0.1

Chapter 4 – Discussion

85	Isoamylisovaterate	1107	1105	0.1
86	NI (MW 85)	1116		0.2
87	NI (MW 170)	1148		<0.1
88	Terpinene-4-ol	1183	1184	<0.1
89	NI (MW 102)	1194		0.1
90	α - terpineol	1197	1197	<0.1
91	NI (MW 101)	1200		0.1
93	NI (MW 168)	1243		0.1
97	NI (MW 168)	1276		<0.1
101	α -Cubebene	1350	1351	4.2
103	α -Cupaene	1380	1380	4.5
105	β -Elemene	1393	1389	1.4
110	α -Gurgenene	1412	1412	0.9
113	β -Caryophyllene	1428	1428	1.9
117	Aromadendrene	1447	1449	1.4
119	NI (MW 204)	1457		2.4
71	β -Cadinene	1474	1471	2.8
127	β -Cadinene	1479	1472	2.8
135	NI (MW 204)	1499		4.4
145	<i>cis</i> -Calamene	1537	1537	22.7
147	NI (MW 254)	1547		11.1
149	α -Calacorene	1552	1548	0.8
152	Caryophyllene oxide	1581	1581	1.2
160	Viridiflorol	1603	1604	0.4
55	Isoleptospermone	1622	1622	5.3
58	Leptospermone	1640	1640	22.4
171	α -Cadinol	1662	1662	1.9
174	NI (MW 218)	1666		0.7
178	NI (MW 220)	1681		0.5
180	NI (MW 220)	1689		0.6
185	NI (MW 206)	1736		0.3
187	NI (MW 266)	1753		<0.1
188	NI (MW 220)	1758		0.2
194	NI (MW 238)	1799		0.3
197	5-Hydroxy-calamenene	1805	1801	0.1
198	NI (MW 236)	1818		0.1
200	NI (MW 236)	1837		0.1

The organic fraction (MO - 1) obtained after the removal of the acetyl- β -triketones by extraction was also analysed for its composition (**Table 4.12**). A total of 27 compounds were detected, of which all but two could be assigned. Only trace amounts of isoleptospermone (**55**) remained in the organic fraction, thus confirming the success of the acid-base extraction.

Table 4.12: Constituents identified from the organic fraction of Manuka oil.

No	Compound	Exp KI	Lit KI	%
72	α -Pinen	934	934	2.4
101	α -Cubebene	1350	1351	7.2
103	α -Cupaene	1380	1380	7.6
105	β -Elemene	1393	1389	2.8
110	α -Gurgenene	1412	1412	2.1
113	β -Caryophyllene	1428	1428	4.0
116	Alloaromadenrene	1443	1442	4.6
119	Epi-Bycyclosesquiphellandrene	1457	1452	5.6
122	Humulene	1462	1462	0.7
71	β -Cadinene	1474	1471	3.8
134	Eremophilene	1499	1498	5.7
139	Dibunol	1505	1504	7.4
145	<i>cis</i> -Calamene	1537	1537	18.1
146	α -Cubenene	1544	1345	9.6
148	Calacorene	1549	1546	1.7
152	Caryophyllene oxide	1581	1581	1.4
154	Espatulenol	1585	1585	1.8
156	Globulol	1591	1590	0.9
160	Viridiflorol	1603	1604	1.6
55	Isoleptospermone	1622	1622	1.2
164	Epicubenol	1632	1632	1.6
166	Cubenol	1641	1641	2.9
172	NI	1663	-	0.9
173	Juniper camphor	1666	1675	0.7
176	Eudesma-4-(15)-7-diene-1b-ol	1679	1685	0.9
179	NI	1687	-	0.8
209	Hexadecanoic acid	1988	1984	2.0

Likewise, the crude aqueous fraction (MO - 2) of the Manuka oil was investigated by GC-analysis (**Table 4.13**). All of the 18 identified compounds could be assigned. The combined amount of the three major acetyl- β -triketones accounted to 88.5%.

Table 4.13: Constituents identified from the aqueous fraction of Manuka oil.

No	Compound	Exp KI	Lit KI	%
101	α -Cubebene	1350	1351	1
103	α -Cupaene	1380	1380	1.2
105	β -Elemene	1393	1389	0.3
106	Eugenol	1397	1389	0.2
110	α -Gurgenene	1412	1412	0.2
113	β -Caryophyllene	1428	1428	0.5
116	Alloaromadenrene	1443	1442	0.3
118	Naphthalene	1454	1458	1.5
71	β -Cadinene	1474	1471	0.8
132	δ -Selinene	1494	1493	0.8
133	Virdiforene	1496	1496	0.3

138	α -Seliene	1501	1498	0.8
141	γ -Cadinene	1517	1517	0.2
144	Calamenene	1528	1528	3.1
54	Flavesone	1541	1546	15.8
159	Guaiol	1602	1600	0.1
55	Isoleptospermone	1622	1622	8.2
58	Leptospermone	1640	1640	64.5

4.3.11. Antimicrobial activity evaluations

Preliminary antimicrobial screening tests were determined by evaluating the extent of inhibition of microbial growth in culture tubes (**Figure 4.43**). Of the 17 samples tested, 8 were synthesized analogues and 9 were plant essential oils and their extracts.

S. epidermidis was susceptible to most of the samples tested. Strong growth inhibitions were achieved mainly by the synthetic trihydroxyphenyl ketones. Moderate activities were found for 6 test compounds, respectively. In particular, the two trihydroxyphenyl ketones analogues **41** and **42** were the most active compounds with >96% inhibition. The acetic Manuka oil extract (MO-2) and the acetyl- β -triketones **54**, **55** and **58** exhibited inhibition rates of 81-86%. Selected synthetic analogues, untreated Manuka oil (MOr) and extracts containing acetyl- β -triketones, *i.e.* *E. cloeziana* and the *X. chrysanthus/X. verticillatus* hybrid, showed reasonable activities at 14-40% inhibition.

E. coli showed moderate susceptibilities to the trihydroxyphenyl ketones **42** and **44** with 28% and 23% of inhibition, respectively. All other compounds showed poor to neglectable growth inhibitions of <10%.

Similarly, *C. albicans* showed high resistance to all the samples screened. Inhibition rates remained <6%, with an average of just 2%.

4.3.12. Larvicidal activity evaluations

Larvicidal screening was conducted with 6 synthetic compounds and 8 essential oils or their extracts. A duplicate 24-well plate assay was used, and the mortality was determined at 95% CI. Generally, most samples exhibited high larvicidal activity (**Figure 4.44**). Particularly, all of the *Xanthostemon* species demonstrated excellent mortality rates of 96-100%. In addition, *E. cloeziana* and untreated Manuka oil achieved activity levels of 98% and 81%, respectively.

Chapter 4 – Discussion

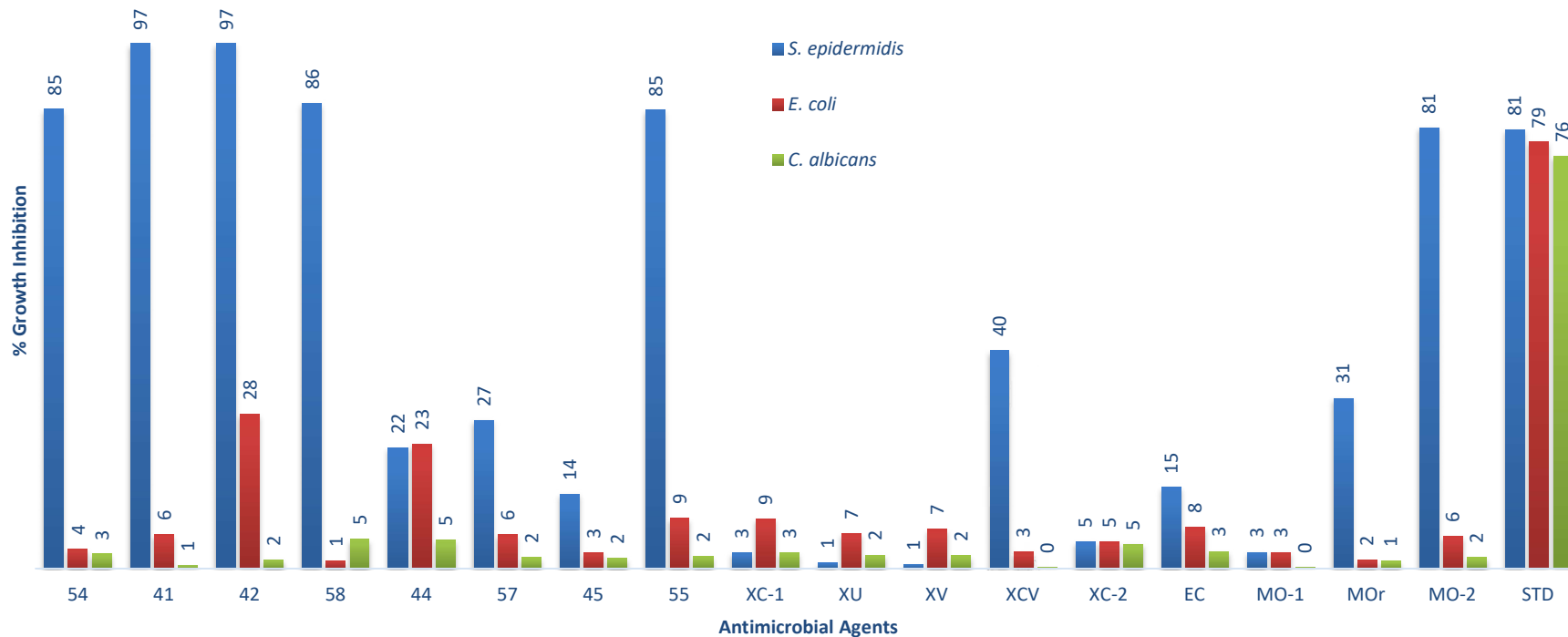


Figure 4.43: Inhibition of *S. epidermidis*, *E. coli* and *C. albicans* after inoculating with selected Myrtaceae extracts, trihydroxyphenyl ketones and acetyl- β -triketones.

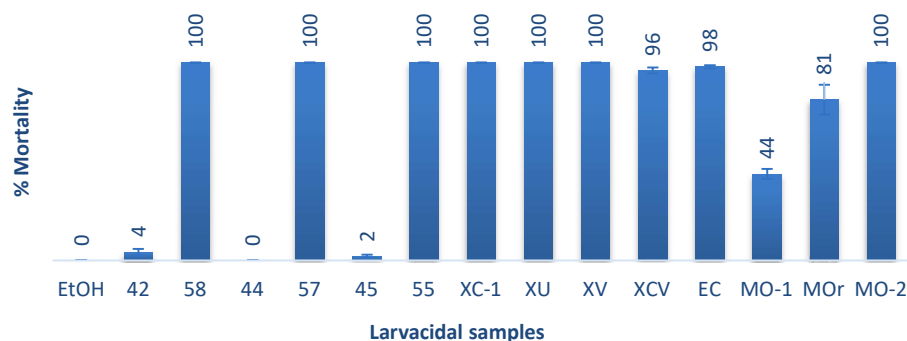


Figure 4.44: Susceptibility of *A. aegypti* larvae after inoculating with selected Myrtaceae extracts, trihydroxyphenyl ketones and acetyl- β -triketones.

An interesting difference was the high mortality displayed by the acetyl- β -triketones **58**, **57** and **55**, while the trihydroxyphenyl ketones **42**, **44** and **45** showed low to no activities. This was supported by the likewise 100% mortality registered for the acetyl- β -triketone-rich acetic fraction of Manuka oil (MO-2), compared to the weaker activity of 44% for the organic (neutral) Manuka oil fraction MO-1.

4.3.13. Adulticidal activity evaluations

Further testing with the untreated Manuka oil (MOr) was conducted using adult *A. aegypti* and WHO bioassay tubes. As visible from **Figure 4.45**, the knock down rate (% KD) directly correlated to the concentration of MOr, but also somewhat to the exposure time.

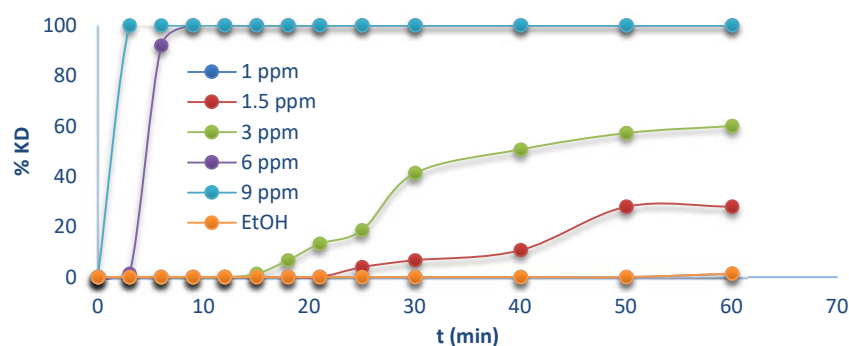


Figure 4.45: Knock down (KD) rates of adult *A. aegypti* towards untreated Manuka oil (MOr).

The control using EtOH showed no lethal effect on the mosquitoes, confirming that adult *A. aegypti* were highly vulnerable to the triketone constituents of MOr. At the lowest concentration of 1 ppm, MOr exhibited only 1.3% KD after hour of exposure. A delayed activity of 4-28% KD was observed at 1.5 ppm within 25-60 minutes. Following this trend, a concentration of 3

ppm showed activities of 1.3-60% KD already within the window of 15-60 minutes. Rapid and 100% KD were achieved at 6 ppm and 9 ppm after just 9 min and 3 min, respectively.

From this data, an LD₅₀ of 3.57 ppm was established for a sample size of 25 adult *A. aegypti* in 60 minutes of exposure (**Figure 4.46**).

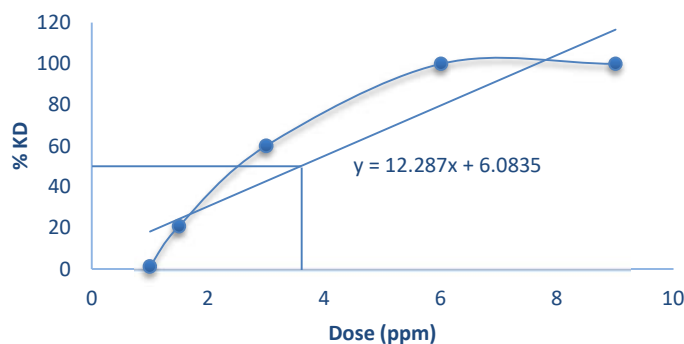


Figure 4.46: LD₅₀-determination for adult *A. aegypti* after 1 h exposure towards untreated Manuka oil (MOr).

A concentration-related trend was also observed for exposures for 24 hours (**Figure 4.47**). At concentrations of 1, 1.5 and 3 ppm, low mortality rates of <5% were established. In contrast, the highest concentrations of 6 and 9 ppm achieved good the excellent mortalities of 81% and 100%, respectively.

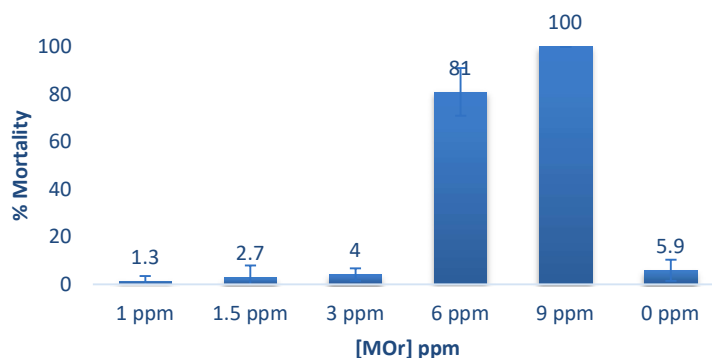


Figure 4.47: Mortality of adult *A. aegypti* towards the untreated Manuka oil (MOr).

For the 25 adult *A. aegypti* and 24 hours exposure, an LD₅₀ of 4.98 ppm was subsequently determined for the untreated Manuka oil (**Figure 4.48**).

Chapter 4 – Discussion

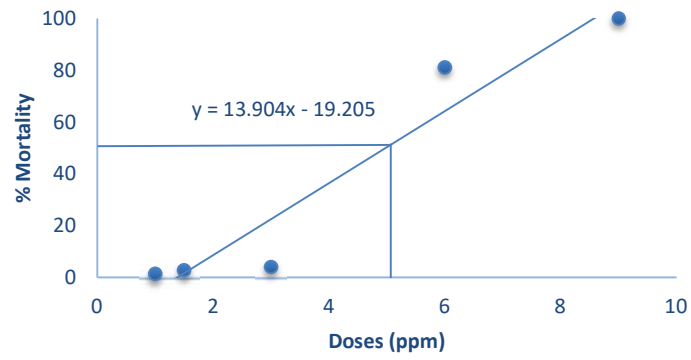


Figure 4.48: LD₅₀-determination for adult *A. aegypti* after 24 hrs exposure towards the untreated Manuka oil (MOr).

CHAPTER 5: SUMMARY AND OUTLOOK

5. Summary and Outlook

5.1. Synthesis of hydroxyfuranone and its alkoxy-derivatives

There has been increasing interest in the production of HF (**2**) as a versatile commodity chemical. Its alkoxy derivatives are another group of potential platform chemicals that can be further transformed by thermal or photochemical reactions. HF (**2**) was relatively easily accessible by photooxygenation of the biomass-derived FAL (**1**). Due to its dark colour, FAL (**1**) was purified by fractional distillation prior to usage.

5.1.1. Photooxygenations

Indoor reactions using a small-scale Rayonet reactor fitted with 16 × 8 W fluorescent lamps achieved 73-100% conversion of FAL. While complete conversions could be achieved within 60 minutes, considerable amounts of ethoxy-derivatives were also detected during the irradiation. Workup proved challenging as significant amounts of HF were transformed to the ethoxy-derivatives. During irradiation, significant sensitizer bleaching was observed. Under controlled conditions, rose Bengal decomposed at a rate of 0.001 mM.min⁻¹ at 27-28°C. Under comparable conditions, the efficiencies of photooxygenations in different alcohols decreased in the order EtOH > *i*-PrOH > *t*-AmOH. This trend was linked to solubility and hence light-transparency differences. In contrast, selectivities increased for *t*-AmOH and *i*-PrOH due to their reduced nucleophilicity. The larger immersion well photoreactor, equipped with a powerful 150 W medium-pressure mercury lamp, consistently achieved high conversions of 94-100%. The device readily produced larger quantities of material, but demanded extended irradiation times compared to the smaller Rayonet system.

For a rapid access to larger quantities of technical-grade to pure hydroxyfuranone, the immersion well reactor is surely preferable. To counter bleaching, regular refeeding or usage of more acid-stable or solid-supported photosensitizers should be employed. Alternative workup and isolation processes should also be developed. For example, neutralization of the formic acid formed during irradiation by washing with aqueous base or filtration over a solid basic material may reduce side-reactions. Alternatively, preparative photooxygenations may be conducted in *i*-PrOH due to its reduced reactivity towards pseudo-esterification, rapid availability and low cost.

Four demonstration-scale solar reactions were conducted in a simple flatbed reactor and achieved significant conversions of hydroxyfuranone of 91-98%. The natural fluctuation of

sunlight demanded variable illumination times. Likewise, reaction temperatures varied depending on the weather conditions between solar experiments. Hourly monitoring of the reactions by NMR- or GC-methods revealed that the compositions of the reaction mixtures were not changing uniformly. These variations were potentially caused by the sample treatment methods as both required thermal processes for isolation or analysis. In particular, it was noticed that spontaneous pseudo-esterification and thermal isomerization already occurred at temperatures $>28^{\circ}\text{C}$. Experiment 22 showed the best result and achieved a conversion of 98% with minimal amounts of side-products and within 8 hours of solar exposure. This reaction was conducted during winter and hence during cooler outside conditions. The importance of temperature was also clearly noticeable from the other solar experiments. The two reactions that experienced average reaction temperatures of 39°C gave larger quantities of follow-up products. The compositions of the reaction mixtures changed again drastically upon evaporation and workup, which induced thermal conversions. The complexity of the dried raw material consequently led to substantial losses of HF (**2**) due to exhaustive recrystallization and washing needs. Nevertheless, the large scales of the solar reaction produced multi-gram quantities of usable material.

Despite its solid performance in terms of conversion rates, the flatbed reactor would clearly benefit from better cooling and also gas-feeding inside the illuminated reaction chamber.

5.1.1.1. Pseudo-esterifications and -transesterifications

Using different C1-C6 alcohols, hydroxyfuranone was successfully converted to the corresponding AFN by formic acid-catalyzed pseudo-esterification. Isolation and purification of the desired compounds was found challenging. The crude MFN (**7**) and *i*PrFN (**8**) were easily obtained by standard rotary evaporation. However, the AFNs derived from the C4-C6 alcohols were difficult to concentrate and dry. A somewhat successful drying approach was achieved by azeotropic distillation of alcohol-water mixtures. Most of the products obtained constituted of 60-100% of the desired AFNs. Their structures and identities were confirmed by a series of spectroscopic analyses. Different batches of MFN (**7**), EFN (**4**) and BFN (**9**) were produced. The heat- and acid-sensitivity of the compounds made purifications on small-scales difficult.

Future studies should utilize alternative purification methods. For example, small-scale reactions may allow chromatographic separation by automated column chromatography or preparative HPLC. Solid acid catalysts may be implemented to minimize undesired ring-opening and acetalization reactions.

All filtrates obtained from the solar reactions contained large residues of HF (**2**) and EFN (**4**), which made them interesting resources for further “blending”. Pseudo-esterifications of this waste material with ethanol indeed achieved complete conversions of any residual HF (**2**). Despite this, purification and isolation of the desired EFN (**4**) caused significant losses due to thermal conversions. Using a combination of micro- and bulb-to-bulb-distillation techniques, the desired EFN (**4**) was obtained in good to high purities of 91-98%.

To avoid material losses, future isolations should use direct fractional distillation using a larger Vigreux column and several collection flasks. The successful large-scale isolation of EFN (**4**) has been indeed described in several patents.

A different approach investigated pseudo-transesterifications of EFN (**4**). It was successfully converted to four different alkoxy-analogues with varying selectivity. Secondary ring-openings and acetalizations were observed as dominant side-reactions.

Future investigation should aim at providing milder reaction conditions or at enforcing complete conversion to the ring-opened acetals instead. The latter compounds may serve as interesting building block materials themselves.

5.2. Sustainable synthesis of *para*-menthane-3, 8-diol

5.2.1. GC-FID method development

The existing GC-analysis method (M1) showed poorly resolved peaks or terminated too early to effectively quantify Cal (**32**) or the various Iso (**37**), PMD (**33**) and PMD-acetal (**39**) isomers. The initially developed and improved method (M2) completely resolved the peaks for Cal (**32**) and its related Iso (**37**) isomers. It also achieved an increased resolution of the main *cis*- and *trans*-PMD isomers (**33a/b**). The extended temperature method (M3) was able to detect higher molecular weight constituents such as the various PMD-acetals. Hence, effective GC-analysis methods were developed to establish the chemical profiles of LSG oils or to monitor the production of PMD (**33**).

Future analyses should consider GC-MS-coupling methods to rapidly proof the identity of constituents. Alternatively, further shortening of the total run-time would enable faster and hence more analyses.

5.2.2. LSG-distillations and chemical profiling

Both, steam- and hydrodistillations produced reasonable quantities of LSG oil that all predominantly contained Cal (**32**). The various aqueous waste streams from the distillation processes, *i.e.* hydrosol and boiler water, were furthermore subjected to continuous liquid-liquid extractions and their organic components analysed. Differences in oil yields and chemical compositions were linked to the design and experimental features of each distillation process. Several commercial LSG oils from distilleries in New Caledonia, Brazil, China, Australia and Madagascar were analysed to determine their chemical compositions. Of these, the oil received from the local Rare Earth (RE) distillery in North QLD showed the highest Cal (**32**) content of >79%.

Alternative separation methods such as salting-out should be investigated in order to recover organic materials, in particular dissolved PMD (**33**), from the aqueous wastes. The chemical composition of LSG, including all higher molecular weight compounds, should always be determined prior to its selection for PMD (**33**) production. The commercial RE-LSG oil is recommended as a feedstock for a future small-scale manufacturing of PMDRBO-containing insect-repellents in Queensland.

5.2.3. Syntheses of PMD

A series of conversions on laboratory- to production-scales were successfully realized. Several aqueous resources, including waste streams from the commercial LSG distillation process, were likewise investigated for the preparation of the citric acid solution.

On small laboratory-scales, conversion rates of Cal (**32**) and selectivities towards the PMD-isomers (**33a/b**) varied significantly between experiments. Nevertheless, conversions of <91% and selectivities of <65% could be achieved. Dissolved organic matter present in some of the aqueous waste streams may have contributed to changes in the chemical composition. More importantly, however, the simple magnetic stirring did not deliver reproducible and stable mixing conditions.

For future studies, the experimental parameters and equipment used should be strictly standardized. Orbital shaking or better suited stirrer magnets, *e.g.* egg-shaped bars that better suit round-bottom flasks, should be furthermore investigated to realize equal mixing conditions between experiments.

Experiments conducted on demonstration-scales produced high conversion rates and PMD (**33**) – yields of up to approx. 71%. While the source of the aqueous layer did not significantly change the outcome of the reaction, the stirring speed of the mechanical paddle did. Notably lower conversions were achieved at lower speeds. Stable emulsion conditions are thus essential for an efficient mass-transfer. At the same time, however, a more effective mixing also favoured the formation of Iso (**37**) and PMD-acetals (**39**).

Three conversions were subsequently conducted on production-scales in an advanced bioreactor. The device enabled highly reproducible reaction conditions. As a result, all transformations showed high and consistent conversions of 99.5% and PMD (**33**) – yields of 67%, respectively. Compared to the demonstration-scale reactor, the formation of Iso (**37**) was reduced, while the amounts of PMD-acetals (**39**) were increased. The high stirring speed, in combination with the baffle inserts, in the advanced bioreactor thus favours hydration (to PMD) over deprotonation (to isopulegol) conditions, but also follow-up reactions of the various PMD-isomers (**33a/b**) with unreacted Cal (**32**).

The impact on stirring speeds and mixing efficiencies needs to be further investigated for standard laboratory experiments. These small-scale transformations are typically the starting point of any technical realization and commercial implementation. While the bioreactor gave excellent results, a more chemically-suitable reactor model should be applied.

5.2.4. Isolation and conversion of PMD

For the isolation and separation of its main stereoisomers, a batch of PMD (**33**) was prepared from neat Cal (**32**). The crude product composed of 50.4% of the *cis*-isomers (**33a**) and 31.4% of the *trans*-PMD (**33b**) isomers, respectively. Repeated recrystallization from *n*-heptane furnished the main *cis*-PMD (**33a**) isomer with 94% purity. The corresponding major *trans*-isomer of PMD (**33b**) was likewise obtained in a purity of 95% through crystallization of the filtrate. Fractional distillation was less effective in separating the diastereoisomers of PMD (**33**). Using crude PMDRBO with approx. 80% purity, distillation and subsequent recrystallization furnished a *cis/trans*-PMD mixture of 84%:16% *trans* PMD.

The formation of PMD-acetals (**39**) from Cal (**32**) and PMD (**33**) was demonstrated but remained ineffective. Intramolecular reactions of Cal (**32**) to the various Iso (**37**) or PMD (**33**) dominated over intermolecular acetalization. Purification by column chromatography and subsequent drying in vacuo produced crude PMD-acetals (**39**) in ca. 87% purity.

Only a limited number of isolation and transformation attempts were conducted. Fractional recrystallization was found to be the superior technique to separate the main diastereoisomers of PMD (**33**) based on their different solubility in heptane. Further optimization of the acetalization conditions by varying reagent ratios or controlling their order of addition may also be performed.

5.3. β -Triketone syntheses and isolation

5.3.1. Syntheses of 2, 4, 6-trihydroxyphenyl ketones and stability testing

A series of 13 trihydroxyphenyl ketones were prepared by Friedel-Crafts acylation. Their yields ranged widely from 1-83%. Subsequent exhaustive methylation furnished the corresponding acetyl- β -triketones in poor to good yields of approx. 1-54%. In both reaction steps, material losses were caused mainly by extensive purification needs. The purities and identities of the synthesized compounds were confirmed by a range of analytical techniques.

A total of 8 photolysis tests were conducted to determine the photostability of selected acetyl- β -triketones towards UV-B light. Preliminary testing with flavesone in Pyrex and Quartz tubes revealed complete stability for 2-3 hours of irradiation. Likewise, follow-up trials conducted in NMR-tubes for rapid monitoring with three additional derivatives showed no changes. It was proposed that photo-keto-enol tautomerization protected the acetyl- β -triketones from Norrish-type reactions. Irradiation of flavesone with visible light irradiation for 10 hours and upon oxygen-purging also showed resistance to photooxidation.

Future studies should further optimize the reaction parameters of the two-step synthesis and should investigate alternative purification methods. Additional photostability testing may involve acetyl- β -triketones with extended side-chains or more drastic irradiation conditions. Photooxidation tests should also investigate simulated solar radiation.

5.3.2. Distillation of Myrtaceae species and chemical profiling

Leaves from six plant species were collected, distilled and the chemical profiles of their essential oils established. GC-analyses proved effective to successfully assign many of the constituents. *X. verticillatus* offered the highest oil yield of 0.58% and largely contains 1, 3-dimethoxy-5-isopropylbenzene (**70**) with 94%. This was followed by *E. cloeziana* with a yield of 0.38% and tasmanone (**67**) as its main constituent in 89%. *X. umbrosus* offered 0.19% oil yield and comprised of 64% of cyclocolorenone (**69**). The hybrid of *X. chrysanthus* and *X. verticillatus* produced only 0.05% of oil, which comprised primarily of 1, 3-dimethoxy-5-

isopropylbenzene (**70**), isoleptospermone (**55**) and β -cadinene (**71**) in quantities of 18%, 13% and 10%, respectively. The results obtained for *X. chrysanthus* varied somewhat with location. While oil yields were comparable with 0.03% and 0.02%, *X. chrysanthus* oil from the Tolga region contained 85% of isotorquatone (**68**), while the extract from the Townsville area gave 22% of isotorquatone (**68**) as main identified component.

Travel restrictions during the Covid pandemic severely limited the collection of plant material in the wider Queensland area. Future studies should thus expand the range of collected Myrtaceae biomass and should include sampling of the same species at different locations to investigate regional changes to their chemical profiles.

5.3.3. Isolation and characterization of selected constituents

A simple acid-base extraction process was used to isolate the acetyl- β -triketones from *E. cloeziana* and commercial *L. scoparium* (Manuka) oil. Following this approach, tasmanone was successfully extracted in 100% purity. NMR-analysis revealed two major tautomeric forms. Extracts from the Manuka oil were further purified by bulb-to-bulb distillation and afforded two fractions containing pure mixtures of flavesone (**54**), isoleptospermone (**55**) and leptospermone (**58**).

Cyclocolorone (**69**) was isolated from *X. umbrosus* oil by flash chromatography in a yield of 42%. Its structural identity was confirmed by 1D- and 2D-NMR techniques and by comparison with simulated spectra. 1, 3-Dimethoxy-5-isopropylbenzene (**70**) was confirmed as the almost sole constituent of *X. verticillatus* oil in approx. 94%. Its structure was confirmed by advanced NMR-analysis.

The distilled oils of the *X. chrysanthus*, *X. umbrosus*, *X. chrysanthus/X. verticillatus* hybrid and *L. scoparium* sourced manuka oils were further assessed by exhaustive GC-analyses to identify other minor constituents. This was successfully accomplished by comparison of experimental KI-values with those reported in the NIST or Wiley database. This further assessment was conducted eight months after the initial distillations of the respective Xanthostemon oils and may have thus caused some variations in the constituents. *X. chrysanthus 1* reported 14 compounds, which farnesoic acid (**199**) and isoleptospermone (**55**) as its main constituents in 35% and 21%, respectively. In contrast, *X. chrysanthus 2* gave 13 compounds with the main components being farnesoic acid (**199**) in 28% and 5-hexenoic acid (**203**) in 26%. *X. umbrosus* revealed 21 compounds and consisted mainly of aristolone (**190**) and farnesoic acid (**178**) with 35% and 11%, respectively. The Xanthostemon hybrid species registered a total of 27

compounds. While three of its major components could not be identified, the presence of isoleptospermone (**58**) in 13% was confirmed. *X. verticillatus* contained only 6 compounds and 1, 3-dimethoxy-5-isopropylbenzene (**70**) was the major compound in 95.5%. *E. cloeziana*, was found to contain 24 compounds, of which all were in <1.1% composition. Tasmanone (**67**) was the dominant constituent with 93.6% composition. The untreated Manuka oil (MOr) registered 47 compounds, of which *cis*-calamene (**71**, 22.7%), leptospermone (**58**, 22.4%) and isoleptospermone (**55**, 5.3%) were the known major constituents.

The organic fraction obtained from the acid-base extraction of Manuka oil (MO-1) confirmed low to no presence of any acetyl- β -triketone. It instead showed 27 compounds with *cis*-calamene (**71**) as the major constituent in 18%. In contrast, the acidic fraction of Manuka oil (MO-2) was confirmed rich in the desired acetyl- β -triketones. Although 18 compounds were detected, the by far major components were leptospermone (**58**, 64%), flavesone (**54**, 16%) and isoleptospermone (**55**, 8%).

Acid-base extractions of the oils and analyses of the neutral and acidic fractions should be further explored for all plant species containing acetyl- β -triketones. Additional analyses should be also conducted to identify more of the so far unknown compounds, in particular in the *Xanthostemon* hybrid species. Isolation of individual compounds by preparative HPLC may further reveal the identity of some of the main components.

5.3.4. Bioactivity screening

Preliminary antimicrobial screening using selected synthetic samples and natural extracts was carried out against three pathogenic indicator organisms: the gram-positive *S. epidermidis*, the gram-negative *E. choli* and the fungi *C. albicans*. The trihydroxyphenyl ketone analogues were the most active agents against *S. epidermidis* with high inhibition rates of 97%, followed by the synthetic acetyl- β -triketone with reasonable inhibitions of approx. 85%. The acid-fraction of Manuka oil (MO-2) showed a similar inhibition strength at 81%, while the *X. chrysanthus*/*X. verticillatus* hybrid and the untreated Manuka oil (MOr) showed moderate activities of 41% and 31%, respectively. In contrast, the acetyl- β -triketone **57** and the chosen trihydroxyphenyl ketone **44** exhibited low activities with 27% and 22%, respectively. A low inhibition against *E. coli* was only exhibited by two of the trihydroxyphenyl ketone analogues, while all other materials tested registered growth inhibition below 10%. In contrast, *C. albicans* was resistant to all tested with 0-5% growth inhibition.

Larvacidal activity against *A. aegypti* was strongly exhibited by most of the samples tested. All synthetic acetyl- β -triketones and the acetic acetyl- β -triketone rich Manuka oil fraction (MO-2) showed 100% mortality. The oils extracted from *X. chrysanthus* (sample 1), *X. umbrosus* and *X. verticillatus* also expressed 100% mortality, while *E. cloeziana* and *X. chrysanthus/X. verticillatus* hybrid oils showed 98% and 96% mortality respectively. Untreated, commercial Manuka oil (MOr), which contained 24% of acetyl- β -triketones, registered 81% mortality, while its neutral fraction expressed 44% mortality. The chosen trihydroxyphenyl ketones were the least active compounds showing 0-4% mortality.

Adulticidal tests on *A. aegypti* for 60 minutes showed that the dose of the untreated Manuka oil (MOr) related directly to the %-KD. Of the concentration range tested, the 6 ppm dose reached 100% KD within 6 minutes, while the 9 ppm dose already expressed 100% KD after 3 minutes. Exposure tests for 24 hours showed the same trend. While low concentrations of 1-3 ppm expressed <5% mortality rates, the 6 ppm and 9 ppm doses exhibited 81% and 100% mortality.

Manuka oil and its easily extracted acetyl- β -triketone rich fraction represent highly active insecticides for the control of *A. aegypti* mosquitos. Testing should thus be extended to other mosquito and blood-sucking insects. A commercial application of Manuka oil or its acidic fraction should likewise be explored.

CHAPTER 6:

EXPERIMENTAL PART

6. Experimental Part

6.1. General methods

6.1.1. Analytical methods

6.1.1.1. Nuclear magnetic resonance spectroscopy

NMR spectra were recorded on a Bruker 400 Ascend™ (¹H: 400 MHz and ¹³C: 100 MHz) equipped with an auto-sampler. Generated data were secured through TopSpin 2.1 and 3.0. NMR spectra and processed using the MestReNova v5.3.2-4936 software. Calibrations were performed with TMS ($\delta = 0$ ppm) or the residual solvent peak as internal standard.

In a clean NMR tube, solid (10-30 mg) or liquid (10-30 μ L) samples were dissolved in approximately 0.6-0.8 ml of deuterated chloroform or deuterated acetone. The sample solution was mixed on a vortexer or in an ultrasonic bath until a homogenous solution was obtained.

6.1.1.2. Mass spectrometry

Mass spectra were obtained on a Shimadzu LCMS-2020 equipped with a DUIS ion source. Samples were directly injected, and the ions generated were detected in either the positive, negative mode or both (mass range: 100-500 m/z). The mobile phase was an aqueous solution of 0.1% formic acid in HPLC grade methanol. Experimentation and data processing were done using the LabSolutions for LCMS-2020 software.

In a clean volumetric flask, 1 mgL⁻¹ sample solutions were prepared by dissolving 10 mg of sample in 10 ml of methanol (HPLC grade). Into a clean amber HPLC vial, approximately 2 ml of the test solution were added, and the vial was capped and vortexed prior to analysis.

6.1.1.3. Infrared spectroscopy

Infrared analysis was conducted on an IR-ATR iD5 (Thermo Scientific) spectrometer. Signals were scanned within 500-4000 cm⁻¹ range with IR peaks given in wavenumbers (cm⁻¹).

Sufficient amounts of solid or liquid sample material were applied to cover the ATR crystal slide.

6.1.1.4. UV-VIS spectrophotometry

Measurements were recorded on a Cary 60 UV-Vis Spectrometer (Agilent Technologies). Signals were scanned within 200-800 nm range. Spectra and λ_{max} of characteristic peaks were processed using the CaryWin UV60 software (Varian).

Sample solutions with concentrations of approx. 10^{-3} - 10^{-4} M in absolute EtOH were prepared in 20 ml volumetric flasks. Aliquots were transferred to 10 mm quartz cuvettes for analysis.

6.1.1.5. Gas chromatography

GC-FID analyses were conducted using a 7890A GC System by Agilent Technologies. Data acquisition was achieved with GC-OpenLab, Version 2.7.

6.1.1.6. High performance liquid chromatography

HPLC analyses were performed on a LC20A (Shimadzu) system with a mobile phase of 0.01% formic acid in MeOH. An AC10 SuperC18 preparative column with dimensions 150 mm \times 12.2 mm ($\text{I}\text{\O}$) was used for separation. Samples were introduced via manual injection and subsequent fractions were auto-collected. The LabSolutions for LCMS-2020 software was used for data acquisition and analysis.

6.1.1.7. Thermogravimetric analysis

A TGA/DSC system model SDT 600 TA, Discovery series was used. Analysis was programmed to ramp at $10^{\circ}\text{C}/\text{min}$ from 0 - 600°C with a N_2 -flow at ~ 50 ml/min. Subsequent TGS (weight vs T) and DSC (T vs heat/enthalpy) data acquisition was conducted with the TRIOS.Inc TA software.

Approximately 3-5 mg samples were transferred to demostured ceramic micro-crucibles and loaded into the oven for thermogravimetric scanning.

6.1.2. Purification methods

6.1.2.1. Thin-layer chromatography

TLC chromatography was performed on 20 cm \times 20 cm \times 0.2 mm plastic sheets coated with silica gel 60 F₂₅₄ (0.2 mm thickness; Merck, Germany). Mixtures of EtOAc and n-hexane were most commonly used as mobile phases. Visualization was achieved by UV-analysis or by dipping into a potassium permanganate solution.

6.1.2.2. Column chromatography

Column chromatographic separations were conducted in glass columns using silica gel 60 (0.04-0.06 mm; Scharlau, Spain) as stationary phase. Mixtures of EtOAc and n-hexane were used as mobile phases for elution.

6.1.2.3. Flash Column chromatography

Flash chromatography was performed using the CombiFlash Lumen (Teledyn ISCO) instrument with an adjustable 32-65 g or 15-25 g solid load cartridge. The cartridges were packed with 50-60 g or 15-21 g of silica gel 60 depending on their sizes. The sample, absorbed on a small amount of silica gel, that added on top of the filled cartridge. Elution were carried out using gradients of EtOAc in n-hexane at a flow rate of 35 ml.min⁻¹. Peaks were detected by UV-Vis analysis at 254 nm and 280 nm, respectively, or evaporative light scattering (ELS) at 30°C. Active fractions were auto collected.

6.2. Synthesis of hydroxyfuranone and its alkoxy-derivatives

6.2.1. Reagents and solvents

Most solvents and reagents were purchased from commercial suppliers and were used without further purification. Furfural was purified by fractional distillation before use. The main reagents and materials used are listed in **Table 6.1**.

Table 6.1: List of reagents and solvents

Name	Purity	Grade	Producer	Country
Rose Bengal sodium salt	-	-	Alfa Aesar	Great Britain
Ethanol	96%	AR	Ajax Finechem	Australia
Ethanol (absolute)	99.9%	AR	Ajax Finechem	Australia
Deuterated chloroform	99.8% atom D	-	Sigma Aldrich	-
Chloroform	99.98%	AR	Fisher Chemicals	UK
Dichloromethane	99.5%	AR	Ajax Finechem	Australia
<i>para</i> -Toluene sulphonic acid monohydrate	≥98%	-	Sigma Aldrich	Japan
Pyridine	99.5%	HPLC	Fisher Chemical	USA
Acetone	99.5%	AR	Chem-Supply	Australia
Tetrahydrofuran	99.9%	HPLC	Fisher Chemicals	USA
Magnesium sulphate (dried)	70%	LR	Ajax Finechem	Australia
Sodium chloride	≥99.5%	-	Sigma Aldrich	USA
Sodium hydrogen carbonate	99.7%	AR	Ajax Finechem	Australia

6.2.2. Photochemical and solar reactors

6.2.2.1. Rayonet chamber reactor

Small-scale batch reactions were conducted in a Rayonet RPR-200 photochemical chamber reactor (Southern New England Ultraviolet Company, USA) equipped with 16 × 8 W fluorescent tubes. Reactions were carried out in Pyrex Schlenk vessels of approx. 100 ml, 200 ml and 300 ml capacity, and equipped with a Pyrex cold finger.

6.2.2.2. Immersion well Reactor

Larger-scale irradiations were conducted in an immersion well reactor from an unknown manufacturer. The reactor had a capacity of 250 ml and was made from Pyrex glass. A 150 W medium-pressure mercury lamp was inserted into the reactor.

6.2.3. Flatbed reactor and illumination procedure

Solar illuminations were performed in a custom-made flatbed reactor by Wexford Viking Glass Ltd in Ireland. A typical experimental procedure is described below.

A 500 ml flask was filled with 250 g (156.15 ml, 2.60 mol) of distilled furfural and 100 ml of absolute ethanol. To the solution, 5.3 g of rose Bengal were added in portions upon occasional shaking until a homogeneous solution was obtained. Cooling water to the external condenser of the flatbed was turned on. Then about 7.8 L of absolute ethanol were filled into the reactor through the top opening and the reactor was covered with black cloth. The furfural-rose Bengal stock solution was subsequently added through the top opening. The air pump was switched on and the solution was thoroughly mixed by air purging. The circulation pump was switched on and the black cloth was removed from the aperture. At the end of the illumination, the reaction mixture and additional ca. 250 ml of wash Ethanol were emptied into three 2.5 L Winchester bottles. Approximately 300 ml portions of the crude reaction mixture were successively evaporated on a Büchi rotavapor R-300 at $<30^{\circ}\text{C}$ and ≤ 100 mbar. The crude concentrates were combined and dissolved in dichloromethane. To this solution, liquid nitrogen was added in small portions until crystals started to form. Alternatively, crystallization was facilitated by seeding with small amounts of pure hydroxyfuranone crystals followed by 12 hours refrigeration. The crystals were collected by filtration on a Büchner funnel.

6.2.3.1. Specific GC-conditions

GC-FID analyses were performed using the conditions described in the table on the next page.

Column:	HP-17 (Agilent-J&W, 19095L-121, 10 m × 0.53 mm × 2 μm)
Detection:	Flame Ionization (FID), 300°C oven temperature
Program:	50°C hold for 2 min, 35°C/min ramp to 80°C and hold for 1 min, ramp at 30°C/min to 220°C and hold for 2 min. Total run time: 10.52 min
Carrier Gas:	He at 57.96 cm/sec
Injection:	1.0 μL, split 20:1, 250°C inlet temperature

Calibration curve and response factor (R_f) determinations were performed using butan-1-ol (>99%) as an internal standard. A stock solution of 0.0928 M was prepared by transferring 1 ml of butan-1-ol (0.81 g, 0.0109 mol) to a 10 ml volumetric flask containing 9 ml of absolute ethanol. Aliquots of the stock solution were transferred to five 2 ml amber GC-vials and diluted with subsequent amounts of ethanol to give five different standard solutions (**Table 6.2**). MS Excel (2010) was used to develop a regression model for the plot of concentration against peak area. The R^2 value and the equation of the plot were derived from the line of best fit. The R_f value was determined firstly from the slope of the line of best fit and secondly calculated as the mean from individual R_f obtained from each standard solution.

Table 6.2: Parameters of calibration standards.

Standard	Aliquot (μL)	Solvent (μL)	Dilution factor	[1-BuOH] (M)
1	200	1400	0.1250	0.1366
2	400	1200	0.2500	0.2732
3	600	1000	0.3750	0.4098
4	800	8000	0.4375	0.4781
5	1000	600	0.5000	0.5464

6.3. Sustainable synthesis of *para*- menthane-3, 8-diol

6.3.1. Reagents and solvents

Most solvents and reagents were purchased from commercial suppliers and were used without further purification. The main reagents and materials used are listed in **Table 6.3** below.

Table 6.3: List of reagents and solvents

Name	Purity	Grade	Producer	Country
Anhydrous Diethyl ether	99.5%	AR	Ajax Finechem	Australia
Sodium chloride	≥99.5%	AR	Sigma Aldrich	USA
Sodium sulphate granular (anhydrous)	99.0%	AR	ChemSupply	Australia
Citronellal	>96%	SR	Alfa Aesar	England
(-)-Isopulegol	>99%	SR	Sigma Aldrich	Japan
(+/-)-Citronellol	>95%	SR	Sigma Aldrich	USA
Lemon-scented gum oil	NA	GP	Essential AUS	Australia
Lemon-scented gum oil	NA	GP	Rear Earths Oil	Australia

Chapter 6 – Experimental

Lemon-scented gum oil	NA	GP	Heritage Oils	Australia
Lemon-scented gum oil	NA	GP	Unknown	China
Lemon-scented gum oil	NA	GP	Distillerie de Boulouparis	New Caledonia
Lemon-scented gum oil	NA	GP	JCU	Australia
Citric acid monohydrate	≥99.5%	AR	ChemSupply	Australia
Heptane	99.0%	AP	Sigma Aldrich	South Korea
Deuterated chloroform	99.8%	AR	Cambridge Isotope Lab	USA
<i>cis</i> -PMD ^a	98%	GP	JCU (in house)	Australia
<i>trans</i> -PMD ^a	95%	GP	JCU (in house)	Australia
Dichloromethane	99.8%	AR	Ajax Finechem	Australia
Sulfuric acid	98%	AR	Ajax Finechem	Australia
Sand	NA	NA	Ajax Finechem	Australia
Potassium permanganate	99.0%	LR	ChemSupply	Australia

SR: standard reagent; GP: general purpose; NA: not applicable; ^a: used for seeding; LA: laboratory reagent.

6.3.1.1. Specific GC-conditions

GC-FID analyses were performed using the following conditions for the three methods M1-M3 developed.

Column:	Zebtron™ ZB-5 (7HG-G002-11, Phenomenex Inc), 30 m × 0.25 mm × 0.25 μm
Detection:	Flame Ionization (FID), 340°C (M1) and 290°C (M2 and M3) oven temperature
Programs:	M1: 50°C hold for 1 min, 15°C/min ramp to 155°C and hold for 5 min, ramp at 1°C/min to 160°C, ramp again at 15°C/min to 240°C and hold for 5 minutes. Total run time: 27.33 min. M2: 70°C hold for 2 min, 3°C/min ramp to 112°C, ramp at 1°C/min to 120°C, ramp again at 8°C/min to 166°C and finally ramp at 20°C/min to 240°C. Total run time: 34.45 min. M3: 70°C hold for 2 min, 3°C/min ramp to 112°C, ramp at 1°C/min to 120°C, ramp again at 8°C/min to 166°C and finally ramp at 20°C/min to 270°C. Total run time: 43.95 min.
Carrier Gas:	He at 40.01 cm/sec (M1), 19.5 cm/sec (M2) and 19.6 cm/sec (M3)
Injections:	1.0 μL, split 20:1 (M1) and 50:1 (M2 and M3), 250°C (M1) and 280°C (M2 and M3) inlet temperature

6.4. β-Triketone syntheses and isolation

6.4.1. Reagents and solvents

Most solvents and reagents were purchased from commercial suppliers and were used without further purification. The main reagents and materials used are listed in **Table 6.4** below.

Table 6.4: List of reagents and solvents

Name	Purity	Grade	Producer	Country
Nitrobenzene	99%	RP	Sigma Aldrich	Portugal
Phloroglucinol	>99%	HPLC	Sigma Aldrich	China
Aluminium trichloride	98%	R	Sigma Aldrich	Germany
Ethyl acetate	99.5%	AR	Ajax Finechem	Australia
Sodium sulphate granular (anhydrous)	99.0%	AR	ChemSupply	Australia

Chapter 6 – Experimental

<i>n</i> -Hexane	95%	AR	Ajax Finechem	Australia
Potassium permanganate	99.0%	LR	ChemSupply	Australia
Isobutyryl chloride	98%	R	Sigma Aldrich	China
2-Methylbutyryl chloride	98%	R	Sigma Aldrich	China
Benzoyl chloride	>99%	RP	Sigma Aldrich	Germany
Propionyl chloride	98%	R	Sigma Aldrich	USA
Isovaleryl chloride	98%	R	Sigma Aldrich	Switzerland
Valeroyl chloride	98%	R	Sigma Aldrich	Switzerland
Butyryl chloride	98%	R	Sigma Aldrich	Switzerland
Hexanoyl chloride	97%	R	Sigma Aldrich	Japan
Nonanoyl chloride	96%	R	Sigma Aldrich	USA
Octanoyl chloride	99%	R	Sigma Aldrich	Germany
Heptanoyl chloride	99%	R	Sigma Aldrich	USA
Acetyl chloride	99%	R	Sigma Aldrich	USA
Cyclohexanecarbonyl chloride	98%	RP	Sigma Aldrich	China
Trimethylacetyl chloride	99%	R	Sigma Aldrich	Switzerland
Hydrocinnamoyl chloride	98%	R	Sigma Aldrich	France
Sodium methoxide	25%	AR	Sigma Aldrich	USA
Iodide	>99%	AR	Sigma Aldrich	USA
Hydrochloric acid	99%	AR	Ajax Finechem	Australia
Methanol (absolute)	99.5%	HPLC	Ajax Finechem	Australia
Diethyl ether (anhydrous)	99.5%	AR	Ajax Finechem	Australia
Sodium carbonate	99%	AR	ChemSupply	Australia
Sodium chloride	≥99.5%	AR	Sigma Aldrich	USA

RP: reagent plus, HPLC: HPLC grade. R: reagent grade, AR: analytical grade. LR: laboratory reagent.

6.4.1.1. Specific GC-conditions

GC-FID analyses were performed using the following conditions.

Column:	DB-5ms Ultra Inert, 122-5532UI (Agilent), 30 m × 0.25 mm × 0.25 μm
Detection:	Flame Ionization (FID), 280°C oven temperature
Program:	40°C hold for 1 min, 6°C/min ramp to 250°C and hold for 4 min. Total run time: 40 min.
Carrier Gas:	He at 42.99 cm/sec
Injection:	1.0 μL, split 50:1, 250°C inlet temperature

REFERENCES

References

1. Koseki, K., Ebata, T., Kawakami, H., Matsushita, H., Naoi, Y., and Itoh, K. (1990). A Method for Easy Preparation of Optically Pure (S)-5-Hydroxy-2-penten-4-olide and (S)-5-Hydroxypentan-4-olide. *HETEROCYCLES* *31*, 423. 10.3987/COM-89-5300.
2. Khayyat, S.A., and Roselin, L.S. (2018). Recent progress in photochemical reaction on main components of some essential oils. *Journal of Saudi Chemical Society*.
3. Koseki, K., Ebata, T., Kawakami, H., Matsushita, H., Naoi, Y., and Itoh, K. (1990). ChemInform Abstract: A Method for Easy Preparation of Optically Pure (S)-5-Hydroxy-2-penten-4-olide and (S)-5-Hydroxypentan-4-olide. *ChemInform* *21*. 10.1002/chin.199040170.
4. Mumtaz, S., Sattler, C., and Oelgemöller, M. (2015). Solar Photochemical Manufacturing of Fine Chemicals: Historical Background, Modern Solar Technologies, Recent Applications and Future Challenges. In.
5. Burguete, M.I., Gavara, R., Galindo, F., and Luis, S.V. (2010). Synthetic application of photoactive porous monolithic polymers. *Tetrahedron Letters* *51*, 3360-3363. 10.1016/j.tetlet.2010.04.065.
6. Bano, U., Khan, A.F., Mujeeb, F., Maurya, N., Tabassum, H., Siddiqui, M.H., Haneef, M., Osama, K., and Farooqui, A. (2016). Effect of plant growth regulators on essential oil yield in aromatic plants. *Journal of Chemical and Pharmaceutical Research* *8*, 733-739.
7. Kumar, P., and Pandey, R.K. (2000). An efficient synthesis of 5-hydroxy-2(5H)-furanone using a titanium silicate molecular sieve catalyst. *Green Chemistry* *2*, 29-32. 10.1039/A907690E.
8. Smith, R.B., Bennett, J.E., Rantakokko, P., Martinez, D., Nieuwenhuijsen, M.J., and Toledano, M.B. (2015). The Relationship between MX [3-Chloro-4-(dichloromethyl)-5-hydroxy-2(5H)-furanone], Routinely Monitored Trihalomethanes, and Other Characteristics in Drinking Water in a Long-Term Survey. *Environmental Science & Technology* *49*, 6485-6493. 10.1021/es5062006.
9. Glaser, K.B., de Carvalho, M.S., Jacobs, R.S., Kernan, M.R., and Faulkner, D.J. (1989). Manoalide: structure-activity studies and definition of the pharmacophore for phospholipase A2 inactivation. *Mol Pharmacol* *36*, 782-788.
10. Pour, P.M., Behzad, S., Asgari, S., Khankandi, H.P., and Farzaei, M.H. (2020). Chapter 10 - Sesterterpenoids. In *Recent Advances in Natural Products Analysis*, A. Sanches

References

- Silva, S.F. Nabavi, M. Saedi, and S.M. Nabavi, eds. (Elsevier), pp. 347-391. 10.1016/B978-0-12-816455-6.00010-X.
11. Patt, W.C., Edmunds, J.J., Repine, J.T., Berryman, K.A., Reisdorph, B.R., Lee, C., Plummer, M.S., Shahripour, A., Haleen, S.J., Keiser, J.A., et al. (1997). Structure–Activity Relationships in a Series of Orally Active γ -Hydroxy Butenolide Endothelin Antagonists. *Journal of Medicinal Chemistry* *40*, 1063-1074. 10.1021/jm9606507.
 12. Lattmann, E., Coombs, J., and Hoffmann, H. (2010). ChemInform Abstract: Pyranofuranones via Lewis Acid Mediated Hetero-Diels-Alder Reactions of 4Furan2(5H)-ones: A Convergent Route to the Manoalide Substructure. *Cheminform* *27*. 10.1002/chin.199625318.
 13. Tokoroyama, T., Matsuo, K., Kotsuki, H., and Kanazawa, R. (1980). Synthetic studies on terpenic compounds—XI: Stereospecific total synthesis of portulal11Preliminary communications, aT. Tokoroyama, K. Matsuo, R. Kanazawa, H. Kotsuki and T. Kubota, *Tetrahedron Letters* 3093 (1974); bR. Kanazawa, H. Kotsuki and T. Tokoroyama, *Ibid.* 3651 (1975).,22Part VI, ref. 4; Part VII, ref. 35; Part VIII, ref. 33; Part IX, H. Koike and T. Tokoroyama, *Tetrahedron Letters* 4531 (1978); Part X, H. Koike and T. Tokoroyama, *Chemistry Letters* 333 (1979). *Tetrahedron* *36*, 3377-3390. 10.1016/0040-4020(80)80188-8.
 14. Brooks, D.W., Bevinakatti, H.S., Kennedy, E., and Hathaway, J. (1985). Practical total synthesis of (+-)-strigol. *The Journal of Organic Chemistry* *50*, 628-632. 10.1021/jo00205a014.
 15. BRASLAVSKY, E.S. (2007). Glossary of terms used in photochemistry, 3rd edition (IUPAC Recommendations 2006). *Chemistry International* *29*, 26.
 16. Hoffmann, N. (2008). Photochemical Reactions as Key Steps in Organic Synthesis. *Chemical Reviews* *108*, 1052-1103. 10.1021/cr0680336.
 17. Bochet, C.G. (2004). Chromatic Orthogonality in Organic Synthesis. *Synlett* *2004*, 2268-2274. 10.1055/s-2004-832848.
 18. Rohatgi-Mukherjee, K.K. (1978). *Fundamentals of photochemistry* (Wiley).
 19. Schuster, D.I. (1992). *Photochemical technology*. Von A. M. Braun, M.-T. Maurette und E. Oliveros. Wiley, Chichester, 1991. XII, 559 S., geb. £95.00.-ISBN 0-471-92652-3. *Angewandte Chemie* *104*, 1563-1564. 10.1002/ange.19921041147.
 20. Hammond, G.S., and Turro, N.J. (1963). *Organic Photochemistry*. *Science* *142*, 1541.

References

21. Giraud, R.J., Williams, P.A., Sehgal, A., Ponnusamy, E., Phillips, A.K., and Manley, J.B. (2014). Implementing Green Chemistry in Chemical Manufacturing: A Survey Report. *ACS Sustainable Chemistry & Engineering* 2, 2237-2242. 10.1021/sc500427d.
22. Lichtman, J., and Conchello, J. (2006). Fluorescence Microscopy. *Nature methods* 2, 910-919. 10.1038/nmeth817.
23. Khayyat, S.A., and Roselin, L.S. (2018). Recent progress in photochemical reaction on main components of some essential oils. *Journal of Saudi Chemical Society* 22, 855-875. 10.1016/j.jscs.2018.01.008.
24. Mayerhöfer, T., and Popp, J. (2018). Beer's Law-Why Absorbance Depends (Almost) Linearly on Concentration. *ChemPhysChem* 20. 10.1002/cphc.201801073.
25. Fox, J.J., Van Praag, D., Wempen, I., Doerr, I.L., Cheong, L., Knoll, J.E., Eidinoff, M.L., Bendich, A., and Brown, G.B. (1959). Thiation of Nucleosides. II. Synthesis of 5-Methyl-2'-deoxycytidine and Related Pyrimidine Nucleosides¹. *Journal of the American Chemical Society* 81, 178-187.
26. Moradei, O.M., and Paquette, L.A. (2003). (5 S)-(d-Menthyloxy)-2 (5 H)-Furanone: (2 (5 H)-Furanone, 5 [[(1 S, 2 R, 5 S)-5-Methyl-2-(1-Methylethyl) cyclohexyl] oxy]-, (5 S)-. *Organic syntheses* 80, 66-74.
27. Morita, Y., Tokuyama, H., and Fukuyama, T. (2005). Stereocontrolled Total Synthesis of (-)-Kainic Acid. Regio- and Stereoselective Lithiation of Pyrrolidine Ring with the (+)-Sparteine Surrogate. *Organic Letters* 7, 4337-4340. 10.1021/ol051408+.
28. Carney, J.M., Hammer, R.J., Hulce, M., Lomas, C.M., and Miyashiro, D. (2012). Microphotochemistry using 5-mm light-emitting diodes: Energy-efficient photooxidations. *Synthesis (Germany)* 44, 2560-2566. 10.1055/s-0031-1289764.
29. Rodenas, Y., Mariscal, R., Fierro, J.L.G., Martín Alonso, D., Dumesic, J.A., and López Granados, M. (2018). Improving the production of maleic acid from biomass: TS-1 catalysed aqueous phase oxidation of furfural in the presence of γ -valerolactone. *Green Chemistry* 20, 2845-2856. 10.1039/c8gc00857d.
30. Annangudi, S.P., Sun, M., and Salomon, R.G. (2005). An Efficient Synthesis of 4-Oxoalkenoic Acid from 2-Alkylfurans. *ChemInform* 36. 10.1002/chin.200541060.
31. Chavan, S.P., and Kadam, A.L. (2021). Practical synthesis of 5-hydroxy-2(5H)-furanone from furan. *Results in Chemistry*.
32. Poskonin, V.V., and Badovskaya, L.A. (1998). Catalytic oxidation of furan and hydrofuran compounds. *Chemistry of Heterocyclic Compounds* 34, 646-650. 10.1007/BF02252269.

References

33. Murzin, D., Bertrand, E., Tolvanen, P., Devyatkov, S., Rahkila, J., Eränen, K., Wärnå, J., and Salmi, T. (2020). Heterogeneous Catalytic Oxidation of Furfural with Hydrogen Peroxide over Sulfated Zirconia. *Industrial & Engineering Chemistry Research XXXX*. 10.1021/acs.iecr.0c02566.
34. Wu, H., Song, J., Liu, H., Xie, Z., Xie, C., Hu, Y., Huang, X., Hua, M., and Han, B. (2019). An electrocatalytic route for transformation of biomass-derived furfural into 5-hydroxy-2(5H)-furanone. *Chem Sci 10*, 4692-4698. 10.1039/c9sc00322c.
35. Yuste, F., and Sanchez-Obregon, R. (1982). 4-Hydroxy-2-butenolide. A versatile reagent for the synthesis of heterocyclic compounds. *The Journal of Organic Chemistry 47*, 3665-3668. 10.1021/jo00140a015.
36. Doerr, I.L., and Willette, R.E. (1973). .alpha.,.beta.-Unsaturated lactones. I. Condensation of 5-bromo-2(5H)-furanones with adenine and uracil derivatives. *The Journal of Organic Chemistry 38*, 3878-3887. 10.1021/jo00962a014.
37. Wang, Y., and Chen, Q. (1999). Synthesis of novel chiral compounds of purine and pyrimidine bases. *Science in China Series B: Chemistry 42*, 121-130. 10.1007/BF02875507.
38. Moradei, O.M., and Paquette, L.A. (2003). (5S)-(d-Menthyloxy)-2(5H)-Furanone: (2(5H)-Furanone, 5[[[(1S,2R,5S)-5-Methyl-2-(1-Methylethyl)cyclohexyl]oxy]-, (5S)-). In *Organic Syntheses*, W. John, and I. Sons, eds. (John Wiley & Sons, Inc.), pp. 66-74.
39. Trost, B.M., and Toste, F.D. (2003). Palladium Catalyzed Kinetic and Dynamic Kinetic Asymmetric Transformations of γ -Acyloxybutenolides. Enantioselective Total Synthesis of (+)-Aflatoxin B1 and B2a. *Journal of the American Chemical Society 125*, 3090-3100. 10.1021/ja020988s.
40. Marinković, S., Brulé, C., Hoffmann, N., Prost, E., Nuzillard, J.-M., and Bulach, V. (2004). Origin of Chiral Induction in Radical Reactions with the Diastereoisomers (5R)- and (5S)-5-l-Menthyloxyfuran-2[5H]-one. *The Journal of Organic Chemistry 69*, 1646-1651. 10.1021/jo030292x.
41. Yan, Z., Wei, W., Xun, H., and Anguo, S. (2012). Rose Bengal Immobilized on Wool as an Efficiently “Green” Sensitizer for Photooxygenation Reactions. *Chemistry Letters 41*, 1500-1502. 10.1246/cl.2012.1500.
42. Linthorst, J.A. (2010). An overview: origins and development of green chemistry. *Foundations of Chemistry 12*, 55-68. 10.1007/s10698-009-9079-4.
43. Paul, L. (1956). *The Columbia Encyclopedia*. In L. Paul, ed. 6 ed. Columbia University Press.

References

44. Danon, B., Marcotullio, G., and de Jong, W. (2014). Mechanistic and kinetic aspects of pentose dehydration towards furfural in aqueous media employing homogeneous catalysis. *Green Chemistry* *16*, 39-54. 10.1039/C3GC41351A.
45. Fang, C., Wu, W., Li, H., Yang, T., Zhao, W., Wang, Z., and Yang, S. (2017). Production of bio-based furfural from xylose over a recyclable niobium phosphate (NbOPO₃) catalyst. *Energy Sources, Part A: Recovery, Utilization, and Environmental Effects* *39*, 2072-2077. 10.1080/15567036.2017.1402103.
46. Gebre, H., Fisha, K., Kindeya, T., and Gebremichal, T. (2015). Synthesis of Furfural from Bagasse. *International Letters of Chemistry, Physics and Astronomy* *57*, 72-84. 10.18052/ILCPA.57.72.
47. Council, A.S.M. (2022). Raw Sugar Industry Overview.
48. Australia, P.H. (2018). Sugar cane. <https://www.planthealthaustralia.com.au/industries/sugarcane/>.
49. Rezende, C.A., de Lima, M.A., Maziero, P., deAzevedo, E.R., Garcia, W., and Polikarpov, I. (2011). Chemical and morphological characterization of sugarcane bagasse submitted to a delignification process for enhanced enzymatic digestibility. *Biotechnology for Biofuels* *4*, 54. 10.1186/1754-6834-4-54.
50. Mariscal, R., Maireles-Torres, P., Ojeda, M., Sádaba, I., and López Granados, M. (2016). Furfural: a renewable and versatile platform molecule for the synthesis of chemicals and fuels. *Energy & Environmental Science* *9*, 1144-1189. 10.1039/C5EE02666K.
51. Holtzapple, M.T. (2003). Hemicellulose. In B. Caballero, ed. *Encyclopedia of Food Science and Nutrition*. 2 ed. Elsevier Science Ltd.
52. Mamman, A.S., Lee, J.-M., Kim, Y.-C., Hwang, I.T., Park, N.-J., Hwang, Y.K., Chang, J.-S., and Hwang, J.-S. (2008). Furfural: Hemicellulose/xylose-derived biochemical. *Biofuels, Bioproducts and Biorefining* *2*, 438-454. 10.1002/bbb.95.
53. Lange, J.-P., van der Heide, E., van Buijtenen, J., and Price, R. (2012). Furfural—A Promising Platform for Lignocellulosic Biofuels. *ChemSusChem* *5*, 150-166. 10.1002/cssc.201100648.
54. Gupta, K., Rai, R.K., Dwivedi, A.D., and Singh, S.K. (2017). Catalytic Aerial Oxidation of Biomass-Derived Furans to Furan Carboxylic Acids in Water over Bimetallic Nickel–Palladium Alloy Nanoparticles. *ChemCatChem* *9*, 2760-2767. /10.1002/cctc.201600942.
55. Li, X.-L., Deng, J., Shi, J., Pan, T., Yu, C.-G., Xu, H.-J., and Fu, Y. (2015). Selective conversion of furfural to cyclopentanone or cyclopentanol using different preparation methods of Cu–Co catalysts. *Green Chemistry* *17*, 1038-1046. 10.1039/C4GC01601G.

References

56. Li, H., Zhang, S., and Luo, H. (2004). A Ce-promoted Ni–B amorphous alloy catalyst (Ni–Ce–B) for liquid-phase furfural hydrogenation to furfural alcohol. *Materials Letters* *58*, 2741-2746. 10.1016/j.matlet.2004.04.003.
57. Motagamwala, A.H., Won, W., Maravelias, C.T., and Dumesic, J.A. (2016). An engineered solvent system for sugar production from lignocellulosic biomass using biomass derived γ -valerolactone. *Green Chemistry* *18*, 5756-5763. 10.1039/C6GC02297A.
58. Yan, B., Zang, H., Jiang, Y., Yu, S., and Chen, E.Y.X. (2016). Recyclable montmorillonite-supported thiazolium ionic liquids for high-yielding and solvent-free upgrading of furfural and 5-hydroxymethylfurfural to C10 and C12 furoins. *RSC Advances* *6*, 76707-76715. 10.1039/C6RA14594A.
59. Singh, E., Shankar, V.S.B., Tripathi, R., Pitsch, H., and Sarathy, S.M. (2018). 2-Methylfuran: A bio-derived octane booster for spark-ignition engines. *Fuel* *225*, 349-357. 10.1016/j.fuel.2018.03.169.
60. An, S., Song, D., Lu, B., Yang, X., and Guo, Y.-H. (2015). Morphology Tailoring of Sulfonic Acid Functionalized Organosilica Nanohybrids for the Synthesis of Biomass-Derived Alkyl Levulinates. *Chemistry-A European Journal* *21*, 10786-10798. 10.1002/chem.201501219.
61. Gainsford, G., and Hinkley, S. (2013). Alkyl levulinates as 'green chemistry' precursors: Butane-1,4-diyl bis(4-oxopentanoate) and hexane-1,6-diyl bis(4-oxopentanoate). *Acta crystallographica. Section C, Crystal structure communications* *69*, 654-657. 10.1107/S0108270113011980.
62. Esser, P., Pohlmann, B., and Scharf, H.-D. (1994). The Photochemical Synthesis of Fine Chemicals with Sunlight. *Angewandte Chemie International Edition in English* *33*, 2009-2023. 10.1002/anie.199420091.
63. Settle, A.E., Berstis, L., Rorrer, N.A., Roman-Leshkóv, Y., Beckham, G.T., Richards, R.M., and Vardon, D.R. (2017). Heterogeneous Diels–Alder catalysis for biomass-derived aromatic compounds. *Green Chemistry* *19*, 3468-3492. 10.1039/C7GC00992E.
64. Houk, K.N., Lin, Y.T., and Brown, F.K. (1986). Evidence for the concerted mechanism of the Diels-Alder reaction of butadiene with ethylene. *Journal of the American Chemical Society* *108*, 554-556. 10.1021/ja00263a059.
65. Doerr, I.L., and Willette, R.E. (1973). Alpha, beta-unsaturated lactones. I. Condensation of 5-bromo-2(5H)-furanones with adenine and uracil derivatives. *The Journal of organic chemistry* *38* 22, 3878-3887.

References

66. Yan, Z., Wei, W., Xun, H., and Anguo, S. (2012). Rose Bengal Immobilized on Wool as an Efficiently “Green” Sensitizer for Photooxygenation Reactions. *Chemistry Letters* *41*, 1500-1502.
67. Huang, H., and Chen, Q. (1999). A valuable synthetic route to spiro-cyclopropane derivatives containing multiple stereogenic centers. *Tetrahedron: Asymmetry* *10*, 1295-1307. 10.1016/S0957-4166(99)00123-8.
68. WANG, Y., and CHEN, Q. (1999). Synthesis of novel chiral compounds of purine and pyrimidine bases. *Science in China Series B-Chemistry* *42*, 121. 10.1360/yb1999-42-2-121.
69. Marinkovic, S., Brulé, C., Hoffmann, N., Elise, P., Nuzillard, J.-M., and Bulach, V. (2004). Origin of Chiral Induction in Radical Reactions with the Diastereoisomers (5R)- and (5S)-5-I-Menthyloxyfuran-2[5H]-one. *The Journal of organic chemistry* *69*, 1646-1651. 10.1021/jo030292x.
70. Faber, W.S., Kok, J., de Lange, B., and Feringa, B.L. (1994). Catalytic kinetic resolution of 5-alkoxy-2(5H)-furanones. *Tetrahedron* *50*, 4775-4794. 10.1016/S0040-4020(01)85016-X.
71. Victoria Martin, M., Farina, F., Rosario Martin, M., and Martinez de Guereñu, A. (1994). Cycloaddition of Nitrile Oxides to 4-Oxobut-2-enoic Acid Derivatives. *HETEROCYCLES* *38*, 1307. 10.3987/COM-94-6679.
72. Kernan, M.R., and Faulkner, D.J. (1988). Regioselective oxidation of 3-alkylfurans to 3-alkyl-4-hydroxybutenolides. *The Journal of Organic Chemistry* *53*, 2773-2776. 10.1021/jo00247a021.
73. Huang, H., and Chen, Q. (1998). Synthesis of enantiomerically pure spiro-cyclopropane derivatives containing multichiral centers. *Tetrahedron: Asymmetry* *9*, 4103-4107. 10.1016/S0957-4166(98)00416-9.
74. Gassama, A., Ernenwein, C., Youssef, A., Agach, M., Riguet, E., Marinkovic, S., Estrine, B., and Hoffmann, N. (2013). Sulfonated surfactants obtained from furfural. *Green Chemistry* *15*, 1558-1566. 10.1039/C3GC00062A.
75. Keller, E., de Lange, B., Rispens, M.T., and Feringa, B.L. (1993). 1,3-Dipolar cycloadditions to 5-methoxy-2(5H)-furanone. *Tetrahedron* *49*, 8899-8910. 10.1016/S0040-4020(01)81909-8.
76. Mise, T., Hong, P., and Yamazaki, H. (1983). Rhodium carbonyl catalyzed carbonylation of unsaturated compounds. 2. Synthesis of 5-alkoxy-2 (5H)-furanones by the carbonylation of acetylenes in alcohol. *The Journal of Organic Chemistry* *48*, 238-242.

References

77. Zimmer, H., Amer, A., Van, P.C., and Schmidt, D.G. (1988). On the synthesis of 4-alkoxy-2 (5H)-furanones. *The Journal of Organic Chemistry* *53*, 3368-3370.
78. Weigele, M., Tengi, J.P., De Bernardo, S., Czajkowski, R., and Leimgruber, W. (1976). Fluorometric reagents for primary amines. Syntheses of 2-alkoxy- and 2-acyloxy-3(2H)-furanones. *The Journal of Organic Chemistry* *41*, 388-389. 10.1021/jo00864a051.
79. Martin, H., Hoffmann, R., Schmidt, B., and Wolff, S. (1989). Preparation of 5-bromotetronates [4-alkoxy-5-bromo-2(5H)-furanones] and a new concept for the synthesis of aflatoxins and related structure types. Tributyltin hydride versus palladium-promoted intramolecular hydroarylation. *Tetrahedron* *45*, 6113-6126. 10.1016/S0040-4020(01)85124-3.
80. Wei, M.-X., Zhang, J., Ma, F.-L., Li, M., Yu, J.-Y., Luo, W., and Li, X.-Q. (2018). Synthesis and biological activities of dithiocarbamates containing 2(5H)-furanone-piperazine. *European Journal of Medicinal Chemistry* *155*, 165-170. 10.1016/j.ejmech.2018.05.056.
81. Feringa, B.L., and De Lange, B. (1988). Asymmetric 1,4-additions to 5-alkoxy-2(5h)-furanones: An efficient synthesis of (r)- and (s)- 3,4-epoxy-1-butanol. *Tetrahedron* *44*, 7213-7222. 10.1016/S0040-4020(01)86092-0.
82. de Lange, B., van Bolhuis, F., and L. Feringa, B. (1989). Asymmetric 1, 4-additions to 5-alkoxy-2 (5H)-furanonesenantioselective synthesis and absolute configuration determination of β -amino- δ -butyrolactones and amino diols. *Tetrahedron* *45*, 6799-6818. 10.1016/S0040-4020(01)89149-3.
83. de Jong, J.C., van den Berg, K.J., van Leusen, A.M., and Feringa, B.L. (1991). Phenylsilyl-substituted 5-alkoxy-2(5H)-furanones; a new class of highly reactive chiral dienophiles. *Tetrahedron Letters* *32*, 7751-7754. 10.1016/0040-4039(91)80582-Q.
84. Commerce, U.S.S.o. (2021). p-Menthane-3,8-diol, cis-1,3,trans-1,4-. 2021 ed. National Institute of Standards and Technology
85. Thielmann, J., and Muranyi, P. (2019). Review on the chemical composition of *Litsea cubeba* essential oils and the bioactivity of its major constituents citral and limonene. *Journal of Essential Oil Research* *31*, 361-378. 10.1080/10412905.2019.1611671.
86. Li Z, Y.J., Zhang X, Zhuang Z (1974). Studies on the repellent quwenling. *Malaria Research*, 6.
87. Buescher, M.D., Rutledge, L.C., Wirtz, R.A., Glackin, K.B., and Moussa, M.A. (1982). Laboratory Tests of Repellents Against *Lutzomyia Longipalpis* (Diptera: Psychodidae)1. *Journal of Medical Entomology* *19*, 176-180. 10.1093/jmedent/19.2.176.

References

88. Rutledge, L.C., Collister, D.M., Meixsell, V.E., and Eisenberg, G.H.G. (1983). Comparative Sensitivity of Representative Mosquitoes (Diptera: Culicidae) to Repellents. *Journal of Medical Entomology* *20*, 506-510. 10.1093/jmedent/20.5.506.
89. Barbier, P.L., G. (1897). *A Mentholglycol. Compt. Rend.*, 1308–1311.
90. Curtis, C.F. (1990). Natural and synthetic repellents. 75-92.
91. Toghröl, F. (1998). Index of Cleared Science Reviews for p-Menthane-3,8-diol (Pc Code 011550). 02 / 07 / 1988 ed. United States Environmental Protection Agency.
92. da Silva, K.A., Robles-Dutenhefner, P.A., Sousa, E.M.B., Kozhevnikova, E.F., Kozhevnikov, I.V., and Gusevskaya, E.V. (2004). Cyclization of (+)-citronellal to (-)-isopulegol catalyzed by H3PW12O40/SiO2. *Catalysis Communications* *5*, 425-429. 10.1016/j.catcom.2004.05.001.
93. Lenardão, E.J., Botteselle, G.V., de Azambuja, F., Perin, G., and Jacob, R.G. (2007). Citronellal as key compound in organic synthesis. *Tetrahedron* *63*, 6671-6712. 10.1016/j.tet.2007.03.159.
94. Kabasenche, W.P., and Skinner, M.K. (2014). DDT, epigenetic harm, and transgenerational environmental justice. *Environmental Health* *13*, 62. 10.1186/1476-069X-13-62.
95. Paull, J. (2013). *The Rachel Carson Letters and the Making of Silent Spring*. SAGE Open *3*, 2158244013494861. 10.1177/2158244013494861.
96. Barasa, S.S., Ndiege, I.O., Lwande, W., and Hassanali, A. (2002). Repellent activities of stereoisomers of p-menthane-3,8-diols against *Anopheles gambiae* (Diptera: Culicidae). *Journal of medical entomology* *39*, 736-741.
97. Drapeau, J., Rossano, M., Touraud, D., Obermayr, U., Geier, M., Rose, A., and Kunz, W. (2011). Green synthesis of para-Menthane-3,8-diol from *Eucalyptus citriodora*: Application for repellent products. *Comptes Rendus Chimie* *14*, 629-635. 10.1016/j.crci.2011.02.008.
98. *Insect Repellents Handbook*, 2nd Edition. (2015). Ringgold, Inc.
99. Debboun, M., Frances, S.P., and Strickman, D. (2007). *Insect repellents : principles, methods, and uses* (Taylor & Francis).
100. Uzzan, B., Konate, L., Diop, A., Nicolas, P., Dia, I., Dieng, Y., and Izri, A. (2009). Efficacy of four insect repellents against mosquito bites: a double-blind randomized placebo-controlled field study in Senegal. *Fundamental & clinical pharmacology* *23*, 589-594. 10.1111/j.1472-8206.2009.00731.x.

References

101. Lee, J., Choi, D.B., Liu, F., Grieco, J.P., and Achee, N.L. (2018). Effect of the Topical Repellent para-Menthane-3,8-diol on Blood Feeding Behavior and Fecundity of the Dengue Virus Vector *Aedes aegypti*. *Insects (Basel, Switzerland)* *9*, 60. 10.3390/insects9020060.
102. Isagulyants, V.I., Khaimova, T.G., Melikyan, V.R., and Pokrovskaya, S.V. (1968). Condensation of Unsaturated Compounds with Formaldehyde (the Prins Reaction). *Russian Chemical Reviews* *37*, 17-25. 10.1070/rc1968v037n01abeh001604.
103. Arundale, E., and Mikeska, L.A. (1952). The Olefin-Aldehyde Condensation. The Prins Reaction. *Chemical Reviews* *51*, 505-555. 10.1021/cr60160a004.
104. Marakatti, V. (2015). DESIGN OF SOLID ACID CATALYSTS FOR PRINS REACTION AND TOLUENE METHYLATION.
105. Kenmochi, H., Akiyama, T., Yuasa, Y., Kobayashi, T., and Tachikawa, A. (1999) Method for producing para-menthane-3,8-diol. patent US5959161A, patent application US09179688, 1999/09/28/, and granted 1999-09-28.
106. Yuasa, Y., Tsuruta, H., and Yuasa, Y. (2000). A Practical and Efficient Synthesis of p-Menthane-3,8-diols. *Organic Process Research & Development* *4*, 159-161. 10.1021/op9901036.
107. Cheng, H., Meng, X., Liu, R., Hao, Y., Yu, Y., Cai, S., and Zhao, F. (2009). Cyclization of citronellal to p-menthane-3,8-diols in water and carbon dioxide. *Green Chemistry* *11*, 1227-1231. 10.1039/B823297K.
108. Borrego, L.G., Ramarosandratana, N., Jeanneau, E., Méta, E., Ramanandraibe, V.V., Andrianjafy, M.T., and Lemaire, M. (2021). Correction to Effect of the Stereoselectivity of para-Menthane-3,8-diol Isomers on Repulsion toward *Aedes albopictus*. *Journal of Agricultural and Food Chemistry* *69*, 12919-12919. 10.1021/acs.jafc.1c06211.
109. Batish, D.R., Singh, H.P., Setia, N., Kaur, S., and Kohli, R.K. (2006). Chemical composition and inhibitory activity of essential oil from decaying leaves of *Eucalyptus citriodora*. *Zeitschrift fur Naturforschung. C, Journal of biosciences* *61*, 52-56.
110. Bowers, W.S., Evans, P.H., and Spence, S.P. (2000). Trichomes of *Eucalyptus maculata citriodon* Possess a Single Potent Insect Repellent. *Journal of Herbs, Spices & Medicinal Plants* *7*, 85-89. 10.1300/J044v07n04_10.
111. Su, y.-c., Ho, C.-L., Eugene, Wang, I.C., Shang, and Chang, T. (2006). Antifungal activities and chemical compositions of essential oils from leaves of four eucalypts. *Taiwan J For Sci* *21*, 49-61.

References

112. Tian, Y., Liu, X., Zhou, Y., and Guo, Z. (2005). [Extraction and determination of volatile constituents in leaves of *Eucalyptus citriodora*]. *Se pu = Chinese journal of chromatography* 23, 651-654.
113. Verma, R.S., Padalia, R.C., Pandey, V., and Chauhan, A. (2013). Volatile oil composition of vegetative and reproductive parts of lemon-scented gum (*Eucalyptus citriodora* Hook.). *Journal of Essential Oil Research* 25, 452-457. 10.1080/10412905.2013.782477.
114. Jongkind, J.C.D.a.C.C.H. (2017). *Corymbia citriodora* (PROSEA) - PlantUse English. [https://uses.plantnet-project.org/en/Corymbia_citriodora_\(PROSEA\)](https://uses.plantnet-project.org/en/Corymbia_citriodora_(PROSEA)).
115. Berovic, M., and Legisa, M. (2007). Citric acid production. *Biotechnol Annu Rev* 13, 303-343. 10.1016/S1387-2656(07)13011-8.
116. Sahar, S., Ali, R.A., Jamal, T.R.S., Asemeh, M.M., Pegah, A.A., and Woo, J.S. (2016). CITRIC ACID AS AN EFFICIENT AND GREEN CATALYST FOR THE SYNTHESIS OF HEXABENZYL HEXAAZASOWURTZITANE (HBIW). *iranian journal of catalysis* 6, 65-68.
117. Fahimi, N., and Reza Sardarian, A. (2016). Citric Acid: A Green Bioorganic Catalyst for One-Pot Three-Component Synthesis of 2,3-dihydroquinazoline-4 (1H)-ones. *Current Organocatalysis* 3, 39-44. 10.2174/2213337202666150602221505.
118. Corkran, G., and Ball, D.W. (2004). The relative energies of cyclopropanone, cyclopropanedione, and cyclopropanetrione. Hartree–Fock, density-functional, G2, and CBS calculations. *Journal of Molecular Structure: THEOCHEM* 668, 171-178. 10.1016/j.theochem.2003.10.026.
119. Leighton, P.A. (1938). THE MECHANISM OF ALDEHYDE AND KETONE PHOTOLYSIS I. *The Journal of Physical Chemistry* 42, 749-761. 10.1021/j100901a006.
120. Leighton, P.A., and Blacet, F.E. (1932). THE PHOTOLYSIS OF THE ALIPHATIC ALDEHYDES. I. PROPIONALDEHYDE. *Journal of the American Chemical Society* 54, 3165-3178. 10.1021/ja01347a019.
121. T., G. (1989). Antiparasitic behaviour in New Zealand parakeets (*Cyanoramphus* species). *Notornis* 36, 2.
122. Reed A. Gray (Saratoga, C., Chien K. Tseng (El Cerrito, CA), Ronald J. Rusay (Lafayette, CA) (1988) 1-Hydroxy-2-(alkylketo)-4,4,6,6-tetramethyl cyclohexen-3,5-diones. USA patent 4202840, patent application 5/947,217, May 13, 1980.
123. SPOONER-HART, R., Neil, and BASTA, A., Habib (2010) METHODS AND COMPOSITIONS FOR CONTROLLING PESTS. USA patent 7820,209 patent application 12/134,035, 2006.01, and granted 26/10/2010.

References

124. Bick, I., and Horn, D. (1965). Nuclear magnetic resonance studies. V. The tautomerism of tasmanone and related β -triketones. *Australian Journal of Chemistry* *18*, 1405-1410.
125. Birch, A., and Elliott, P. (1956). Studies in relation to Biosynthesis. VIII. Tasmanone, Dehydroangustione, and Calythrone. *Australian Journal of Chemistry* *9*, 95-104.
126. Hellyer, R., Bick, I., Nicholls, R., and Rottendorf, H. (1963). The structure of tasmanone. *Australian Journal of Chemistry* *16*, 703-708.
127. Brophy, J.J., and Boland, D.J. (1990). Leaf Essential Oil of Two Chemotypes of *Eucalyptus cloeziana* F. Muell. *Journal of Essential Oil Research* *2*, 87-90.
128. Tam, N.G.T., Thuam, D.T., Bighelli, A., Castola, V., Muselli, A., Richomme, P., and Casanova, J. (2004). *Baekkea frutescens* leaf oil from Vietnam: composition and chemical variability. *Flavour and fragrance journal* *19*, 217-220.
129. Matos, I.L.d., Machado, S.M.F., Souza, A.R.d., Costa, E.V., Nepel, A., Barison, A., and Alves, P.B. (2015). Constituents of essential oil and hydrolate of leaves of *Campomanesia viatoris* Landrum. *Quimica Nova* *38*, 1289-1292.
130. Briggs, L., Hassall, C., and Short, W. (1945). 187. Leptospermone. Part II. *Journal of the Chemical Society (Resumed)*, 706-709.
131. Birch, A.J. (1951). 670. β -Triketones. Part I. The structures of angustione, dehydroangustione, calythrone, and flavaspidic acid. *Journal of the Chemical Society (Resumed)*, 3026-3030.
132. Teixeira, A.F., de Souza, J., Dophine, D.D., de Souza Filho, J.D., and Saúde-Guimarães, D.A. (2022). Chemical Analysis of *Eruca sativa* Ethanolic Extract and Its Effects on Hyperuricaemia. *Molecules* *27*, 1506.
133. Cannon, J., Corbett, N., Haydock, K., Tracey, J., and Webb, L. (1962). An investigation of the effect of the dehydroangustione present in the leaf litter of *Backhousia angustifolia* on the germination of *Araucaria cunninghamii*—An experimental approach to a problem in rain-forest ecology. *Australian journal of botany* *10*, 119-128.
134. Perry, N.B., Brennan, N.J., Van Klink, J.W., Harris, W., Douglas, M.H., McGimpsey, J.A., Smallfield, B.M., and Anderson, R.E. (1997). Essential oils from New Zealand manuka and kanuka: chemotaxonomy of *Leptospermum*. *Phytochemistry* *44*, 1485-1494.
135. Hellyer, R., and Pinhey, J. (1966). The structure of grandiflorone, a new β -triketone. *Journal of the Chemical Society C: Organic*, 1496-1498.
136. Alvarez Costa, A., Naspi, C.V., Lucia, A., and Masuh, H.M. (2017). Repellent and Larvicidal Activity of the Essential Oil From *Eucalyptus nitens* Against *Aedes aegypti*

References

- and *Aedes albopictus* (Diptera: Culicidae). *Journal of Medical Entomology* *54*, 670-676. 10.1093/jme/tjw222.
137. Jeong, E.-Y., Lee, M.-J., and Lee, H.-S. (2018). Antimicrobial activities of leptospermone isolated from *Leptospermum scoparium* seeds and structure–activity relationships of its derivatives against foodborne bacteria. *Food science and biotechnology* *27*, 1541-1547.
138. Quijano-Célis, C., Gaviria, M., Vanegas-López, C., and Pino, J.A. (2010). Chemical composition and antibacterial activity of the essential oil of *Callistemon viminalis* (Gaertn.) G. Don leaves from Colombia. *Journal of Essential Oil Bearing Plants* *13*, 710-716.
139. Taylor, S., Walther, D., Fernando, D.D., Swe-Kay, P., and Fischer, K. (2022). Investigating the Antibacterial Properties of Prospective Scabicides. *Biomedicines* *10*, 3287.
140. Gakuubi, M.M. (2016). Steam distillation extraction and chemical composition of essential oils of *Toddalia asiatica* L. and *Eucalyptus camaldulensis* Dehnh. *Journal of Pharmacognosy and Phytochemistry* *5*, 99-104.
141. Hellyer, R. (1964). The structure of agglomerone, a new β -triketone. *Australian Journal of Chemistry* *17*, 1418-1422.
142. Birch, A., and Elliott, P. (1956). β -Triketones. III. Xanthostemone. *Australian Journal of Chemistry* *9*, 238-240.
143. Brophy, J.J., Goldsack, R.J., and Forster, P.I. (2006). A preliminary examination of the leaf oils of the genus *Xanthostemon* (Myrtaceae) in Australia. *Journal of Essential Oil Research* *18*, 222-230.
144. Khamare, Y., Chen, J., and Marble, S.C. (2022). Allelopathy and its application as a weed management tool: A review. *Frontiers in Plant Science* *13*. 10.3389/fpls.2022.1034649.
145. Alsaud, N., Shahbaz, K., and Farid, M. (2021). Evaluation of deep eutectic solvents in the extraction of β -caryophyllene from New Zealand Manuka leaves (*Leptospermum scoparium*). *Chemical Engineering Research and Design* *166*, 97-108. 10.1016/j.cherd.2020.11.028.
146. Killeen, D.P., Larsen, L., Dayan, F.E., Gordon, K.C., Perry, N.B., and van Klink, J.W. (2016). Nortriketones: Antimicrobial Trimethylated Acylphloroglucinols from Mānuka (*Leptospermum scoparium*). *Journal of Natural Products* *79*, 564-569. 10.1021/acs.jnatprod.5b00968.
147. Yong-Hong, L., Li-Zhen, X., Shi-Lin, Y., Jie, D., Yong-Su, Z., Min, Z., and Nan-Jun, S. (1997). Three cyclohexene oxides from *Uvaria grandiflora*. *Phytochemistry* *45*, 729-732.

References

148. Bignell, C.M., Dunlop, P.J., and Brophy, J. (1997). Volatile leaf oils of some southwestern and southern Australian species of the genus *Eucalyptus* (series I). Part XVI: Subgenus *Symphomyrtus*, Section *Bisectaria*, Series *Cneorifoliae*, Series *Porantherae* and Series *Falcatae*. *Flavour and fragrance journal* 12, 261-267.
149. Penfold, A.R., and Simonsen, J.L. (1940). 87. Calythrone. *Journal of the Chemical Society (Resumed)*, 412-415.
150. Barton, J.E.D.C., D.; Carter, C. G.; Cox, J. M.; Lee, D. L.; Mitchell, G., and Walker, F.H.W., F. X. (1988) Herbicidal substituted cyclic diones. Great Britain. patent 0 283 261 B1. , patent application 88302286.5 17/08/94 and granted 15/12/87.
151. Lee, D.L., Knudsen, C.G., Michaely, W.J., Tarr, J.B., Chin, H.-L., Nguyen, N.H., Carter, C.G., Cromartie, T.H., Lake, B.H., Shribbs, J.M., et al. (2000). The Synthesis and Structure—Activity Relationships of the Triketone HPPD Herbicides. In *Agrochemical Discovery*, (American Chemical Society), pp. 8-19. doi:10.1021/bk-2001-0774.ch002
10.1021/bk-2001-0774.ch002.
152. Mitchell, G., Bartlett, D.W., Fraser, T.E.M., Hawkes, T.R., Holt, D.C., Townson, J.K., and Wichert, R.A. (2001). Mesotrione: a new selective herbicide for use in maize. *Pest Management Science* 57, 120-128. 10.1002/1526-4998(200102)57:2<120::AID-PS254>3.0.CO;2-E.
153. Lee, D.L., Knudsen, C.G., Michaely, W.J., Chin, H.-L., Nguyen, N.H., Carter, C.G., Cromartie, T.H., Lake, B.H., Shribbs, J.M., and Fraser, T. (1998). The structure–activity relationships of the triketone class of HPPD herbicides†. *Pesticide Science* 54, 377-384. 10.1002/(SICI)1096-9063(199812)54:4<377::AID-PS827>3.0.CO;2-0.
154. Beraud, J., and Compagnon, J. (1993). [Sulcotrione, a postemergence herbicide for maize crops,[ICIA0051, SC0051, triketones]]. *Phytoma La Defense des Vegetaux (France)*.
155. Wichert, R.A.T., J.K.; Bartlett, D.W.; Foxon, G.A. (1999). Technical review of mesotrione, a new maize herbicide. *Weeds : the 1999 Brighton conference held in Brighton, UK, 15-18, November*. (British Crop Protection Council), pp. 105-110.
156. Muturi, E.J., Selling, G.W., Doll, K.M., Hay, W.T., and Ramirez, J.L. (2020). *Leptospermum scoparium* essential oil is a promising source of mosquito larvicide and its toxicity is enhanced by a biobased emulsifier. *Plos one* 15, e0229076.
157. P, M. (2016). New B - triketone insecticides offer novel mode of action to control resistant insects. *International Pest Control*. 58.
158. Zhan, Q., Wu, Y.-Y., Liu, F., Li, N.-P., Zhou, X., Wang, C.-Q., Wu, Y., Zhao, W., Ye, W.-C., and Wang, L. (2022). (+)- and (–)-Xanthostones A–D: Four Pairs of Enantiomeric

References

- Cinnamoyl- β -Triketone Derivatives from *Xanthostemon chrysanthus*. *Chemistry & Biodiversity* *19*, e202200356. 10.1002/cbdv.202200356.
159. van Klink, J.W., Larsen, L., Perry, N.B., Weavers, R.T., Cook, G.M., Bremer, P.J., MacKenzie, A.D., and Kirikae, T. (2005). Triketones active against antibiotic-resistant bacteria: Synthesis, structure–activity relationships, and mode of action. *Bioorganic & Medicinal Chemistry* *13*, 6651–6662. 10.1016/j.bmc.2005.07.045.
160. Orr, R., and Nelson, P.N. (2021). Eucalyptus cloeziana mulch suppresses Fusarium wilt of banana. *Crop Protection* *147*, 105694. 10.1016/j.cropro.2021.105694.
161. Shestak, O.P., Novikov, V.L., Martyyas, E.A., and Anisimov, M.M. (2009). Synthesis and antimicrobial and antifungal activities of cyclopentene β , β' -triketones and their methyl enol ethers. *Pharmaceutical Chemistry Journal* *43*, 498–501. 10.1007/s11094-009-0338-4.
162. Baigent, D., and Bick, I. (1973). The synthesis of agglomerone. *Australian Journal of Chemistry* *26*, 2065–2066. 10.1071/CH9732065.
163. van Klink, J.W., Brophy, J.J., Perry, N.B., and Weavers, R.T. (1999). β -Triketones from Myrtaceae: Isoleptospermone from *Leptospermum scoparium* and Papuanone from *Corymbia dallachiana*. *Journal of Natural Products* *62*, 487–489. 10.1021/np980350n.
164. Mak, W.C.K. (2022). Comparisons between the Hydro Distillation and the Steam Distillation in the Extraction of Volatile Compounds from and the Anti-oxidative Activity of *Prunella Vulgaris*. *bioRxiv*, 2022.2007.2007.499219. 10.1101/2022.07.07.499219.
165. Ozkan, K., Bayram, Y., Karasu, S., Karadag, A., and Sagdic, O. (2021). Chapter 3 - Extraction of bioactive compounds from saffron species. In *Saffron*, C.M. Galanakis, ed. (Academic Press), pp. 99–141. 10.1016/B978-0-12-821219-6.00003-8.
166. Handa, S. (2008). An overview of extraction techniques for medicinal and aromatic plants. *Extraction technologies for medicinal and aromatic plants* *1*, 21–40.
167. Reche, R.V., Leite Neto, A.F., Da Silva, A.A., Galinaro, C.A., De Osti, R.Z., and Franco, D.W. (2007). Influence of Type of Distillation Apparatus on Chemical Profiles of Brazilian Cachaças. *Journal of Agricultural and Food Chemistry* *55*, 6603–6608. 10.1021/jf0704110.
168. Batish, D.R., Singh, H.P., Setia, N., Kaur, S., and Kohli, R.K. (2006). Chemical Composition and Inhibitory Activity of Essential Oil from Decaying Leaves of *Eucalyptus citriodora*. *Zeitschrift für Naturforschung C* *61*, 52–56. doi:10.1515/znc-2006-1-210.

References

169. Tian, Y., Liu, X., Zhou, Y., and Guo, Z. (2005). [Extraction and determination of volatile constituents in leaves of *Eucalyptus citriodora*]. *Se pu = Chinese journal of chromatography* 23 6, 651-654.
170. Rajeswara Rao, B., Kaul, P., Syamasundar, K., and Ramesh, S. (2003). Comparative composition of decanted and recovered essential oils of *Eucalyptus citriodora* Hook. *Flavour and fragrance journal* 18, 133-135.
171. Kharissova, O.V., Kharisov, B.I., Oliva González, C.M., Méndez, Y.P., and López, I. (2019). Greener synthesis of chemical compounds and materials. *Royal Society Open Science* 6, 191378. doi:10.1098/rsos.191378.
172. Babushok, V.I., Linstrom, P.J., and Zenkevich, I.G. (2011). Retention Indices for Frequently Reported Compounds of Plant Essential Oils. *Journal of Physical and Chemical Reference Data* 40. 10.1063/1.3653552.
173. Borrego, L.G., Ramarosandratana, N., Jeanneau, E., Métay, E., Ramanandraibe, V.V., Andrianjafy, M.T., and Lemaire, M. (2021). Effect of the Stereoselectivity of para-Menthane-3,8-diol Isomers on Repulsion toward *Aedes albopictus*. *Journal of Agricultural and Food Chemistry* 69, 11095-11109. 10.1021/acs.jafc.1c03897.
174. George, J.H., Hesse, M.D., Baldwin, J.E., and Adlington, R.M. (2010). Biomimetic synthesis of polycyclic polyprenylated acylphloroglucinol natural products isolated from *Hypericum papuanum*. *Organic letters* 12, 3532-3535.
175. Riedl, W., and Risse, K.H. (1954). Synthese des Filicinsäurebutanons, III. Mitteil.) über Bestandteile von *Filix mas*. *Chemische Berichte* 87, 865-868. 10.1002/cber.19540870612.
176. Dumas, E., Giraud, M., Goujon, E., Halma, M., Knhili, E., Stauffert, M., Batisson, I., Besse-Hoggan, P., Bohatier, J., Bouchard, P., et al. (2017). Fate and ecotoxicological impact of new generation herbicides from the triketone family: An overview to assess the environmental risks. *Journal of Hazardous Materials* 325, 136-156. 10.1016/j.jhazmat.2016.11.059.
177. Romdhane, S., Devers-lamrani, M., Martin-Laurent, F., Ben Jrad, A., Raviglione, D., Salvia, M.-V., Besse-Hoggan, P., Dayan, F., Bertrand, C., and Barthelmebs, L. (2018). Evidence for photolytic and microbial degradation processes in the dissipation of leptospermone, a natural β -triketone herbicide. *Environmental science and pollution research international* 25. 10.1007/s11356-017-9728-4.

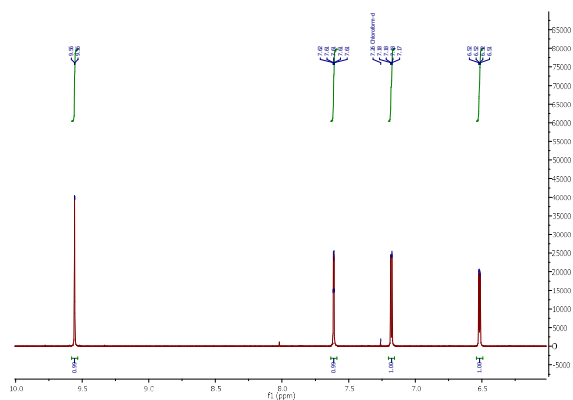
References

178. Trivella, A., Stawinoga, M., Dayan, F.E., Cantrell, C.L., Mazellier, P., and Richard, C. (2015). Photolysis of natural β -triketonic herbicides in water. *Water Research* 78, 28-36. 10.1016/j.watres.2015.03.026.
179. Tam, N.G., Duong, T., Bighelli, A., Castola, V., Muselli, A., Richomme, P., and Casanova, J. (2004). *Baekkea frutescens* leaf oil from Vietnam: Composition and chemical variability. *Flavour and Fragrance Journal* 19, 217-220. 10.1002/ffj.1281.
180. Liu, F., Lu, W.-J., Li, N.-P., Liu, J.-W., He, J., Ye, W.-C., and Wang, L. (2018). Four new cinnamoyl-phloroglucinols from the leaves of *Xanthostemon chrysanthus*. *Fitoterapia* 128, 93-96. 10.1016/j.fitote.2018.05.017.
181. Chaverri, C., and Ciccío, J. (2005). Essential oil of trees of the genus *Ocotea* (Lauraceae) in Costa Rica. I. *Ocotea brenesii*. *Revista de biología tropical* 53, 431-436. 10.15517/rbt.v53i3-4.14611.
182. Silva, M.H.L.d., Andrade, E.H.d.A., Zoghbi, M.G.B., Luz, A.I.R., Silva, J.E.d., and Maia, J.G.S. (1999). The essential oils of *Lantana camara* L. occurring in North Brazil. *Flavour and Fragrance Journal* 14, 208-210.

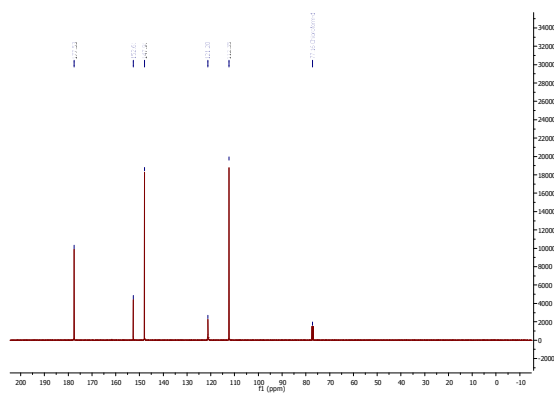
APPENDICES

Appendices

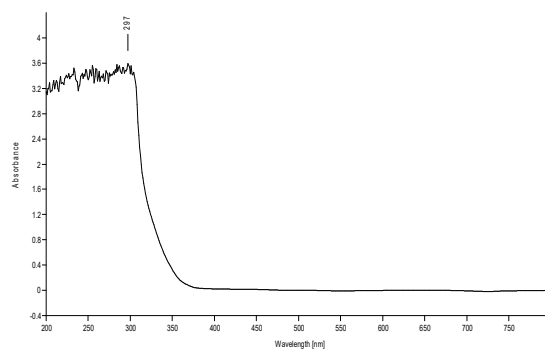
Appendices



Appendix 1: ^1H -NMR of furan-2-carbaldehyde (**1**).

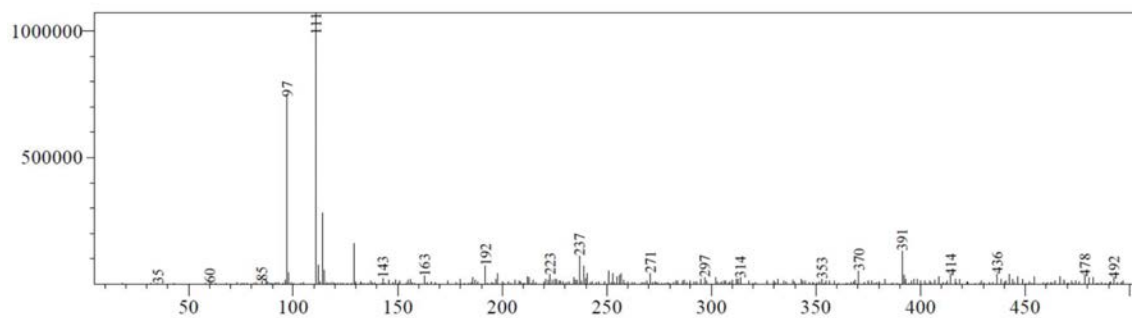


Appendix 2: ^{13}C -NMR of furan-2-carbaldehyde (**1**).

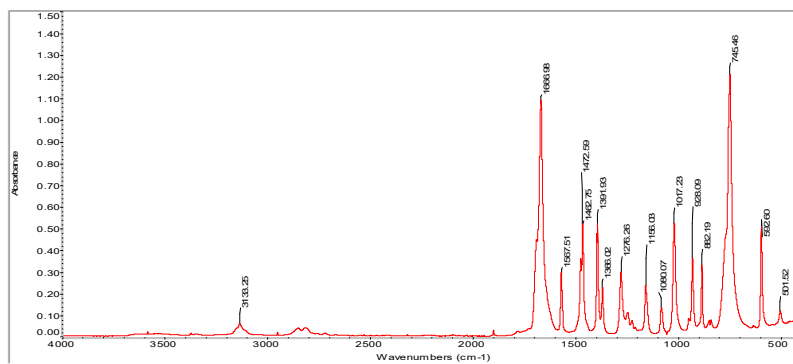


Appendix 3: UV/Vis-Spectrum of furan-2-carbaldehyde (**1**).

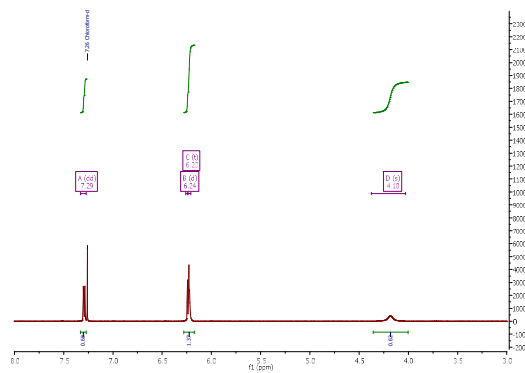
Appendices



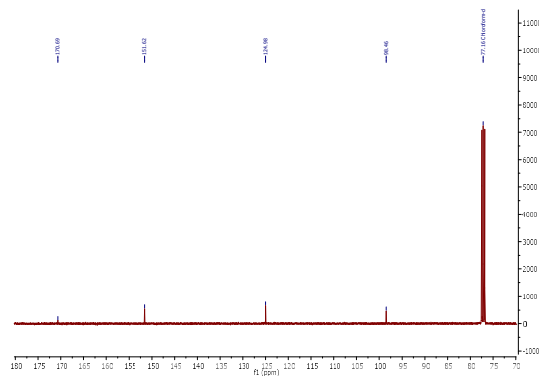
Appendix 4: MS-Spectrum of furan-2-carbaldehyde (1).



Appendix 5: IR-Spectrum of furan-2-carbaldehyde (1).

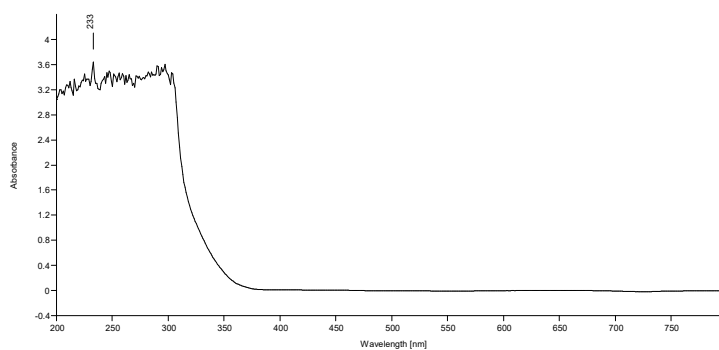


Appendix 6: ¹H-NMR of 5-hydroxyfuran-2(5H)-one (2).

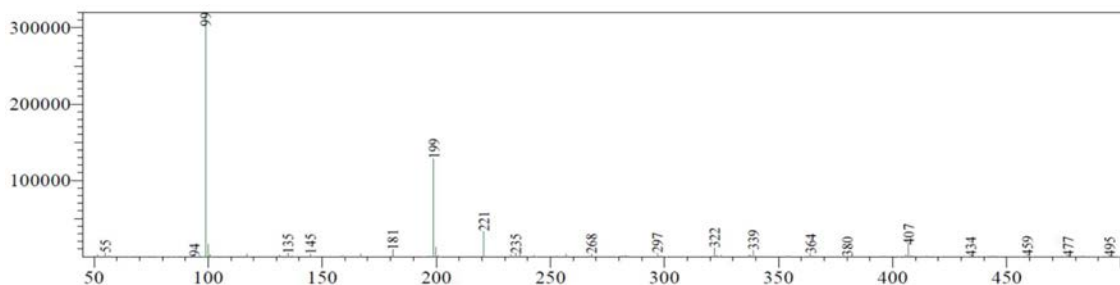


Appendix 7: ¹³C-NMR of 5-hydroxyfuran-2(5H)-one (2).

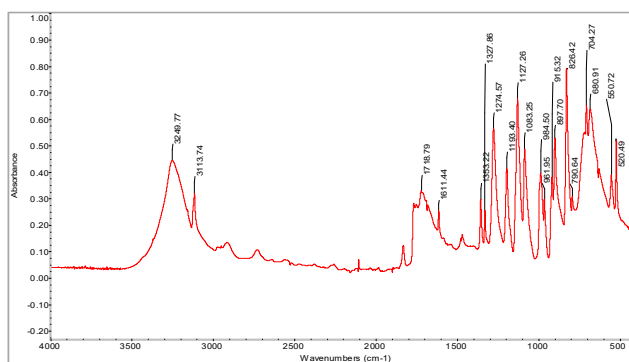
Appendices



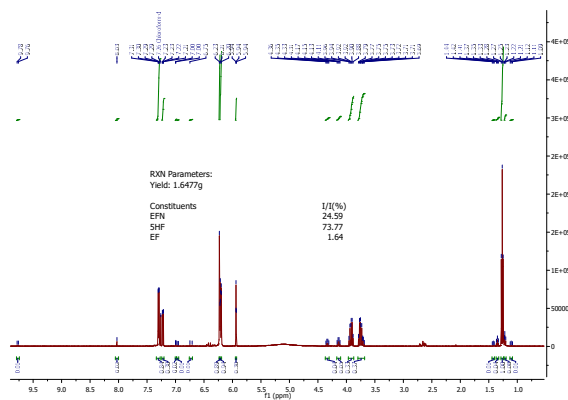
Appendix 8: UV/Vis-Spectrum of 5-hydroxyfuran-2(5H)-one (2).



Appendix 9: MS-Spectrum of 5-hydroxyfuran-2(5H)-one (2).

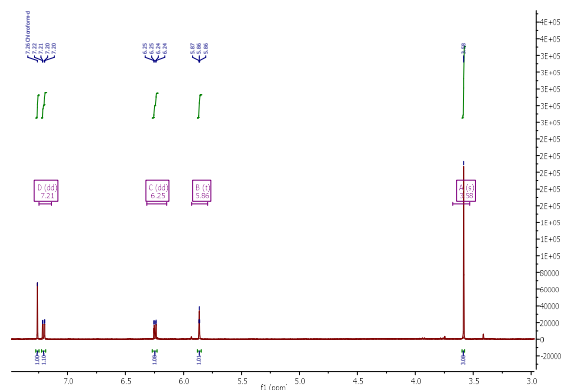


Appendix 10: IR-Spectrum of 5-hydroxyfuran-2(5H)-one (2).

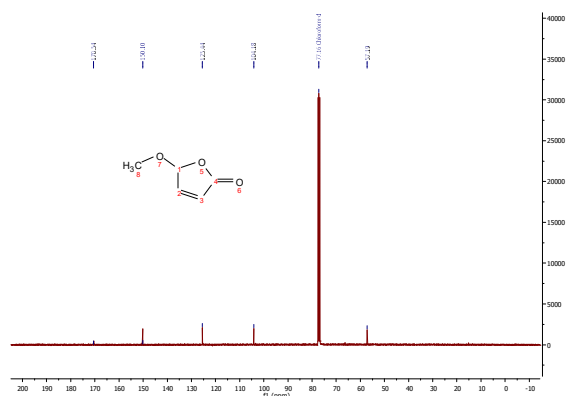


Appendix 11: $^1\text{H-NMR}$ of the crude product of Experiment 3.

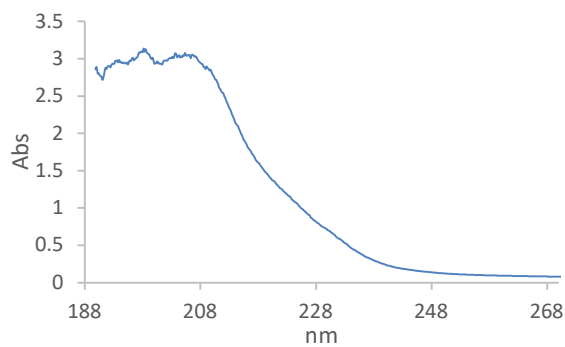
Appendices



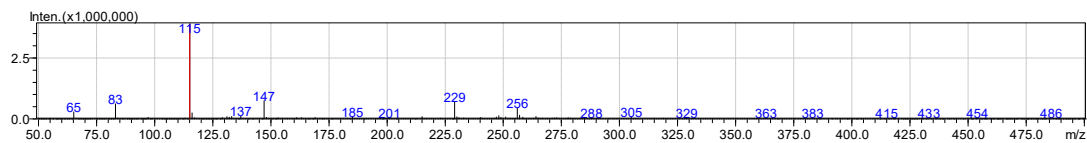
Appendix 12: $^1\text{H-NMR}$ of 5-methoxyfuran-2(5H)-one (7).



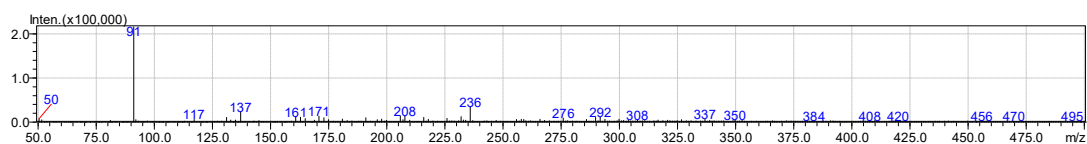
Appendix 13: $^{13}\text{C-NMR}$ of 5-methoxyfuran-2(5H)-one (7).



Appendix 14: UV/Vis-Spectrum of 5-methoxyfuran-2(5H)-one (7).

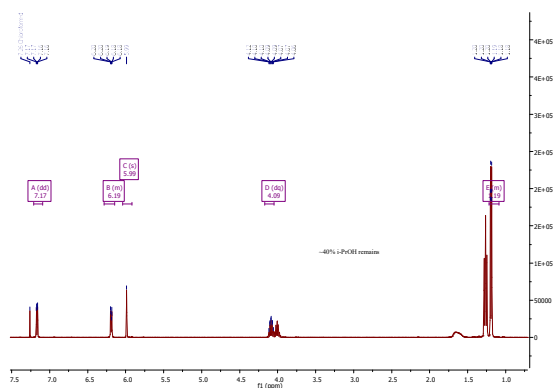


Appendix 15: MS-Spectrum (positive mode) of 5-methoxyfuran-2(5H)-one (7).

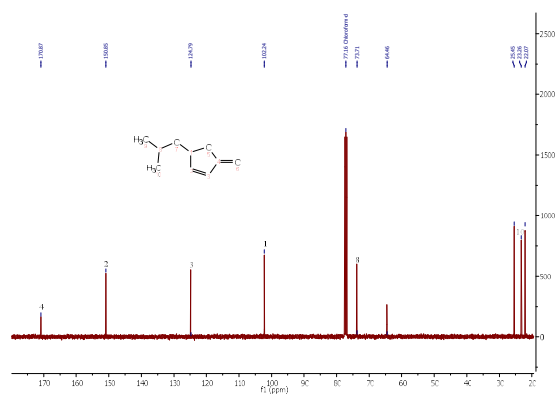


Appendix 16: MS-Spectrum (negative mode) of 5-methoxyfuran-2(5H)-one (7).

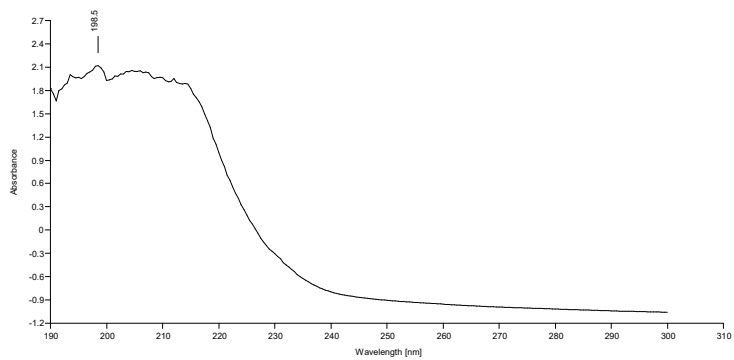
Appendices



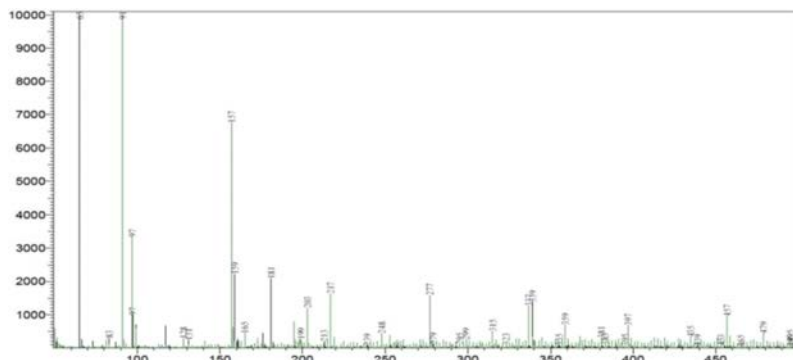
Appendix 17: $^1\text{H-NMR}$ of 5-isopropoxyfuran-2(5H)-one (**8**).



Appendix 18: $^{13}\text{C-NMR}$ of 5-isopropoxyfuran-2(5H)-one (**8**).

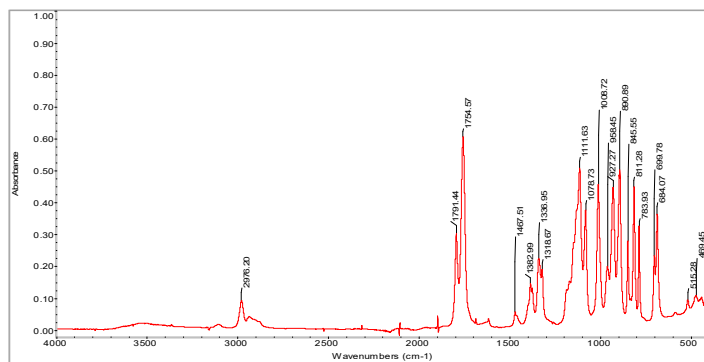


Appendix 19: UV/Vis-Spectrum of 5-isopropoxyfuran-2(5H)-one (**8**).

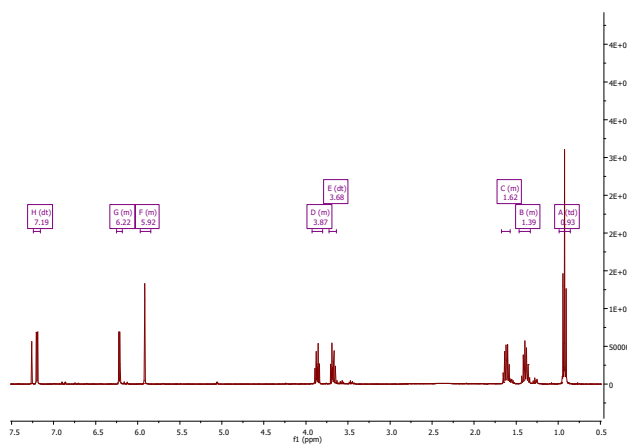


Appendix 20: MS-Spectrum of 5-isopropoxyfuran-2(5H)-one (**8**).

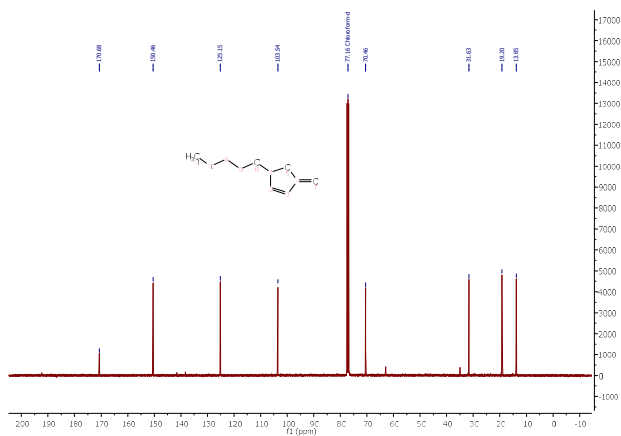
Appendices



Appendix 21: IR-Spectrum of 5-isopropoxyfuran-2(5H)-one (**8**).

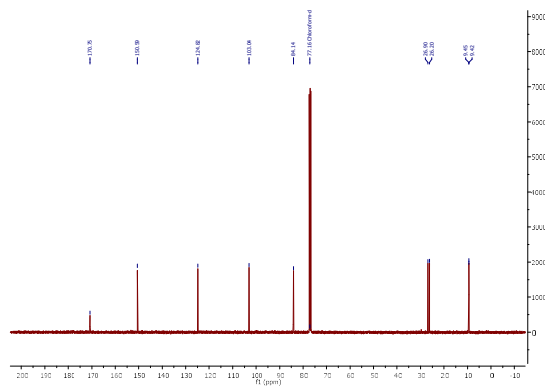


Appendix 22: ^1H -NMR of 5-butoxyfuran-2(5H)-one (**9**).

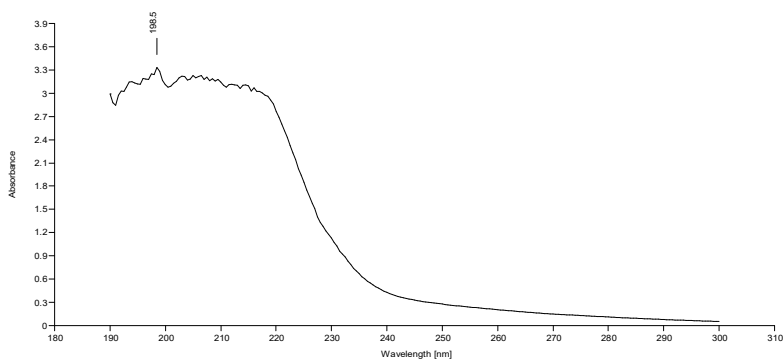


Appendix 23: ^{13}C -NMR of 5-butoxyfuran-2(5H)-one (**9**).

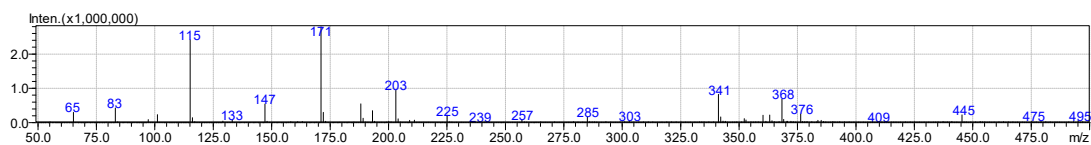
Appendices



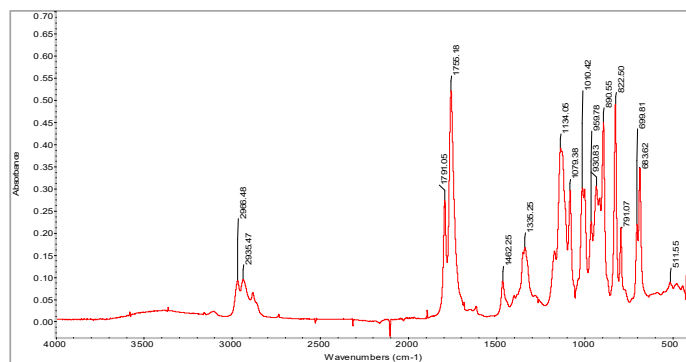
Appendix 28: ^{13}C -NMR of 5-(pentan-3-yloxy) furan-2(5H)-one (**10**).



Appendix 29: UV/Vis-Spectrum of 5-(pentan-3-yloxy) furan-2(5H)-one (**10**).

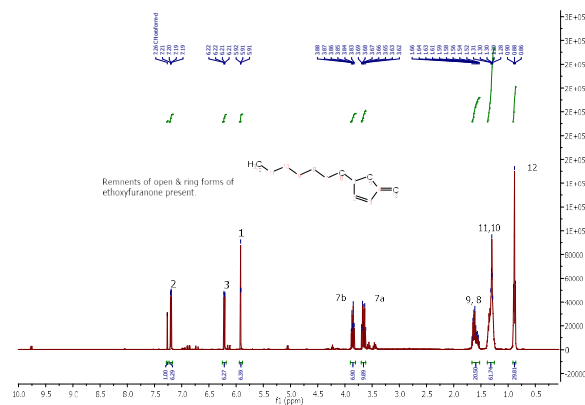


Appendix 30: MS-Spectrum of 5-(pentan-3-yloxy) furan-2(5H)-one (**10**).

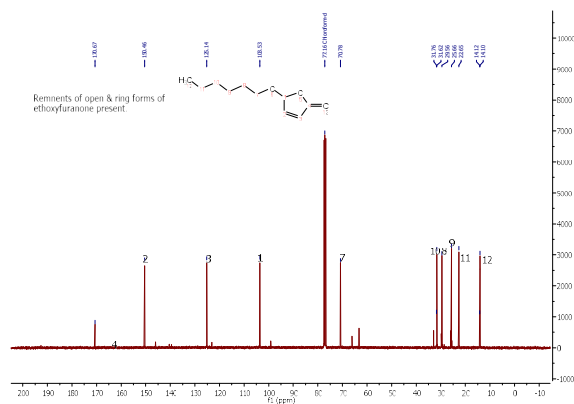


Appendix 31: IR-Spectrum of 5-(pentan-3-yloxy) furan-2(5H)-one (**10**).

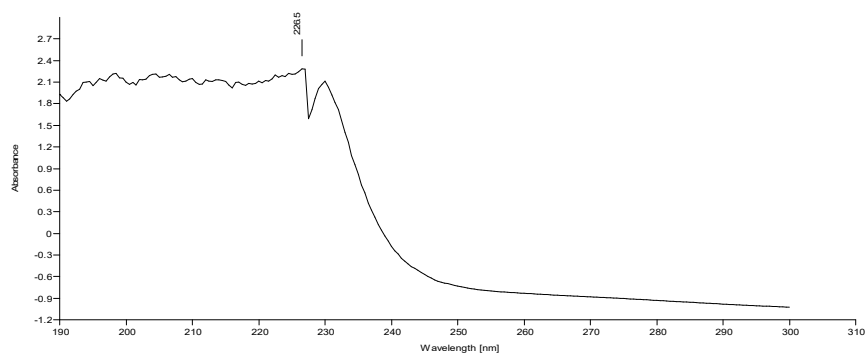
Appendices



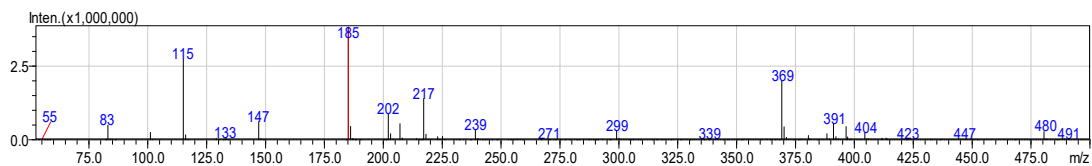
Appendix 32: $^1\text{H-NMR}$ of 5-hexoxyfuran-2(5H)-one (11).



Appendix 33: $^{13}\text{C-NMR}$ of 5-hexoxyfuran-2(5H)-one (11).

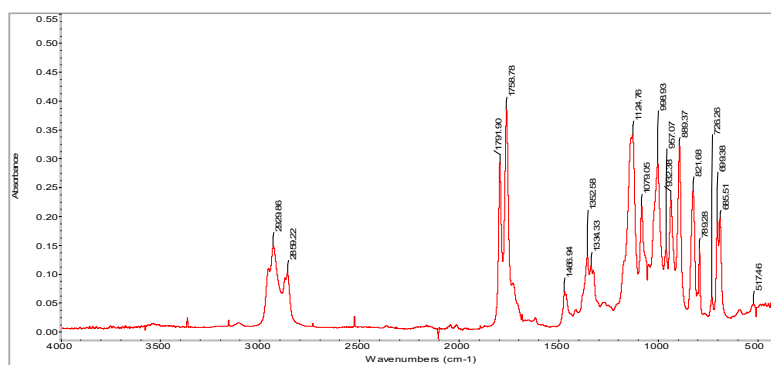


Appendix 34: UV/Vis-Spectrum of 5-hexoxyfuran-2(5H)-one (11).

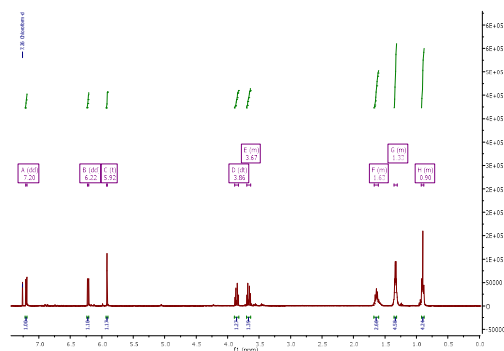


Appendix 35: MS-Spectrum of 5-hexoxyfuran-2(5H)-one (11).

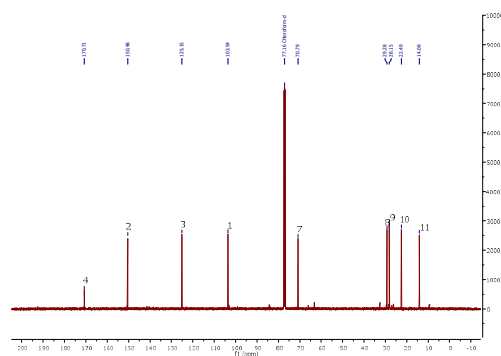
Appendices



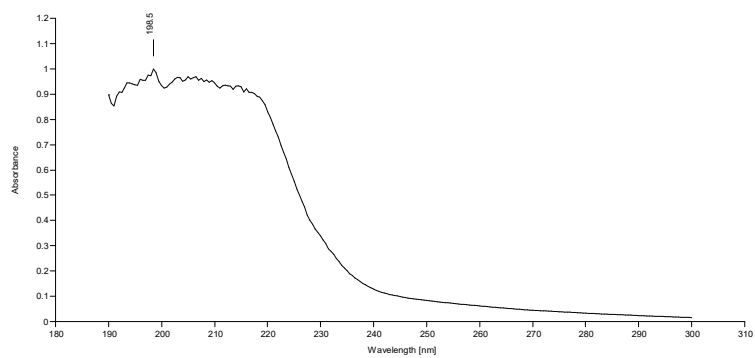
Appendix 36: IR-Spectrum of 5-hexoxyfuran-2(5H)-one (11).



Appendix 37: $^1\text{H-NMR}$ of 5-pentoxifyfuran-2(5H)-one (12).

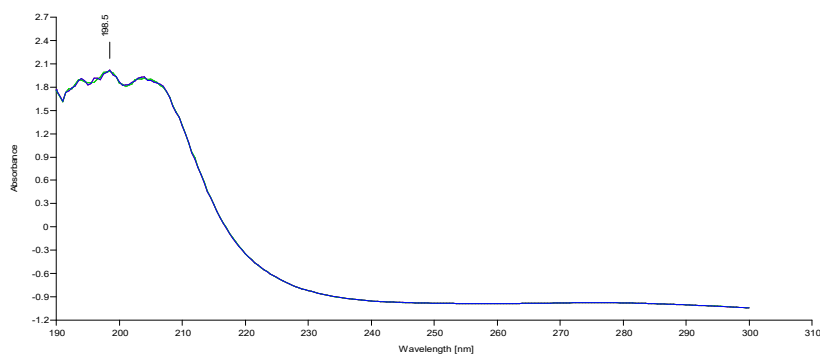


Appendix 38: $^{13}\text{C-NMR}$ of 5-pentoxifyfuran-2(5H)-one (12).

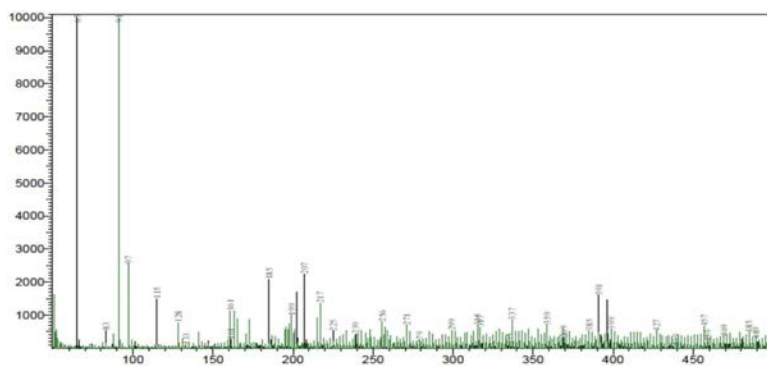


Appendix 39: UV/Vis-Spectrum of 5-pentoxifyfuran-2(5H)-one (12).

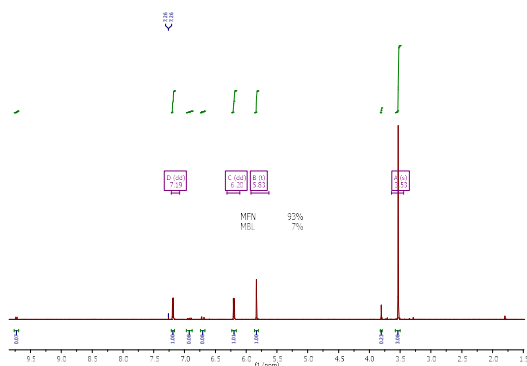
Appendices



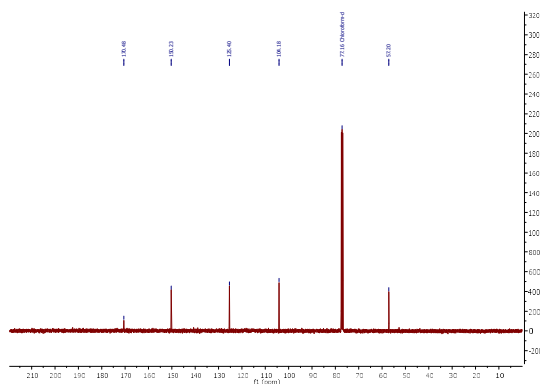
Appendix 44: UV/Vis-Spectrum of 5-cyclopentoxyfuran-2(5H)-one (13).



Appendix 45: MS-Spectrum of 5-cyclopentoxyfuran-2(5H)-one (13).

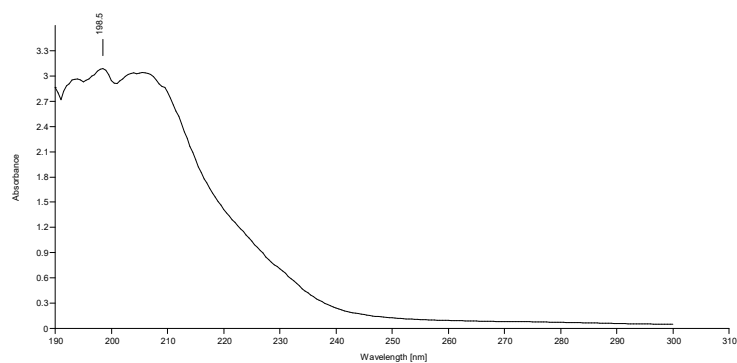


Appendix 46: ¹H-NMR of 5-methoxyfuran-2(5H)-one (7).

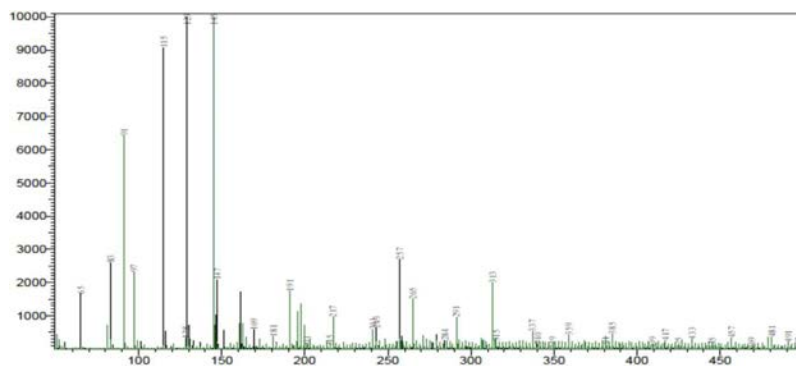


Appendix 47: ¹³C-NMR of 5-methoxyfuran-2(5H)-one (7).

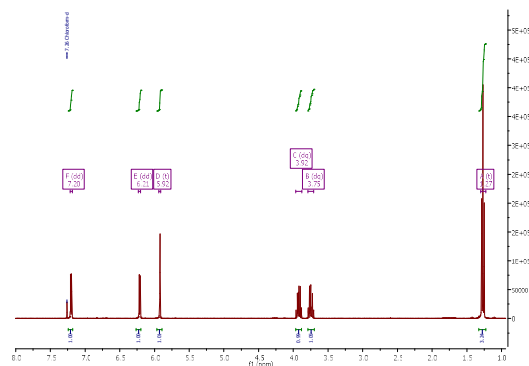
Appendices



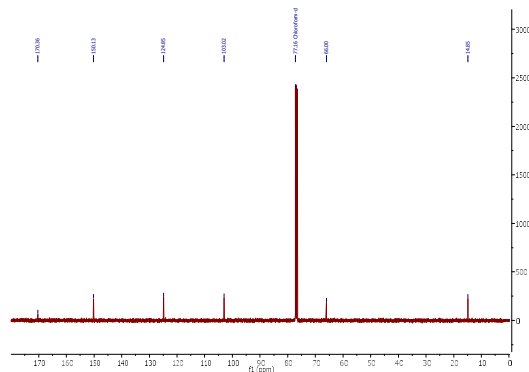
Appendix 48: UV/Vis-Spectrum of 5-methoxyfuran-2(5H)-one (7).



Appendix 49: MS-Spectrum of 5-methoxyfuran-2(5H)-one (7).

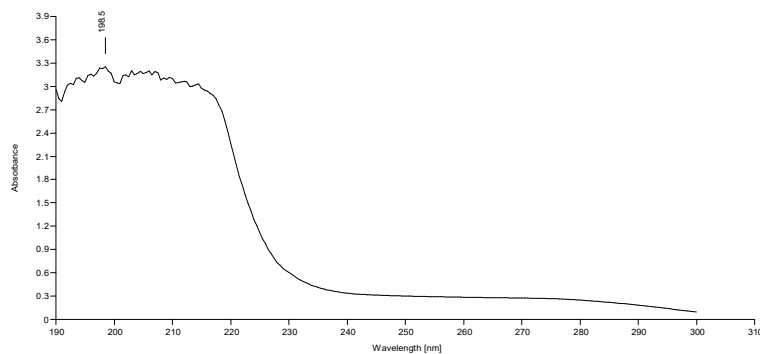


Appendix 50: $^1\text{H-NMR}$ of 5-ethoxyfuran-2(5H)-one (4).

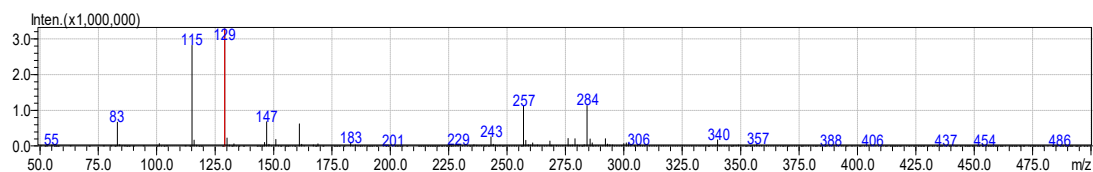


Appendix 51: $^{13}\text{C-NMR}$ of 5-ethoxyfuran-2(5H)-one (4).

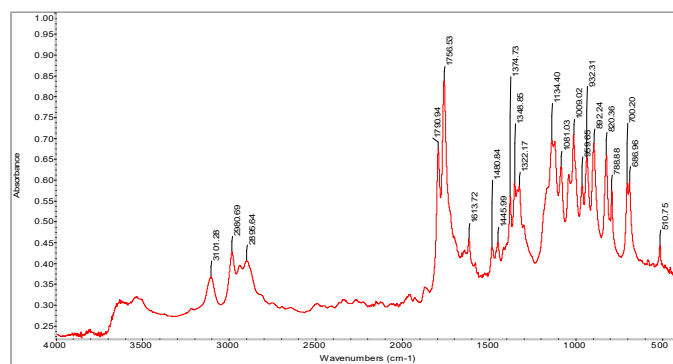
Appendices



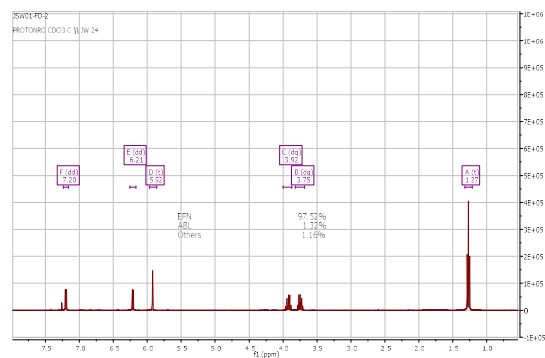
Appendix 52: UV/Vis-Spectrum of 5-ethoxyfuran-2(5H)-one (**4**).



Appendix 53: MS-Spectrum of 5-ethoxyfuran-2(5H)-one (**4**).

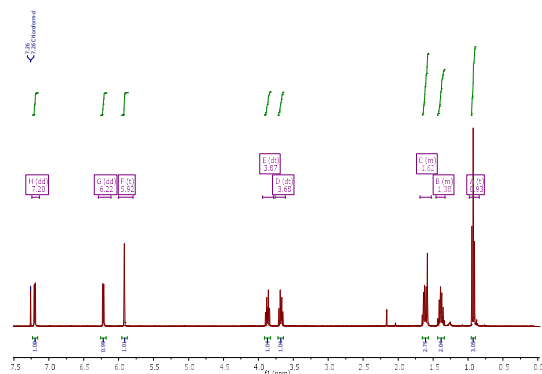


Appendix 54: IR-Spectrum of 5-ethoxyfuran-2(5H)-one (**4**).

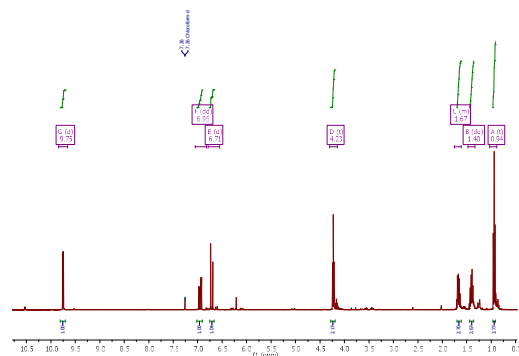


Appendix 55: $^1\text{H-NMR}$ of 5-ethoxyfuran-2(5H)-one (**4**) obtained from BB1.

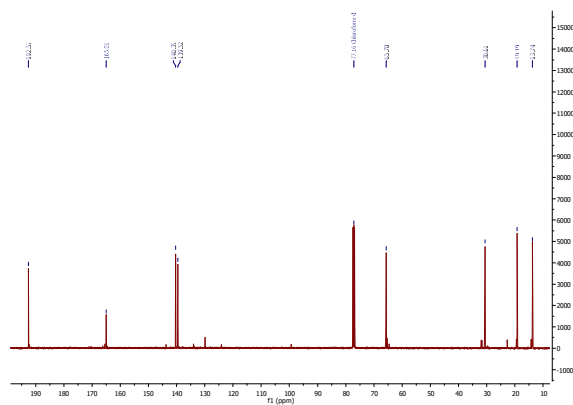
Appendices



Appendix 56: ¹H-NMR of 5-butoxyfuran-2(5H)-one (9).

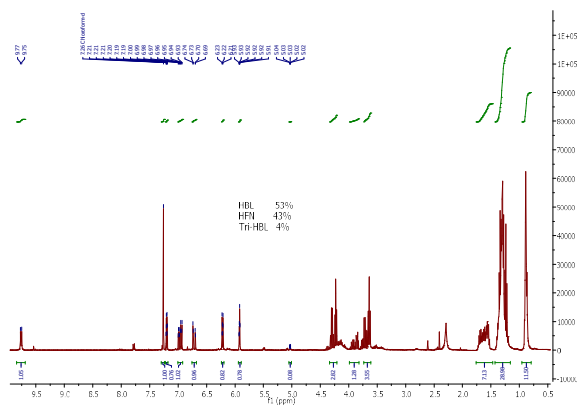


Appendix 57: ¹H-NMR of (*E*)-butyl 4-oxobut-2-enoate (14).

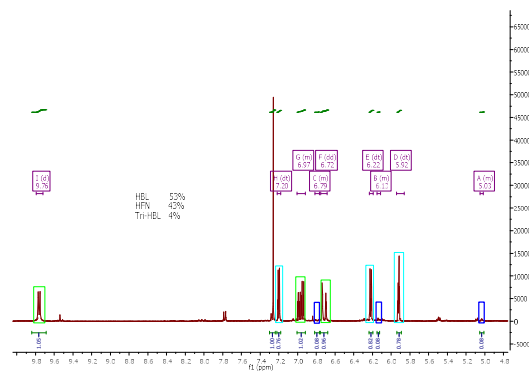


Appendix 58: ¹³C-NMR of (*E*)-butyl 4-oxobut-2-enoate (14).

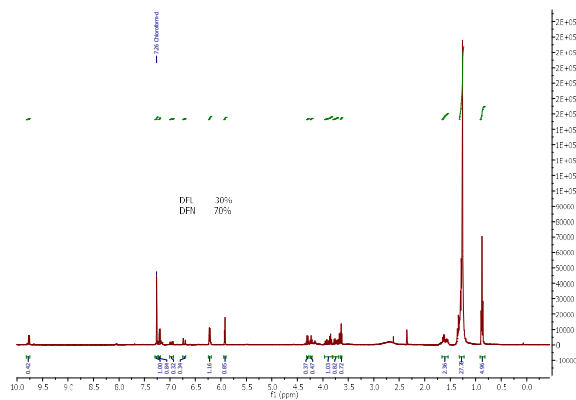
Appendices



Appendix 59: $^1\text{H-NMR}$ of crude pseudo-transesterification 4 to 11 (Experiment 29).

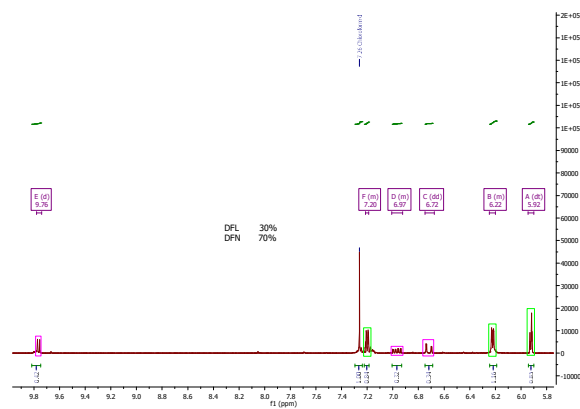


Appendix 60: Expansion of Appendix 59.

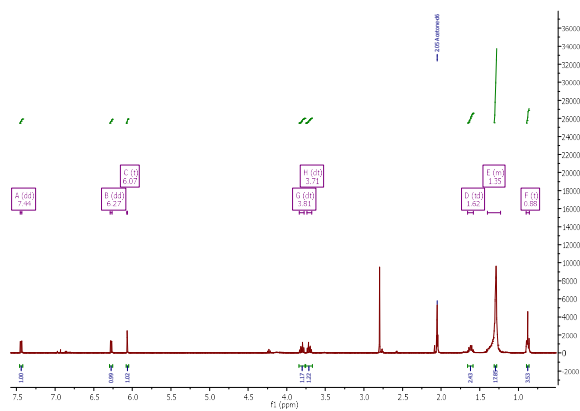


Appendix 61: $^1\text{H-NMR}$ of crude pseudo-transesterification 4 to 23 (Experiment 30).

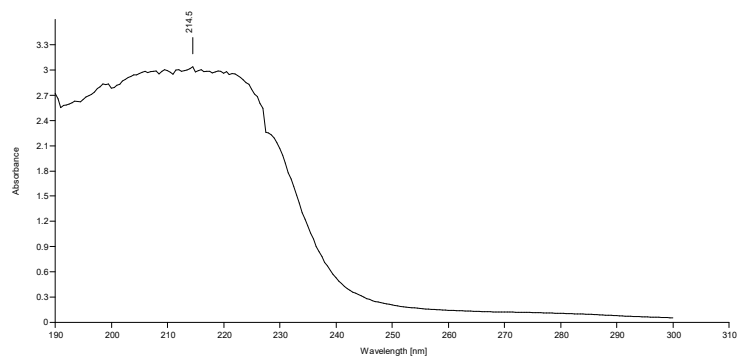
Appendices



Appendix 62: Expansion of Appendix 61.

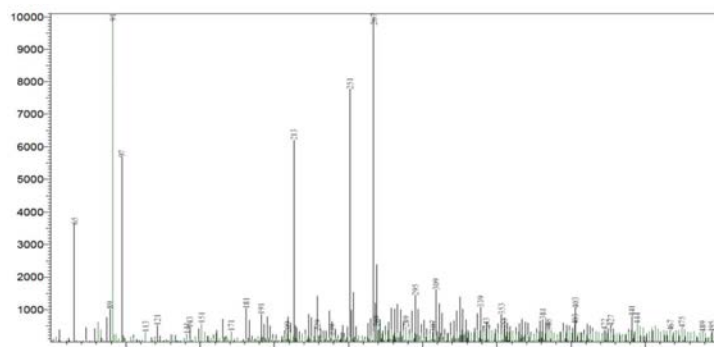


Appendix 63: $^1\text{H-NMR}$ spectra of 5-(Dodecyloxy) furan-2(5H)-one (23).

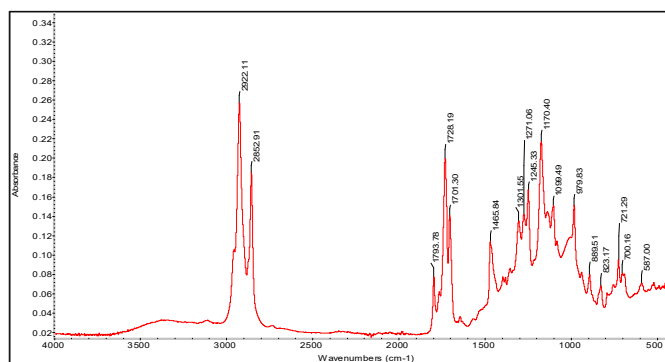


Appendix 64: UV/Vis-Spectrum of 5-(Dodecyloxy) furan-2(5H)-one (23).

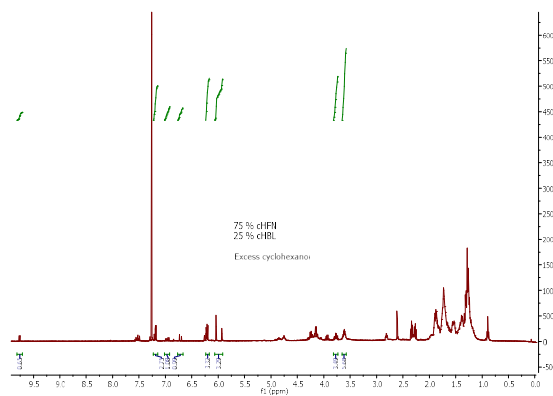
Appendices



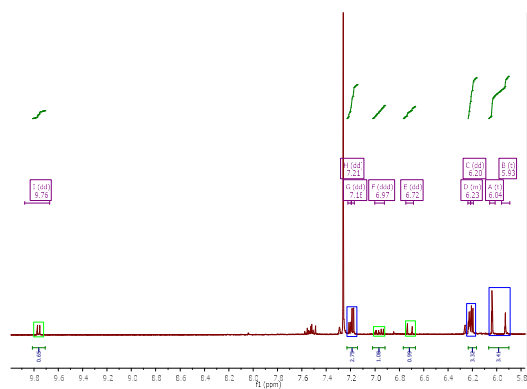
Appendix 65: MS-Spectrum of 5-(Dodecyloxy) furan-2(5H)-one (**23**).



Appendix 66: IR-Spectrum of 5-(Dodecyloxy) furan-2(5H)-one (**23**).

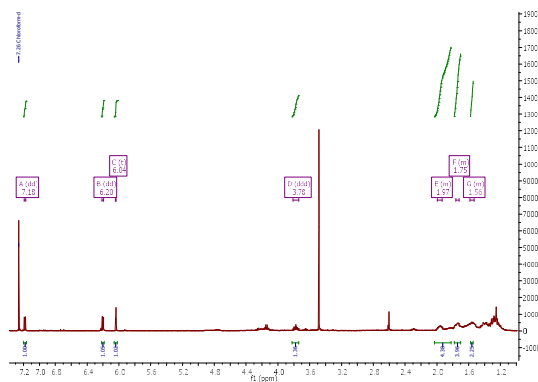


Appendix 67: ¹H-NMR of crude pseudo-transesterification **4** to **25** (Experiment 31).

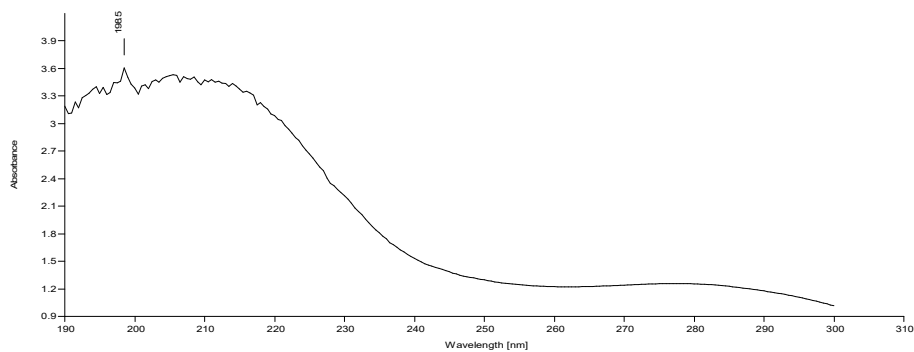


Appendix 68: Expansion of Appendix 67.

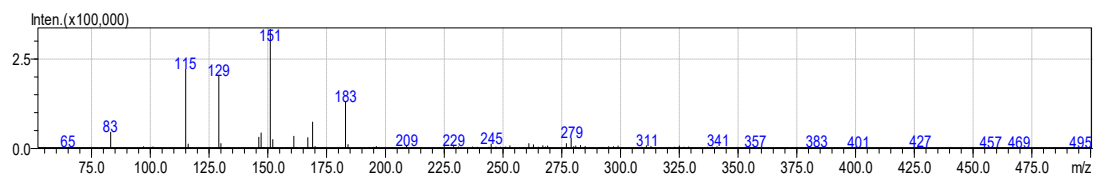
Appendices



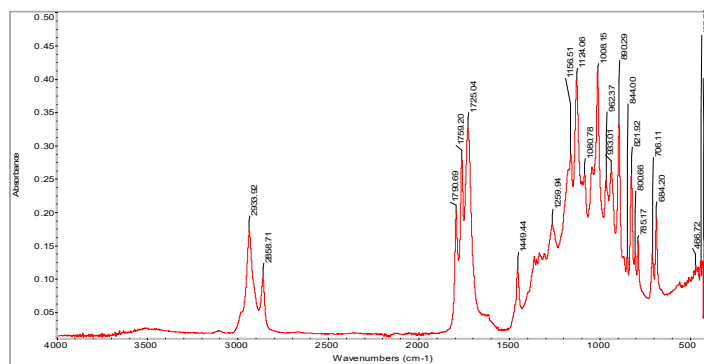
Appendix 69: $^1\text{H-NMR}$ of 5-cyclohexoxyfuran-2(5H)-one (25).



Appendix 70: UV/Vis-Spectrum of 5-cyclohexoxyfuran-2(5H)-one (25).

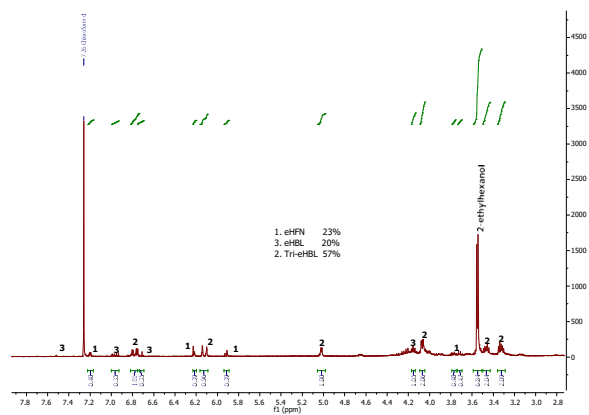


Appendix 71: MS-Spectrum of 5-cyclohexoxyfuran-2(5H)-one (25).

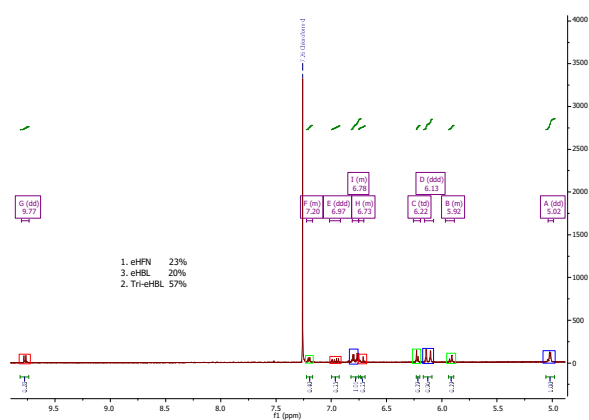


Appendix 72: IR-Spectrum of 5-cyclohexoxyfuran-2(5H)-one (25).

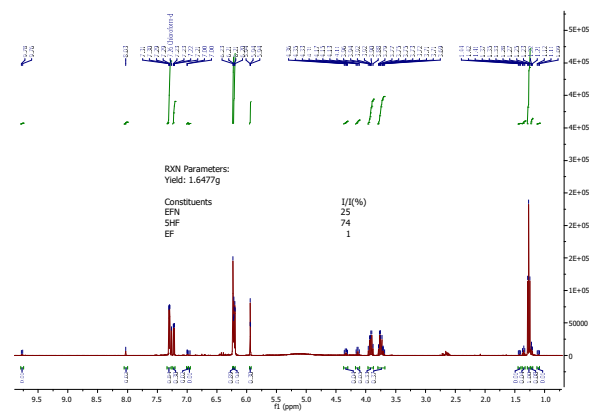
Appendices



Appendix 73: $^1\text{H-NMR}$ of crude pseudo-transesterification **4** to **27** (Experiment 32).

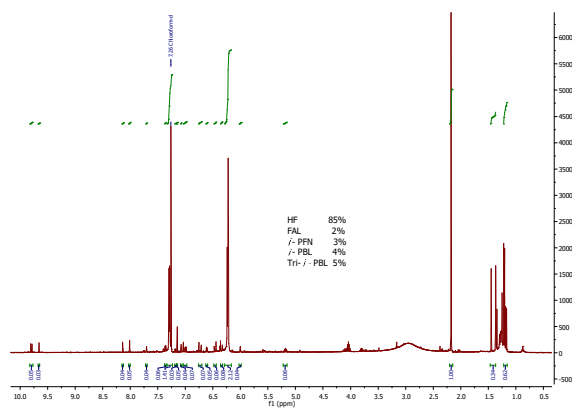


Appendix 74: Expansion of **Appendix 73**.

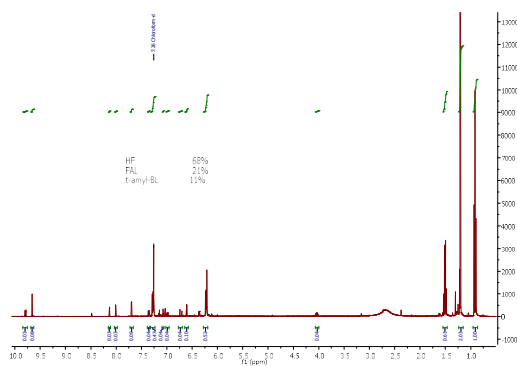


Appendix 75: $^1\text{H-NMR}$ of hydroxyfuranone obtained in EtOH (Experiment 34).

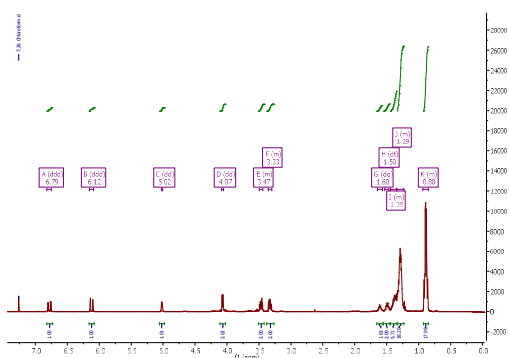
Appendices



Appendix 76: $^1\text{H-NMR}$ of hydroxyfuranone obtained in *i* – PrOH (Experiment 35).

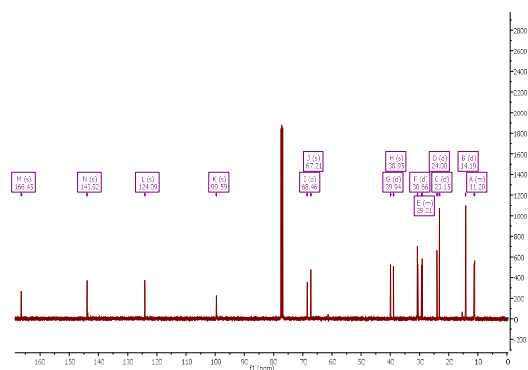


Appendix 77: $^1\text{H-NMR}$ of hydroxyfuranone obtained in *t* – AmOH (Experiment 36).

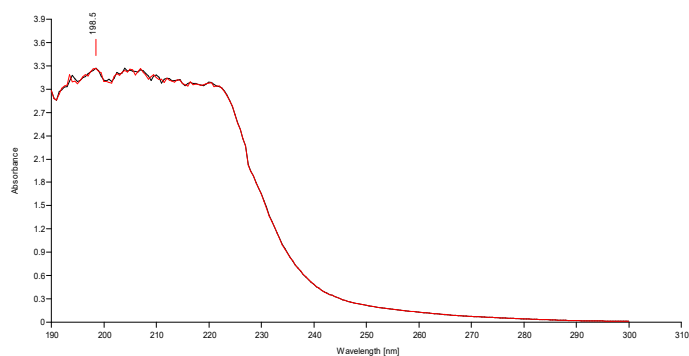


Appendix 78: $^1\text{H-NMR}$ of (*E*)-2-ethylhexyl 4, 4-bis ((2-ethylhexyl) oxy) but-2-enoate (**29**).

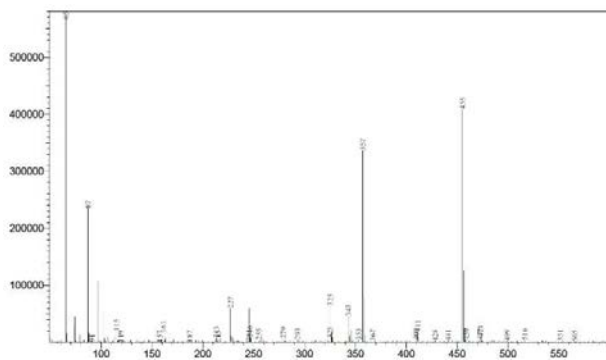
Appendices



Appendix 79: ^{13}C -NMR of (*E*)-2-ethylhexyl 4,4-bis((2-ethylhexyl)oxy)but-2-enoate (**29**).

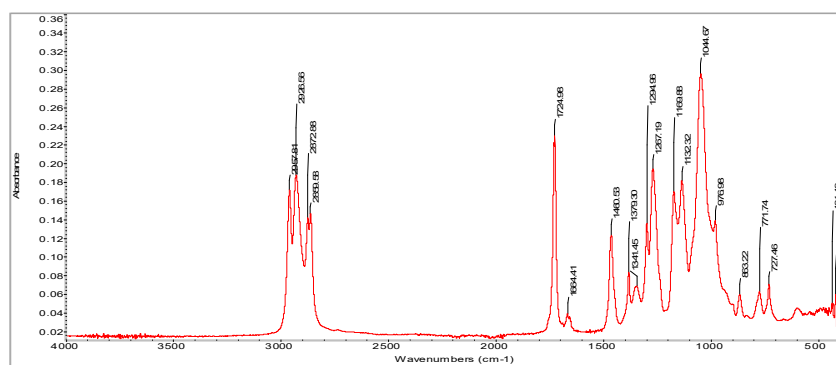


Appendix 80: UV/Vis-Spectrum of (*E*)-2-ethylhexyl 4,4-bis((2-ethylhexyl)oxy)but-2-enoate (**29**).



Appendix 81: MS-Spectrum of (*E*)-2-ethylhexyl 4,4-bis((2-ethylhexyl)oxy)but-2-enoate (**29**).

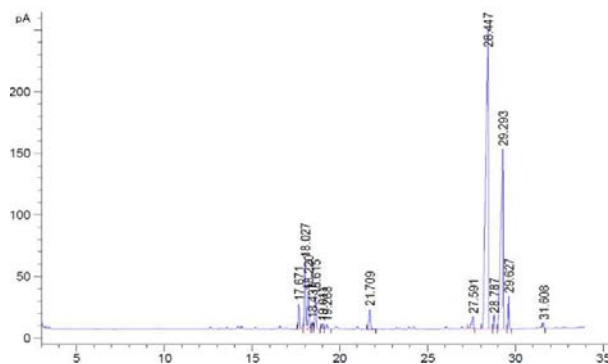
Appendices



Appendix 82: IR-Spectrum of (*E*)-2-ethylhexyl 4, 4-bis ((2-ethylhexyl) oxy) but-2-enoate (29).

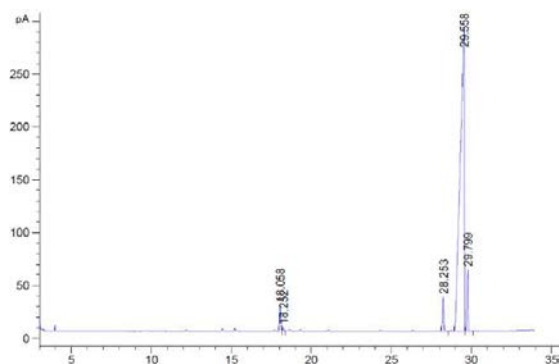
PMD isomers		R_t (min) M1		R_t (min) M2-3
<i>cis</i> -PMD 1		12.720		28.135
<i>trans</i> -PMD 1		13.319		28.035
<i>trans</i> -PMD 2		13.574		28.513
<i>cis</i> -PMD 2		12.991		29.344

Appendix 83: GC-chromatogram and retention times of PMD isomers using method M1 (left) and using methods M2 or M3 (right).

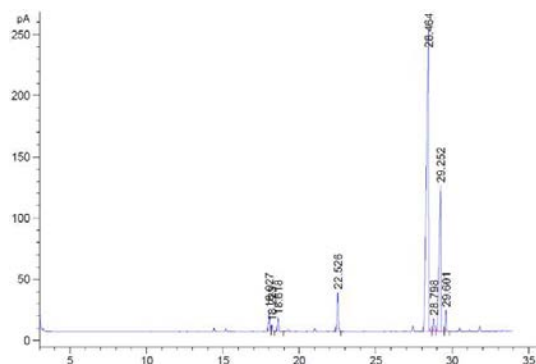


Appendix 84: GC-chromatogram of the crude PMD obtained from Experiment 58.

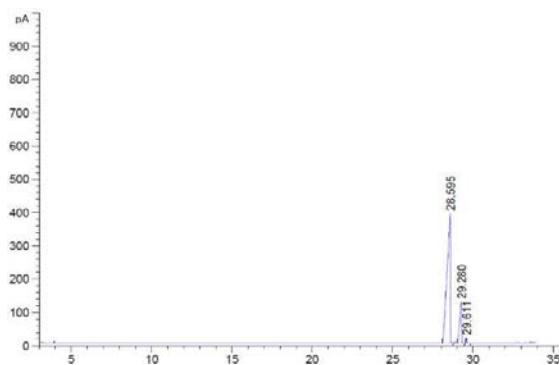
Appendices



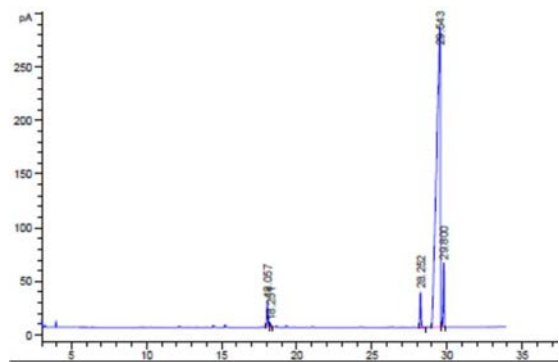
Appendix 85: GC-chromatogram of enriched *trans*-PMD obtained through recrystallization.



Appendix 86: GC-chromatogram of crude PMD in fraction F4 obtained by vacuum distillation from Experiment 59.

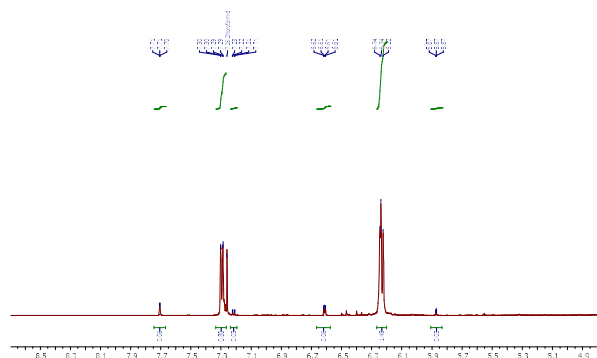


Appendix 87: GC-chromatogram of enriched PMD isomers from recrystallized F4.

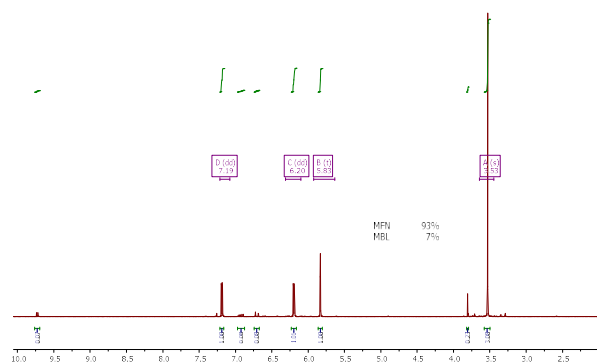


Appendix 88: GC-chromatogram of enriched *trans*-PMD in filtrate.

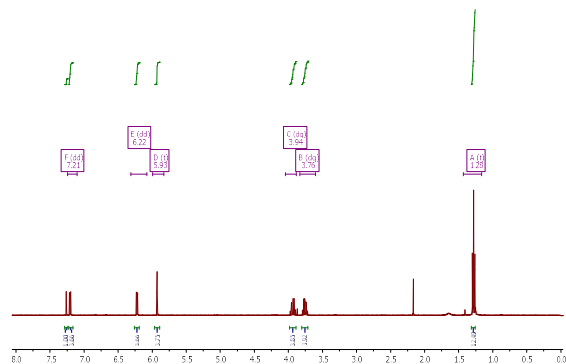
Appendices



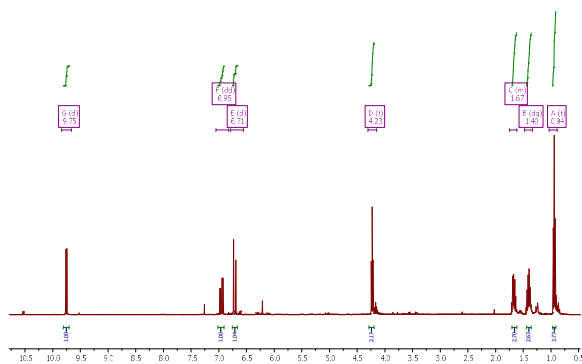
Appendix 89: ¹H-NMR of crude product obtained from Experiment 16.



Appendix 90: ¹H-NMR of crude product obtained from Experiment 18.

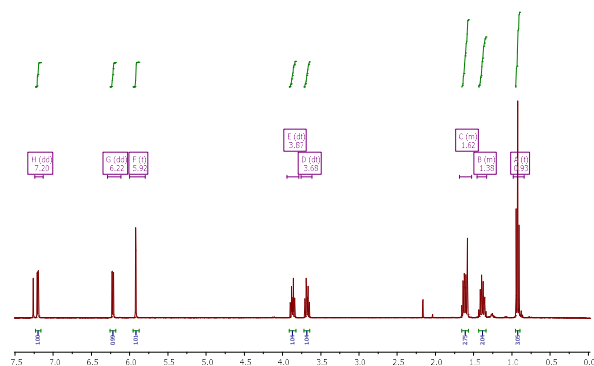


Appendix 91: ¹H-NMR of 5-ethoxyfuran-2(5H)-one (**4**) obtained from Experiment 19.

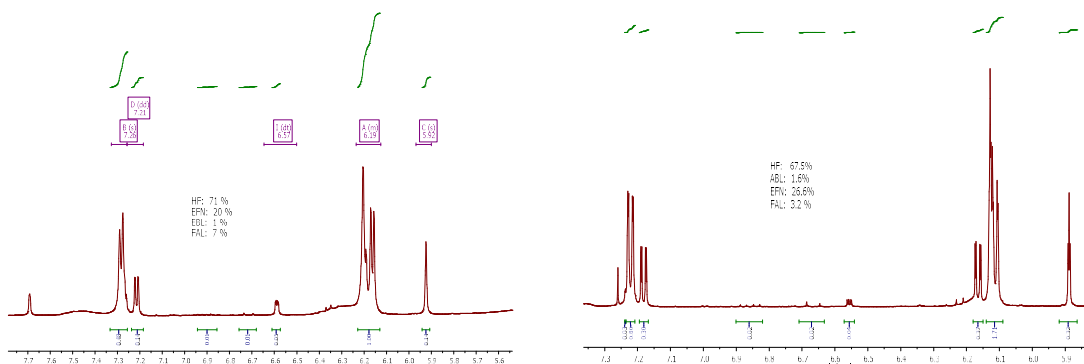


Appendix 92: ¹H-NMR of (*E*)-butyl 4-oxobut-2-enoate (**5**) obtained from Experiment 20.

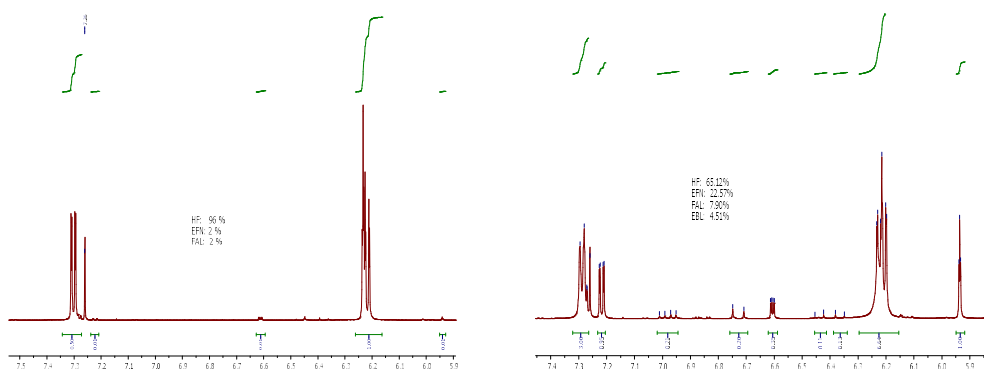
Appendices



Appendix 93: ¹H-NMR of 5-butoxyfuran-2(5H)-one (**9**) obtained from Experiment 21.

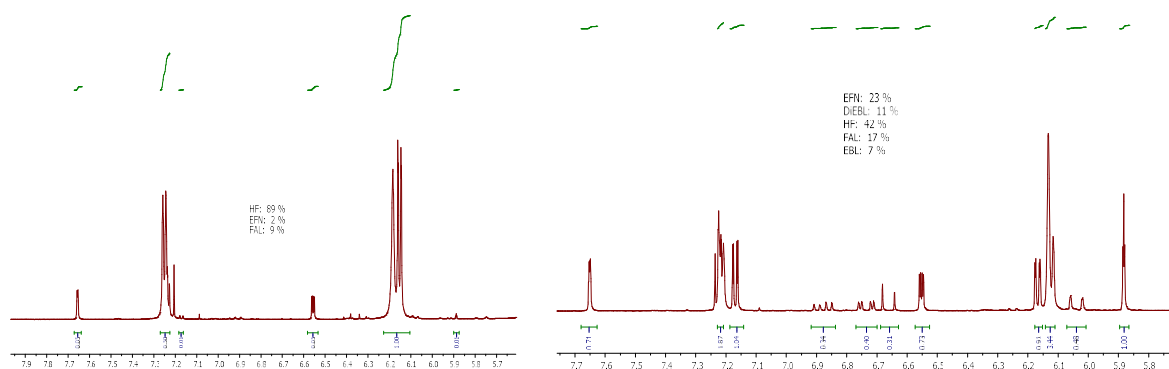


Appendix 94z: ¹H-NMR spectra at completion of reaction (left) and the resulting crude product (right) obtained from Experiment 21 (SR1).

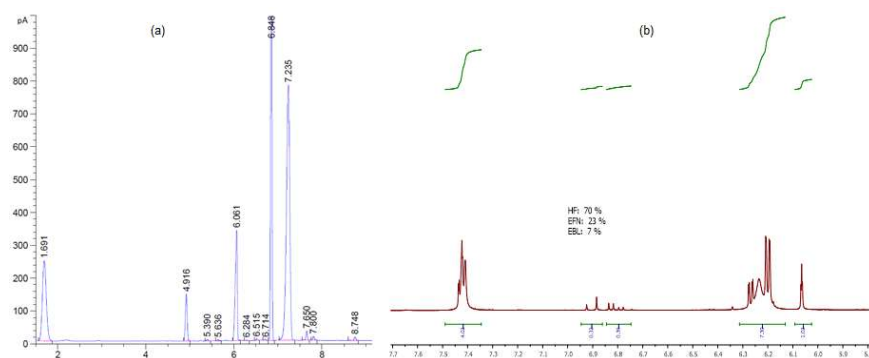


Appendix 95: ¹H-NMR spectra at completion of reaction (left) and the resulting crude product (right) obtained from Experiment 22 (SR2).

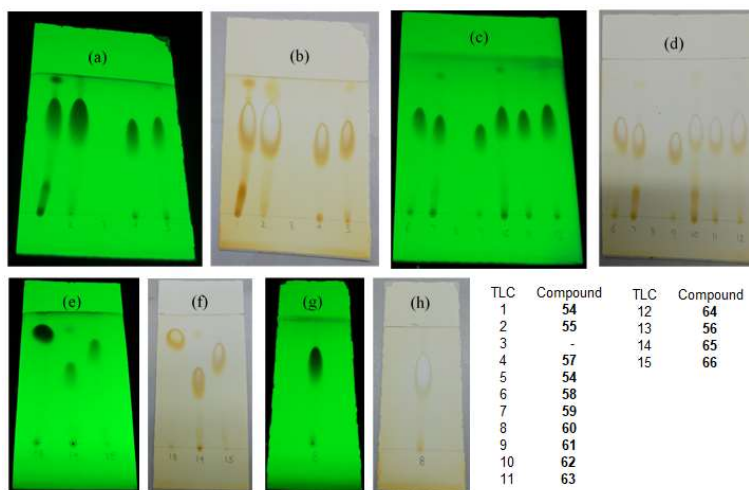
Appendices



Appendix 96: ¹H-NMR spectra at completion of reaction (left) and the resulting crude product (right) obtained from Experiment 23 (SR3).

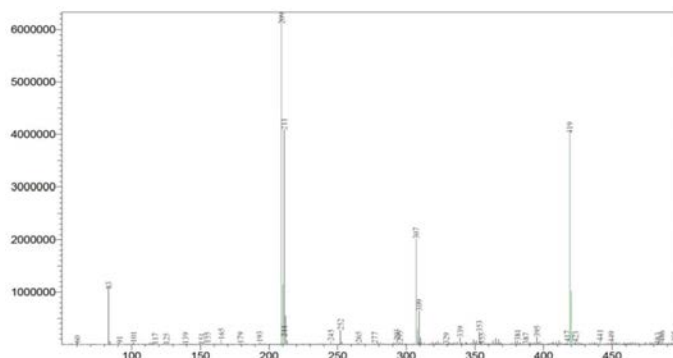


Appendix 97: GC-chromatogram at completion of reaction (left) and ¹H-NMR spectrum of the resulting crude product (right) obtained from Experiment 24 (SR4).

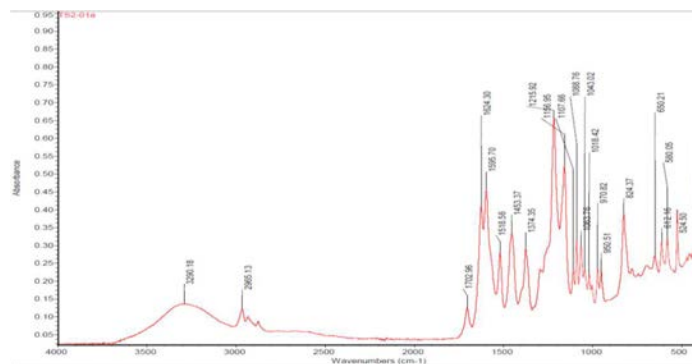


Appendix 98: TLC-plates of the β-triketone precursors for flash chromatography separation.

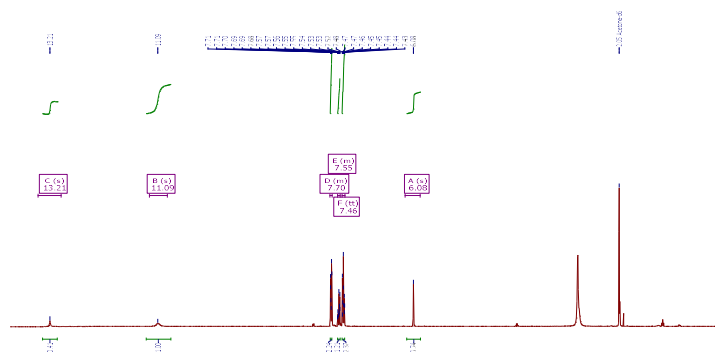
Appendices



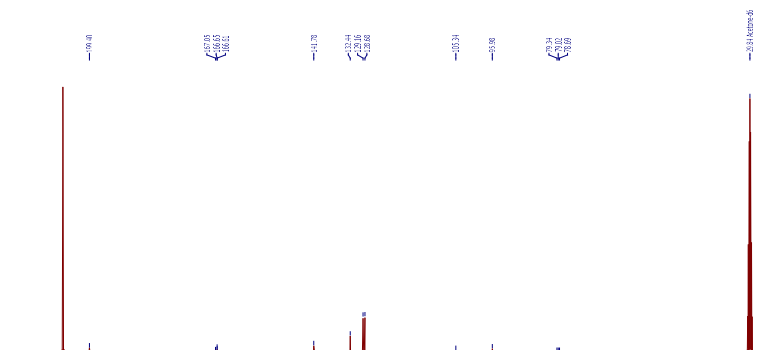
Appendix 107: MS-Spectrum of 2-methyl-1-(2, 4, 6-trihydroxyphenyl) butan-1-one (**42**).



Appendix 108: IR-Spectrum of 2-methyl-1-(2, 4, 6-trihydroxyphenyl) butan-1-one (**42**).

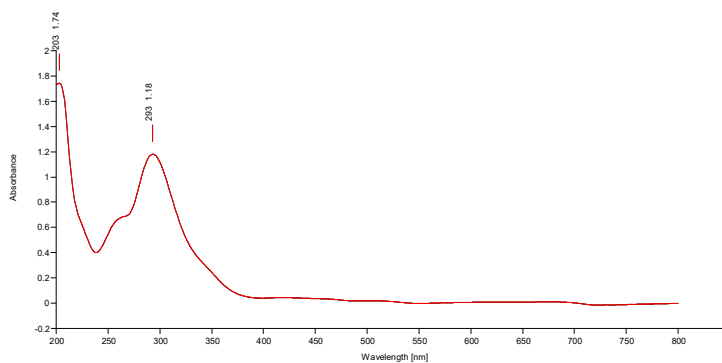


Appendix 109: ¹H-NMR of phenyl (2, 4, 6-trihydroxyphenyl) methanone (**43**).

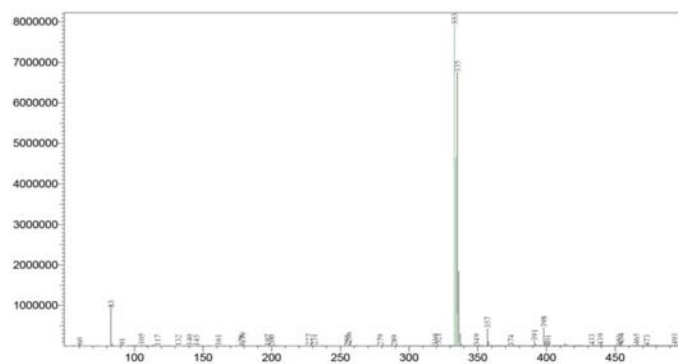


Appendix 110: ¹³C-NMR of phenyl (2, 4, 6-trihydroxyphenyl) methanone (**43**).

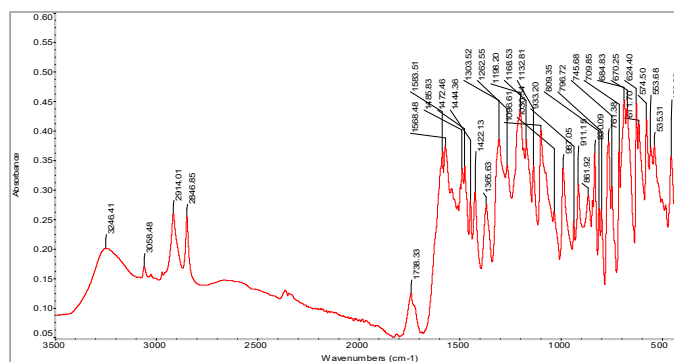
Appendices



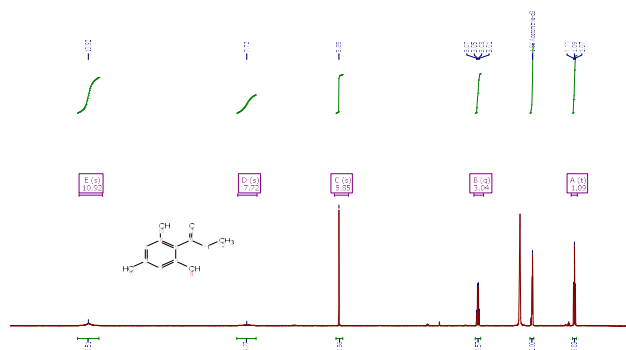
Appendix 111: UV/Vis-Spectrum of phenyl (2, 4, 6-trihydroxyphenyl) methanone (**43**).



Appendix 112: MS-Spectrum of phenyl (2, 4, 6-trihydroxyphenyl) methanone (**43**).

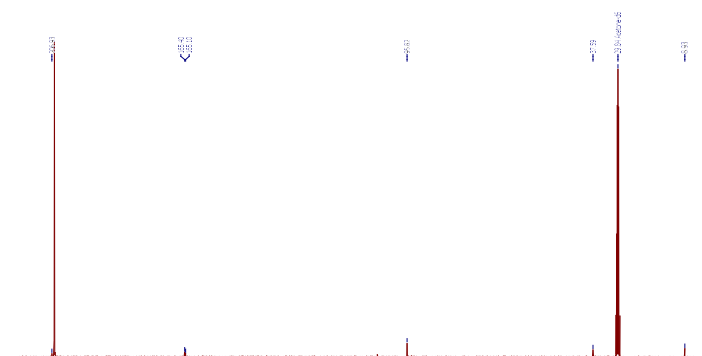


Appendix 113: IR-Spectrum of phenyl (2, 4, 6-trihydroxyphenyl) methanone (**43**).

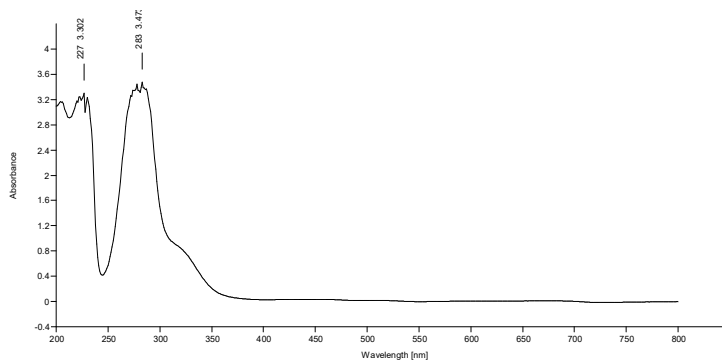


Appendix 114: $^1\text{H-NMR}$ of 1-(2, 4, 6-trihydroxyphenyl) propan-1-one (**44**).

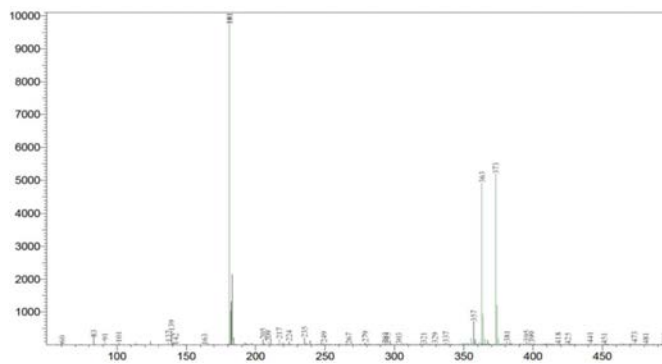
Appendices



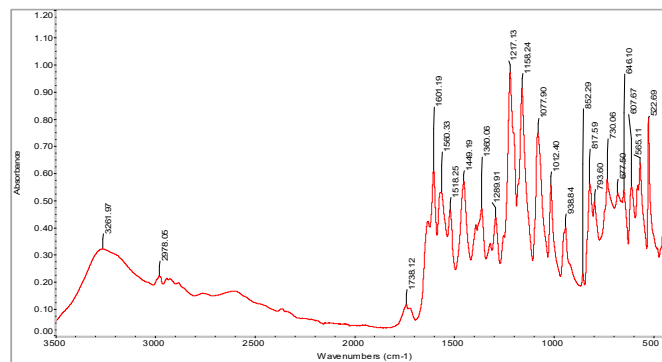
Appendix 115: ^{13}C -NMR of 1-(2, 4, 6-trihydroxyphenyl) propan-1-one (**44**).



Appendix 116: UV/Vis-Spectrum of 1-(2, 4, 6-trihydroxyphenyl) propan-1-one (**44**).

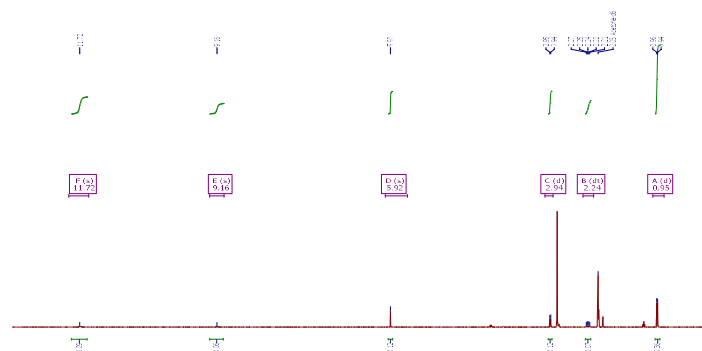


Appendix 117: MS-Spectrum of 1-(2, 4, 6-trihydroxyphenyl) propan-1-one (**44**).

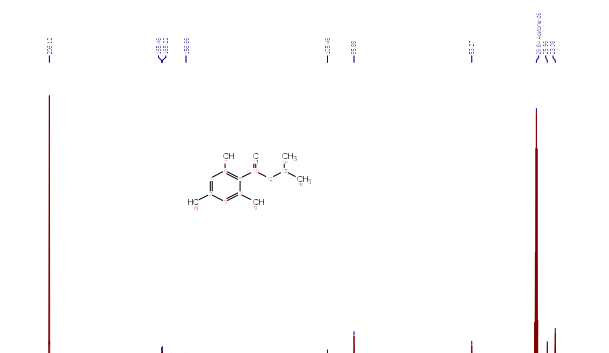


Appendix 118: IR-Spectrum of 1-(2, 4, 6-trihydroxyphenyl) propan-1-one (**44**).

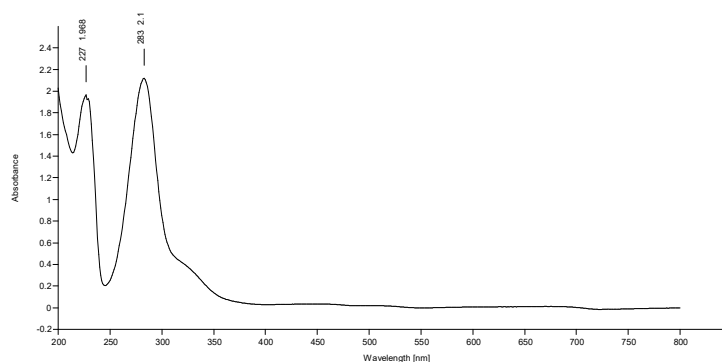
Appendices



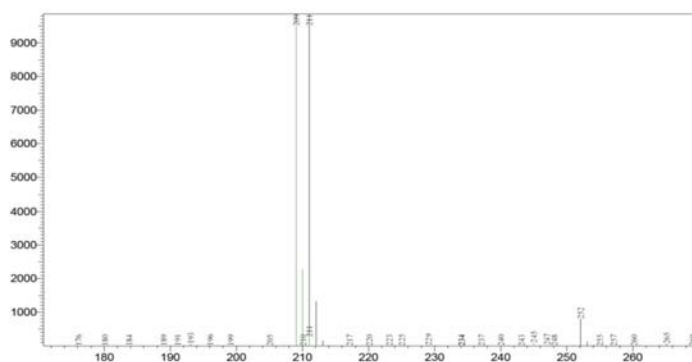
Appendix 119: ¹H-NMR of 3-methyl-1-(2,4,6-trihydroxyphenyl) butan-1-one (45).



Appendix 120: ¹³C-NMR of 3-methyl-1-(2,4,6-trihydroxyphenyl) butan-1-one (45).

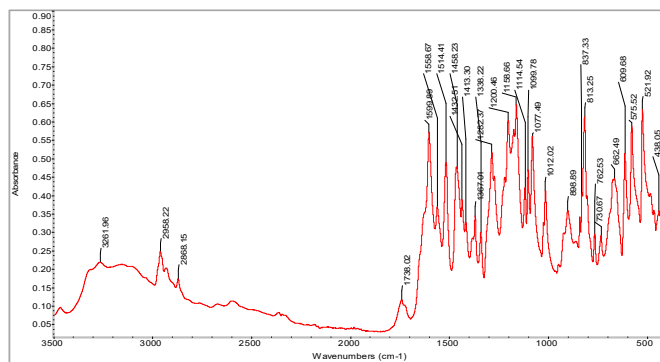


Appendix 121: UV/Vis-Spectrum of 3-methyl-1-(2,4,6-trihydroxyphenyl) butan-1-one (45).

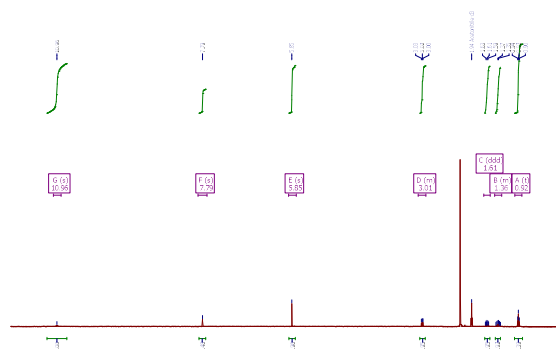


Appendix 122: MS-Spectrum of 3-methyl-1-(2,4,6-trihydroxyphenyl) butan-1-one (45).

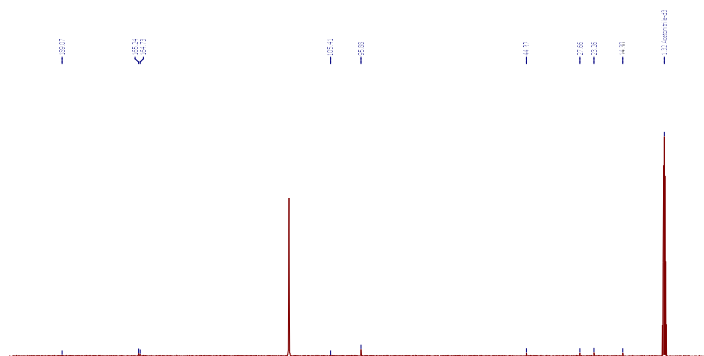
Appendices



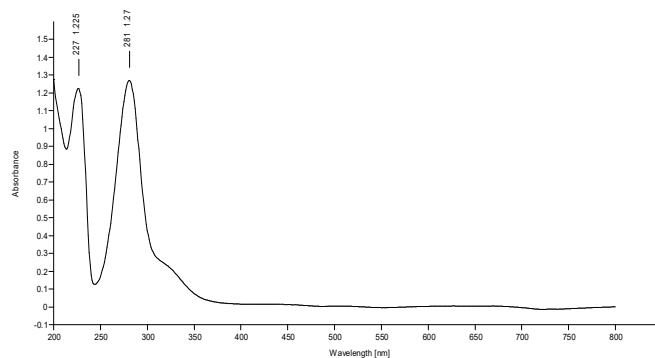
Appendix 123: IR-Spectrum of 3-methyl-1-(2, 4, 6-trihydroxyphenyl) butan-1-one (45).



Appendix 124: $^1\text{H-NMR}$ of 1-(2, 4, 6-trihydroxyphenyl) pentan-1-one (46).

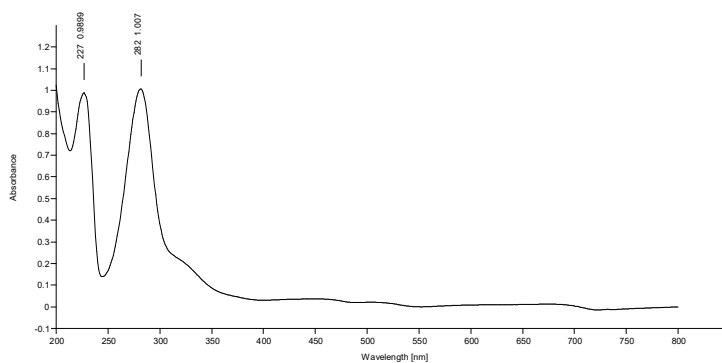


Appendix 125: $^{13}\text{C-NMR}$ of 1-(2, 4, 6-trihydroxyphenyl) pentan-1-one (46).

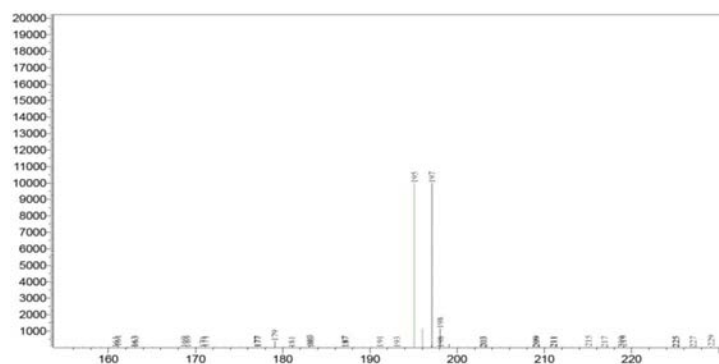


Appendix 126: UV/Vis-Spectrum of 1-(2, 4, 6-trihydroxyphenyl) pentan-1-one (46).

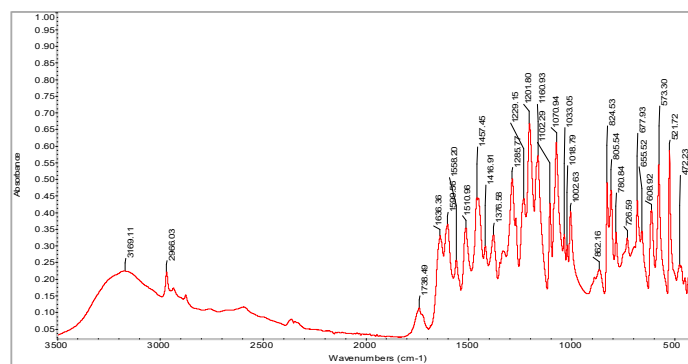
Appendices



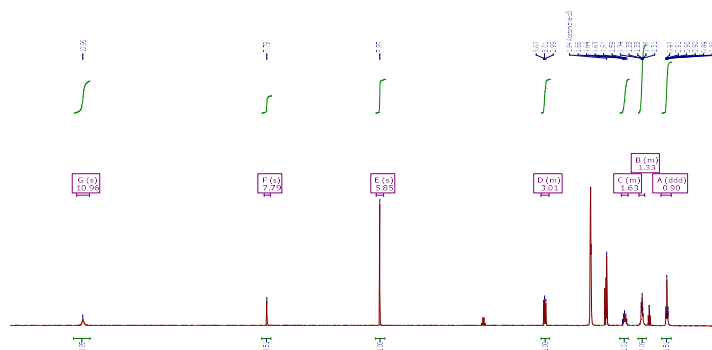
Appendix 131: UV/Vis-Spectrum of 1-(2, 4, 6-trihydroxyphenyl) butan-1-one (47).



Appendix 132: MS-Spectrum of 1-(2, 4, 6-trihydroxyphenyl) butan-1-one (47).

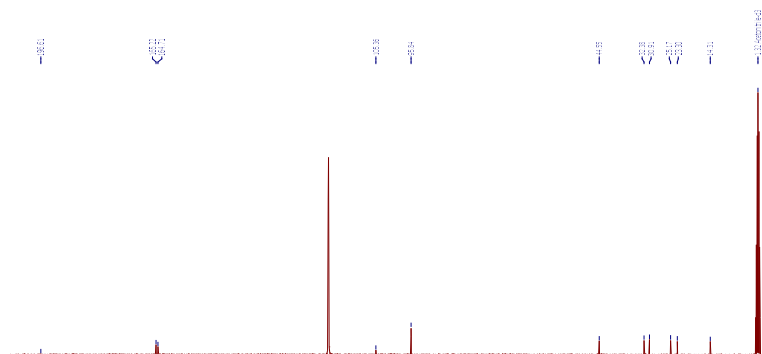


Appendix 133: IR-Spectrum of 1-(2, 4, 6-trihydroxyphenyl) butan-1-one (47).

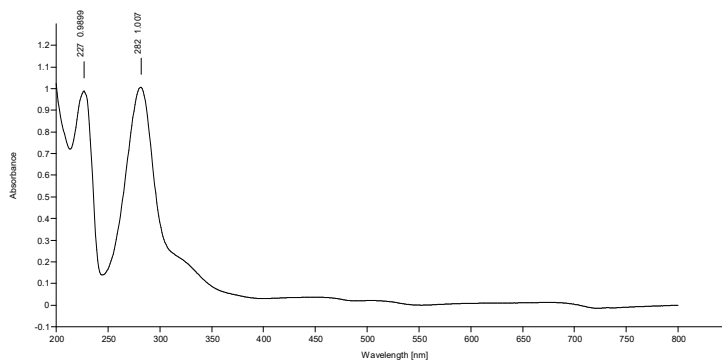


Appendix 134: $^1\text{H-NMR}$ of 1-(2, 4, 6-trihydroxyphenyl) hexan-1-one (48).

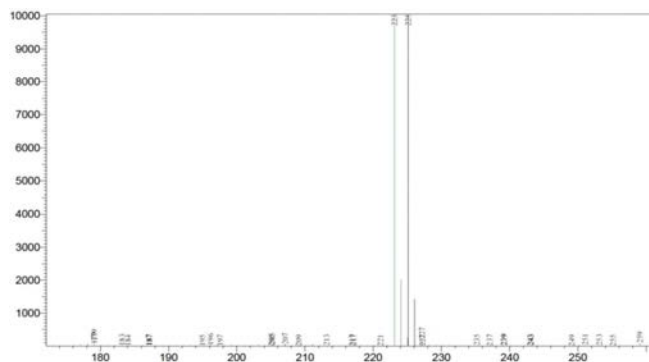
Appendices



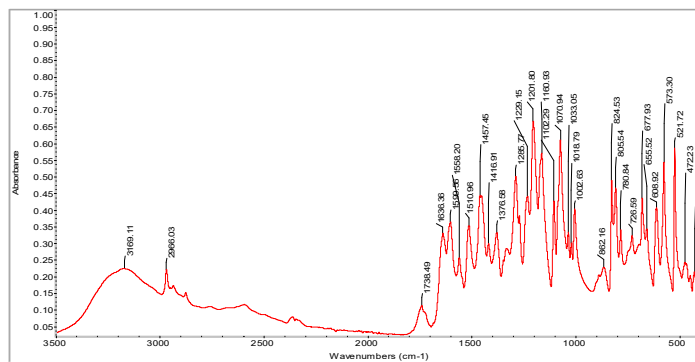
Appendix 135: ^{13}C -NMR of 1-(2, 4, 6-trihydroxyphenyl) hexan-1-one (48).



Appendix 136: UV/Vis-Spectrum of 1-(2, 4, 6-trihydroxyphenyl) hexan-1-one (48).

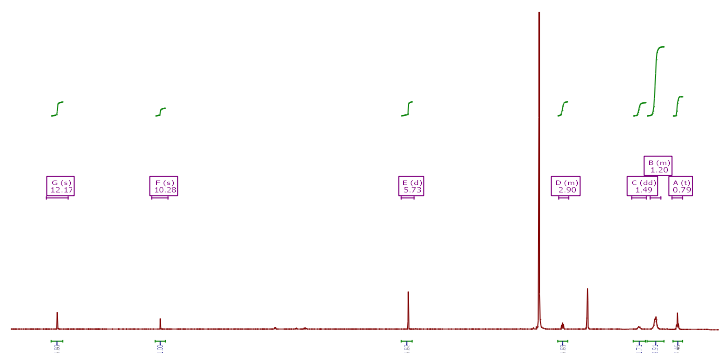


Appendix 137: MS-Spectrum of 1-(2, 4, 6-trihydroxyphenyl) hexan-1-one (48).

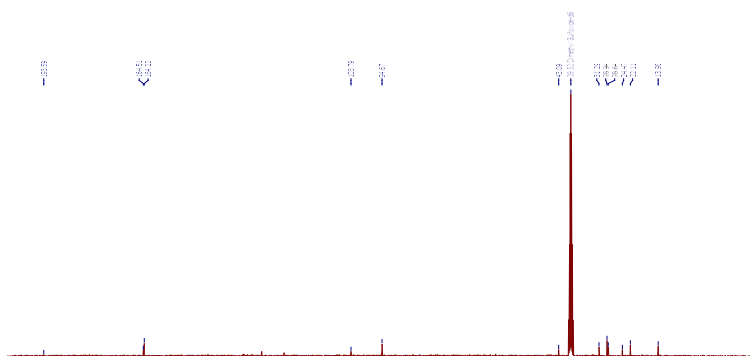


Appendix 138: IR-Spectrum of 1-(2, 4, 6-trihydroxyphenyl) hexan-1-one (48).

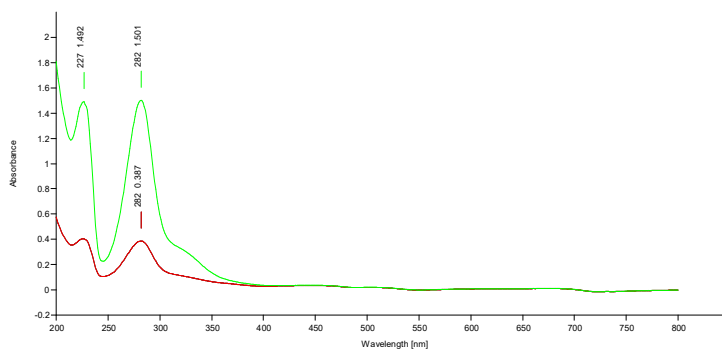
Appendices



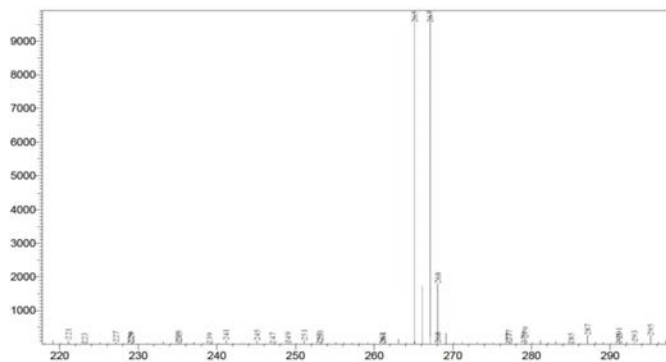
Appendix 139: $^1\text{H-NMR}$ of 1-(2, 4, 6-trihydroxyphenyl) nonan-1-one (**49**).



Appendix 140: $^{13}\text{C-NMR}$ of 1-(2, 4, 6-trihydroxyphenyl) nonan-1-one (**49**).

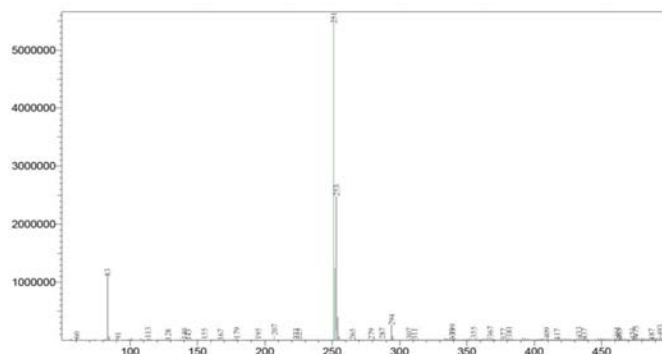


Appendix 141: UV/Vis-Spectrum of 1-(2, 4, 6-trihydroxyphenyl) nonan-1-one (**49**).

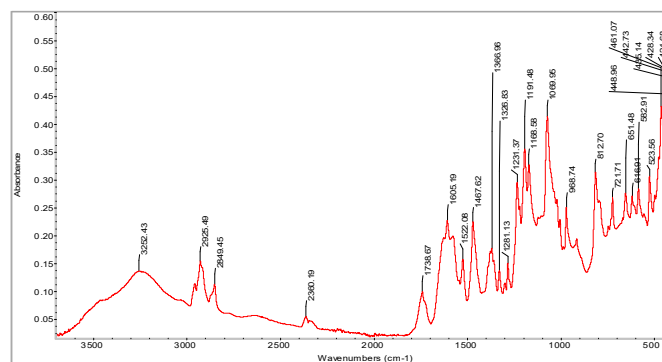


Appendix 142: MS-Spectrum of 1-(2, 4, 6-trihydroxyphenyl) nonan-1-one (**49**).

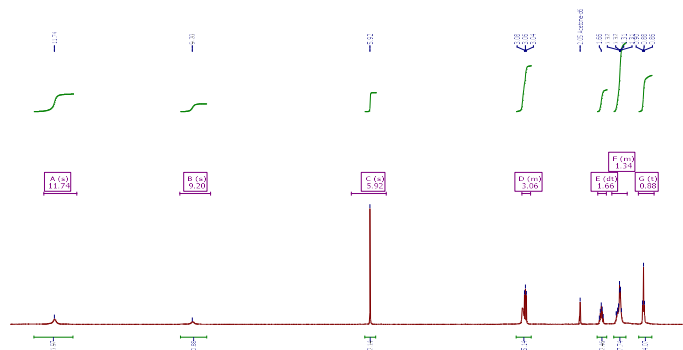
Appendices



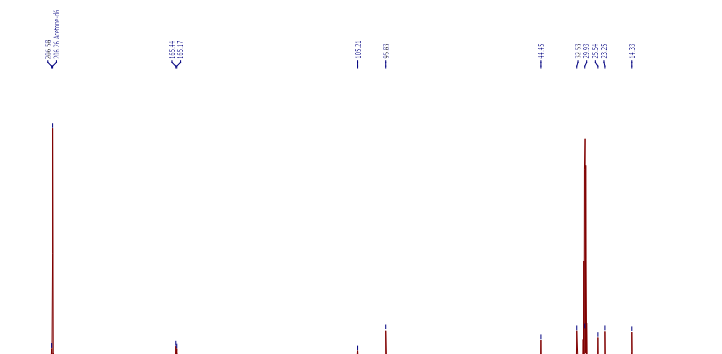
Appendix 147: MS-Spectrum of 1-(2, 4, 6-trihydroxyphenyl) octan-1-one (**50**).



Appendix 148: IR-Spectrum of 1-(2, 4, 6-trihydroxyphenyl) octan-1-one (**50**).

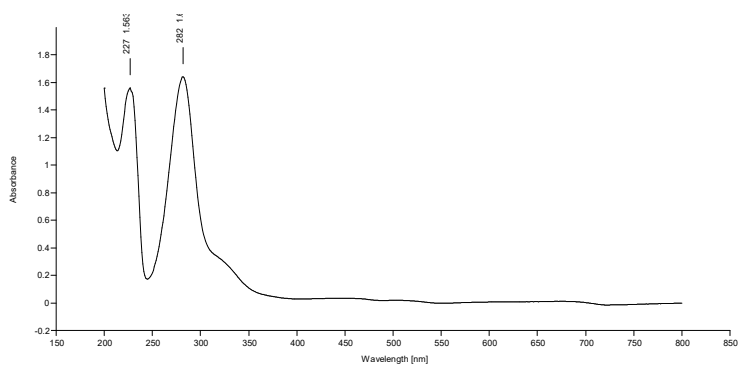


Appendix 149: ¹H-NMR of 1-(2, 4, 6-trihydroxyphenyl) heptan-1-one (**51**).

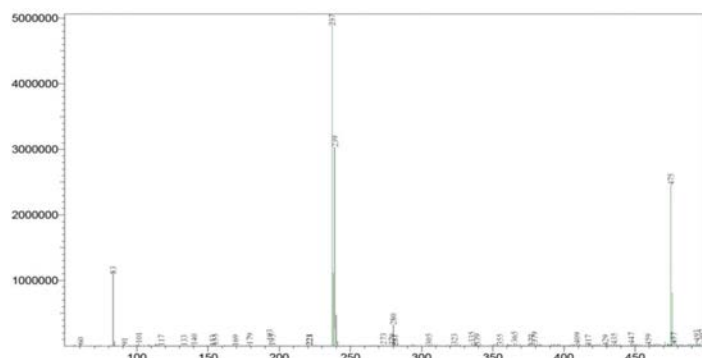


Appendix 150: ¹³C-NMR of 1-(2, 4, 6-trihydroxyphenyl) heptan-1-one (**51**).

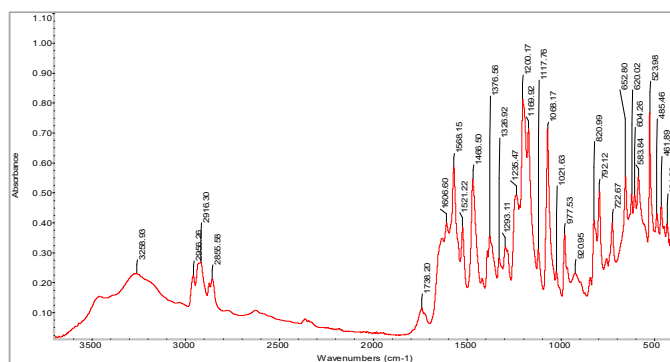
Appendices



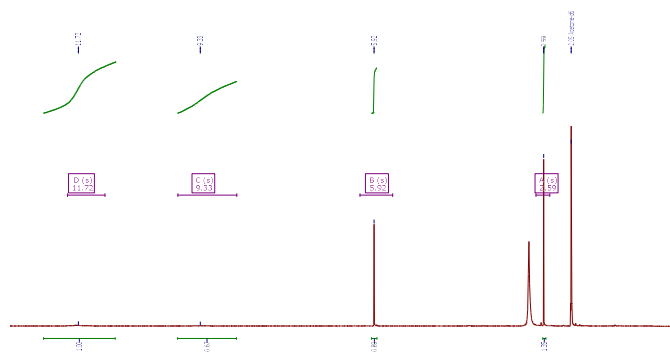
Appendix 151: UV/Vis-Spectrum of 1-(2, 4, 6-trihydroxyphenyl) heptan-1-one (**51**).



Appendix 152: MS-Spectrum of 1-(2, 4, 6-trihydroxyphenyl) heptan-1-one (**51**).

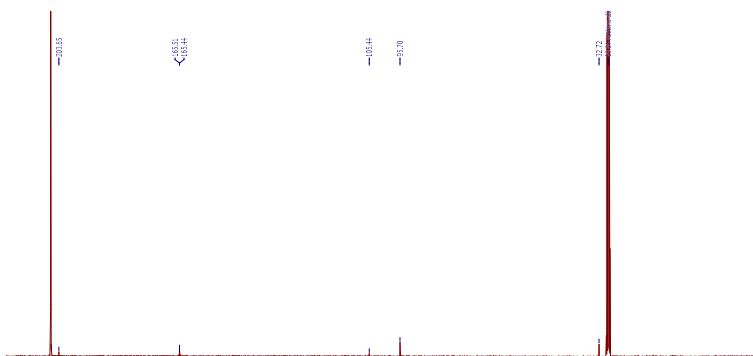


Appendix 153: IR-Spectrum of 1-(2, 4, 6-trihydroxyphenyl) heptan-1-one (**51**).

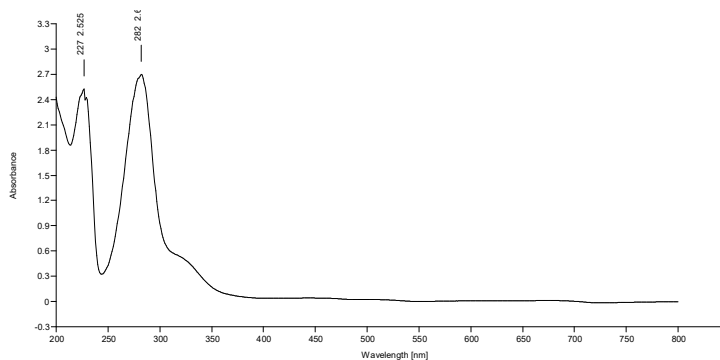


Appendix 154: $^1\text{H-NMR}$ of 1-(2, 4, 6-trihydroxyphenyl) ethanone (**52**).

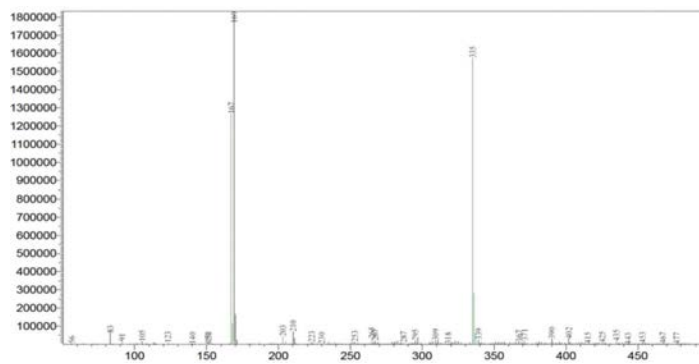
Appendices



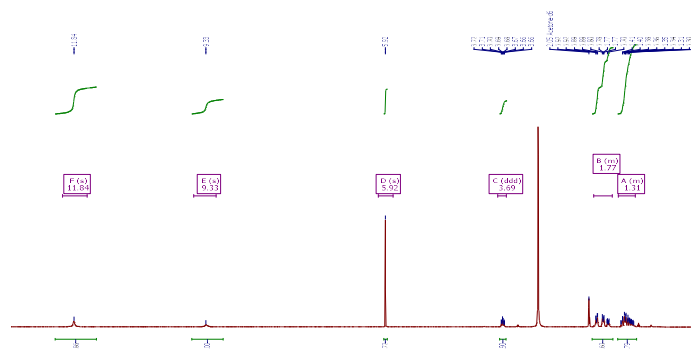
Appendix 155: ^{13}C -NMR of 1-(2, 4, 6-trihydroxyphenyl) ethanone (**52**).



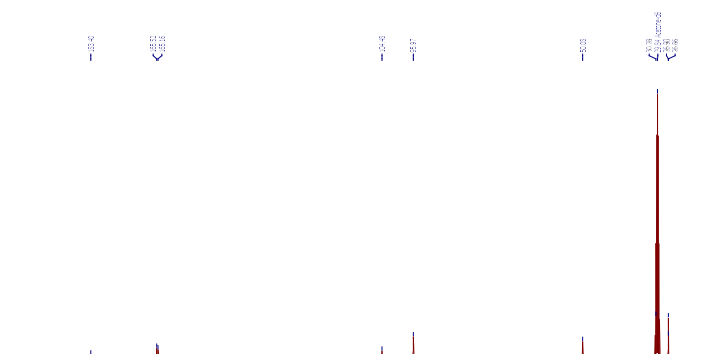
Appendix 156: UV/Vis-Spectrum of 1-(2, 4, 6-trihydroxyphenyl) ethanone (**52**).



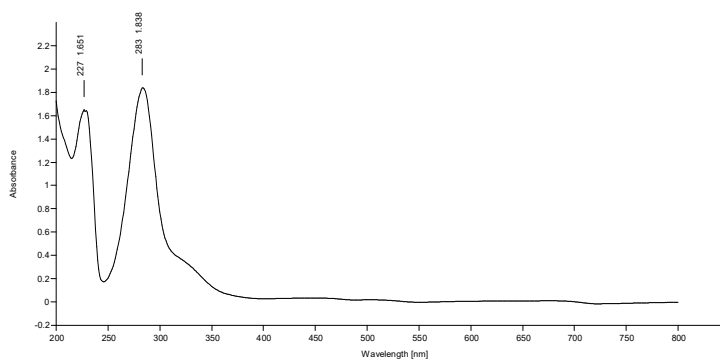
Appendices



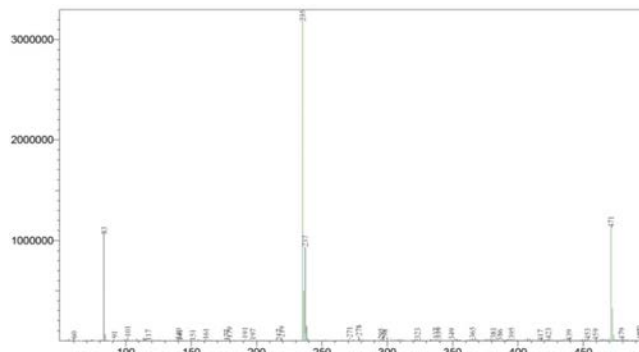
Appendix 159: $^1\text{H-NMR}$ of cyclohexyl (2, 4, 6-trihydroxyphenyl) methanone (**53**).



Appendix 160: $^{13}\text{C-NMR}$ of cyclohexyl (2, 4, 6-trihydroxyphenyl) methanone (**53**).

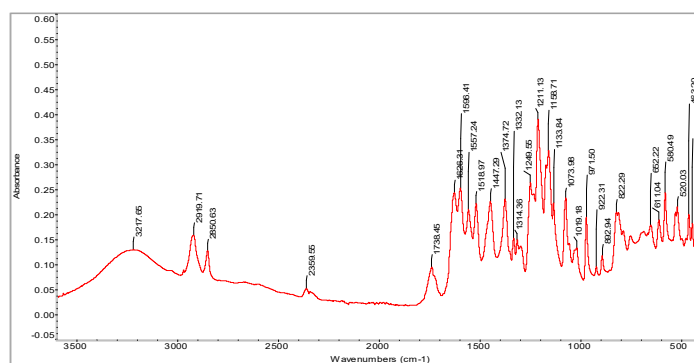


Appendix 161: UV/Vis-Spectrum of cyclohexyl (2, 4, 6-trihydroxyphenyl) methanone (**53**).

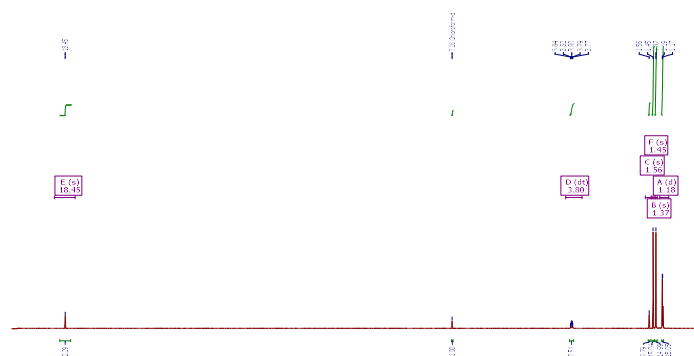


Appendix 162: MS-Spectrum of cyclohexyl (2, 4, 6-trihydroxyphenyl) methanone (**53**).

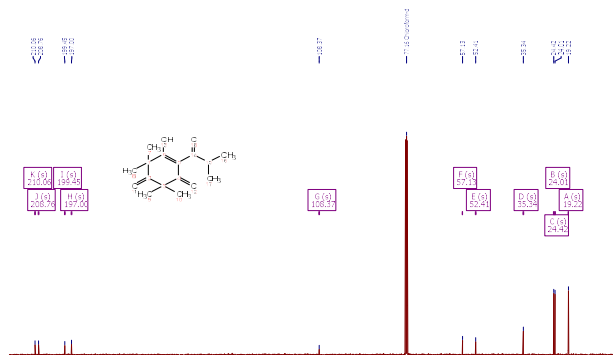
Appendices



Appendix 163: IR-Spectrum of cyclohexyl (2, 4, 6-trihydroxyphenyl) methanone (**53**).

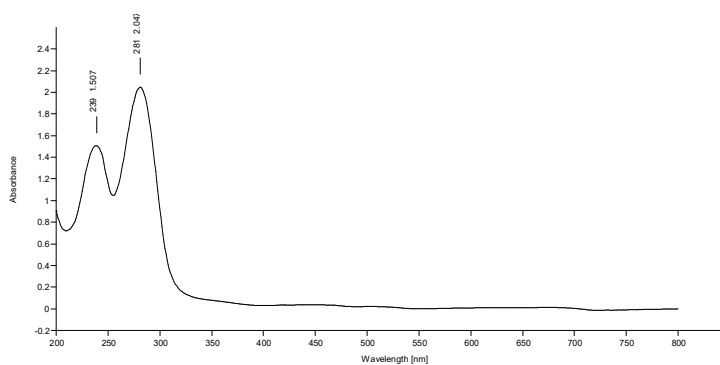


Appendix 164: $^1\text{H-NMR}$ of 5-hydroxy-4-isobutyryl-2, 2, 6, 6-tetramethylcyclohex-4-ene-1, 3-dione (**54**).

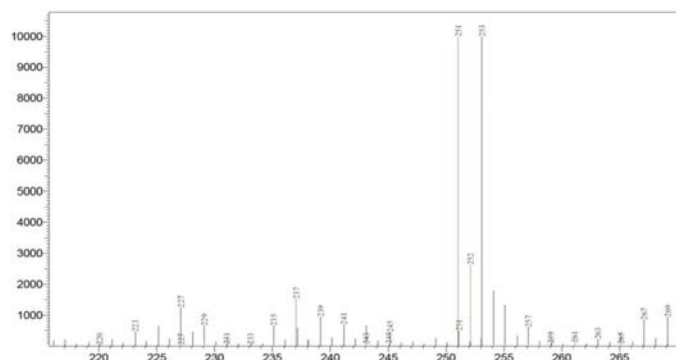


Appendix 165: $^{13}\text{C-NMR}$ of 5-hydroxy-4-isobutyryl-2, 2, 6, 6-tetramethylcyclohex-4-ene-1, 3-dione (**54**).

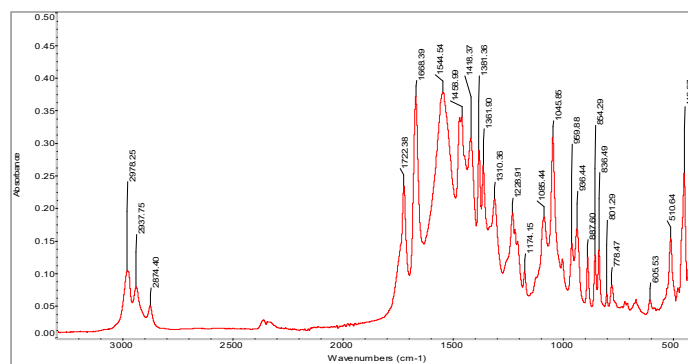
Appendices



Appendix 166: UV/Vis-Spectrum of 5-hydroxy-4-isobutyryl-2, 2, 6, 6-tetramethylcyclohex-4-ene-1, 3-dione (**54**).

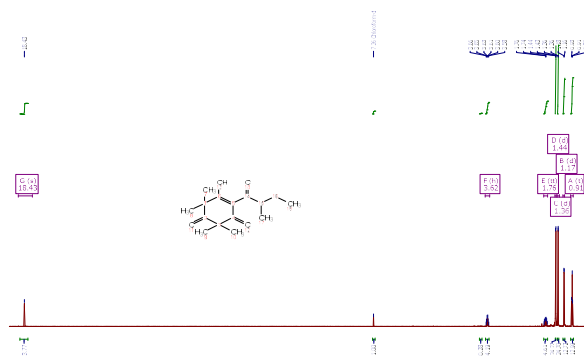


Appendix 167: MS-Spectrum of 5-hydroxy-4-isobutyryl-2, 2, 6, 6-tetramethylcyclohex-4-ene-1, 3-dione (**54**).

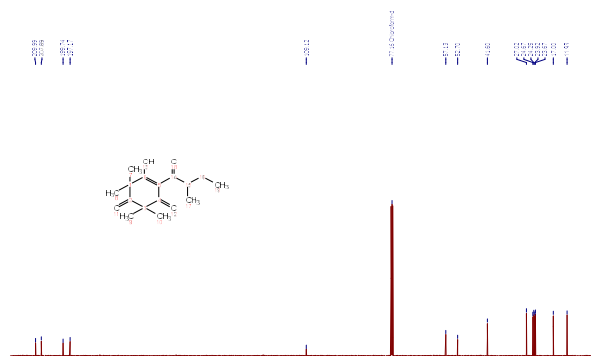


Appendix 168: IR-Spectrum of 5-hydroxy-4-isobutyryl-2, 2, 6, 6-tetramethylcyclohex-4-ene-1, 3-dione (**54**).

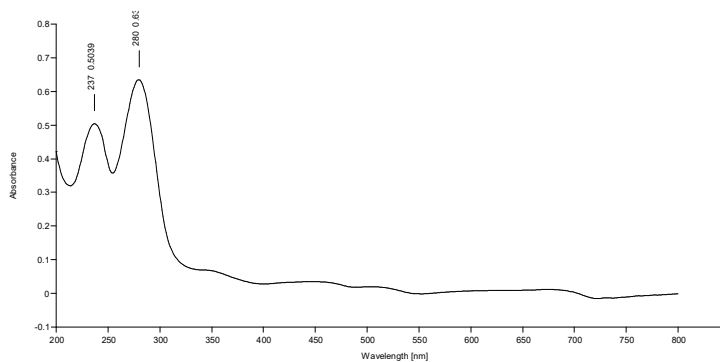
Appendices



Appendix 169: $^1\text{H-NMR}$ of 5-hydroxy-2, 2, 6, 6-tetramethyl-4-(2-methylbutanoyl) cyclohex-4-ene-1, 3-dione (**55**).

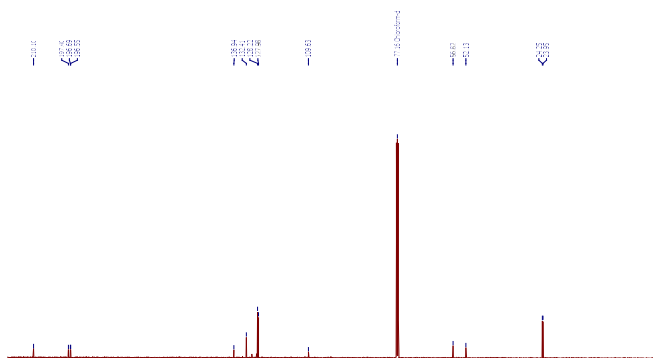


Appendix 170: $^{13}\text{C-NMR}$ of 5-hydroxy-2, 2, 6, 6-tetramethyl-4-(2-methylbutanoyl) cyclohex-4-ene-1, 3-dione (**55**).

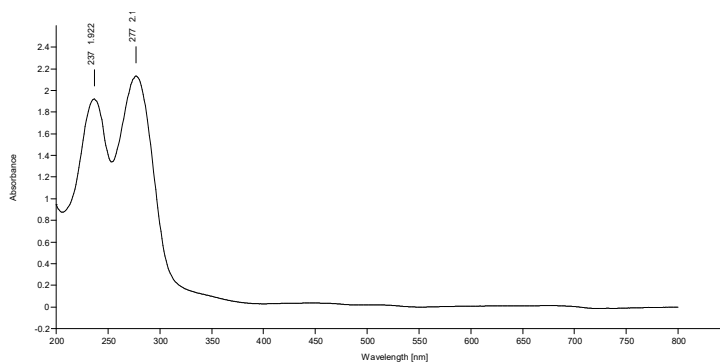


Appendix 171: UV/Vis-Spectrum of 5-hydroxy-2, 2, 6, 6-tetramethyl-4-(2-methylbutanoyl) cyclohex-4-ene-1, 3-dione (**55**).

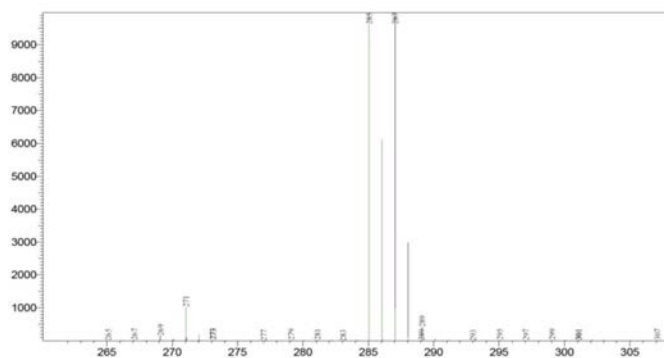
Appendices



Appendix 175: ^{13}C -NMR of 4-benzoyl-5-hydroxy-2,2,6,6-tetramethylcyclohex-4-ene-1,3-dione (**56**).

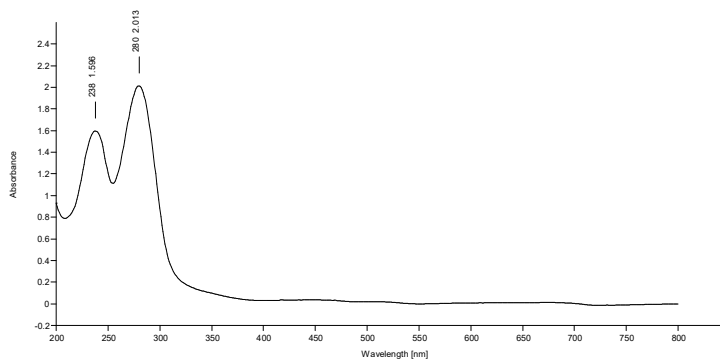


Appendix 176: UV/Vis-Spectrum of 4-benzoyl-5-hydroxy-2,2,6,6-tetramethylcyclohex-4-ene-1,3-dione (**56**).

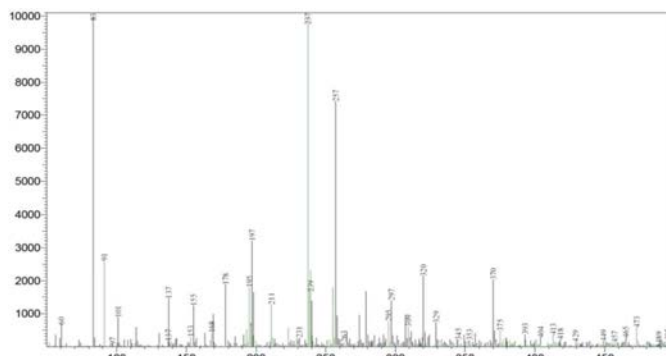


Appendix 177: MS-Spectrum of 4-benzoyl-5-hydroxy-2,2,6,6-tetramethylcyclohex-4-ene-1,3-dione (**56**).

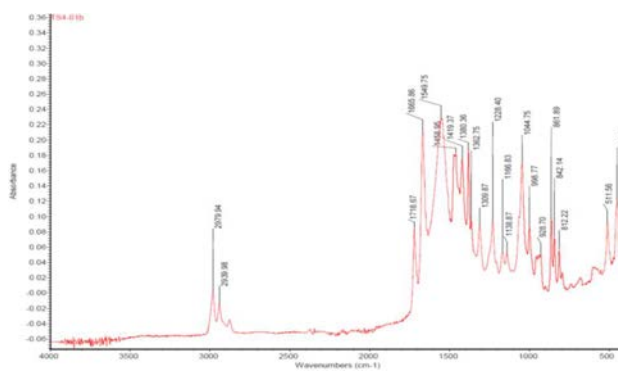
Appendices



Appendix 181: UV/Vis-Spectrum of 5-hydroxy-2,2,6,6-tetramethyl-4-propionylcyclohex-4-ene-1,3-dione (**57**).

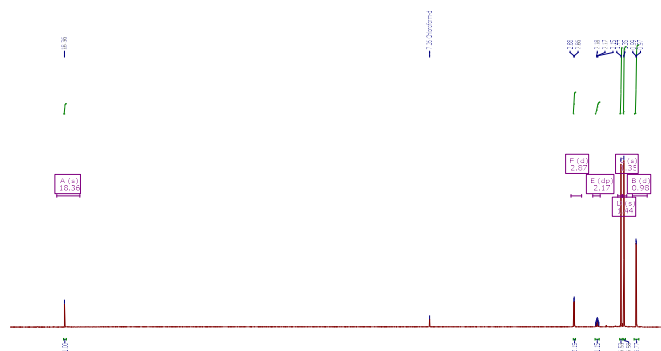


Appendix 182: MS-Spectrum of 5-hydroxy-2,2,6,6-tetramethyl-4-propionylcyclohex-4-ene-1,3-dione (**57**).

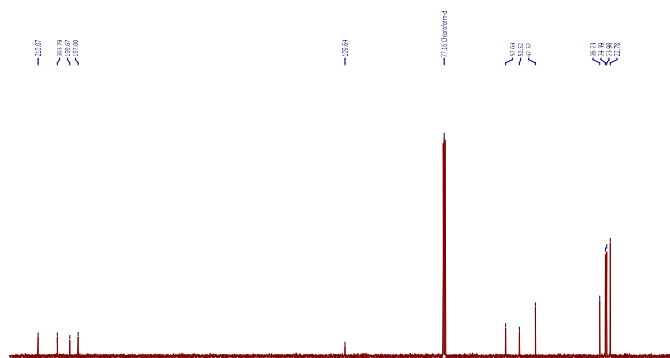


Appendix 183: IR-Spectrum of 5-hydroxy-2,2,6,6-tetramethyl-4-propionylcyclohex-4-ene-1,3-dione (**57**).

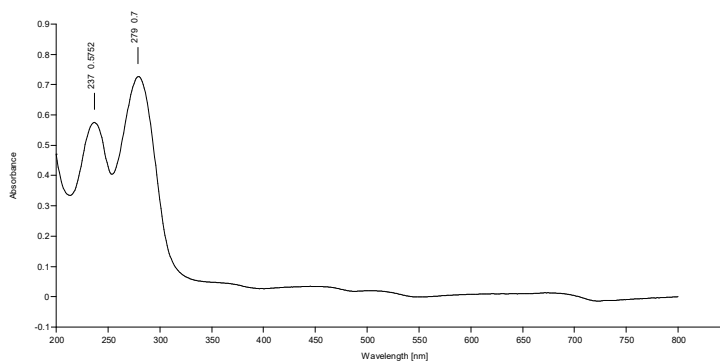
Appendices



Appendix 184: $^1\text{H-NMR}$ of 5-hydroxy-2,2,6,6-tetramethyl-4-(3-methylbutanoyl)cyclohex-4-ene-1,3-dione (**58**).

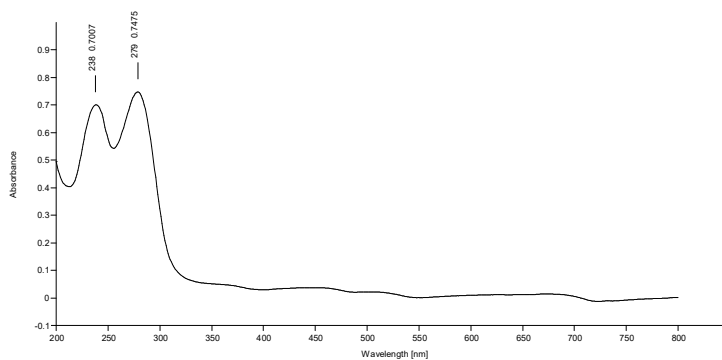


Appendix 185: $^{13}\text{C-NMR}$ of 5-hydroxy-2,2,6,6-tetramethyl-4-(3-methylbutanoyl)cyclohex-4-ene-1,3-dione (**58**).

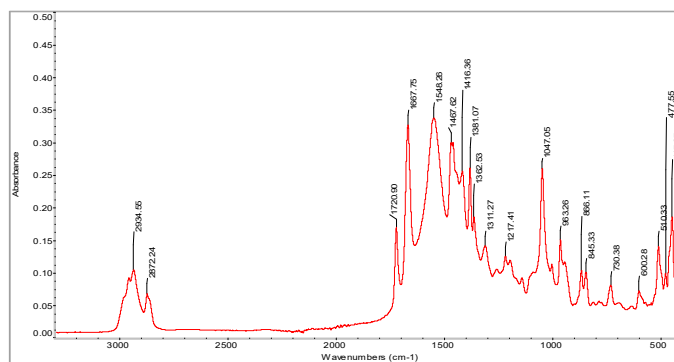


Appendix 186: UV/Vis-Spectrum of 5-hydroxy-2,2,6,6-tetramethyl-4-(3-methylbutanoyl)cyclohex-4-ene-1,3-dione (**58**).

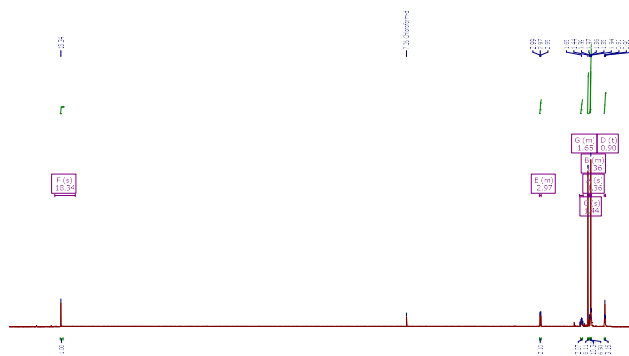
Appendices



Appendix 196: ^{13}C -NMR of 4-butyl-5-hydroxy-2,2,6,6-tetramethylcyclohex-4-ene-1,3-dione (**60**).

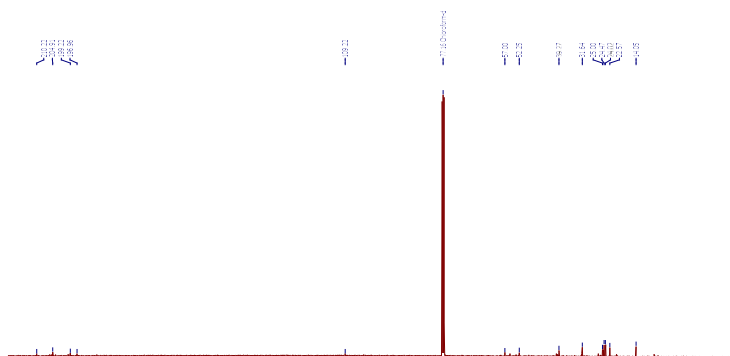


Appendix 197: IR-Spectrum of 4-butyl-5-hydroxy-2,2,6,6-tetramethylcyclohex-4-ene-1,3-dione (**60**).

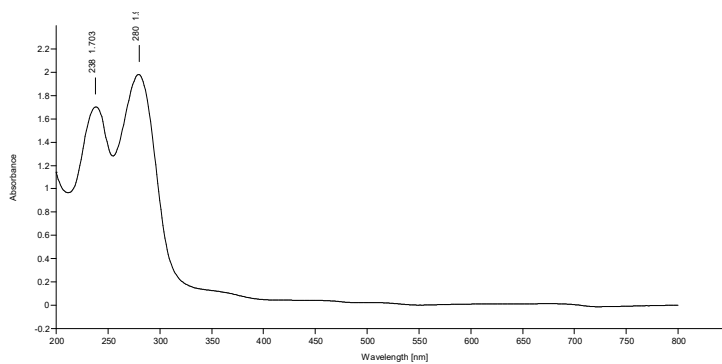


Appendix 198: ^1H -NMR of 4-hexanoyl-5-hydroxy-2,2,6,6-tetramethylcyclohex-4-ene-1,3-dione (**61**).

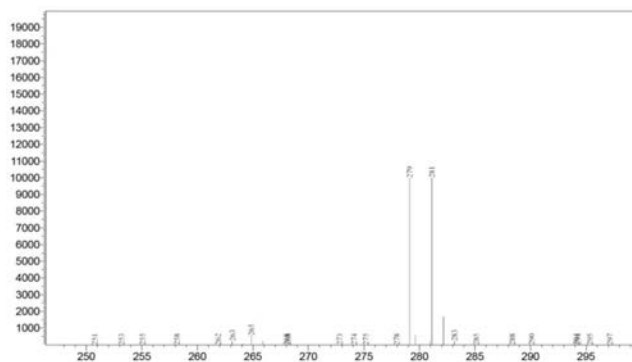
Appendices



Appendix 199: ¹³C-NMR of 4-hexanoyl-5-hydroxy-2,2,6,6-tetramethylcyclohex-4-ene-1,3-dione (**61**).

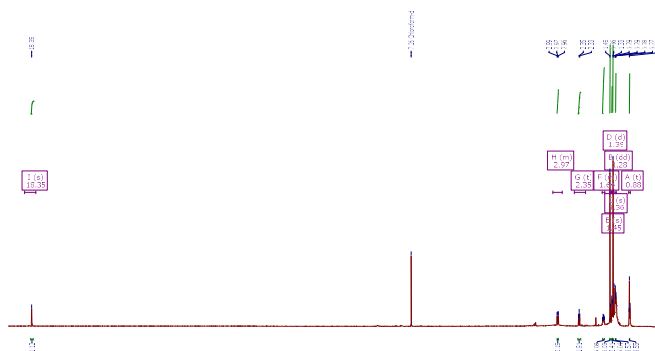


Appendix 200: UV/Vis-Spectrum of 4-hexanoyl-5-hydroxy-2,2,6,6-tetramethylcyclohex-4-ene-1,3-dione (**61**).

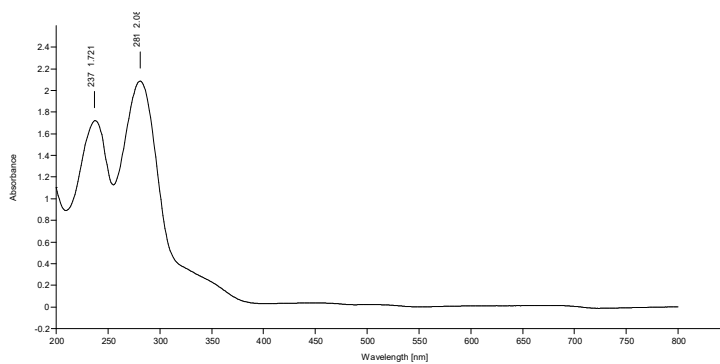


Appendix 201: MS-Spectrum of 4-hexanoyl-5-hydroxy-2,2,6,6-tetramethylcyclohex-4-ene-1,3-dione (**61**).

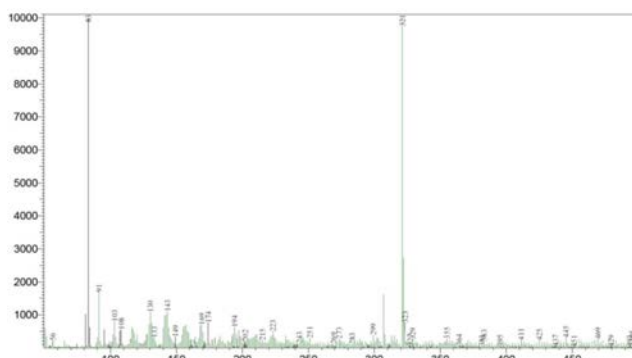
Appendices



Appendix 202: $^1\text{H-NMR}$ of 5-hydroxy-2,2,6,6-tetramethyl-4-nonanoylcyclohex-4-ene-1,3-dione (**62**).

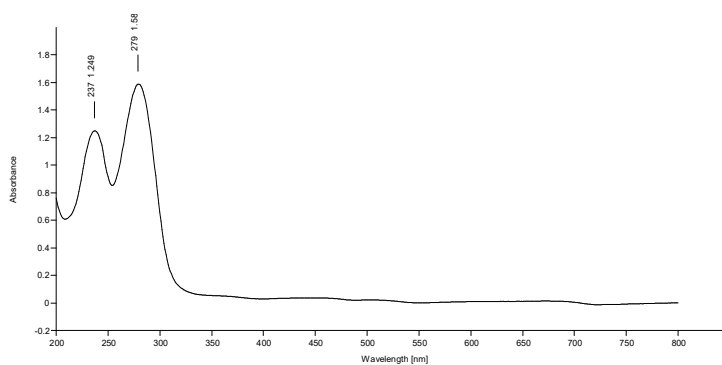


Appendix 203: UV/Vis-Spectrum of 5-hydroxy-2,2,6,6-tetramethyl-4-nonanoylcyclohex-4-ene-1,3-dione (**62**).

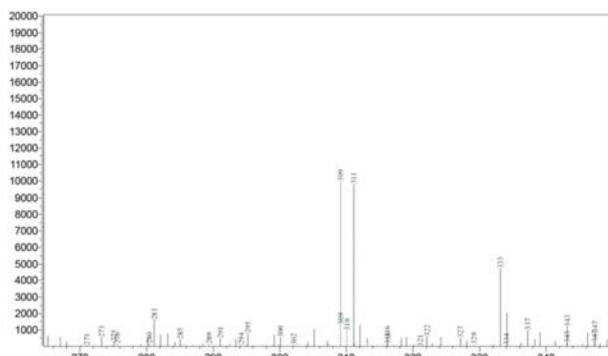


Appendix 204: MS-Spectrum of 5-hydroxy-2,2,6,6-tetramethyl-4-nonanoylcyclohex-4-ene-1,3-dione (**62**).

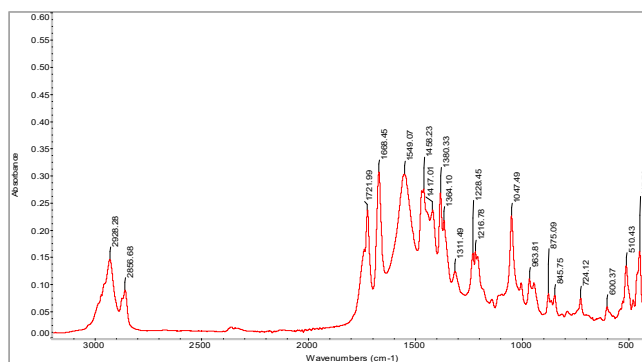
Appendices



Appendix 208: UV/Vis-Spectrum of 5-hydroxy-2, 2, 6, 6-tetramethyl-4-octanoylcyclohex-4-ene-1, 3-dione (**63**).

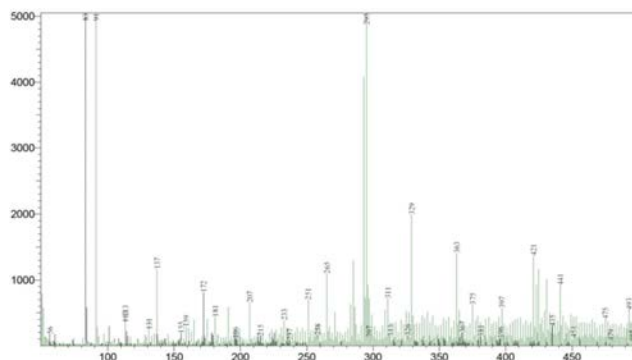


Appendix 209: MS-Spectrum of 5-hydroxy-2, 2, 6, 6-tetramethyl-4-octanoylcyclohex-4-ene-1, 3-dione (**63**).

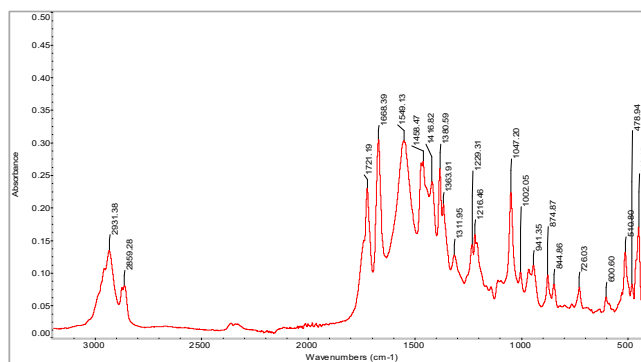


Appendix 210: IR-Spectrum of 5-hydroxy-2, 2, 6, 6-tetramethyl-4-octanoylcyclohex-4-ene-1, 3-dione (**63**).

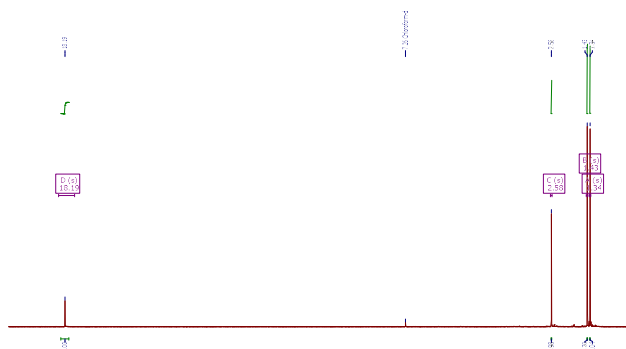
Appendices



Appendix 214: MS-Spectrum of 4-heptanoyl-5-hydroxy-2, 2, 6, 6-tetramethylcyclohex-4-ene-1, 3-dione (**64**).

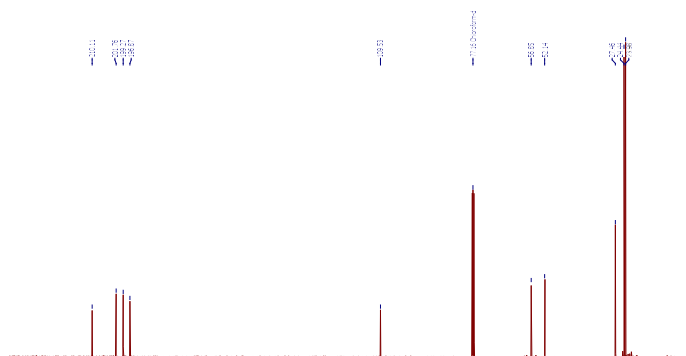


Appendix 215: IR-Spectrum of 4-heptanoyl-5-hydroxy-2, 2, 6, 6-tetramethylcyclohex-4-ene-1, 3-dione (**64**).

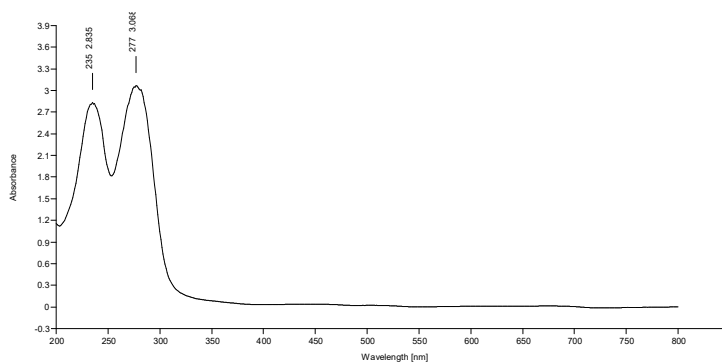


Appendix 216: $^1\text{H-NMR}$ of 4-acetyl-5-hydroxy-2, 2, 6, 6-tetramethylcyclohex-4-ene-1, 3-dione (**65**).

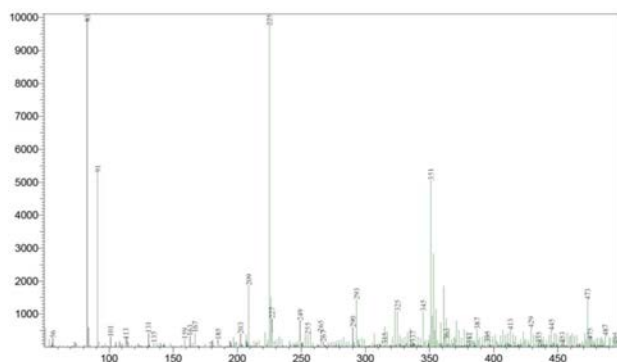
Appendices



Appendix 217: ^{13}C -NMR of 4-acetyl-5-hydroxy-2,2,6,6-tetramethylcyclohex-4-ene-1,3-dione (**65**).

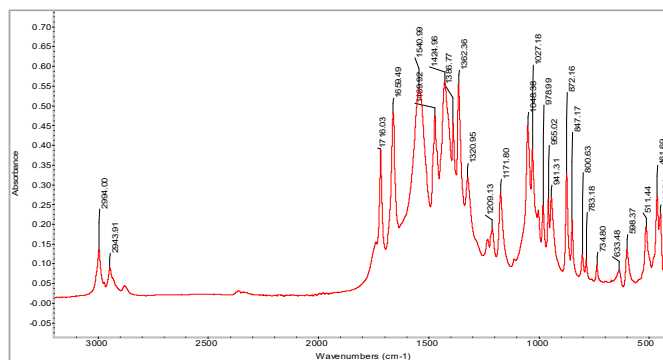


Appendix 218: UV/Vis-Spectrum of 4-acetyl-5-hydroxy-2,2,6,6-tetramethylcyclohex-4-ene-1,3-dione (**65**).

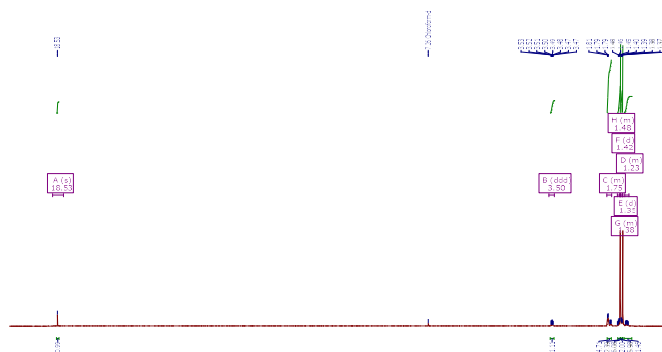


Appendix 219: MS-Spectrum of 4-acetyl-5-hydroxy-2,2,6,6-tetramethylcyclohex-4-ene-1,3-dione (**65**).

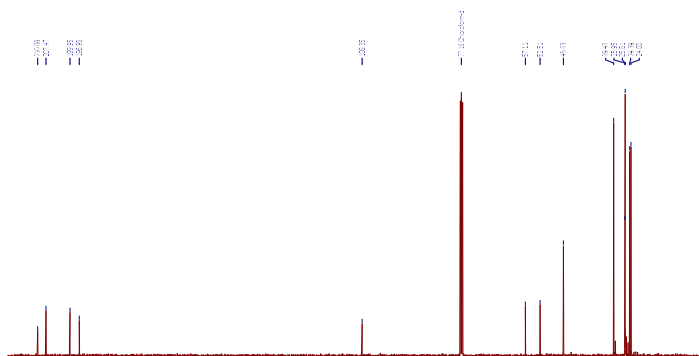
Appendices



Appendix 220: IR-Spectrum of 4-acetyl-5-hydroxy-2, 2, 6, 6-tetramethylcyclohex-4-ene-1, 3-dione (**65**).

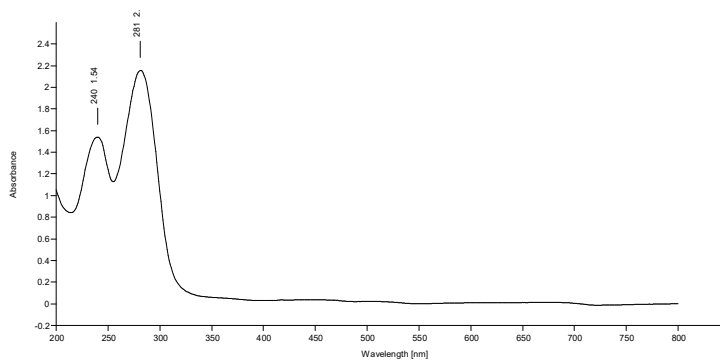


Appendix 221: ^1H -NMR of 4-(cyclohexane carbonyl)-5-hydroxy-2, 2, 6, 6-tetramethylcyclohex-4-ene-1, 3-dione (**66**).

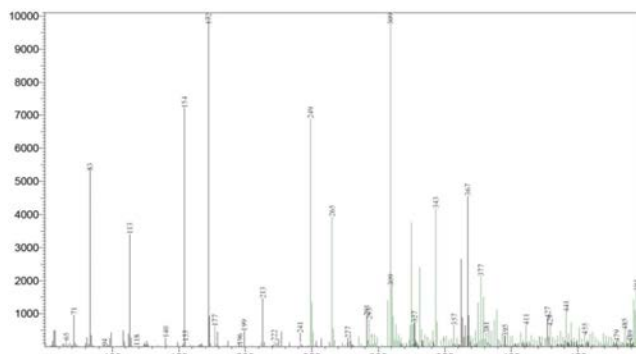


Appendix 222: ^{13}C -NMR of 4-(cyclohexane carbonyl)-5-hydroxy-2, 2, 6, 6-tetramethylcyclohex-4-ene-1, 3-dione (**66**).

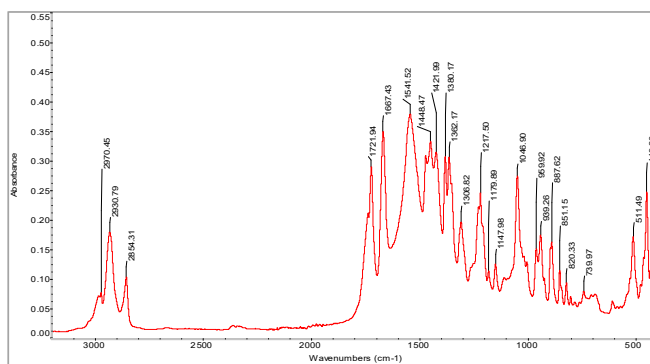
Appendices



Appendix 223: UV/Vis-Spectrum of 4-(cyclohexane carbonyl)-5-hydroxy-2, 2, 6, 6-tetramethylcyclohex-4-ene-1, 3-dione (**66**).

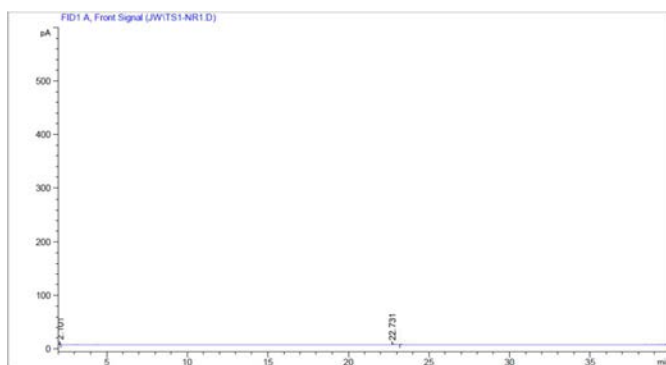


Appendix 224: MS-Spectrum of 4-(cyclohexane carbonyl)-5-hydroxy-2, 2, 6, 6-tetramethylcyclohex-4-ene-1, 3-dione (**66**).

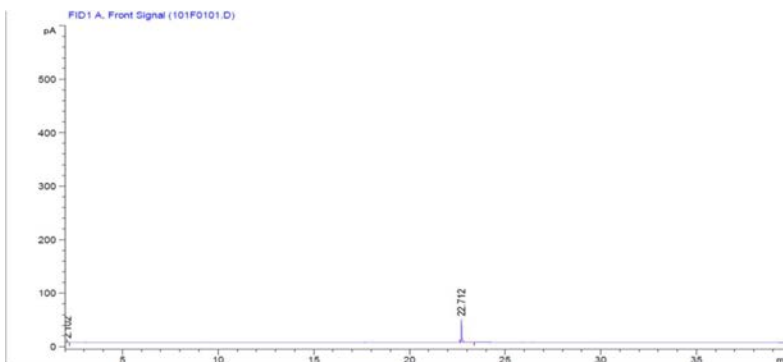


Appendix 225: IR-Spectrum of 4-(cyclohexane carbonyl)-5-hydroxy-2, 2, 6, 6-tetramethylcyclohex-4-ene-1, 3-dione (**66**).

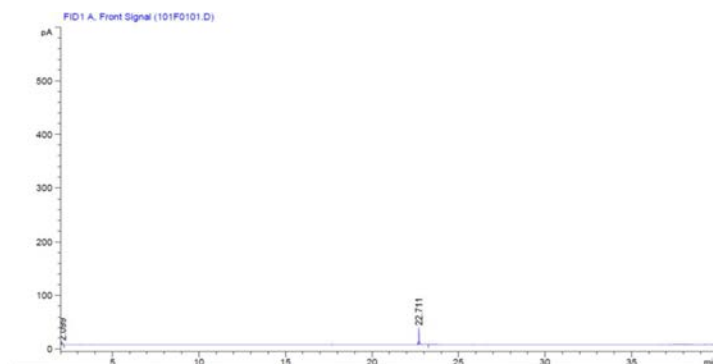
Appendices



Appendix 226: GC-chromatogram of Experiment 94.



Appendix 227: GC-chromatogram of Experiment 95.

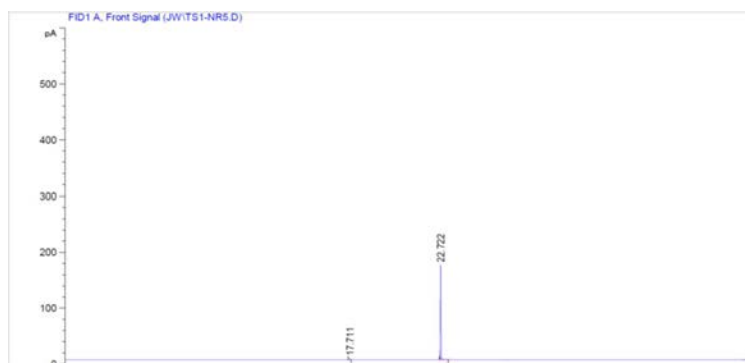


Appendix 228: GC-chromatogram of Experiment 95.



Appendix 229: ¹H-NMR of Experiment 96.

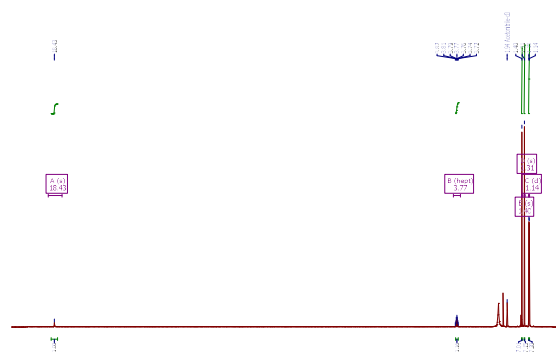
Appendices



Appendix 230: GC-chromatogram of Experiment 97.



Appendix 231: ¹H-NMR of Experiment 97.



Appendix 232: ¹H-NMR of Experiment 98.



Appendix 233: ¹H-NMR of Experiment 99.

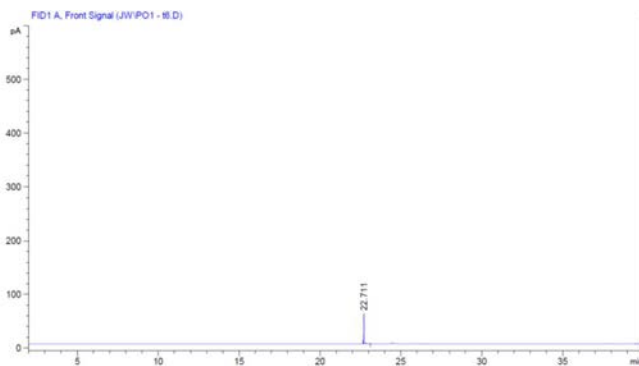
Appendices



Appendix 234: ¹H-NMR of Experiment 100.



Appendix 235: ¹H-NMR of Experiment 101.

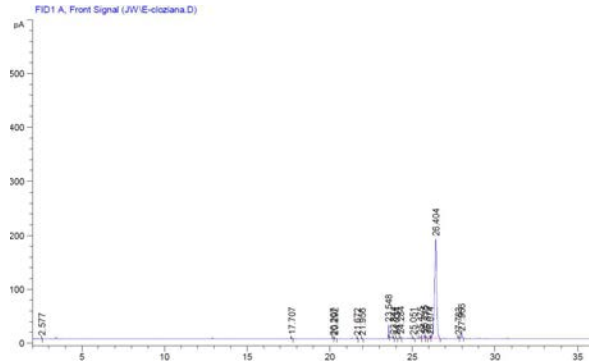


Appendix 236: GC-chromatogram of Experiment 102.

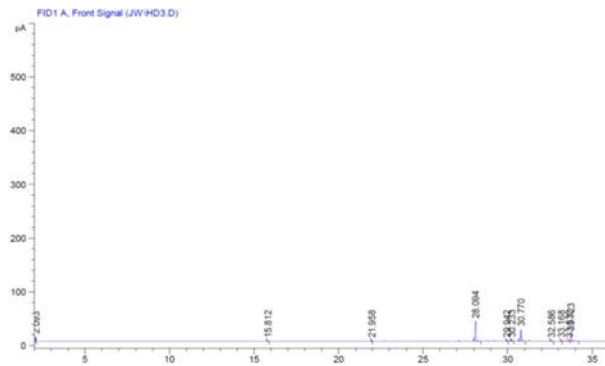


Appendix 237: GC-chromatogram of C8-C20 alkanes used for KI calculations.

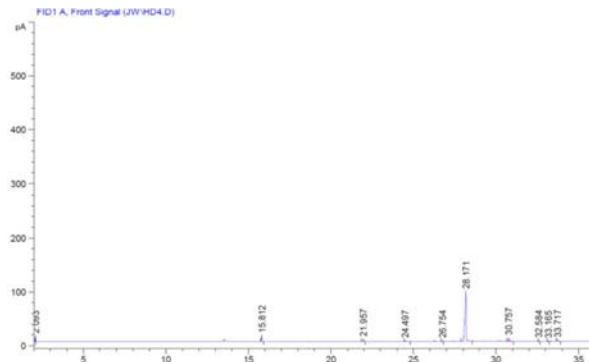
Appendices



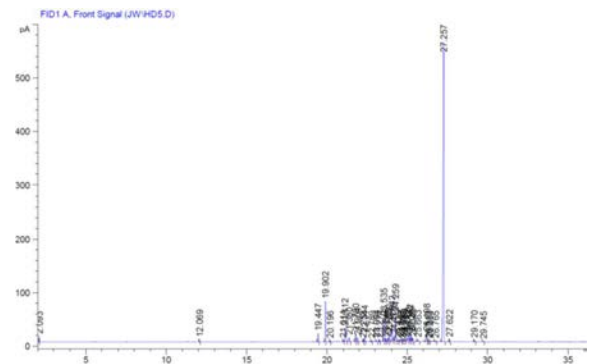
Appendix 238: GC-chromatogram of *E. cloeziana* essential oil.



Appendix 239: GC-chromatogram of *X. chrysanthus 1* (Townsville) essential oil.

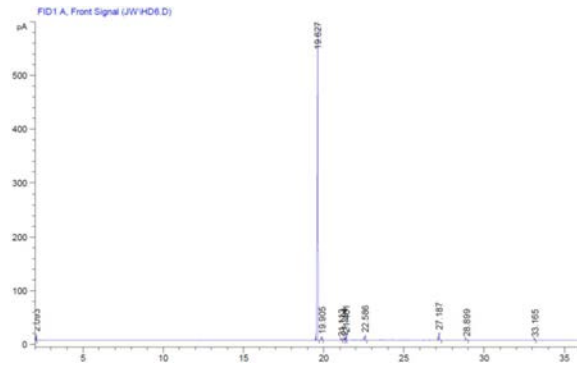


Appendix 240: GC-chromatogram of *X. chrysanthus 2* (Tolga) essential oil.

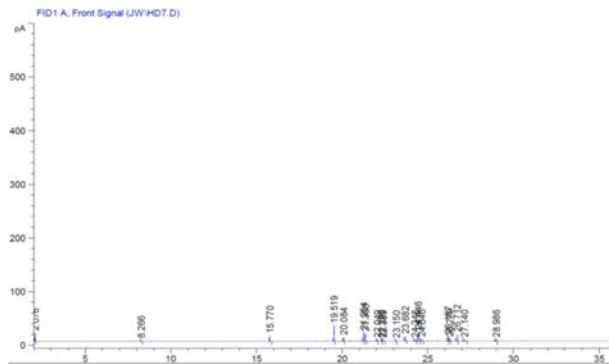


Appendix 241: GC-chromatogram of *X. umbrosus* (Tolga) essential oil.

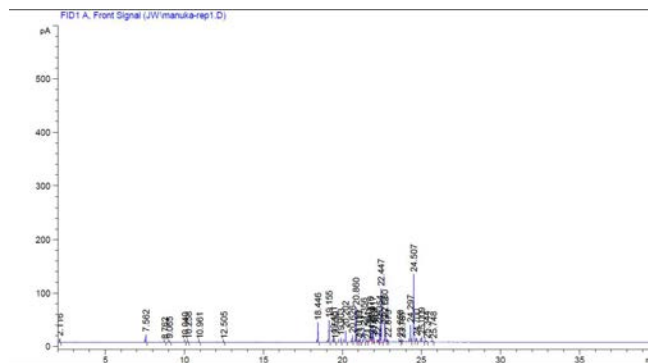
Appendices



Appendix 242: GC-chromatogram of *X. verticillatus* (Tolga) essential oil.

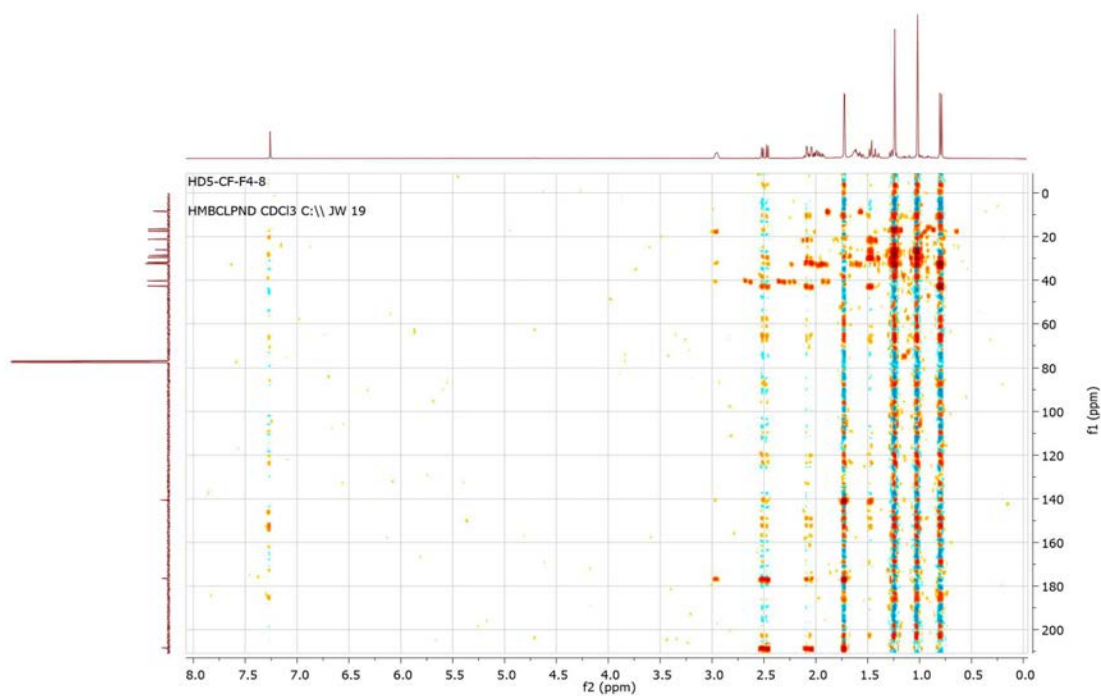


Appendix 243: GC-chromatogram of *X. verticillatus*/*X. chrysanthus* hybrid (Tolga) essential oil.

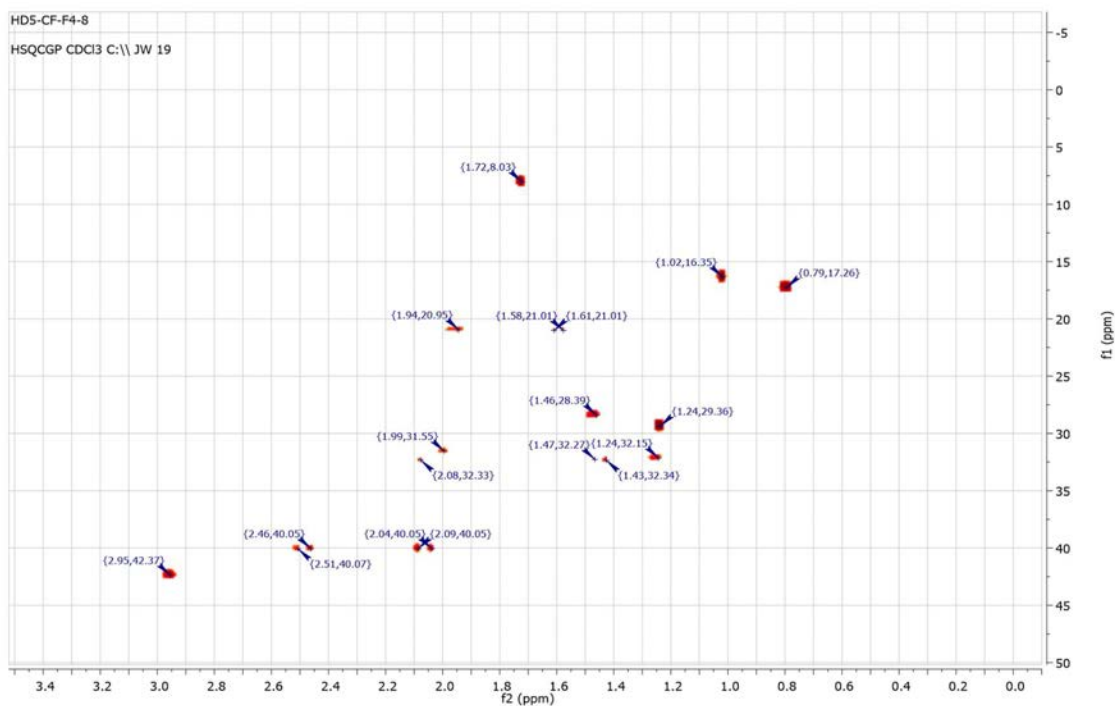


Appendix 244: GC-chromatogram of *L. scoparium*/Manuka oil (Plant Essentials®).

Appendices

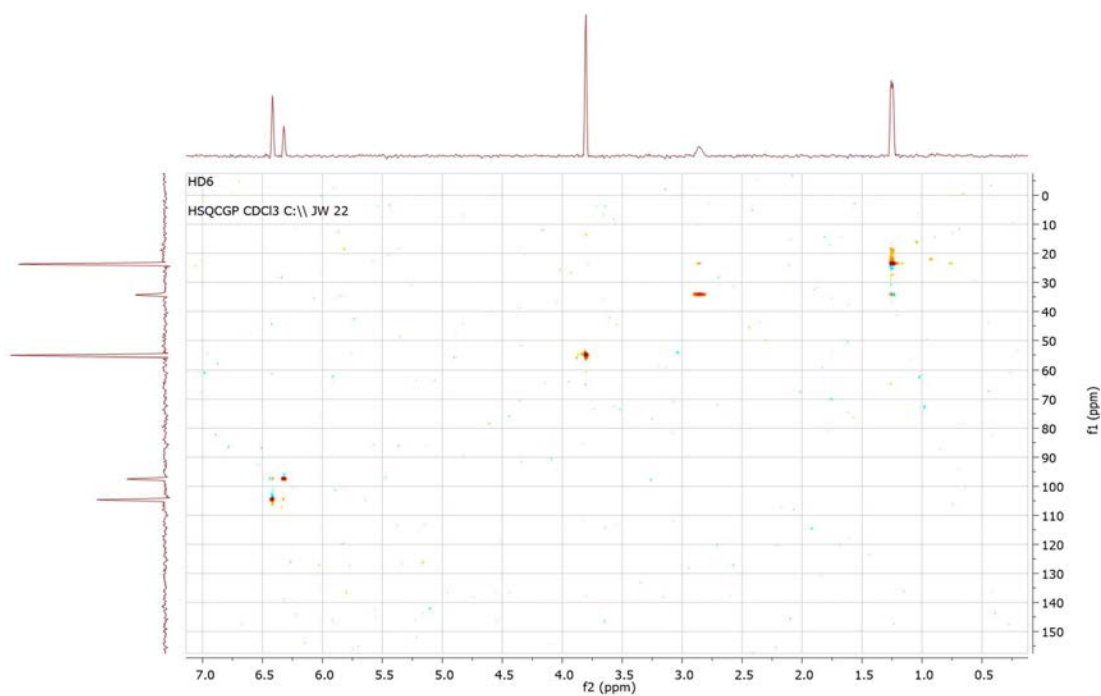


Appendix 245: HMBC-NMR of cyclocolorenone (69).

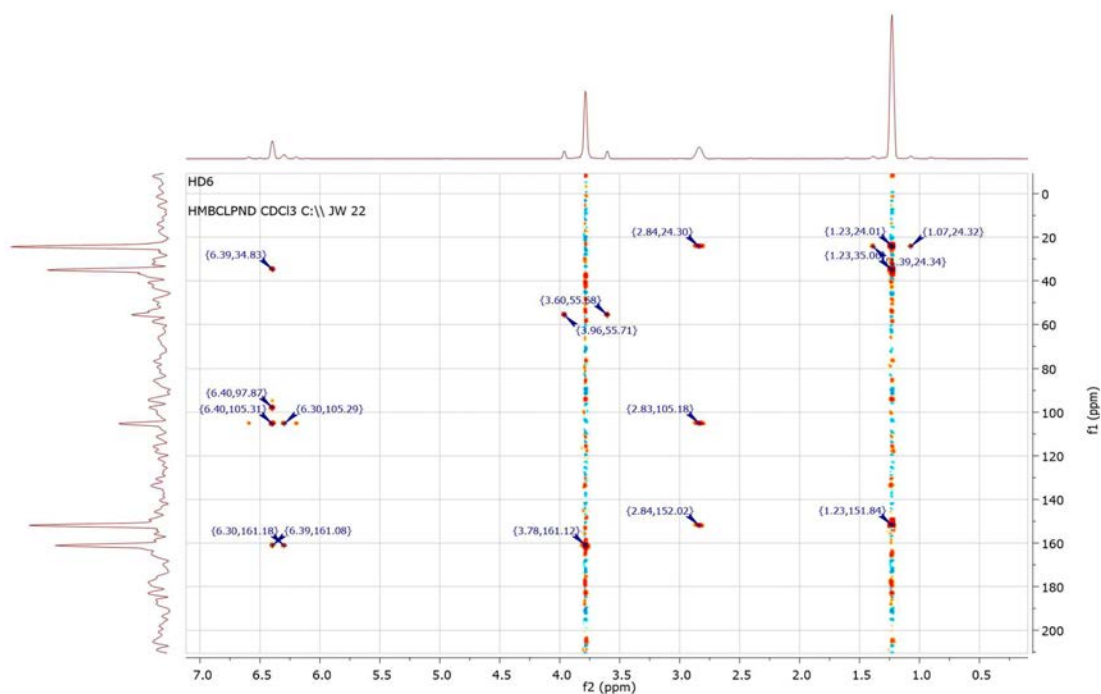


Appendix 246: HSQC-NMR of cyclocolorenone (69).

Appendices



Appendix 247: HSQC-NMR of 1, 3-dimethoxy-5-isopropylbenzene (**70**).



Appendix 248: HMBC-NMR of 1, 3-dimethoxy-5-isopropylbenzene (**70**).